Proton induced spallation reactions in the energy range 0.1 - 10 GeV

Anna Kowalczyk

Contents

2

Chapter 1

Introduction

Several possible scenarios of proton - nucleus reaction are considered nowadays. According to one of the scenarios, incoming proton deposits energy into target nucleus. It knocks out a few nucleons and leaves excited residual nucleus. Then, nucleons and various fragments are emitted from the excited residuum. This scenario is called *spallation*. It is also possible, that the residuum splits up slowly (*fissions*) into two parts, which then emit particles. This scenario is known as emission from *fission* fragments. But, it could be also that all fragments appear simultaneously. This would have features of a phase transition in nuclear matter and is called *fragmentation*. These reaction scenarios are based on experimental observations of different final states. Generally, observation of one heavy nucleus (in respect to the mass of initial target), a small number of light fragments and numerous individual nucleons indicates spallation. Detection of a large number of intermediate size fragments indicates fragmentation. Nevertheless, spallation and fragmentation are correlated. Their differentiation is not clear, difficult and still under discussions. Previous studies indicate, that spallation is the most probable scenario of proton - nucleus reaction, what will be shown also in this dissertation. The main idea of this work concerns theoretical study of proton induced spallation reactions in wide range of incident energy and mass of target nuclei; fission and fragmentation are not discussed in details.

The following definition of spallation process can be found in Nuclear Physics Academic press: *"Spallation - a type of nuclear reaction in which the high-energy of incident particles causes the nucleus to eject more than tree particles, thus changing both its mass number and its atomic number."* So, the term *spallation* means a kind of nuclear reactions, where hadron with high kinetic energy (100 MeV up to several GeV) interacts with a target. First, this term was connected with observation of residuum of reaction corresponding to losses of mass of target nucleus from few up to several dozen

nucleons. Nowadays, it means mechanism, in which high energy light particle causes production of numerous secondary particles from target nucleus, leaving cold residuum of spallation. As a result of such process also various Intermediate Mass Fragments (IMF), i.e. fragments with masses in range $4 < M_{IMF} < 20$, are observed.

From historical point of view, the possibility of heating a nucleus via bombarding by neutrons was suggested first time in 1936 by N. Bohr [1]. Studies of similar reactions were possible due to development of accelerator technics. It was in the end of fourties, when accelerators could provide projectiles with energies higher than 100 MeV [2]. Experimentally, two - component spectra of emitted particles are observed: anisotropic high energy part, which dominates in forward angles (i.e. the high energy tail decreases at backward angles, as it is seen in the example Fig. 1.1) and isotropic, low energy part. These general features of spallation process are established experimentally. A theoretical picture of an incident particle colliding successively with several nucleons inside target nucleus, losing a large fraction of its energy was proposed by Serber in 1947 [3]. Before, in 1937 Weisskopf considered possibility of emission of neutron from excited target nucleus [4]. In the end of fifties, Metropolis [5] and Dostrovsky [6] (who used the ideas of Serber and Weisskopf) suggested description of spallation as two step process involving energy deposition and subsequent evaporation. They formulated and performed first Monte Carlo calculations of the reactions. Such treatment of spallation reactions is used from that time up to now. In more details, the first, so-called fast stage of the spallation is highly non-equilibrated process. High energy proton causes an intra-nuclear cascade on a time scale $\sim 10^{-22}$s. The incident projectile goes through the target nucleus and deposits a significant amount of excitation energy and angular momentum, while ejecting only a few high energy nucleons and, with a minor yield, pions and light ions. The result of the first stage is excited residual nucleus in thermodynamical equilibrium (totally or partly equilibrated), with excitation energy $\sim$ a few MeV/nucleon.

In case of thick target, i.e. system of several nuclei, the ejectiles, as secondary projectiles can cause so-called inter-nuclear cascade, placing individual nuclei into excited states, as illustrated in Fig. 1.2.

The second, so-called slow stage of the spallation, consists in deexcitation of the residuum by evaporation of particles. The isotropic emission (in the system of nucleus) of nucleons (mainly neutrons), light and heavy ions (d, t, He, Li, Be, B, ..., γ) takes place on a time scale $\sim 10^{-18}$ - 10^{-16}s.

From many years spallation reactions of medium and high energy protons with atomic nuclei are still of interest for many reasons. First of all, because knowledge of the reaction mechanism is still not complete. This is interesting
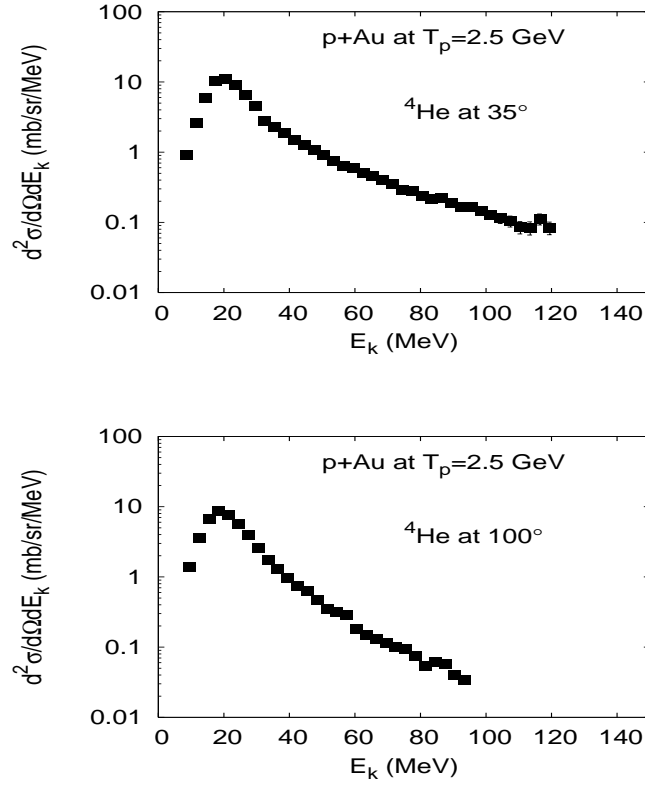
Figure 1.1: *Experimental observations of an example 2.5 GeV proton induced spallation reaction on Au target; inclusive alpha particles spectra measured by PISA at COSY [7]*

both from theoretical and experimental point of view. Experimental data of double differential cross sections of emitted particles in the reactions are necessary for testing, validation and developing of theoretical models. It means, experimentally measured cross sections for exclusive elementary reactions (e.g. NN, Nπ, ...) are implemented in theoretical models. Then, results of calculations are compared with results of inclusive measurements. It is reasonable to study the reaction mechanism on the base of proton - nucleus rather than nucleus - nucleus collisions, where all processes start to be much more complicated (e.g. presence of distortions due to collective processes like compression, deformation, high spin [8]). Moreover, proton - nucleus reactions are important and indispensable also for experiments of nucleus -

Figure 1.2: *The Spallation Process*

nucleus collisions (e.g. HADES [9], CHIMERA [10]). Results of proton - nucleus reactions facilitate extraction and interpretation of results of nucleus - nucleus reactions. Other reasons concern very broad range of applications (e.g. in medicine (radiation therapy), cosmology, accelerator technology).
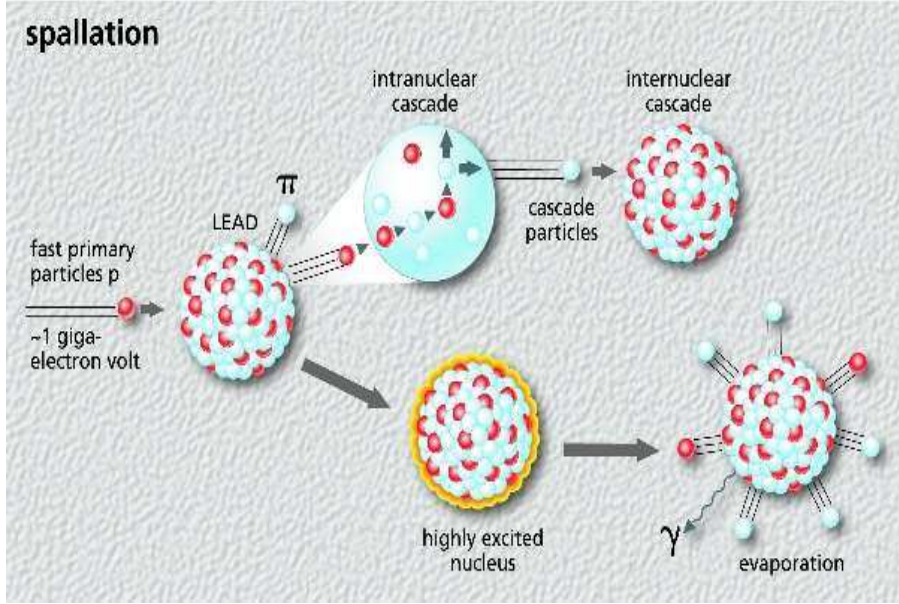
Relatively huge number of produced neutrons suggested the idea of using spallation reactions as neutron sources. Nowadays, neutron beams are produced in nuclear reactors. Reactors dedicated for such production generate also a lot of heat; about 190 MeV of energy is dissipated for single produced neutron. In accelerator based sources, neutrons are produced in a spallation process, with only about 30 MeV of energy dissipated for one generated neutron. During last decade several spallation sources (IPNS [11], ISIS [11], LANSCE [12], SINQ [13]) became operational.

Spallation reactions are very important in accelerator technology (e.g. activation of detectors, radiation protection). The reactions are used for energy amplification, also for production of energy from nuclear waste and furthermore, transmutation of long - lived radioactive nuclei of nuclear waste to stable or short - lived, in order to avoid their long term storing [14].

 Astrophysical models have to include spallation processes. If one compares abundances of cosmic rays and solar system elements, it is seen that Li, Be and B in cosmic rays are enriched by more than 6 orders of magnitude, as shown in Fig. 1.3. They were evidently produced in spallation reactions of
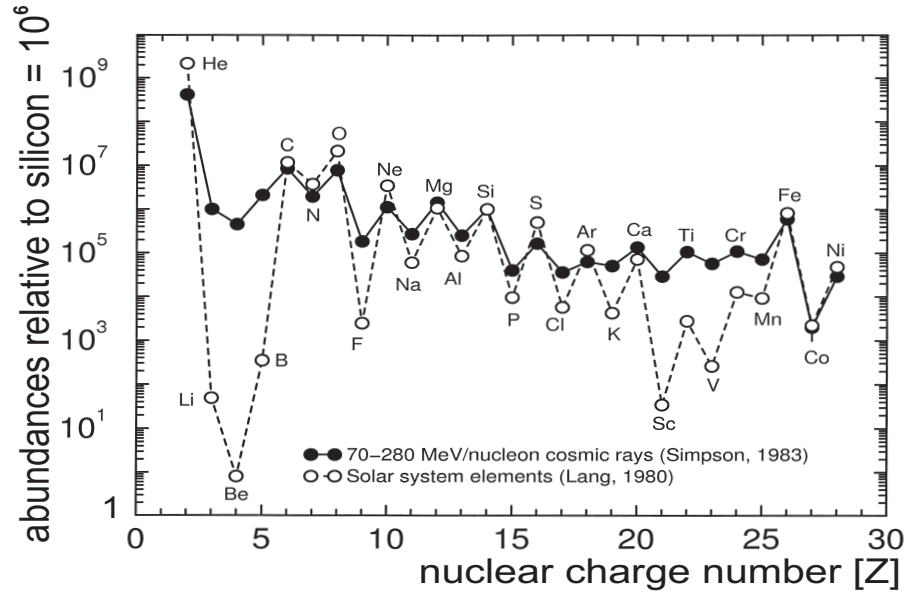
Figure 1.3: *The relative abundances of elements in cosmic rays measured at Earth and in the solar system, taken from [16]*

hydrogen nuclei (which consist about 87 % of cosmic rays) with heavy elements (produced due to stars explosions). For more informations see [15, 16].

Theoretical predictions of the process are important in each of mentioned above cases. Several models have been constructed in order to describe the spallation process. First stage of the reaction is described by a class of microscopic models, e.g. [17, 18, 19]. For the second stage statistical models are used, e.g. [20, 21]. Nevertheless, the theoretical investigations are rather fragmentary and still not satisfactory. Global qualitative and quantitative informations of the spallation reactions are needed.

Description of global average properties of proton induced spallation reactions in wide range of projectile energy and mass of target nuclei is the main subject of this work. This is investigated within a transport model based on Boltzmann - Uehling - Uhlenbeck (BUU) equation supplemented by a statistical evaporation model. The used transport model has been specially developed in the frame of this work, in order to enable description of such reactions.

This work is organized as follows. In Chapter 2, present knowledge of the reaction dynamics and review of various theoretical models is given. Chapter 3 includes description of the Hadron String Dynamics (HSD) approach

of the first stage of the spallation reaction. In Chapter 4 and Chapter 5, results concerning properties of the first stage of the reaction are presented and discussed. Chapter 6 concerns pions, which could be produced only in the first stage of reaction. In Chapter 7, statistical evaporation models for the second stage are recalled. Chapter 8 contains bulk model predictions of both stages of proton - nucleus reactions. In Chapter 9 and Chapter 10, the models results and comparison with available experimental data and with results of other models are presented, respectively. Finally, in Chapter 11, a summary and conclusions are given.

Chapter 2

Present knowledge of the reaction dynamics - basic theoretical models

Our understanding of physical phenomena is expressed as modelling. At present, the broadest platform for such modelling is quantum mechanics approach. Unfortunately, many - body systems are usually an extreme challenge for existing methods of quantum mechanics. One has to rely on rather simple, much more straight formed concepts. In this Chapter, such general basic concepts will be shown as ingredients of typical models of nuclear reaction.

Several microscopic models have been constructed in order to describe the first stage of proton - nucleus reaction. All of them have the same basis, they describe the reaction as a cascade of nucleon - nucleon collisions, but employing different assumptions. The main difference concerns implemented potential of nucleon - nucleus interaction. One can distinguish the simplest models, which neglect features of the mean field dynamics and employ constant static potential, like a class of Intra - Nuclear Cascade (INC) models. Other, more sophisticated approaches comprise dynamically changing field and minimal fluctuations obtained due to use of test particle method, i.e. models based on Boltzmann - Uehling - Uhlenbeck (BUU) transport equation. There are also models, which include real fluctuations and particles correlations, employing two- and three- body potentials, e.g. Quantum Molecular Dynamics models. The main ideas of the different types of nuclear reaction approaches are described below.

In this Chapter, devoted for model-like approach of investigation of nucleon - nucleus reactions, also so-called percolation model is presented. This rather basic model describes fragment mass distributions very well (Section 2.3).

2.1 Intranuclear Cascade model

Intranuclear cascade (INC) model is used as a base in many existing codes for the first stage calculations. Description of the nucleon - nucleus reaction in terms of binary nucleon - nucleon collisions inside nucleus is the basic assumption of the model. In principle, the single particles approach of the INC is justified as long as the de Broglie wavelength λ of the cascade particles is smaller than the average internucleon distance in the nucleus ($\approx$ 1.3 fm). This indicates the low energy limit of the model (e.g. for projectile kinetic energy $T_p = 100$ MeV $\Rightarrow \lambda = 2.7$ fm, for $T_p = 1000$ MeV $\Rightarrow \lambda = 0.7$ fm). The INC calculations follow the history of individual nucleons that becomes involved in the nucleon - nucleon collisions in a semi - classical manner. It means, the momenta and coordinates (trajectories) of the particles are treated classically. The only quantum mechanical concept incorporated in the model is the Pauli principle.

The first code of INC has been created by Bertini [22], in 1963. Later, the conception was used also in other codes, e.g. by Yariv in his ISABEL code [23]. In the 80's and 90's, the next versions of INC model was developed by Cugnon et al. [17].

The main features of the standard INC approach are the following.

The initial positions of target nucleons are chosen randomly in a sphere of radius $R = 1.12 \cdot A_T^{1/3}$ fm, where: A_T is the mass number of target nucleus. Momenta of the nucleons are generated inside a Fermi sphere of radius $p_F = 270$ MeV/c. Neutrons and protons are distinguished according to their isospin. All nucleons are positioned in a fixed and constant, attractive potential well of $V_0 = 40$ MeV depth, inside the nuclear target volume. The depth value is taken a bit higher than the Fermi energy ($E_F \approx 38$ MeV), so that the target is stable during the reaction. The idea of fixed average potential is based on a relatively low number of particles emitted during the INC stage of reaction, which disturbes the mean field only slightly. The incident particle (of incident energy T_p) is provided with an impact parameter b, chosen randomly on a disc of radius R. It is positioned at the surface of nucleus, in the potential V_0. Its kinetic energy is equal to $T_p + V_0$. Relativistic kinematics is used for description of the reaction (i.e. the total energy of a nucleon is connected with its momentum and mass by relation: $E^2 = p^2 + m^2$). All nucleons are propagated in time; their momenta and positions are evolved in time as follows: $\vec{r}(t + \delta t) = \vec{r}(t) + \frac{\vec{p}}{E}\delta t$, $\vec{p}(t + \delta t) = \vec{p}(t) - \nabla_r V_0 \delta t$.

At time $t = 0$, the incident nucleon is hitting the nuclear surface. Next, all particles are moving along straight line trajectories, until two of them reach their minimum relative distance, or until one of them hits the nuclear surface. When a particle hits the nucleus surface from inside, two cases are consid-

ered. If the kinetic energy of the particle is lower than the V_0, it is reflected on the surface. If the kinetic energy is higher than the V_0, the particle is transmitted randomly with some probability, see Ref. [17].

A collision takes place, if the minimum relative distance d_{min} between two particles fulfills the condition: $d_{min} \leq \sqrt{\frac{\sigma_{tot}(\sqrt{s})}{\pi}}$, where: $\sqrt{s}$ is the energy in the center of mass of the two particles, σ_{tot} is the total collision cross section. The two particles are scattered elastically or inelastically, according to the energy - momentum conservation. Inelastic collisions with high probability lead to the formation of Deltas (Δ's). Mass of Δ is introduced with the Lorentzian distribution centered on the mean value equal to 1232 MeV, with the width Γ=110 MeV.

The following reactions are considered in the model:

$NN \Leftrightarrow NN$, $NN \Leftrightarrow N\Delta$, $N\Delta \Leftrightarrow N\Delta$, $\Delta\Delta \Leftrightarrow \Delta\Delta$, $\Delta \Leftrightarrow N\pi$.

All used cross sections and angular distributions are based on available experimental data [17].

Additional condition restricting a collision is Pauli blocking. Collisions and Δ - decays are avoided, when the presumed final states are already occupied. The final states phase - space occupation probability (f_i and f_j, where i and j denote two particles predicted to be created in the final state) is evaluated by counting particles of the same kind, inside a reference volume in phase - space. The collision or decay is realized, when: $P_{ij} = (1 - f_i)(1 - f_j)$ is larger than a random number chosen between 0 and 1.

The interaction process is stopped at time $t = t_{stop}$, determined by the average behaviour of some quantities (e.g. an excitation energy of the nucleus, see Ref. [17]). At the end of the cascade, all remaining Δ's are forced to decay.

2.2   Quantum Molecular Dynamics model

Quantum Molecular Dynamics (QMD) [19, 24] model has been developed mainly in order to investigate fragments formation during proton - nucleus or nucleus - nucleus collisions. The model, as a N-body theory, describes the time evolution of correlations between particles, what is essential in consideration of the fragments formation.

In the approach, nucleons are spread out in phase - space with a Gaussian distribution. The coordinates and momenta of nucleons are designated simultaneously. The wave function of each nucleon (i) is assumed to have the following Gaussian form:

$$\psi_i(\vec{r}, \vec{p}, t) = \frac{1}{(2\pi L)^{3/4}} e^{-\frac{(\vec{r} - \vec{r}_{i0})^2}{4L}} e^{i\vec{p}\vec{r}} \qquad (2.1)$$

where: the Gaussian width - $L = 1.08 fm^2$ - corresponds to a root mean square radius of the nucleon of 1.8 fm, $\vec{r}_{i0}$ are the coordinates of the centers of the Gaussian wave packets.

The normalized Gaussian function represents one nucleon.

In the model, Szilard-Wigner densities are applied. Those give a semi-classical approximation, depending simultaneously on coordinates and momenta. The Szilard-Wigner density is defined by the following expression, constructed of a wave function: $\psi(x_1, ..., x_n)$ [25]:

$$P(x_1, ..., x_n; p_1, ..., p_n) = (\frac{1}{\hbar\pi})^n \int_{-\infty}^{\infty} ... \int_{-\infty}^{\infty} dy_1 ... dy_n \psi(x_1 + y_1, ..., x_n + y_n)^*$$
$$\psi(x_1 - y_1, ..., x_n - y_n)e^{\frac{2i}{\hbar}(p_1 y_1 + ... + p_n y_n)} \quad (2.2)$$

This is called the probability function of the simultaneous values of coordinates: $x_1, ..., x_n$ and momenta: $p_1, ..., p_n$. It has the following properties. Integrated with respect to the p, it gives probabilities for the different values of the coordinates:

$$\int P(x_1, ..., x_n; p_1, ..., p_n)dp = |\psi(x_1, ..., x_n)|^2. \quad (2.3)$$

Also, integrated with respect to the x, it gives quantum mechanical probabilities for the momenta $p_1, ..., p_n$:

$$\int P(x_1, ..., x_n; p_1, ..., p_n)dx = |\int_{-\infty}^{\infty} ... \int_{-\infty}^{\infty} \psi(x_1, ..., x_n)e^{\frac{-i}{\hbar}(p_1 x_1 + ... + p_n x_n)}dx_1 ... dx_n|^2. \quad (2.4)$$

Based on upper definition, the Szilard-Wigner representation of considered in the model system is given by:

$$f(\vec{R}, \vec{p}, t) = \sum_i \frac{1}{(\pi\hbar)^3} exp(-\frac{(\vec{R} - \vec{R}_i(t))^2}{2L} - \frac{2L \cdot (\vec{p} - \vec{p}_i(t))^2}{\hbar^2}) \quad (2.5)$$

The boundary distributions, i.e. the densities in coordinate and momentum space are given by:

$$n(\vec{R}, t) = \int f(\vec{R}, \vec{p}, t)d^3p = \sum_i \frac{1}{(2\pi L)^{3/2}} exp(-\frac{(\vec{R} - \vec{r}_{i0}(t))^2}{2L}), \quad (2.6)$$

$$g(\vec{p}, t) = \int f(\vec{R}, \vec{p}, t)d^3R. \quad (2.7)$$

In order to construct the initial system, the centers of the Gaussians (i.e. nucleons) are chosen randomly in coordinate and momentum space, in the following way. First, the positions $(\vec{r}_i)$ of nucleons are determined in a sphere

of the radius $R = 1.14 \cdot A^{1/3}$. The numbers are chosen randomly, rejecting those which would position the centers of two nucleons closer than $r_{min} = 1.5$ fm. In the next step, the local density $(\rho(\vec{r_i}))$, at the centers of all nucleons, generated by all the other nucleons is determined. Then, the local Fermi momentum (p_F^l) is calculated: $p_F^l = \hbar(\frac{3}{2}\pi^2\rho(\vec{r_i}))^{1/3}$. Finally, the momenta $(\vec{p_i})$ of all nucleons are chosen randomly, between zero and the local Fermi momentum (p_F^l). Then, all random numbers, which position two nucleons in phase - space closer than: $(\vec{r_i} - \vec{r_j})^2(\vec{p_i} - \vec{p_j})^2 = d_{min}$ are rejected, and must be chosen again. The initialization process lasts long time. Typically, only 1 of 50 000 initializations is accepted under the criteria. But the finally accepted configurations are quite stable, usually no nucleon escapes from the nucleus in 300 fm/c, see [19].

After successful initialization, the nuclei (in case of nucleus - nucleus collisions) are boosted towards each other with the proper center of mass velocity.

During propagation, only positions (r_i) and momenta (p_i) of nucleons (i) are changed, the width of the wave function is kept fixed. The mean values (r_{i0}, p_{i0}) are evaluated at time under the influence of two- and three- body interactions (important for preserving the correlations and fluctuations among nucleons), according to the classical Newtonian equation of motion:

$$\dot{r}_{i0} = \frac{\partial H}{\partial p_{i0}},$$
$$\dot{p}_{i0} = -\frac{\partial H}{\partial r_{i0}}, \tag{2.8}$$

with the Hamiltonian $H = T + U$, where: T is total kinetic energy and U is total potential energy of all nucleons.

Usually, the differential equations are solved using an Eulerian integration routine with a fixed time step Δt, where the momentum is evaluated at time points halfway between the times of the position determinations:

$$p_{i0}(n + 1) = p_{i0}(n) - \nabla_r U_i(n + \frac{1}{2})\Delta t,$$
$$r_{i0}(n + \frac{1}{2}) = r_{i0}(n - \frac{1}{2}) + \frac{p_{i0}(n)}{(p_{i0}(n)^2 + m_i^2)^{1/2}}\Delta t + \nabla_p U_i(n)\Delta t. \tag{2.9}$$

Assumed in the model total interaction is composed of a short range interactions between nucleons $(V^{loc} \approx \delta(r_1 - r_2) + \delta(r_1 - r_2)\delta(r_1 - r_3))$, a long range Yukawa interaction $(V^{Yuk} \approx \frac{e^{-|r_1-r_2|/\nu}}{|r_1-r_2|/\nu}, \nu = 0.8$ fm) and a charge Coulomb interaction $(V^{Coul} \approx \frac{Z_1 \cdot Z_2}{|r_1-r_2|}, Z_{1,2}$ stands for charges).

Potential acting on each particle is given by the expectation value of the two and three body interaction:

$$U_i(t) = U_i^{(2)}(t) + U_i^{(3)}(t) \tag{2.10}$$

where the two body potential $U_i^{(2)}$ is given by local, Yukawa and Coulomb interaction terms, while the three body potential $U_i^{(3)}$ includes only the local interactions term, see Ref. [19].

Two nucleons can collide if they come closer than $r = \sqrt{\sigma/\pi}$, where σ is a total nucleon - nucleon cross section. Additionally, Pauli principle is taken into account. In the model, the measured free nucleon - nucleon scattering cross section is used. However, the effective cross section is smaller because of the Pauli blocking of the final state. It means, whenever a collision has occurred, the phase - space around the final states of the scattering partners is checked. It is calculated, which percentage, P_1 and P_2, of the final phase - space for each of the two scattering partners, respectively, is already occupied by other nucleons. Then, the collision is blocked with a probability $P_{block} = P_1 P_2$, or allowed with the probability $1 - P_{block}$. If a collision is blocked, the momenta of scattering partners are kept with values, which they had before scattering.

The scattering angles of the single nucleon - nucleon collisions are chosen randomly, with the probability distribution known from the experimental nucleon - nucleon scattering [26].

Inelastic collisions lead to the formation of Deltas, which can be reabsorbed by the inverse reactions.

It is assumed in the QMD approach, that only these beam energies are accepted, at which no more than 84% of all collisions are blocked. Therefore, the low energy limit of the model is kinetic energy $T_{lab} = 20$ MeV/nucleon [19].

2.3 Percolation model

Percolation model has been introduced in the eighties as minimum information approach, based on purely topological and statistical concepts. It was in order to describe fragment size distributions, as an outcome of nuclear fragmentation process within the simplest possible physical framework [27]. However the model is flexible enough to allow for the inclusion of different physical mechanisms.

In general, one distinguishes between bond and site percolation model.

Site percolation corresponds to the case where each site is either occupied by one particle or is empty. One fixes a probability $p \in [0, 1]$, and for each site generates a random number ξ, taken from a uniform distribution in the interval $[0, 1]$. If $\xi \leq p$ the site is said to be occupied, if $\xi > p$ it is empty. Checking all sites, one obtains an ensemble of occupied and empty sites. Sets of occupied sites are called clusters. Finally, space is topologically covered with clusters and empty space.

Bond percolation corresponds to the case where each site is occupied, but neighbouring sites being bound or not to each other. The number of neighbouring sites is fixed by the bonds, which depend on the geometric structure of space occupation. A similar procedure, as in case of site percolation, works also in this case. For a fixed bond probability p one considers a pair of neighbouring sites and generates a random number $\xi \in [0, 1]$. If $\xi \leq p$ the sites are linked by a bond, if $\xi > p$ they are not. Checking all possible bonds between neighbouring sites one obtains clusters made of connected particles. There are clusters of different sizes, appearing with a given multiplicity, which depends on p.

The first applications of percolation concepts were proposed by W. Bauer and collaborators [28, 29], Campi and Desbois [30]. While Campi and Desbois used a site percolation, Bauer with his group have proposed a model based on bond percolation theory. Nowadays, the bond percolation has been used as a base for models of fragmentation more often than the site one. Below, an outline of model proposed by Bauer et al. is presented.

As any percolation model, it is based on two crucial ingredients: a description of the distribution of a set of points (i.e. nucleons) in a space and a criterion for deciding whether two given points are connected. The target nucleons are represented by points occupying uniformly an approximately spherical volume on a simple cubic three-dimensional lattice in coordinate space. The lattice spacing d is computed from the normal nuclear density: $d = \frac{1}{\rho_0^{1/3}} \approx 1.8 \ fm$, where: $\rho_0 = 0.16 \ nucleons/fm^3$. The number of points is equal to the number of target nucleons and is conserved during the calcula-

tion, therefore the conservation law of mass in the calculated fragmentation process is fulfilled. Initially, each nucleon is connected by bonds (representing the short-ranged nuclear interactions) to its maximum six nearest neighbors, depending on its location in the target. Then, a point-like proton, with an interaction radius r collides the target. Because it is assumed that the motion of the nucleons in the target is neglected, the projectile sees a frozen image of the target (it is feasible, as typical Fermi motion speed of nucleon is significantly lower than speed of incoming proton). For a given impact parameter b, the proton removes from the lattice nucleons occupying a cylindrical channel with the radius r along his straight path in the target. It is typically 6-8 nucleons. All of remained nucleons, called spectators, are still connected via bonds. These bonds are then broken with a probability p, which is a percolation parameter. The parameter p should be related to some physical input. For example, it is reasonable to assume that p is a linear function of kinetic energy of the projectile, and also an increasing function of the excitation energy (E^*) of the spectators: $p = E^*/E_B$, where: E_B is the nuclear matter binding energy per nucleon (16 MeV) [31].

The breaking probability has to be also dependent on the impact parameter b of the proton. Bauer et al. have used following dependence: $p(b) = \frac{p_0}{1+exp[(b-R)/a]}$, where: $p_0 = p(b = 0)$, R is a radius of the target nucleus, $a = 1.0\ fm$ is a diffuseness parameter [29, 31].

For given parameter b, the breaking probability is assumed to be uniform for all bonds, independent of their position on the lattice.

Using the breaking probability p as an input parameter, a Monte-Carlo algorithm decides for each bond individually whether it is broken or not, as follows. For a given $p(b)$, a random number $\xi_{ijk} \in [0, 1]$ is generated for each bond B_{ijk}, where: the indices ijk correspond to the spatial location of the center of the bond on the lattice. If $\xi_{ijk} > p$, the bond B_{ijk} is unbroken, if $\xi_{ijk} \leq p$, the bond is broken. Then a cluster search algorithm [29] is used to find out which nucleons are still connected by bonds i.e. form clusters. Taking into account all impact parameters, inclusive mass and multiplicity distributions can be obtained. That can be compared to experimental results.

It is surprising that using only one free parameter and simple geometrical considerations, this model is able to reproduce experimental mass yield curves with a good accuracy, in particular, the power law behavior ($\sim A_F^{-\lambda}$) at small masses and the U-shape distribution of the whole mass range.

Bauer's group have used such model also to study the possibility of observing a phase transition of nuclear matter in collisions of high energy protons (> 10 GeV) with heavy targets. Since inclusive fragment mass distributions

follow a power law behavior: $\sigma(A_F) \approx A_F^{-\lambda}$, for $A_F < A_T/3$, ($\lambda = 2.6$ is independent of target mass for heavy targets) [32] similar to the mass yield distribution of droplets condensing at the critical point in a van der Waals gas ($\sigma(m) \approx m^{-\tau}$, with the critical exponent $\tau = \frac{7}{3}$), they suggested that nuclear multifragmentation proceeds via a liquid-gas phase transition of nuclear matter.

Bauer et al. have accented the importance of their result for experimental study of the phase transition, that the critical events are not the ones with the highest multiplicities, but the ones with the highest value of standard deviation of mass distribution.

In the percolation models, such as described above, it is assumed that nucleons are distributed uniformly in the sphere, and the total excitation energy is assumed to be uniformly distributed over the whole excited system of the spectators, what is equivalent to assumption that equilibrium is reached. In this picture, the angular distribution of fragments should be forward peaked, because the momentum transfer from incident proton to the nucleus is in average in forward direction. In reality, as the incident energy increases, the mass fragments angular distribution grows from forward to sideward ($E_p \geq 10$ GeV) [33] or backward ($E_p \geq 100$ GeV) [34] peaked in laboratory frame, what contradicts to the picture of the fragmentation from an equilibrated system, and indicates that the nucleons may not be uniformly distributed spatially and the excitation may depend on the position inside the nucleus.

For the understanding of this sideward emission (for which not satisfactory explanation has been given so far) Hirata et al. [35] investigated the non-equilibrium dynamical effects, such as non-spherical nuclear formation. They formulated Non-Equilibrium Percolation (NEP) model, which they use in a combined framework with a transport model [35]. The main differences between equilibrium percolation and the NEP model are following. The initial conditions of percolation, instead of putting nucleons on sites with some assumed occupation probability, is taken from the results of the dynamical transport model calculations. The bond breaking probability is assumed to be dependent on the position and momenta of the nucleons. It is calculated by considering excitation energy, distance and momentum difference between the nucleon pairs, instead of giving a common breaking probability for the bonds connecting nearest neighbor sites.

Analysing fragmentation process with the NEP model, considering calculated effects, Hirata et al. have found following mechanism of sideward enhanced fragments emission. Based on fragments formation point distributions, both in case of central and peripheral collisions, the fragments are formed mainly near the surface of the nuclei. It is due to fact, that along the

incident proton path, nucleons collide with the leading proton or secondary cascade particles. Since they have large kinetic energies, they increase the bond breaking probability. As a result the fragment formation is suppressed along the incident proton path. Fragments are formed mainly in the cold region around the hot zone. Their formation points are distributed non-spherically, in a doughnut shaped region. Hirata et al. noticed that this effect alone does not generate any anisotropy in angular distributions.

Based on analysis of fragments energy distributions, they found that the energy distribution is effected by Coulomb repulsion. Calculated results after the Coulomb expansion well reproduce the qualitative behavior of experimental data [35]. This is Coulomb repulsion between formed fragments that pushes and accelerates them sideways of the doughnut region. It means, the Coulomb repulsion modifyies the angular distribution from forward peaked to sideward peaked.

Bond percolation model with non-equilibrium effects, have been investigated also by Yamaguchi and Ohnishi [36]. They introduced to the model isospin dependence, by assuming that neutron-neutron and proton-proton bonds are always broken, while neutron-proton bonds make the nucleus bound. Additionally, by comparing calculated fragments energy spectra with experimental data, they have got an agreement, when taken density of fragmenting nuclei is not equal the normal nuclear density ρ_0, but of around $\sim \rho_0/3$. It means, target nucleus, after being heated by incident proton, would expand up to rather low, mechanically unstable density.

They have also considered, that the incident proton heats up either cylindrical or conic shaped region around its path in the target. They have found, that in case of cylindrical heated region, formed fragments are pushed, by Coulomb repulsion, more strongly in sideward directions. If a conic shaped region is heated up, fragments are pushed in rather backward directions.

Chapter 3

Specific models for fast stage of proton-nucleus collision

In the frame of this work, dynamical analysis of fast stage of proton - nucleus reactions are performed within transport approaches: Boltzmann-Uehling-Uhlenbeck (BUU) [18, 37] and Hadron String Dynamics (HSD) [38, 39] models. The models have been specially developed in order to enable description of considered here reactions.

The BUU model is used to calculate proton - nucleus reactions in projectile kinetic energy range only up to about 2.5 GeV. That is because included in the model processes go mainly through single resonances excitations (i.e. Δ, $N(1440)$, $N(1535)$), what is correct in this energy range. While an incident energy increases, the density of produced resonances also increases. In this case, a possible proper description of processes requires taking into consideration hadron - hadron reactions on the level of elementary quark - quark interactions. This can be done by employment of a string model (e.g. FRITIOF model [40]), where during inelastic collision, two interacting hadrons are excited due to longitudinal energy-momentum transfer [40]. The formed excitation, so-called string, represents a prehadronic stage. It is characterized by the incoming quarks and a tubelike colour force field [41] spanned in between. The string is then allowed to decay into final state hadrons, with conservation of the four-momentum, according to e.g. Lund string fragmentation model [42].
The HSD approach includes the FRITIOF scheme of string dynamics and the Lund model of hadron production through string fragmentation. It is employed, in particular, for incident energies higher than projectile energy 2.5 GeV. For projectile energies lower than about 2.5 GeV, the BUU code is used in the frame of the HSD model.

Below, a description of the approaches is given.

Both the models are based on transport equation.

3.1   Transport equation

Historically, the transport equation originate from classical Boltzmann equation for one-body phase-space distribution function $f(\vec{r}, \vec{v}, t)$ defined such that
$\int f(\vec{r}, \vec{v}, t)\, d^3v\, d^3r$ is the number of particles at time t positioned in element volume d^3r around $\vec{r}$, which have velocities in volume element of velocity space d^3v around $\vec{v}$.
Let's consider particles, in which an external force F with mass m acts and assume initially that no collisions take place between the particles. In time $t + \delta t$ the velocity $\vec{v}$ of each particle will change to $\vec{v} + (\frac{\vec{F}}{m})\delta t$ and its position $\vec{r}$ will change to $\vec{r} + \vec{v}\delta t$. Thus the number of particles $f(\vec{r}, \vec{v}, t)\, d^3v\, d^3r$ is equal to the number of particles $f(\vec{r} + \vec{v}\delta t\,,\ \vec{v} + (\frac{\vec{F}}{m})\delta t\,,\ t + \delta t)\, d^3r' d^3v'$, what is explained by the Liouville theorem:

> *The volume of phase-space element is constant, if movement of all particles inside is consistent with canonical Hamilton equation of motion.*

and written as:

$$f(\vec{r} + \vec{v}\delta t\,,\ \vec{v} + (\frac{\vec{F}}{m})\delta t\,,\ t + \delta t) - f(\vec{r}, \vec{v}, t) = 0 \qquad (3.1)$$

If collisions occur between the particles, an additional element, i.e. collision term is needed. This gives the following equation describing evolution of the distribution function:

$$f(\vec{r} + \vec{v}\delta t\,,\ \vec{v} + (\frac{\vec{F}}{m})\delta t\,,\ t + \delta t) - f(\vec{r}, \vec{v}, t) = (\partial f/\partial t)_{coll}\delta t \qquad (3.2)$$

Letting $\delta t \to 0$ and expanding into the Taylor series gives the Boltzmann equation:

$$((\partial/\partial t) + \nabla_r \cdot \vec{v} + (\frac{\vec{F}}{m})\nabla_V)f(\vec{r}, \vec{v}, t) = (\partial f/\partial t)_{coll} \qquad (3.3)$$

An apparent form of the collision term $(\partial f/\partial t)_{coll}$ can be found considering an element volume A at time t, around position $(\vec{r}, \vec{v})$ and an element volume

B at time $t + \delta t$, around position $(\vec{r} + \vec{v}\delta t, \vec{v} + (\frac{\vec{F}}{m})\delta t)$. These two element volumes are so similar, that letting $\delta t \to 0$, particles knocked out from A, due to collisions, will not get into B. Particles being outside A, during time δt, will get into A, and they will be inside B. So, the number of particles inside B, at time $t + \delta t$, at $\delta t \to 0$, is equal to the initial number of particles inside A, at time t, and a magnitude of relative modification of number of particles due to collisions, during time δt. Therefore, a form of the collision term $(\partial f / \partial t)_{coll}$ can be calculated as a difference between the number of collision in a time range $(t, t + \delta t)$, when one of particles *after* collision is situated in element volume $d^3r \, d^3v$ around position $(\vec{r}, \vec{v})$, and the number of collision in a time range $(t, t + \delta t)$, when one of particles *before* collision is situated in the same element volume $d^3r \, d^3v$ around position $(\vec{r}, \vec{v})$. It can be done by assuming that the density of particles is low enough, that only binary collisions need be considered. It is also assumed that the velocity of particle is uncorrelated with its position in the space. It means that in element volume d^3r the number of particles pairs with velocities in volume elements of velocity space d^3v_1 around v_1 and d^3v_2 around v_2 is equal to:
$[f(\vec{r}, \vec{v_1}, t) \, d^3r \, d^3v_1][f(\vec{r}, \vec{v_2}, t) \, d^3r \, d^3v_2]$.

The number of binary collisions $(\vec{v_1}, \vec{v_2} \to \vec{v_3}, \vec{v_4})$ inside element d^3r, in time range $(t, t + \delta t)$ is equal to: $[f(\vec{r}, \vec{v_2}, t)d^3v_2]|\vec{v_1} - \vec{v_2}|\sigma(\Omega)d\Omega\delta t$,
where:
$\vec{v_1}$ and $\vec{v_2}$ are the velocities of the two particles before collision,
$\vec{v_3}$ and $\vec{v_4}$ are their velocities after the collision,
$\sigma(\Omega)$ is the differential cross section for a reaction, in the centre of mass reference frame,
Ω is the solid angle the particles are scattered into (the angle between vectors $\vec{v_1} - \vec{v_2}$ i $\vec{v_3} - \vec{v_4}$),
$|\vec{v_1} - \vec{v_2}|$ is the magnitude of the particles relative velocity before the collision,
$[f(\vec{r}, \vec{v_2}, t)d^3v_2]|\vec{v_1} - \vec{v_2}|$ is the density of particles flux equal to the product of particles density and their velocity.
The total number of collisions, where one of the particle *before* collision is situated inside element $d^3r \, d^3v_1$ around $(\vec{r}, \vec{v_1})$ is obtained multiplying the number of binary collisions by number of particles with velocity $\vec{v_1}$, inside element d^3r and integrating over all possible $\vec{v_2}$ and Ω:

$$\int d^3v_2 \int d\Omega \sigma(\Omega) f(\vec{r}, \vec{v_2}, t)|\vec{v_1} - \vec{v_2}|[f(\vec{r}, \vec{v_1}, t)d^3r \, d^3v_1]\delta t \qquad (3.4)$$

Taking into consideration the inverse binary collision: $(\vec{v_3}, \vec{v_4} \to \vec{v_1}, \vec{v_2})$, and using analogical method as above, the total number of collisions, where one of the particle *after* collision is situated inside element $d^3r \, d^3v_1$ around $(\vec{r}, \vec{v_1})$

is obtain:

$$\int d^3v_4 \int d\Omega \sigma'(\Omega) f(\vec{r}, \vec{v_4}, t) |\vec{v_3} - \vec{v_4}| [f(\vec{r}, \vec{v_3}, t) d^3r \, d^3v_3] \delta t \qquad (3.5)$$

Because collisions $\vec{v_1}, \vec{v_2} \to \vec{v_3}, \vec{v_4}$ and $\vec{v_3}, \vec{v_4} \to \vec{v_1}, \vec{v_2}$ are inverse collisions, so: $\sigma(\Omega) = \sigma'(\Omega)$.
From covservarion law for energy and momentum: $|\vec{v_1} - \vec{v_2}| = |\vec{v_3} - \vec{v_4}|$.
From Liouville theorem: $d^3v_1 d^3v_2 = d^3v_3 d^3v_4$. Subtracting equations (3.5) and (3.4), and using above assumptions the collision term can be written as:

$$(\partial f/\partial t)_{coll} = \int d^3v_2 d^3v_3 \sigma(\Omega) d\Omega |\vec{v_1} - \vec{v_2}| (f_3 f_4 - f_1 f_2) \qquad (3.6)$$

where: $f_1 \equiv f(\vec{r}, \vec{v_1}, t)$, $f_2 \equiv f(\vec{r}, \vec{v_2}, t)$, $f_3 \equiv f(\vec{r}, \vec{v_3}, t)$, $f_4 \equiv f(\vec{r}, \vec{v_4}, t)$.

   Joining equations (3.3) and (3.6) one obtains the classical Boltzmann equation:

$$\{\frac{\partial}{\partial t} + (\frac{\vec{p_1}}{m_1} + \frac{\partial U(\vec{r}, \vec{p_1}, t)}{\partial \vec{p_1}}) \frac{\partial}{\partial \vec{r}} - \frac{\partial U(\vec{r}, \vec{p_1}, t)}{\partial \vec{r}} \frac{\partial}{\partial \vec{p_1}}\} f(\vec{r}, \vec{p_1}, t) =$$

$$\frac{4}{(2\pi)^3} \int d^3p_2 \, d^3p_3 \, d\Omega \, \sigma(\Omega) |\vec{v_1} - \vec{v_2}| \, \delta^3(\vec{p_1} + \vec{p_2} - \vec{p_3} - \vec{p_4}) \cdot [f_3 f_4 - f_1 f_2] (3.7)$$

where:
$\vec{v} = \vec{p}/m$,
$\vec{F} = -(\partial U(\vec{r})/\partial \vec{r})$, $U(\vec{r})$ is position dependent potential.

   In 1933 Uehling and Uhlenbeck have developed the equation by adding the Pauli factors [43].
Due to Pauli blocking, a collision can occur only if in the final state, there are free quantum states.
Probability of finding the free quantum state in a phase-space volume is equal to: $[1 - f(\vec{r}, \vec{p}, t)]$, what is responsible for fermion Pauli blocking.
The probability of two particles collision with momenta $\vec{p_1}$ and $\vec{p_2}$ is equal to:

$$[1 - f(\vec{r}, \vec{p_3}, t)][1 - f(\vec{r}, \vec{p_4}, t)] \equiv \overline{f}_3 \overline{f}_4 \qquad (3.8)$$

Probability of inverse occurrence is equal to:

$$[1 - f(\vec{r}, \vec{p_1}, t)][1 - f(\vec{r}, \vec{p_2}, t)] \equiv \overline{f}_1 \overline{f}_2 \qquad (3.9)$$

Expression (3.8) and (3.9) are Pauli factors.

Including in (3.7) the Pauli factors gives:

$$\{\frac{\partial}{\partial t} + (\frac{\vec{p_1}}{m_1} + \frac{\partial U(\vec{r}, \vec{p_1}, t)}{\partial \vec{p_1}})\frac{\partial}{\partial \vec{r}} - \frac{\partial U(\vec{r}, \vec{p_1}, t)}{\partial \vec{r}}\frac{\partial}{\partial \vec{p_1}}\}f(\vec{r}, \vec{p_1}, t) =$$

$$\frac{4}{(2\pi)^3}\int d^3p_2\, d^3p_3\, d\Omega\, \sigma(\Omega)|\vec{v_1} - \vec{v_2}|\, \delta^3(\vec{p_1} + \vec{p_2} - \vec{p_3} - \vec{p_4})$$

$$\cdot[f_3 f_4 \overline{f}_1 \overline{f}_2 - f_1 f_2 \overline{f}_3 \overline{f}_4] \quad (3.10)$$

The equation is named Boltzmann-Uehling-Uhlenbeck (BUU) equation.

3.2   Boltzmann-Uehling-Uhlenbeck model

The theory based on the transport equation (3.10) (it means the Boltzmann equation with a self-consistent potential field, and with a collision term that respects the Pauli principle) was used first time to nuclear collisions description by Bertsch, in 1984 [44].
The BUU equation is solved numericaly, using Monte Carlo method, representing the one-body phase-space distribution by discretized test particles:

$$f(\vec{r}, \vec{p}, t) = \frac{1}{N}\sum_{i=1}^{N \cdot A(t)} \delta^3(\vec{r} - \vec{r_i}(t))\, \delta^3(\vec{p} - \vec{p_i}(t)) \quad (3.11)$$

where:
N is a number of test particles,
$A(t)$ is a number of real particles at time t

Likewise, one collision is replaced by parallel collisions.

All of the test particles give part to the density of nuclear matter not in single points, but they are smeared with Gauss distribution. This way, the effect of quantum smearing is included.
The density is calculated on the grid r_g:

$$\rho(\vec{r_g}) = \frac{1}{N}\sum_{i=1}^{NA}\frac{1}{(2\pi\Delta^2)^{3/2}}exp(\frac{-(\vec{r_g} - \vec{r_i})^2}{2\Delta^2}) \quad (3.12)$$

where: Δ is the Gauss width parameter (taken usually equal 1).

The initial coordinates of particles of target nucleus have Wood-Saxon distribution form:

$$\rho(r) = \frac{\rho_0}{1 + exp(\frac{r - R}{a})} \quad (3.13)$$

where:
$a = 0.025 \cdot A^{1/3} + 0.29 \ [fm] = 0.5 \ [fm]$
$R = 1.124 \cdot A^{1/3} \ [fm]$
$\rho_0 = 0.168 \ [nukleon/fm^3]$.

Initially, the target nucleus is in the rest, the total momentum (i.e. the sum of momenta of all particles) is equal to 0, but the local momenta of particles are determined homogeneously on the Fermi sphere with radius $p_F(r)$:

$$p_F(r) = (\frac{3\pi^2}{2}\rho(r))^{1/3} \tag{3.14}$$

The projectile is a single proton. The test particles replacing the proton are distributed homogeneously on a thin cylinder, with a radius equal the radius of target. Thanks to this approach, each test particle has different impact parameter, so the results of calculations are averaged over all impact parameters.

The solution of the transport equation is the single-particle phase-space distribution function, depending on time.

The collision is numericaly evolved by fixed time steps.

The test particles propagate between collisions according to the classical Hamilton equations of motion:

$$\dot{\vec{p}}_i = -\frac{\partial U(\vec{r}_i, \vec{p}_i, t)}{\partial \vec{r}_i} \tag{3.15}$$

$$\dot{\vec{r}}_i = \vec{p}_i/\sqrt{m^2 + p^2} + \frac{\partial U(\vec{r}_i, \vec{p}_i, t)}{\partial \vec{p}_i} \tag{3.16}$$

where: $U(\vec{r}_i, \vec{p}_i, t)$ is a mean field potential, dynamically changing, calculated as a function of local density:

$$U(\vec{r}) = \frac{3}{4}t_0\rho(\vec{r}) + \frac{7}{8}t_3\rho(\vec{r})^{4/3} + V_0 \int d^3\vec{r'}\frac{exp(-\mu|\vec{r} - \vec{r'}|)}{\mu|\vec{r} - \vec{r'}|}\rho(\vec{r'}) + V_{Coul} \tag{3.17}$$

where: t_0=-1124 MeV·fm³, t_3=2037 MeV·fm⁴, V_0=-378 MeV, μ=2.175 fm⁻¹, see Ref. [18].

The momentum and coordinates of all particles taking part in reaction are calculated in the successive time steps. Using the values of momentum and coordinates, all other quantities (i.e. nucleon density, mean field potential) are calculated.

The nucleon - nucleon collision at a fixed time step is introduced as follows: when two nucleons come closer than the distance $b_{max} = \sqrt{\sigma_{NN}^{max}/\pi}$ (where σ_{NN}^{max} is the maximal cross section for nucleon - nucleon interaction in nuclear matter (30 mb [18])) they are made to scatter, but if the final state is Pauli blocked, this collision is canceled.

The BUU model describes the propagation and mutual interaction of nucleons, Delta's, N^* - resonances, and also π and η - mesons.
In the model, the following reaction channels are included:
$NN \leftrightarrow NN$,
$NN \leftrightarrow NR$,
$NR \leftrightarrow NR$,
$\Delta\Delta \leftrightarrow NR$,
$R \leftrightarrow N\pi$,
$N(1535) \leftrightarrow N\eta$,
$NN \leftrightarrow NN\pi$,
$\pi N \to \pi N$,
$\pi N \to \pi\pi N$,
where: N is a nucleon, R stands for a resonance Δ, $N(1440)$ or $N(1535)$.
Cross sections for the reactions, used in the model calculations, are parametrizations of the experimental cross sections taken from [45].

All resonances are allowed to decay into two particles (besides the decays due to collisions with other particles, e.g. $NR \to NN$). The decay of a resonance is determined by its width $\Gamma(M)$. The decay probability P is calculated in every step of time, according to the exponential decay law: $P = 1 - e^{-\Gamma(M)/(\hbar\gamma)\delta t}$, where: $\Gamma(M)$ is the energy dependent width of the resonance, γ is a Lorentz factor related to the velocity of the resonance, δt is a time step size of the calculations.
For the Δ decay the parametrization given by Koch et al. [46] is used. Details concerning higher resonances can be found in [47].
In each step of time it is decided if the resonance may decay and to which final state it may go. If the final state is Pauli blocked, the resonance decay is rejected.

3.3 Hadron String Dynamics model

The HSD model is based on the same transport equation (3.10) as the BUU approach and solved also by use of the test particle method.
In the HSD model, propagation of the following real particles are included:

baryons (p, n, Δ, $N(1440)$, $N(1535)$, Λ, Σ, Σ^*, Ξ, Ω), the corresponding antibaryons and mesons (π, K, η, η', ρ, ω, ϕ, K^*, a_1).

3.3.1   Cross sections

The **low-energy baryon-baryon** and **meson-baryon** collisions (i.e. with the invariant energies below "string threshold": $\sqrt{s} < 2.65$ GeV and $\sqrt{s} < 2.1$ GeV [39], respectively) are described using the explicit cross section, as in the BUU code. The following parametrization of the experimental total and elastic $p + p$, $p + n$, $\pi^+ p$, $\pi^- p$, $K^+ p$, $K^- p$ cross sections, taken from [45], is used:

$$\sigma(p) = A + B \cdot p^n + C \cdot ln^2(p) + D \cdot ln(p) [mb], \qquad (3.18)$$

where: p is a momentum of incident proton in laboratory frame,
A, B, n, C, D are constants, with adequate values for different processes cross sections, see Ref. [48].
For reaction channels: $\pi N \to \pi N$ and $\pi N \to \pi \pi N$, to have them consistent with the experimental inelastic pion-proton cross section below the string threshold, instead of (3.18), the following parametrization is used [48]:

$$\begin{aligned} \sigma_{tot}(p_\pi) &= 25.0 + 16.0 \cdot p_\pi^{-1.4} [mb], \\ \sigma_{el}(p_\pi) &= 3.5 + 14.0 \cdot p_\pi^{-1.1} [mb], \end{aligned} \qquad (3.19)$$

where: p_π is a momentum of incident pion (in GeV/c).
Additionally, the channels:
$\rho N \to N \pi \pi$, $\rho \Delta \to N \pi \pi$ and
$\omega N \to N \pi \pi \pi$, $\omega \Delta \to N \pi \pi \pi$,
are included with an energy independent cross section equals to 30 mb.
Because of very low number of produced hyperons in low-energy proton-nucleus collisions, the hyperon(Λ, Σ) - nucleon interactions are neglected in the model.

Angular distribution of elastic collisions depends on energy [48], therefore the following parametrization of the **differential elastic nucleon - nucleon cross section**, taken from Cugnon et al. [26], is applied:

$$\frac{d\sigma}{d\Omega} = e^{A(s)t}, \qquad (3.20)$$

where: s is the invariant energy of collision squared (in GeV),
t is the four-momentum transfer squared,
$A(s) = 6 \frac{[3.65(\sqrt{s} - 1.8776)]^6}{1 + [3.65(\sqrt{s} - 1.8776)]^6}$.

In the approach, the **high-energy elastic** and **total baryon - baryon** and **meson - baryon** collisions (i.e. with energies above the "string threshold"), are related to the measured cross sections by:

$\sigma_{el}^{N\Delta}(\sqrt{s}) = 0.5(\sigma_{el}^{pp}(\sqrt{s}) + \sigma_{el}^{pn}(\sqrt{s}))$,

$\sigma_{el}^{\rho N}(\sqrt{s}) = \sigma_{el}^{\rho\Delta}(\sqrt{s}) = \sigma_{el}^{\omega\Delta}(\sqrt{s}) = ... = 0.5(\sigma_{el}^{\pi^+ N}(\sqrt{s}) + \sigma_{el}^{\pi^- N}(\sqrt{s}))$,

$\sigma_{el}^{KN}(\sqrt{s}) = \sigma_{el}^{K\Delta}(\sqrt{s}) = ... = \sigma_{el}^{K^+ p}(\sqrt{s})$,

$\sigma_{el}^{\overline{K}N}(\sqrt{s}) = \sigma_{el}^{\overline{K}\Delta}(\sqrt{s}) = ... = \sigma_{el}^{K^- p}(\sqrt{s})$,

where dots stand for other combination in the incoming channel, with $K = (K^+, K^0, K^{*+}, K^{*0})$ and $\overline{K} = (K^-, \overline{K}^0, K^{*-}, \overline{K}^{*0})$. The same relations are applied for the total cross sections.

The **high-energy inelastic baryon - baryon** and **meson - baryon** cross sections obtained by this procedure are equal to 30 mb and 20 mb, respectively. This corresponds to the typical geometrical cross section (i.e. $\sigma_{inel} \approx \pi R^2$), so it should be reasonable input for the calculations.

Due to this fact, in order to include all baryon - baryon and meson - baryon high-energy inelastic cross sections, only final state rates must be specified. Therefore, the string model (i.e. FRITIOF model) is employed, which will be described hereafter in this work.

In the HSD model, the following **meson - meson** reaction channels are included:

$\pi\pi \leftrightarrow \rho$,

$\pi\rho \leftrightarrow \phi$,

$\pi\rho \leftrightarrow a_1$,

$K\overline{K} \leftrightarrow \phi$,

$\pi K \leftrightarrow K^*$.

They are more probable at high-energy proton - nucleus collisions, but as they appear as secondary or higher order reactions, the average energy for such processes is rather low. In this case, the cross section within the Breit-Wigner parametrization is employed. Therefore, the reactions $a + b \rightarrow m_R \rightarrow c + d$, where: a, b, c, d are the mesons in the initial and final state, respectively, and m_R denotes the intermediate mesonic resonance (ρ, a_1, ϕ, K^*), are described by:

$$\sigma(ab \rightarrow cd) = \frac{2J_R + 1}{(2S_a + 1)(2S_b + 1)} \frac{4\pi}{p_i^2} \frac{s\Gamma_{R\rightarrow ab}\Gamma_{R\rightarrow cd}}{(s - M_R^2)^2 + s\Gamma_{tot}^2}, \qquad (3.21)$$

where:

S_a and S_b are spins of the particles, J_R is spin of resonance;

$\Gamma_{R\rightarrow ab}$ and $\Gamma_{R\rightarrow cd}$ are partial decay widths in the initial and final channels, M_R is the mass of the resonance, Γ_{tot} is the total resonance width,

p_i is the initial momentum in the resonance rest frame.

The decay widths and the branching ratios for the mesonic channels are adopted from the nuclear data tables [45], without introducing new parameters.

Additionally, strangeness production in meson - meson collisions is included, with an isospin averaged cross section [49]:

$$\sigma_{mm \to K\overline{K}}(s) = 2.7(1 - \frac{s_0}{s})^{0.76}[mb], \tag{3.22}$$

where: $s_0 = 4m_K^2$, mm stands for all possible non-strange mesons in the incoming channel (e.g. $\pi\pi \to K\overline{K}$, $\pi\rho \to K\overline{K}$).

3.3.2   String Model

Quarks, as colour-charged particles cannot be found individually. They are confined in two- or three-quarks systems, i.e. colour neutral hadrons. The quarks, in a given hadron, exchange gluons. If one of the quarks is pulled away from the other quarks in the hadron, the colour force field, which consists of gluons holding the quarks together, stretches between this quark and its neighbers. Because of interaction between gluons [41], the colour field lines are not spread out over all space, as the electromagnetic field lines do, but they are constrained to a thin tube-like region. While the quarks are pulled apart, more and more energy is added to the colour force field. So, in such a formation, the four-momentum can be accumulated. At some point, it is energetically possible for the field to break into new quarks. The four-momentum is conserved, because the energy of the colour force field is converted into the mass of the new quarks. Finally, the colour force field comes back to an unstretched state.

With this picture in mind, high-energy hadron - hadron interactions models, called string models [39] have been created, where the formation composed of quarks and the colour field between is called a string.

In the HSD approach, in order to describe the high-energy inelastic hadron - hadron collisions, FRITIOF model is applied [40]. In the model, hadronic collision corresponds to large longitudinal and small transversal energy - momentum transfer. It means, to the stretching of longitudinally extended string-like colour force field along the beam direction, between constituent quarks of the incoming hadron. The created excitation, i.e. string is a dynamical object, which may decay into final state hadrons, according to the Lund fragmentation scheme [42], implemented in the FRITIOF model. The field between quarks is confined into a tube, called "flux tube", which is

one-dimensional object. The uniform colour field contains constant amount
of energy stored per unit length. The total energy (E) of the field is pro-
portional to the length (L): $E = \kappa \cdot L$, where $\kappa \cong 1$ GeV/fm, is a string
tension [42]. Due to longitudinal energy-momentum transfer, spread over
some region, the colour separation occurs, i.e. as seen in CM string frame,
there will be two extended parts of the string moving forward and backward,
along the beam direction. The potential between quarks is linearly rising.
As result, the system breaks. Because of colour confinement there is never
a single quark in isolation. After the string breaks, on its ends new quarks
appear. The new $q\bar{q}$ pair is created from the available field energy. By that
means, the energy of the initial string decrease (a part of the energy is used
for $q\bar{q}$ pair production), but the breaking process is not finished yet. The
quarks of the new created strings are also moving in opposite directions in
the strings rest frames. Thereby the original system breaks into smaller and
smaller pieces, until only physical hadrons remain, (i.e. baryons as bound
systems of three quarks, antibaryons - three antiquarks and mesons as quark
- antiquark systems).
In the HSD approach, baryonic ($qq - q$) and mesonic ($q - \bar{q}$) strings are con-
sidered.
The implementation of the string model into the transport approach implies
introduction of a time scale for the particle production processes. The time
scale is given by a formation time t_f, which includes formation of a string,
fragmentation of the string into small substrings due to $q\bar{q}$ and $qq\bar{q}\bar{q}$ pro-
duction, and formation of physical hadrons. The formation time should be
also related to the spatial extension of the interacting hadrons. It means, it
should be big enough so that quark - antiquark pair could reach a distance
corresponding to a typical hadron radius, i.e. 0.6 - 0.8 fm [48]. In the HSD
model, the formation time is a single fixed parameter for all hadrons, it is
set to $t_f = 0.8$ fm/c in the rest frame of the new produced particles [50].
The particles production proceeds as follows.
If a system contains originally e.g. $\bar{q}_0$ and q_0, moving in opposite directions
with large energies, it breaks after some time into two parts by a production
of a pair $q_1 \bar{q}_1$, at a space-time point (x_1, t_1). The new produced quarks also
move in opposite directions. Two subsystems are created by $\bar{q}_0 q_1$ and $\bar{q}_1 q_0$.
As a result, a colour force field between the new pair $q_1 \bar{q}_1$ vanishes. At a
later time another pair $q_2 \bar{q}_2$ can be produced at (x_2, t_2), due to breaking e.g.
$\bar{q}_1 q_0$ subsystem. Analogically, new subsystems $\bar{q}_1 q_2$ and $\bar{q}_2 q_0$ are created.
A colour force field between the new quark pair $q_2 \bar{q}_2$ vanishes. Created sub-
systems either are hadrons or else will fragment further, until only hadrons
remain. In the model, string fragmentation starts always in its center (in the
CM frame of the string). All quark pairs production points are separated

in a space-time. A total momentum in the rest frame of a string is equal to zero. The energy and momentum in the production process is conserved. Masses of the finally produced hadrons are equal to the masses of physical hadrons.

In the HSD model, the production probability (P) of massive $s\bar{s}$ or $qq\overline{qq}$ pairs is supressed in comparison to light quarks pairs production ($u\bar{u}$, $d\bar{d}$). Inserting the following constituent quark masses: $m_u = m_d = 0.3$ GeV and $m_s = 0.5$ GeV, one gets: $\frac{P(s\bar{s})}{P(u\bar{u})} = 0.3$ and $\frac{P(qq\overline{qq})}{P(u\bar{u})} = 0.07$.

So, the suppression factors used in the model are:

$u : d : s : uu = 1 : 1 : 0.3 : 0.07$, see Ref. [48].

As a result, mainly mesons are produced.

The model assumes that there is no final state interaction of the produced hadrons included in the model.

Because most of the strings, in a given space-time volume, fragment within a small time interval, the interaction of the string field spanned between the constituent quarks with other hadrons is not taken into account. But the secondary interactions of the quarks or diquarks inside the strings are considered in the approach. The following cross sections of such interactions are used [48]:

$\sigma(q - B) = \frac{1}{3}\sigma(B - B) \approx 10$ mb,

$\sigma(qq - B) = \frac{2}{3}\sigma(B - B) \approx 20$ mb,

$\sigma(qq - q) = \frac{2}{9}\sigma(B - B) \approx 6.6$ mb.

Because most of strings are stretched longitudinally, parallelly to each other, and radius of string is small, equal to about 0.2 - 0.3 fm [51], there is no string - string interaction included in the HSD model.

The characterized above version of the HSD code has been used and developed in order to describe proton induced spallation reactions in wide energy range, and mass of target nuclei in the following aspects. First of all, to calculate properties of residual nuclei remaining after first stage of the reaction, forming an input for models of the second stage calculations.

Additionally, the code has been developed for description of pions produced in proton - nucleus spallation reactions. Moreover, a version of HSD code that allows for calculations of pion induced reactions has been prepared.

Each of the directions of the HSD code development will be presented and discussed in the next sections of this work.

3.4 Further development of the model

As a result of the first stage of proton - nucleus reaction, apart from emitted particles (mainly nucleons and pions), a hot excited nucleus remained. Properties of the residual nucleus, i.e. mass (A_R), charge (Z_R), excitation energy (E_R^*), three - momentum ($\vec{p_R}$) and angular momentum (L_R) form an input for the second stage models. In order to calculate the properties, the original version of the HSD code has been modified. Corrections ensuring energy and charge conservations have been made, which are important here, but played minor role in the original version. Also, corrections enabling calculations of various quantities in function of time, for very large times of propagation have been found.

The properties are evaluated in the following way.

First, using that in the models calculations, four-momenta of all hadrons are propagated in time, the particles that have left the residual heavy fragment are identified. This can be done in two ways. In case of low-energy collisions, a sphere of observation, with radius equal to $R_A + 2$ fm, where: R_A denotes the radius of the target with mass number A, can be considered. All the particles inside the sphere are treated as belonging to residual nucleus, the particles outside - as emitted. In case of high-energy collisions, when target nucleus is moving faster during reaction, it is easier to consider a baryon density criterion. It means, particles, which are positioned in baryon density lower than 0.02 nucleon/fm^3 are treated as emitted, the rest of the particles form a residual nucleus. At intermediate proton impact energy (0.1 - 2.0 GeV) both methods are equivalent. In the frame of this work, the second criterion is used. Nevertheless, both of the methods of classification are connected with some inaccuracy, concerning the very low energetical particles. Distributions of particles escaped from the sphere of observation characterize absence of very low energetical part. In contrary, distributions of particles classified on the base of the baryon density criterion characterize overabundance in the very low energetical part. In this second case, it is because the density condition classifies incorrectly nucleons placed in the lowest density level of a residual nucleus, as emitted. Therefore, the density method needs to be completed by an additional condition concerning the particles kinetic energy. Particles in the nucleon density equal to 0.02 nucleon/fm^3 acquire momentum with a value from the range from zero to the local Fermi momentum, equal to about 130 MeV/c, what corresponds to about 10 MeV of kinetic energy. Compliance of that information gives a complete and correct condition, i.e. particles in nuclear density lower than 0.02 nucleon/fm^3 and with kinetic energy higher than 10 MeV are considered as emitted.

Then, by exploring the conservation of total energy, mass number, momen-

tum and angular momentum, for each parallel ensemble (see description of models), the average values of properties of the residual nuclei are calculated as function of time, according to formulas:

$$< E_R^* > (t) = E_{tot} - \sum_{i=1}^{N_p(t)} \sqrt{p_i^2 + m_i^2} - M_R - E_C,$$

$$< A_R > (t) = A_T + A_P - N_p(t),$$

$$< \vec{p_R} > (t) = \vec{p_{tot}} - \sum_{i=1}^{N_p(t)} \vec{p_i}(t),$$

$$< L > (t) = L_{tot} - \sum_{i=1}^{N_p(t)} \vec{r_i}(t) \times \vec{p_i}(t), \qquad (3.23)$$

where: $N_p(t)$ denotes the number of emitted particles, M_R is the mass of the residual nucleus, A_T is a mass of original target, $A_P = 1$ stands for incoming proton and E_C is the the energy of Coulomb interaction between the emitted particles and the residual nucleus.

3.5 Stopping time criteria for the first stage model calculations

In order to describe both stages of the reaction, model of the first stage must be used together with a statistical model for the second stage of reaction. The outcome of the transport model calculations determines an input for the second stage model. Thus, it is important to assume a proper duration time of the first stage calculations. In order to define the time at which the first stage calculations should be stopped, it must be verified, whether informations obtained from the transport models are sensitive to the time duration of the first stage of the reaction. For this purpose, time variation of the average values of four physical quantities: excitation energy per nucleon, momentum in beam direction per nucleon, angular momentum and mass number of the excited residual nucleus after the first stage, have been analysed. As example, the dependences for p + Bi collision, at 3.0 GeV proton beam energy are discussed below. The average values of presented quantities are evaluated according to the equations (3.23).
First, let's look at the time evolution of the average value of excitation energy per nucleon of the residual nucleus shown in Fig. 3.1. It is evident from the Figure, that it takes some time before proton approaches nucleus, i.e. about 10 fm/c (at the time _zero_, projectile is placed in some distance from

the target nucleus, ensuring that density distributions of projectile and target are not overlapping). Next, up to about 18 fm/c, the excitation energy gains some maximal value, which corresponds to the energy introduced into target nucleus by incoming proton. Then, the excitation energy drops very quickly in the range 20 - 30 fm/c of the duration time of the first stage of the reaction, whereas it is varying only a little at larger times. It is seen that the average value of excitation energy per nucleon starts to stabilize at time 35 - 40 fm/c.

Looking at Fig. 3.2, it is seen, that the average value of the momentum of
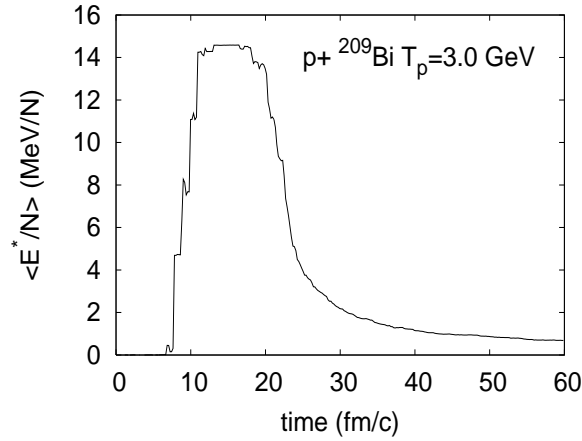
Figure 3.1: *Time variation of the average value of excitation energy per nucleon of the residual nucleus in p + Bi collision, at 3 GeV proton beam energy; results of the HSD model calculations*

the nucleus in the beam direction behaves very similar during first stage of the reaction as the average value of excitation energy. Starting from about 10 fm/c, when proton reaches target nucleus, up to about 18 fm/c, the longitudinal momentum per nucleon of the residual nucleus has a maximal value, adequate to the value of momentum introduced into target nucleus by incoming proton. Then, the average value drops quickly in the range 20 - 30 fm/c of the duration time of the first stage of the reaction, because the momentum is carried out by nucleons escaping from the nucleus. At larger times the value varies only a little.

Very similar behavior is observed for the average value of angular momentum of the residual nucleus during first stage of the reaction, presented in Fig. 3.3. At about 10 fm/c, incoming proton, having in average a non zero impact parameter, introduces some angular momentum into the nucleus. At around
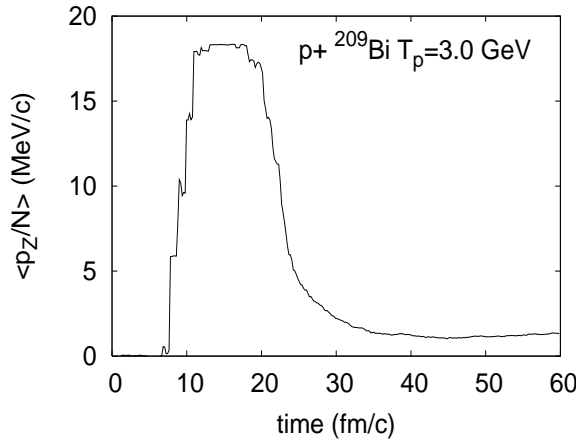
Figure 3.2: *Time variation of the average value of longitudinal momentum per nucleon of the residual nucleus in p + Bi collision, at 3 GeV proton beam energy; results of the HSD model calculations*
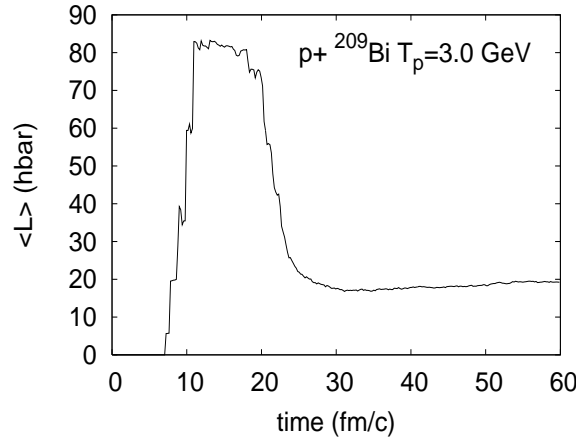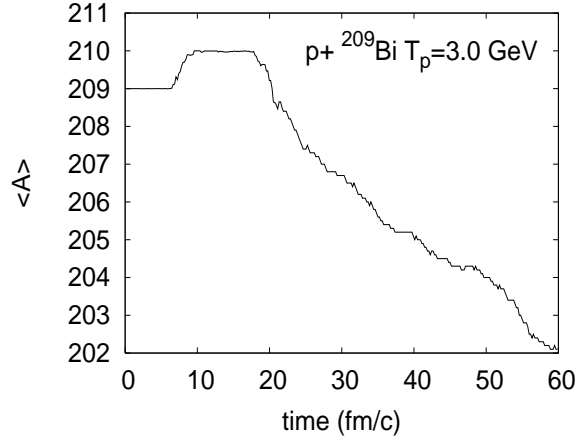

Figure 3.3: *Time variation of the average value of angular momentum of the residual nucleus in p + Bi collision, at 3 GeV proton beam energy; results of the HSD model calculations*

18 fm/c and later the angular momentum lowers significantly due to nucleons escaping from the nucleus. This leakage of angular momentum stops at around 30 fm/c and the average value stabilizes. At later time, i.e. from about 40 fm/c, spurious slow increase of angular momentum is observed, which is unphysical and results from building-up inaccuracies of numerical

calculations. That also indicates that the first stage calculations should be terminated at about 35 fm/c.

Looking at the time evolution of the average mass number of the residual nucleus, presented in Fig. 3.4, quite different behavior is observed. It is seen,

Figure 3.4: *Time variation of the average value of mass number of the residual nucleus in p + Bi collision, at 3 GeV proton beam energy; results of the HSD model calculations*

that at about 10 fm/c the projectile come into the target nucleus. As expected, the mass number is increased by one. But then, starting from about 18 fm/c, the mass number of the residual nucleus decreases monotonically with duration time of the first stage of reaction and does not stabilize at larger times, as it was in case of the other quantities. This indicates, that emission of particles in this model takes place all the time. Duration time of the cascade of the nucleon - nucleon collisions cannot be determined on the basis of behavior of the average mass number of the nucleus. Nevertheless, it accents the importance of assumption of a proper stopping time for the calculations, which has influence on a value of multiplicity of emitted particles. It has a negligible meaning for energy distributions of ejectiles, since, as a time evolution of excitation energy shows, from about 18 fm/c, particles with lower and lower energies are emitted.

The behavior of excitation energy, longitudinal momentum and angular momentum as a function of time shows that choice of the stopping time is limited from two sides. The first stage calculations cannot be terminated too early, when interacting system is highly nonequilibrated. From the other side, also not too late, since for longer times numerical inaccuracies are increasing. Based on above dependences, it is concluded that the most reasonable dura-

tion time of transport models calculations of the first stage of proton induced reactions is equal to 35 fm/c.

Behavior of the time dependences in case of reactions on other targets nuclei and other values of incident energy is displayed in Fig. 3.5. It is seen
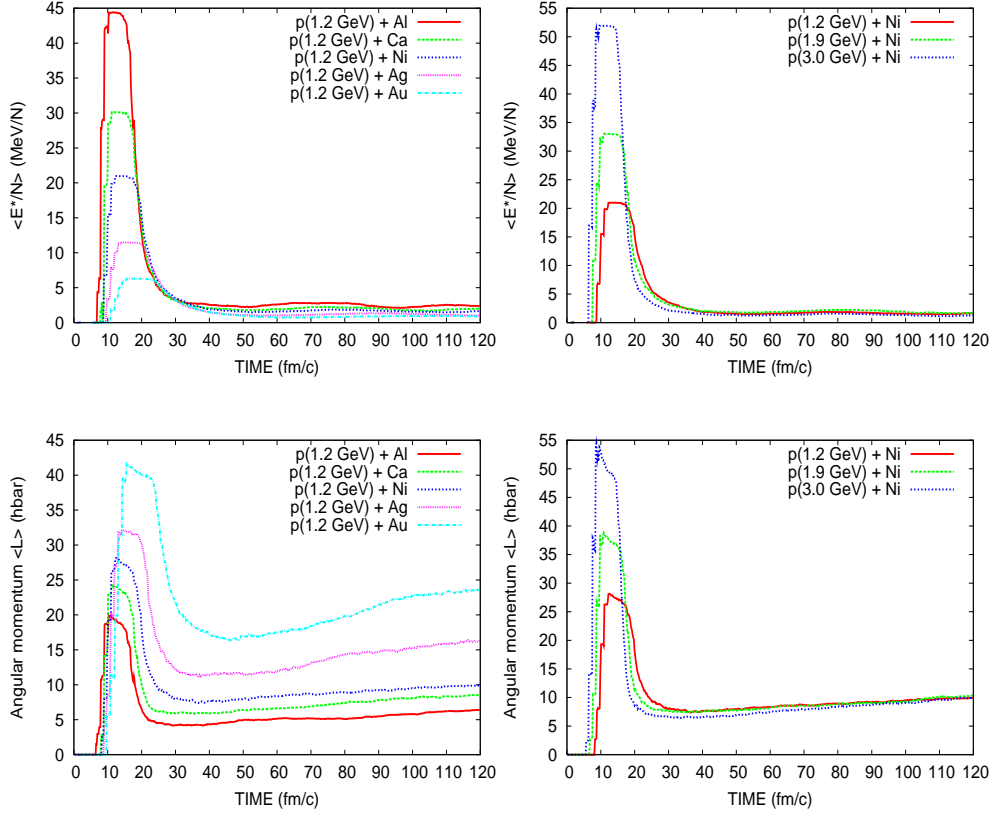

Figure 3.5: *Time variation of the average values of excitation energy per nucleon and angular momentum of residual nuclei in proton induced reactions on various targets, at different projectile energies; results of the HSD model calculations*

that stabilization of the average values in time depends both on incident energy and mass of target. The heavier target is used, the later stabilization occurs. Similarly, the lower projectile energy, the longer time of first stage calculations is needed in order to reach equilibrium. Unfortunately, it cannot be assumed one maximal time for all systems, because of building up of the numerical inaccuracies (see the time dependences of angular momentum), what starts at different time for different systems. Nevertheless, the deduced

above stopping time equal to 35 fm/c will be treated in the frame of this work as an optimal time for each system. It is optimal for all used targets, since it has been established on the example of one of the heaviest targets. But taking into consideration dependence on incident energy, the following exceptions must be included. Calculations of first stage of reactions at projectile energies greater than or equal to 3.0 GeV, on all targets will be terminated after 35 fm/c. At energies lower than 3.0 GeV, the HSD calculations will be stopped later, especially for heavier targets.

The above considerations are based on the results of calculations averaged over all impact parameters. For particular reaction p+Au at Tp=2.5 GeV, for specific impact parameters, e.g. b = 1 fm, 4 fm, 6 fm, the following dependences: time evolution of average excitation energy (presented in Fig. 3.6), angular momentum (Fig. 3.7) and momentum in beam direction (Fig. 3.8) are obtained.
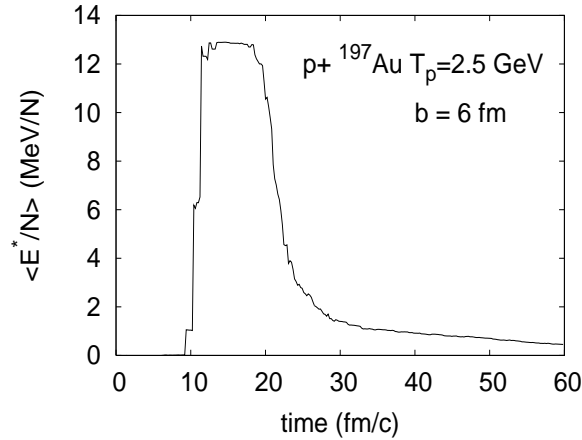
Figure 3.6: *Time variation of the average value of excitation energy per nucleon of the residual nucleus in p + Au collision at 2.5 GeV proton beam energy, the impact parameter b=6 fm; results of the HSD model calculations*

The example dependences calculated for specific impact parameters agree with results obtained with averaging over all impact parameters; choice of time of calculations of first stage of the reaction ($\approx$ 35 - 45 fm/c) is satisfactory.
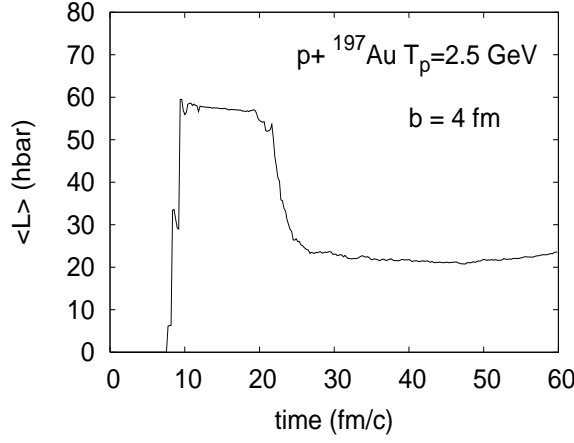
Figure 3.7: *Time variation of the average value of angular momentum of the residual nucleus in p + Au collision at 2.5 GeV proton beam energy, the impact parameter b=4 fm; results of the HSD model calculations*
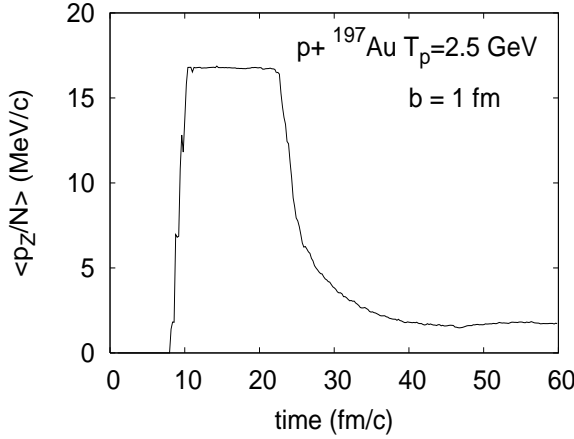
Figure 3.8: *Time variation of the average value of longitudimal momentum of the residual nucleus in p + Au collision at 2.5 GeV proton beam energy, the impact parameter b=1 fm; results of the HSD model calculations*

Chapter 4

Bulk properties of the first stage of proton induced reactions

The following scenario of the first stage of proton - nucleus reactions takes place. High energy proton ($T_p > 100$ MeV) hits a target nucleus. The intra-nuclear cascade starts to develop: the incoming proton, on its way, collides with several target nucleons, transfers energy and momentum to them and may excite them into higher baryonic states. Depending on the position of the cascade nucleons inside the target, they either escape directly from the nucleus or collide secondarily with a few other nucleons transfering further the energy and momentum. Some of the nucleons may leave the nucleus. Development of the cascade can be seen by observing variations of spatial nucleon density with the reaction time. It indicates that proton induced reactions are low-invasive processes.

In Figure 4.1 the HSD simulations of time evolution of nucleon density in central collisions of 2.5 GeV and 5.0 GeV proton with Au nucleus are presented. The density of nucleons with kinetic energies $E_k > 50$ MeV has been calculated, in order to see more clearly the development of the intra - nuclear cascade. Initially, before proton strikes the target nucleus, the max-imal kinetic energy of nucleons in the target is equal to the Fermi energy ($E_F \approx 35$ MeV). As a consequence of interaction nucleons get more ener-getical. At the beginning of reaction, the incident proton is in distance of 15 fm from the center of target nucleus. Projectile enters the target from the left, z is the axis in beam direction. One can see in the Fig. 4.1, that after 5 fm/c ($1\text{fm/c} \approx \frac{1}{3} \cdot 10^{-23}$ s), when proton has not entered the target yet, none of target nucleons has kinetic energy more than 50 MeV. Then, looking at the situation corresponding to density distribution sampled after
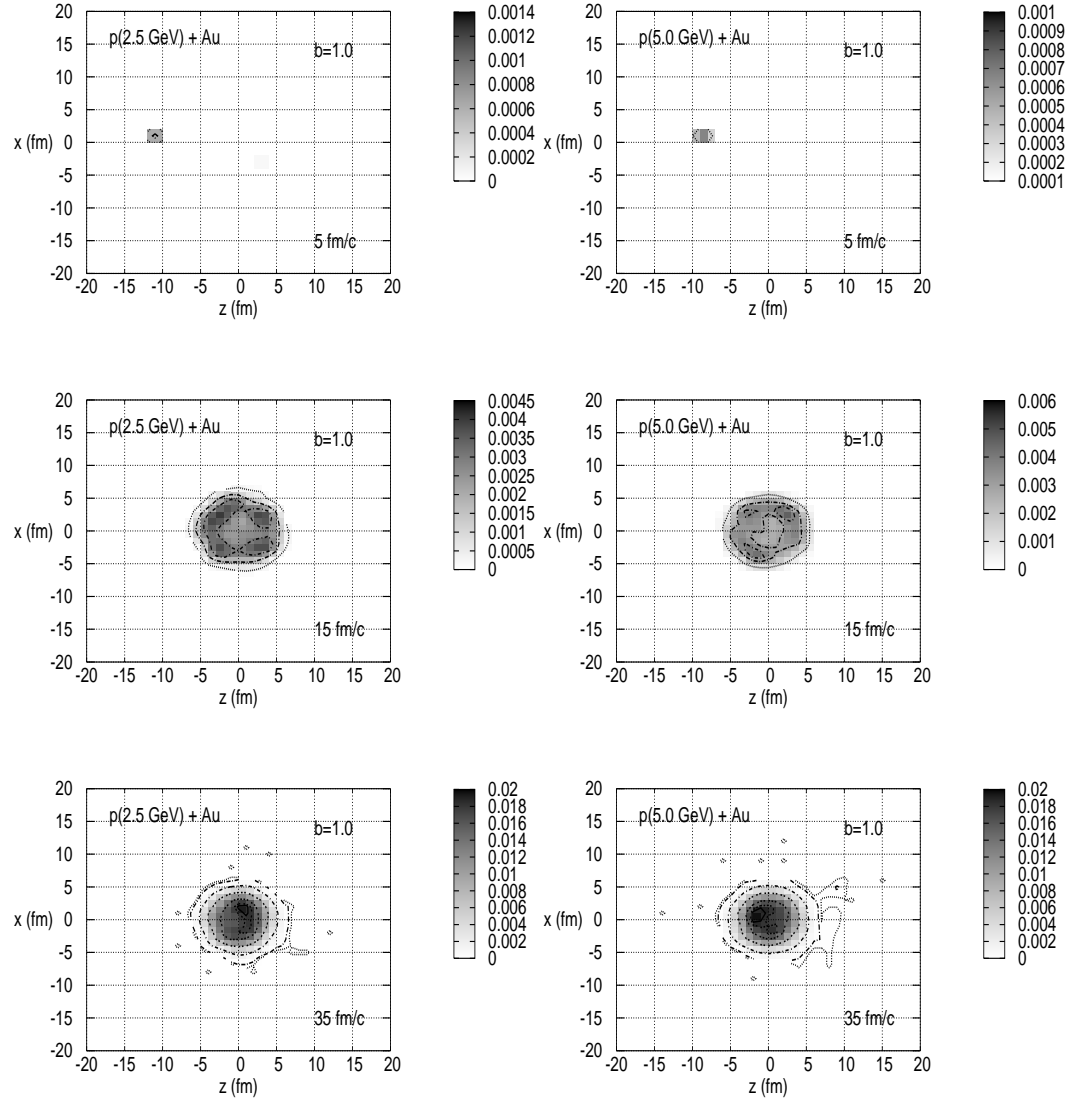
Figure 4.1: *Time evolution of nucleon density of nucleons with kinetic energies $E_k > 50$ MeV, in central collisions of 2.5 GeV (left column) and 5.0 GeV (right column) proton with Au nucleus; results of the HSD model calculations (projections on xz plane)*

15 fm/c, one observes something like a wave going near the surface of target nucleus. Mainly nucleons from the most outer area of nucleus take part in the cascade. The center of target is not touched yet. Situation after 35 fm/c, it means after first fast stage of the reaction is shown on the bottom plots of the Fig. 4.1. It is seen that the center of the nucleon density distribution is now occupied by the cascade nucleons. But the density is not spatially uniform. The central area corresponds to the maximum of the distribution. Levels of constant nucleon density (in units nucleon/fm^3), with values increasing to the center of the circular shaped distribution are clearly visible. It means that in the residual nuclei, the density distribution of shape like of initial target nucleus is reproduced (the density of initial nucleus have the Wood-Saxon distribution form (3.13)). Nevertheless, a small expansion of the nucleus is observed. The level corresponding to the spatial density of value less than about 0.002 nucleon/fm^3 is associated with the free nucleons knocked out of the target.

Distribution of the nucleon density of residual nuclei, in general, does not depend significantly on the centrality of proton - nucleus collision. This is illustrated in Fig. 4.2, where two-dimensional projections of the nucleon density of residual nuclei, for different centralities of 5.0 GeV proton with Au nucleus collision are compared (i.e. for impact parameters of b=1.0, 2.5 and 5.0 fm). However, on the level corresponding to the lowest spatial density, associated with emitted nucleons, some differences are observed. They indicate that more nucleons are emitted in central than in peripheral collisions.

All the presented distributions of nucleon density show that in general, the incoming proton has caused only minor changes of density inside target nucleus.

One of characteristics of created target nucleus is its maximal density. Modification of the density due to penetration of the nucleus by incoming proton is the characteristic feature of proton induced reactions. Such modifications are presented qualitatively in Fig. 4.3, as time evolution of a ratio of maximal nuclear density in case of p+Au reaction at 0.5 GeV, 1.0 GeV, 2.5 GeV and 5.0 GeV of incident energy and the standard nuclear density ρ^0_{max}. It is evident from the Figure, that the incoming proton causes negligible modifications of nuclear density. Though, it is seen, that in case of low energy projectile the maximal density is first slightly increased and then it decreases. In case of higher energetical proton, first slight decrease and then an increase is observed. That could be explained by a fact that incoming low energy projectile almost stops inside target nucleus, causing increase of density, while higher energy projectile goes faster through the nucleus, pushing nucleons away. Then, the situation is changed respectively, due to acting of mean field potential. Nevertheless, the deviations of the presented ratios

from the unity are of order of few percent, what proves that proton induced reactions are quite non-invasive processes.

In order to check, how the kinetic energy is distributed inside the residual nuclei, the following test has been made. Based on p+Au reaction, at 2.5 GeV proton beam energy, nucleons, which take part in the intra-nuclear cascade have been observed. It means, nucleons which gained a significant part of the energy of the projectile (i.e. of $E_k > 75$ MeV, $E_k > 100$ MeV). Most of the observed cases indicated homogeneous distribution of kinetic energy inside the residual nuclei. Partial heating up of the nuclei has been noticed in only about 1% of the cases, in peripheral collisions. Illustration of the exceptional situation is shown in Fig. 4.4, where, starting from the top, the nucleon density of residual nuclei of nucleons with kinetic energies $E_k > 50$ MeV, $E_k > 75$ MeV and $E_k > 100$ MeV, respectively are plotted. Looking at the plot in the bottom of Fig. 4.4 one can distinguish two differently excited parts. One part of nucleus is composed of nucleons with kinetic energies greater than 100 MeV, the second part - of nucleons with kinetic energies lower than 100 MeV. The highly excited group of nucleons, it is about 10 nucleons with an average total momentum equal to about 560(+/-80) MeV/c. The less excited part, it is till about 184 nucleons with an average total momentum equal to only about 190(+/-60) MeV/c.

Similar situation is observed, if looking at a bit lower energetical nucleons, the central plot of Fig. 4.4, nucleons with kinetic energies greater or lower than 75 MeV. In this case, the highly excited part consists of about 20 nucleons with an average total momentum equal to about 470(+/-90) MeV/c, and less excited part composed of 174 nucleons with an average total momentum equal to about 190(+/-60) MeV/c.

One can conclude, that the HSD simulations predict something like formation of two excited sources of evidently unequal masses. The smaller source consists of relatively few nucleons (up to ~ 20) and is rather fast, $\beta \sim 0.025$ c. The larger source is built of $\sim$ 170 - 180 nucleons and has velocity $\beta \sim 0.0012$ c. Similar observation has been drawn from phenomenological analysis of experimental data presented in [7].
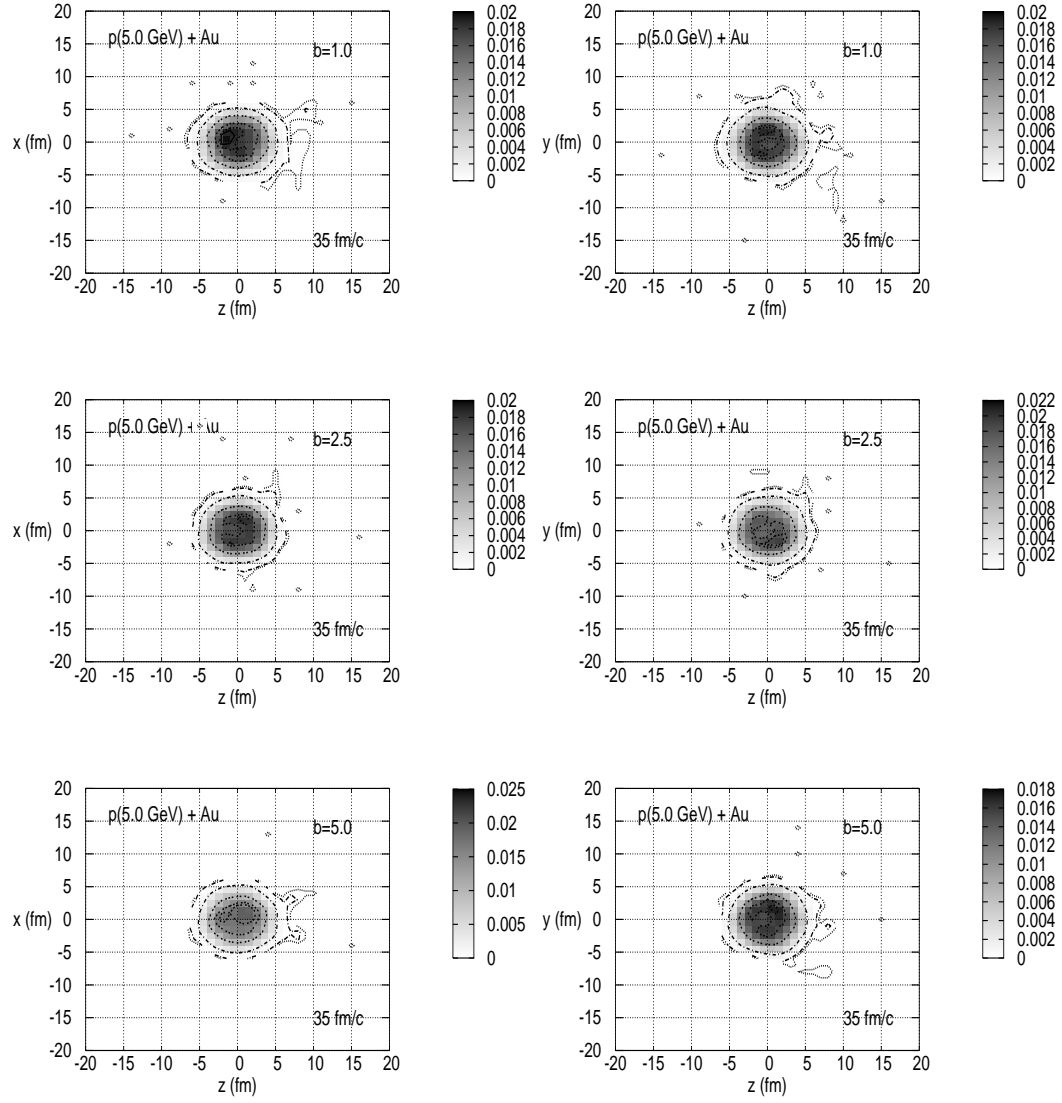
Figure 4.2: *Nucleon density of residual nuclei of nucleons with kinetic energies $E_k > 50$ MeV, in central (starting from the top, b=1fm), midcentral (b=2.5fm) and peripheral (b=5fm) collisions of 5.0 GeV proton with Au nucleus; results of the HSD model calculations (the density projections on xz (left column) and yz (right column) planes)*
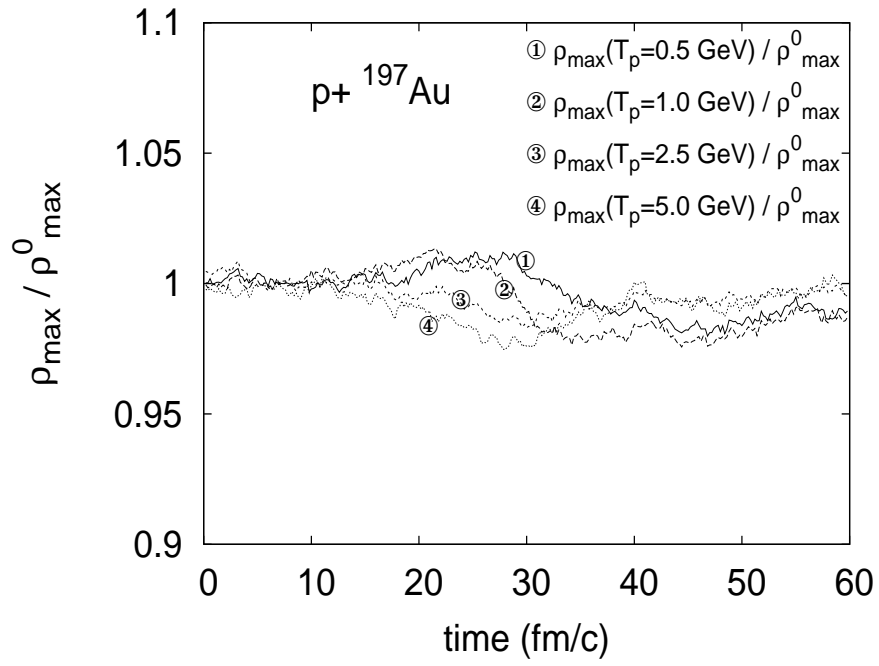
Figure 4.3: *Modifications of maximal nucleon density in the case of p+Au collisions at 0.5 GeV, 1.0 GeV, 2.5 GeV and 5.0 GeV proton beam energy; results of the HSD model calculations*
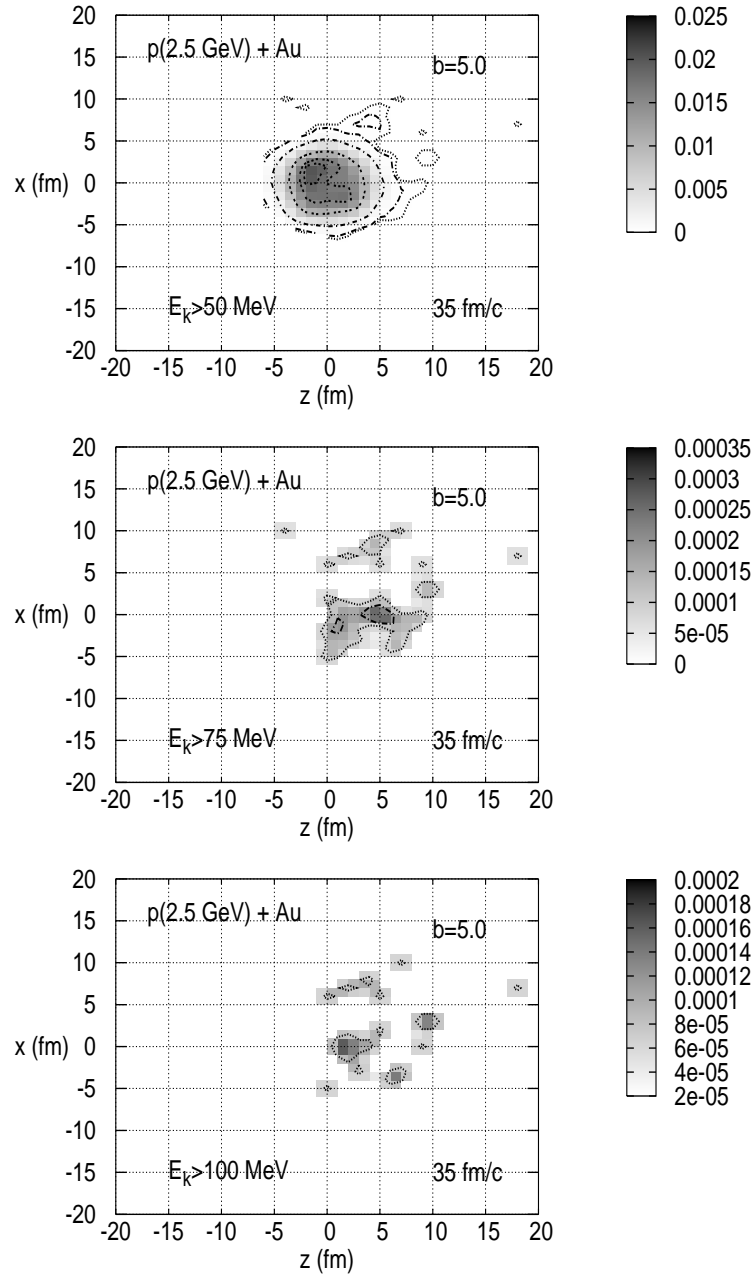
Figure 4.4: *Nucleon density of residual nuclei of nucleons with kinetic energies $E_k > 50$ MeV (starting from the top), $E_k > 75$ MeV and $E_k > 100$ MeV, respectively, in peripheral (b=5fm) collisions of 2.5 GeV proton with Au nucleus; results of the HSD model calculations*

Chapter 5

Properties of residual nuclei after the first stage of proton - nucleus reactions

As it is mentioned above in this work, as result of the first stage of proton - nucleus reaction, beside emitted particles, an excited nucleus remains. It differs from the initial target, in average, by only a few nucleons in mass number. Properties of the residual nucleus (i.e. mass (A_R), charge (Z_R), excitation energy (E_R^*), three - momentum ($\vec{p_R}$) and angular momentum (L_R)) are evaluated, in the frame of the HSD model, by exploring conservation laws, according to formulas 3.23. Results of calculations for reactions on various target nuclei, at different values of incident energy in range from 0.1 GeV to about 10 GeV, are discussed below.

Let's look first at one - dimensional distributions of the quantities evolving with projectile energy and mass of target. Histogrammed properties for exemplary reactions of 1.9 GeV proton on light (^{27}Al), heavy (^{197}Au) and two intermediate mass (^{58}Ni and ^{107}Ag) targets are displayed in Fig. 5.1. Distributions for proton induced reaction on example Al target, at several values of proton beam energy are shown in Fig. 5.2. The average values and standard deviations for the presented distributions are collected in Tables 5.1 and 5.2.

The Figures 5.1 and 5.2 and values collected in the Tables 5.1 and 5.2 indicate, that all of the distributions differ significantly with mass of target, but behave similarly for varied projectile energies.

Table 5.1: *The average values and standard deviations for the one - dimensional distributions of properties of residual nuclei from 1.9 GeV proton induced reactions on several targets*

reaction	p+Al	p+Ni	p+Ag	p+Au
$< A >_R$	23.96±2.25	54.71±2.65	102.24±3.55	192.39±3.69
$< Target\ Mass\ loss >$	3.036±2.25	3.29±2.65	4.76±3.55	4.61±3.69
$< Z >_R$	11.64±1.42	26.53±1.64	45.05±1.98	77.34±1.92
$< Target\ Charge\ loss >$	1.36±1.42	1.47±1.64	1.96±1.98	1.66±1.92
$< E^* >_R$ [MeV]	74.56±81.77	122.84±120.41	144.16±125.65	222.16±171.24
$< E^*/N >_R$ [MeV/N]	3.27±3.63	2.30±2.29	1.43±1.27	1.16±0.91
$< L >_R$ [ℏ]	4.77±3.25	7.41±3.59	11.76±5.50	17.14±8.08
$< p_z >_R$ [GeV/c]	0.18±0.24	0.22±0.27	0.29±0.35	0.34±0.38
$< p_x >_R$ [GeV/c]	-0.0011±0.28	-0.0014±0.31	-0.0058±0.36	-0.0045±0.37

Table 5.2: *The average values and standard deviations for the one - dimensional distributions of properties of residual nuclei from proton induced reactions on Al target, at several incident energies*

| impact energy	1.0 GeV	2.0 GeV	3.0 GeV	4.0 GeV
$< A >_R$	23.51±2.17	24.032±2.20	24.23±1.99	24.12±2.085
$< Z >_R$	11.28±1.35	11.66±1.37	11.78±1.31	11.71±1.33
$< E^* >_R$ [MeV]	65.76±54.067	73.46±84.27	70.31±88.081	74.50±98.023
$< E^*/N >_R$ [MeV/N]	2.94±2.61	3.22±3.75	3.026±3.84	3.25±4.35
$< L >_R$ [ℏ]	4.75±2.65	4.71±3.072	4.85±4.48	4.99±5.23
$< p_z >_R$ [GeV/c]	0.18±0.24	0.17±0.23	0.16±0.24	0.16±0.25
$< p_x >_R$ [GeV/c]	-0.0021±0.27	-0.00088±0.27	-0.0030±0.27	0.0033±0.27
impact energy	5.0 GeV	6.0 GeV	7.0 GeV	8.0 GeV
$< A >_R$	24.027±2.19	23.94±2.26	23.86±2.35	23.75±2.41
$< Z >_R$	11.66±1.39	11.603±1.41	11.58±1.46	11.54±1.47
$< E^* >_R$ [MeV]	74.61±90.60	76.48±98.98	79.64±129.89	81.92±137.73
$< E^*/N >_R$ [MeV/N]	3.29±4.13	3.41±4.55	3.58±5.8	3.71±6.29
$< L >_R$ [ℏ]	5.034±5.66	5.48±8.25	5.15±7.32	6.035±11.044
$< p_z >_R$ [GeV/c]	0.16±0.24	0.16±0.25	0.17±0.27	0.18±0.28
$< p_x >_R$ [GeV/c]	-0.000024±0.27	0.0053±0.28	0.0026±0.28	-0.0051±0.29
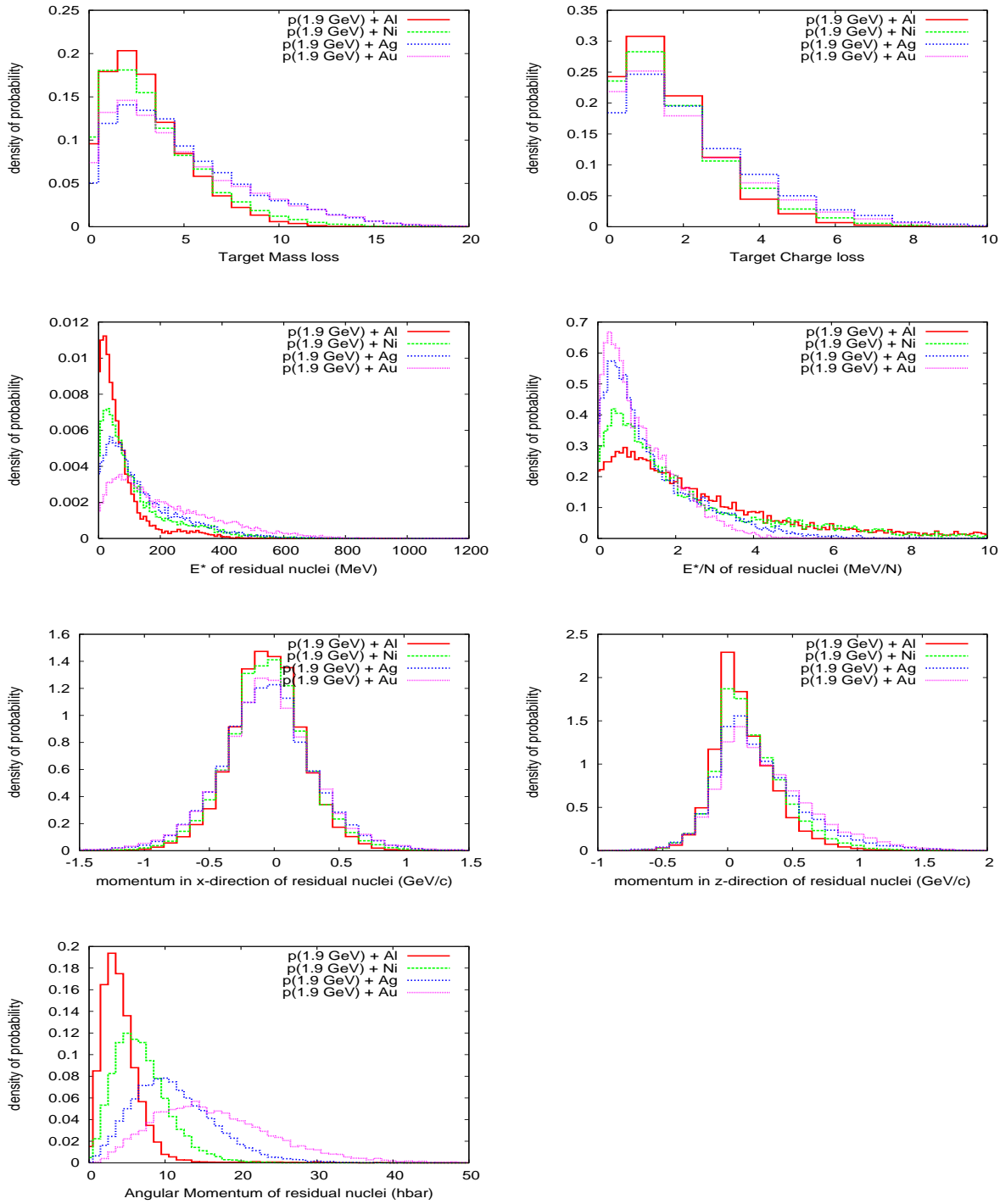
Figure 5.1: *One - dimensional distributions of properties of residual nuclei after first stage of 1.9 GeV proton induced spallation reactions on ^{27}Al, ^{58}Ni, ^{107}Ag and ^{197}Au targets; results of the HSD model calculations*
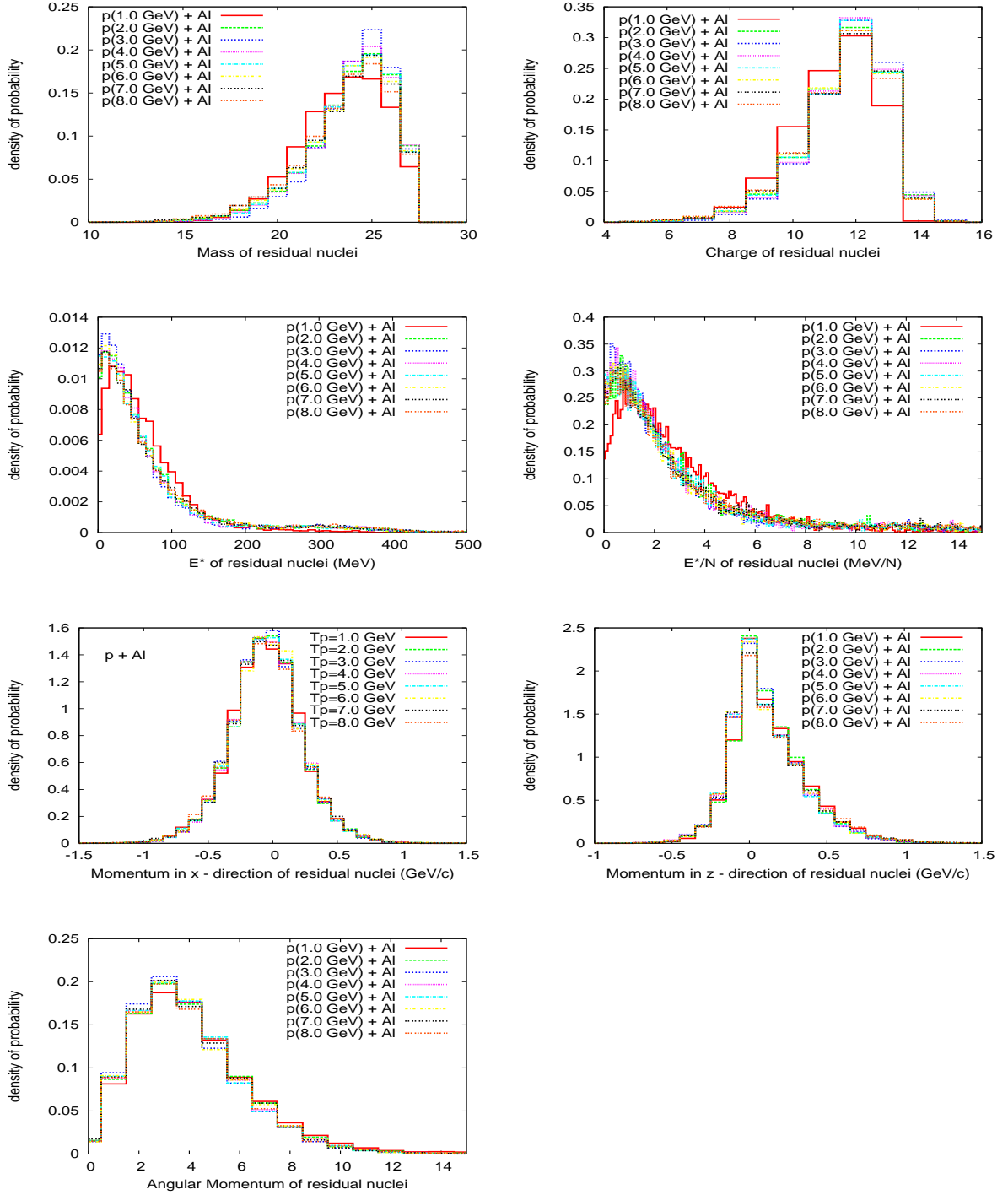
Figure 5.2: *One - dimensional distributions of properties of residual nuclei after first stage of proton induced spallation reactions on ^{27}Al target, at few values of projectile energy; results of the HSD model calculations*

Reason for these behaviors is connected with finite size of nuclei. Average values of excitation energy (E_R^*) and angular momentum (L_R) of residual nucleus and width of the distributions increase with mass of target nuclei, at fixed projectile energy. For a chosen target, the distributions of E_R^* very slightly depend on incident energy. Distributions of L_R almost do not depend on incident energy. This can be explained in an intuitive way by analyzing how the energy and momentum are deposited into a target nucleus. The E_R^* left in the residual nucleus after the first stage of reaction is in average only a small fraction of the energy, which has been introduced into a target nucleus by incoming proton. Most of the energy is carried away by emitted particles (example energy balance is presented in Sec. 8.1). The number of ejected particles should be treated as a signature how many nucleons were involved in the intra - nuclear cascade. The more nucleon - nucleon collisions inside target nuclei, the larger part of the energy and angular momentum introduced by a projectile is deposited into the residual nucleus. E.g. due to a collision of the incident proton with a nucleon inside a target, a resonance, mainly Delta resonance could be excited. The Delta resonance has a short time of life, i.e. about 1 - 2 fm/c. It decays into nucleon and meson (mainly pion) or collides with other nucleon before the decay. As result, energy is accumulated inside target nucleus. The heavier target, the more collisions can occur, because the cascade of collisions can last for a longer time. For light targets, the excitation energy (E_R^*) is respectively small, because a number of collisions made by a projectile is low. In case of the excitation energy per nucleon (E_R^*/N) the situation is opposite, i.e. E_R^*/N is a decreasing function of mass of target. This is just because in heavier targets, the amount of energy is distributed among more nucleons.

Similarly, distribution of angular momentum of residual nuclei almost does not depend on value of incident energy, but strongly depends on mass of target. The heavier target, the more angular momentum is deposited inside. This is because in the HSD model, quasi - classical approximation for calculations of angular momentum is used; at fixed impact energy, the maximal angular momentum of projectile is proportional to radius of target nuclei. Therefore, in case of heavier targets, more angular momentum is introduced by a projectile.

Distributions of momentum in beam direction (z-component) and the momentum perpendicular to the beam direction (x-component) indicate that residual nuclei are moving according to initial direction of projectile. It is evidently seen (both from the Fig. 5.1 and Table 5.1), that the average values of momentum in x-direction of residual nuclei are consistent with zero.

Table 5.3: *The average values and standard deviations for distributions of velocity of residual nuclei ($< v_z >_R$ [c]) from proton induced reactions on several targets*

$< v_z >_R$ [c]	p+Al	p+Ni	p+Ag	p+Au
T_p=1.2 GeV	0.0082±0.011	0.0046±0.0056	0.0036±0.0036	0.0035±0.0027
T_p=1.9 GeV	0.0078±0.011	0.0044±0.0054	0.0029±0.0033	0.0025±0.0024
T_p=2.5 GeV	0.0069±0.010	0.0036±0.0052	0.0024±0.0032	0.0019±0.0021

Similar information about the reaction could be extracted from distributions of velocity in beam direction of residual nuclei. The distributions differ significantly with mass of target, but behave similarly for varied projectile energies, as shown in Fig. 5.3. The average values and standard deviations of the values are presented in Table 5.3. It is seen that the lighter target, the broader is the distribution. These are asymmetric, peaked in forward direction, with tails in backward direction. This indicates, that in average, the residual nuclei tend to move forward, according to the initial direction of projectile.

In order to have a better view of the dependences, average values of the quantities and standard deviation of the average values, have been expressed as a function of incident energy and mass of target and presented in Figures 5.4 and 5.5.

Average values and standard deviations of mass number and charge of residual nuclei remaining after first stage of p+Al reaction, in function of projectile energy are presented in Figures 5.6 and 5.7. It is interesting, that both the mass number and the charge, in average, increase up to 3.0 GeV of incident energy. Then decreasing is observed. The ratio of average values of the mass number and charge is constant as function of projectile energy, as shown in Fig. 5.8. Additionally, it exceeded the ratio for initial target nucleus.

Average values and standard deviations of momentum in beam direction of residual nuclei after first stage of proton induced reaction on several targets, at various incident energies are presented in Fig. 5.9. One can conclude, that the heavier the target, the more momentum in beam direction is deposited inside. What more, the maximum in mass dependence on projectile kinetic energy (at the incident energy equal to 3.0 GeV) for given target, see Fig. 5.6, corresponds to the minimum of dependence of momentum in beam direction of residual nuclei in function of projectile energy.
Behavior of standard deviations as function of projectile kinetic energy is

noteworthy. It is observed, that the higher incident energy, the broader are distributions of excitation energy, momentum, angular momentum, mass number, charge of residual nuclei. This can be qualitatively explained taking into account results of simulations presented in the Fig. 5.10 (i.e. dependence of multiplicity and energy of emitted nucleons during the first stage of the reactions on incident energy). The behavior of multiplicity of emitted nucleons as function of projectile energy perfectly agrees with the behavior of mass and charge of residual nuclei. It means, first, up to about 3.0 GeV of incident energy, number of emitted nucleons decreases, so that mass of residuum increases. With further increase of impact energy, more and more nucleons are emitted, so that mass of the residuum decreases. Obviously, average kinetic energy carried by emitted nucleons is a monotonically increasing function of projectile energy in the whole considered range of projectile energy, as shown in Fig. 5.10. Protons carried out in average more kinetic energy than neutrons, since more protons than neutrons are emitted during first stage of reaction. The p/n ratio is larger than unity, because of the extra proton correspondig to the incident particle (see Fig. 5.10). One can conclude that information of type of projectile is somehow remembered by the system during the first stage of reaction (this topic is undertaken also in Sec. 8.2).

Looking at behaviors of average values of properties of residual nuclei, especially their momentum in beam direction, mass number and multiplicity of emitted nucleons during first stage of reaction as function of incident energy, it is seen that the average values first continuously decrease (or increase, respectively) with the incident energy, up to about 3 GeV and then consistently, the opposite tendency is observed. The precise explanation of such behavior is difficult, it must be a result of a few simultaneous effects. Newertheless, considering elementary processes (implemented to the model, based on experimental data), one can suggest the following qualitative explanation. Such behaviors should be connected with contribution of different resonances excitations, which depends on the energy introduced by a projectile into the target nucleus. At low projectile energy (about 1.0 GeV) nucleons are emitted mainly due to elastic nucleon - nucleon scattering. More probable than at higher energies is also, that incoming proton stops inside target nuclei. At higher incident energies possibility of excitation of resonances (mainly, the most important here Δ resonance) increases. A bit less, but more energetic nucleons are emitted. In result, the average multiplicity of emitted nucleons decreases, so mass of residual nuclei increases and the average longitudinal momentum decreases. At higher incident energy (equal to about 3.0 GeV), from one side the probability of Δ resonance excitation becomes smaller, and from the other side probability of excitation of higher resonance is still too

low. This corresponds to the minimum (or maximum) of the incident energy dependences of the considering quantities. Then, with further increase of projectile energy, probability of excitation of other resonances increases. This causes, that more energy and momentum is deposited into residual nuclei. So, the average longitudinal momentum of residual nuclei increases. Simultaneously, more particles could be produced, since the ratio of inelastic to elastic collision increases. The multiplicity of emitted nucleons increases, so the average mass of remnants decreases.

Behavior of multiplicity and average kinetic energy of emitted nucleons, as function of target mass number, at an example impact energy is shown in Fig. 5.11. One can see, that the heavier target, the smaller differences in number of emitted protons and neutrons. For the heaviest presented target, the p/n ratio is equal to the unity. One can conclude that in heavy targets, the information about a type of projectile is lost due to possible large number of mutual reactions. Total number of emitted nucleons increases with mass of target nucleus and stabilizes for heavier targets (with mass numbers greater than 60). In heavier targets, the cascade of intra-nuclear collisions can last longer, so that emitted nucleons carries in average less kinetic energy. The nucleon, on its way, going outside the nucleus, has to penetrate through nuclear skin of the nucleus, with high probability undergoes further collisions. As result, more particles with suppressed energies are emitted.

More informations about the excited nuclei is provided by two - dimensional correlation plots of their properties. Example dependences of excitation energy, mass of residual nuclei and their velocity in the beam direction are shown in Fig. 5.12 (velocity versus excitation energy per nucleon and velocity versus residual mass). It is meaningful, that velocity in beam direction of residual nuclei increases with increasing excitation energy deposited inside the residual nuclei. This indicates, that the energy is comprised also in onward movement of residual nuclei. Simultaneously, the velocity increases with decreasing mass of residual nuclei, what is equivalent to increase of number of ejected particles. One can conclude that also excitation energy of residual nuclei should increase with decrease of mass of the nuclei. In Figures 5.13 and 5.14, regression function of excitation energy on target mass loss and regression function of angular momentum on target mass loss are presented (for residual nuclei formed in p+Al reaction, at a few impact energies and proton induced reaction on several targets at example 4.0 GeV incident energy, respectively). The dependences are roughly linear functions of the target mass loss.

It is seen, that the heavier remnants (for the same initial target), the lower average excitation energy is deposited inside. The average excitation energy increases with decreasing of the remnant mass. Based on the Fig.

5.14, one can conclude that particularly the dependence on mass of target is quite pronounced. It is because, as it is already mentioned above, in heavier targets, where the cascade lasts longer, more energy can be accumulated. In the Figures 5.13 and 5.14, it is also seen, that in the cases of the lowest mass of residual nuclei, (i.e. the target mass loss higher than about 7 nucleons), the increase of excitation energy and angular momentum is not only less pronounced, but even a slight decreases is observed. In such cases, i.e. more ejected particles, the intra - nuclear cascade is lasting for longer time, so that particles with rather moderated energies are emitted.

Example two - dimensional distributions of mass and excitation energy of residual nuclei formed in p+Al reaction, at several projectile energies are displayed in Fig. 5.15. Again, one observes that the higher excitation energy of residual nuclei, the smaller their mass.

Dependence of excitation energy on angular momentum of residual nuclei is presented in Fig. 5.16. The five lines (in upper part of the Fig. 5.16) correspond to the Yrast lines (definition is given in Chapter 7) calculated according to the formula: $E^* = \frac{\hbar^2}{2I} L_R(L_R + 1)$ with different values of the moment of inertia (I), where: I is the moment of inertia of rigid body ($I = \frac{2}{5}MR^2$, where M and R stand for mass and radius of nucleus, respectively), $I/50$ corresponds to the hydrodynamical limit of nucleus (meaning that only a part of nucleus behaves like the rigid body, the other part - in uncorrelated way, see Ref. [52]). One observes that angular momentum increases with increase of the average value of excitaton energy. It is evident, that the dependence is not inconsistent with the Yrast line.

Physicists, who are studing fragmentation have found that this process occurs at some particular value of projectile energy (T_p) (based on (p,^{7}Be) reaction, for various targets at different T_p, see [53]). Fragmentation is a phase transition, what means, that a proper amount of energy needs to be pumped into a system. It follows, that fragmentation occurs at some particular value of $(E^*/N)_R$, which experimentally has been found to be at least equal to about 5 MeV/N [54, 55]. Using the condition of 5 MeV/N to the HSD model results, presented in Fig. 5.17, it is seen that fragmentation is a very low probable process in proton induced reactions. For example, in p+Al reaction at T_p=5.0 GeV, fragmentation of excited nucleus may occur in about 17 % of cases (i.e. the part of spectrum for $(E^*/N)_R > 5$ MeV/N is 17 % of the whole $(E^*/N)_R$ spectrum), whereas in p+Au reaction at the same incident energy, only in about 5 % of cases. These are cases from the tail of $(E^*/N)_R$ distribution. Based in the Fig. 5.17 one can conclude that fragmentation process is more probable in reactions on light than on heavy targets, and at higher incident energies.

One can suppose that fragmentation of only a part of nucleus could be more probable. This requires inhomogeneous excitation of residual nucleus. It means, not all of nucleons inside the nucleus are involved in carrying of the excitation, i.e. for different target, $(E^*/N)_R$ should be calculated not per each nucleon, but only per some amount of nucleons, which take active part in the cascade. However based on observations of evolution of nucleon density and distribution of kinetic energy inside excited nuclei, it is seen that such partial heating up of nucleus is very low probable. It occurs only in about 1 % of cases, as discussed in Chapter 4.

Additionally, experimentalists, who are interested in fragmentation, look for it in central collisions, accompanied with high multiplicity of emitted particles, as it is shown qualitatively by results of the HSD model calculations, presented in Fig. 4.2. Nevertheless, in the HSD simulations, the very low probable partial heating up of nucleus has been found in peripheral collisions (see Fig. 4.4).

Investigated here reactions are very low invasive processes, involving only a few nucleons, causing only minor fluctuations of nucleon density. So, it is evident that there is a negligible probability for fragmentation in proton - nucleus interacting system, in energy range considered in the frame of this work. Spallation is evidently dominant process.
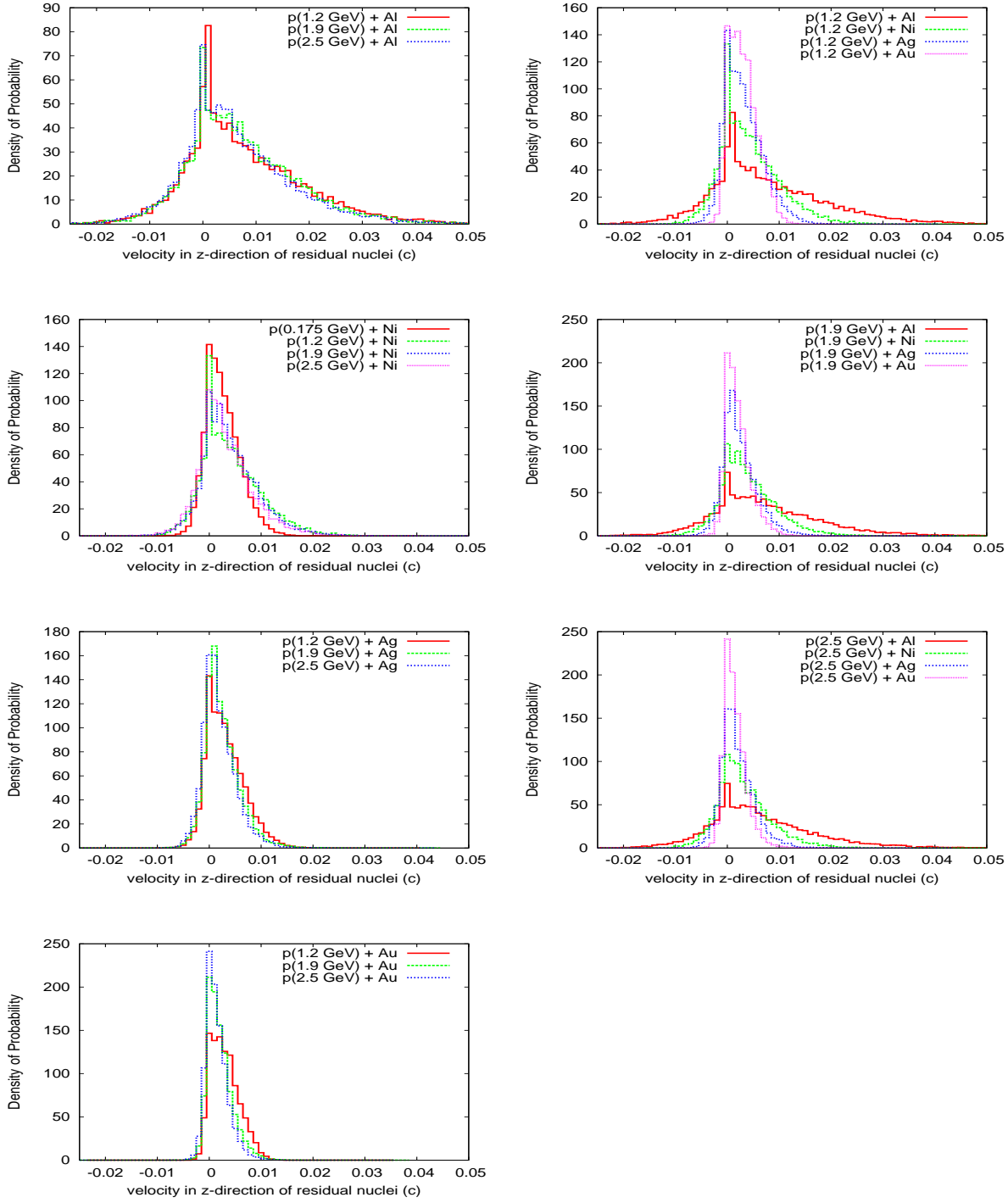
Figure 5.3: *One - dimensional distributions of velocity in beam direction of residual nuclei at the end of first stage of proton induced spallation reactions on various targets, at few example values of projectile energy; results of the HSD model calculations*
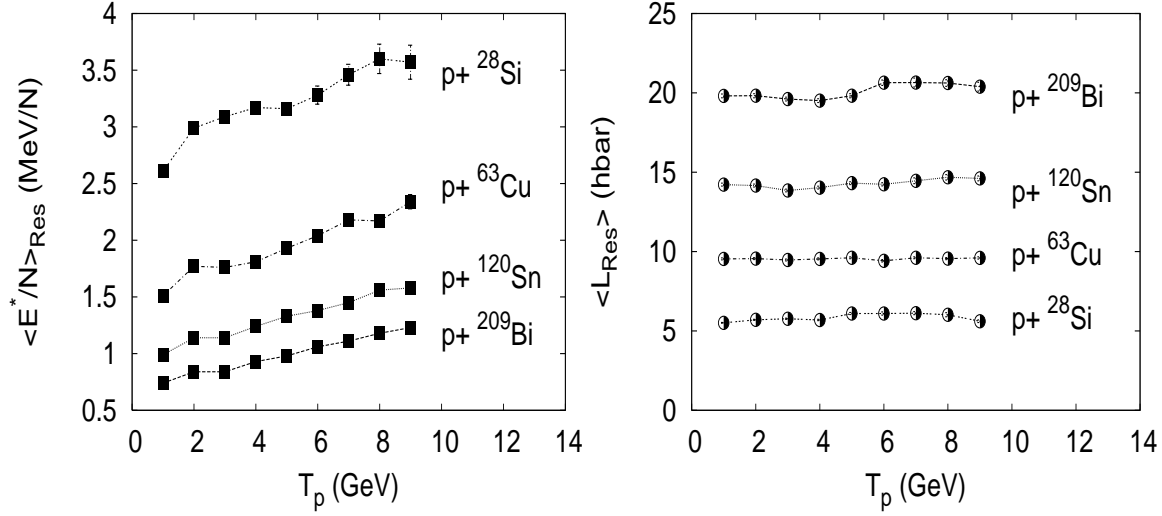
Figure 5.4: *Average values of excitation energy per nucleon (left) and angular momentum (right) of residual nuclei from proton induced reactions on Si, Cu, Sn and Bi target in functi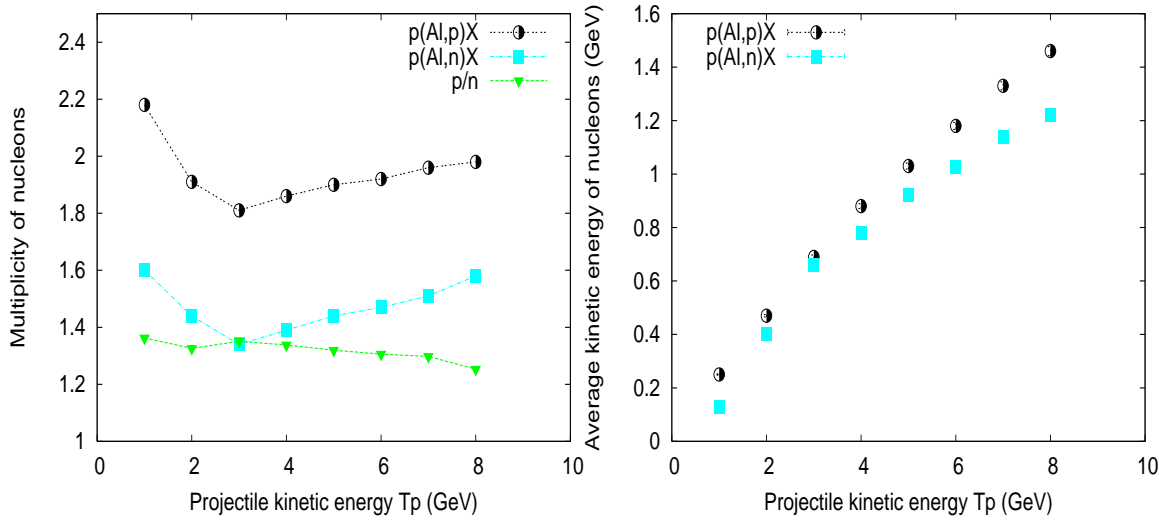on of incident energy; results of the HSD model calculations (error bars indicate values of standard deviation of the average values, divided by a square root of number of events)*
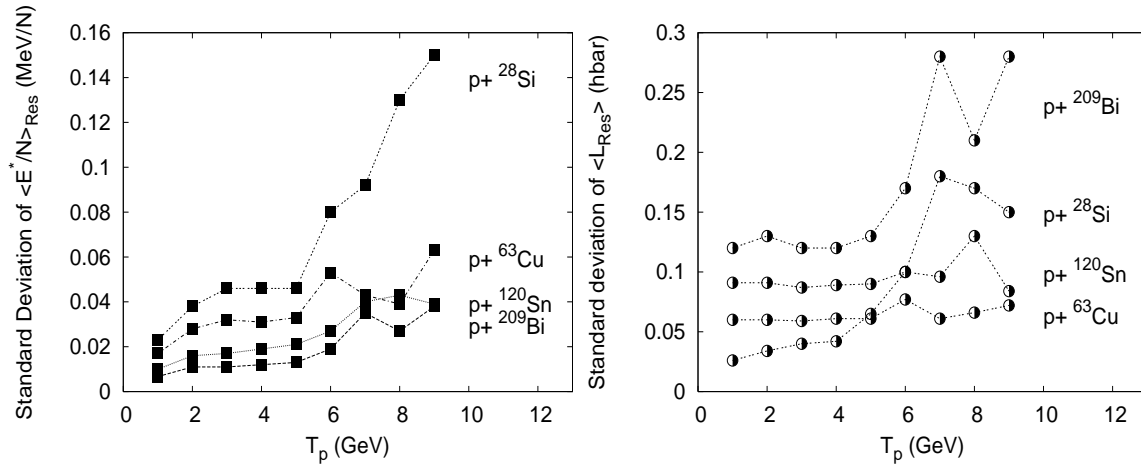
Figure 5.5: *Standard deviation of average values of excitation energy per nucleon (left) and of angular momentum (right) of residual nuclei from proton induced reactions on Si, Cu, Sn and Bi target, in function of incident energy; results of the HSD model calculations*
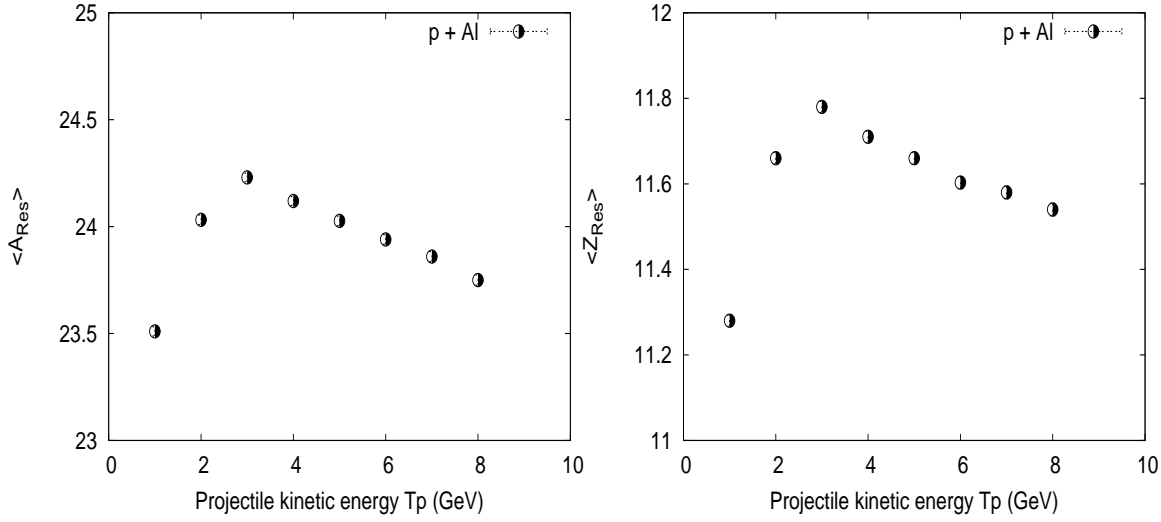
Figure 5.6: *Average values of mass number (left) and charge (right) of residual nuclei from proton induced reaction on Al target, in function of incident energy; results of the HSD model calculations (error bars indicate values of standard deviation of the average values, divided by a square root of number of events)*
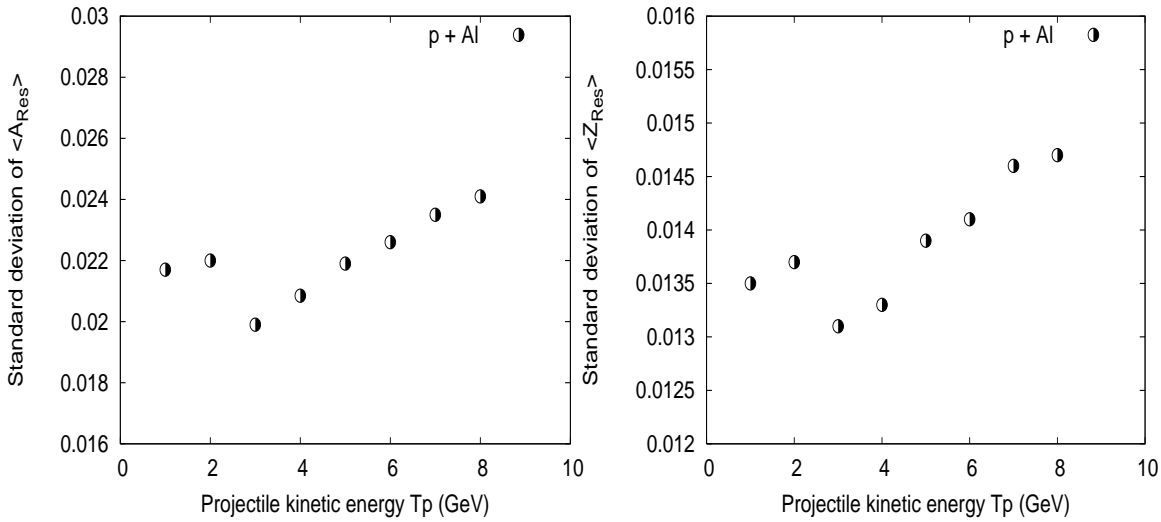

Figure 5.7: *Standard deviation of average values of mass number (left) and charge (right) of residual nuclei from proton induced reactions on Al target, in function of incident energy; results of the HSD model calculations*
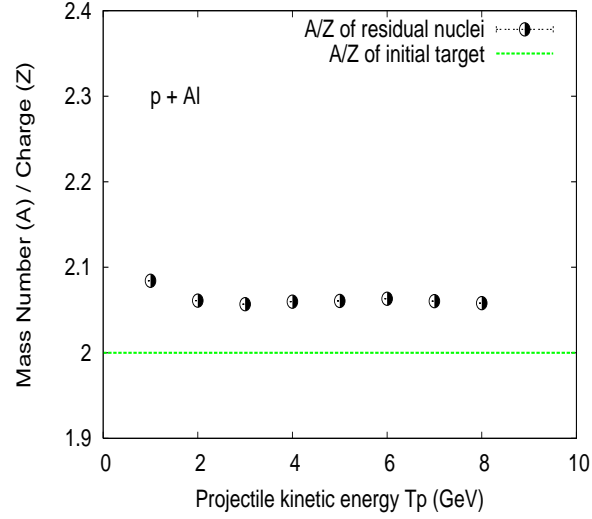
Figure 5.8: *Ratio of average values of mass number and charge of residual nuclei from proton induced reactions on Al target, in function of incident energy; results of the HSD model calculations*
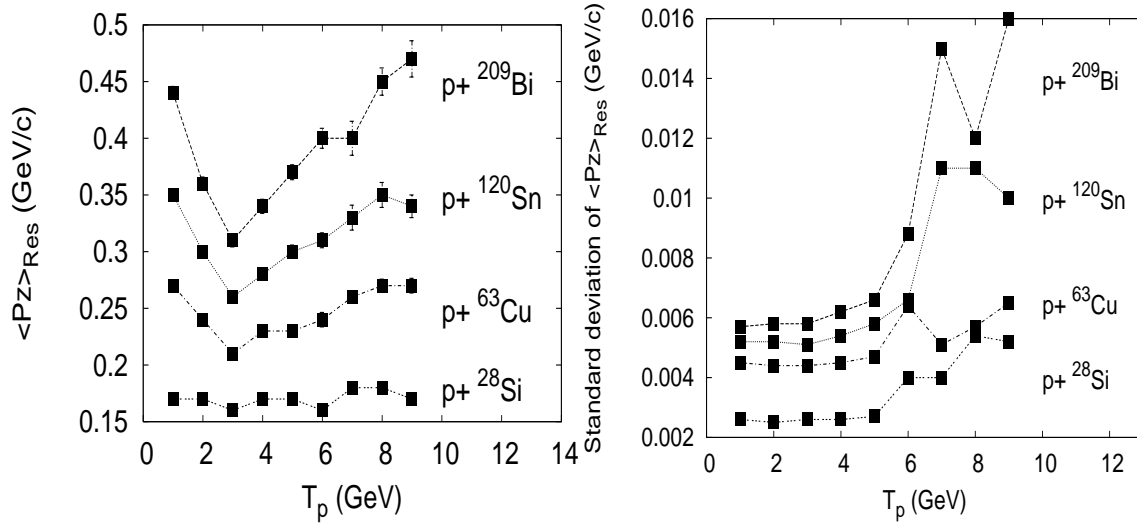
Figure 5.9: *Average values (left) and standard deviation (right) of the average values of momentum in beam direction of residual nuclei from proton induced reactions on several targets, in function of incident energy; results of the HSD model calculations*

Figure 5.10: *Multiplicity (left) and average values of kinetic energy per individual nucleon (right) of nucleons emitted during first stage of proton induced reaction on Al target, as function of incident energy; results of the HSD model calculations (error bars indicate values of standard deviation of the average values, divided by a square root of number of events)*
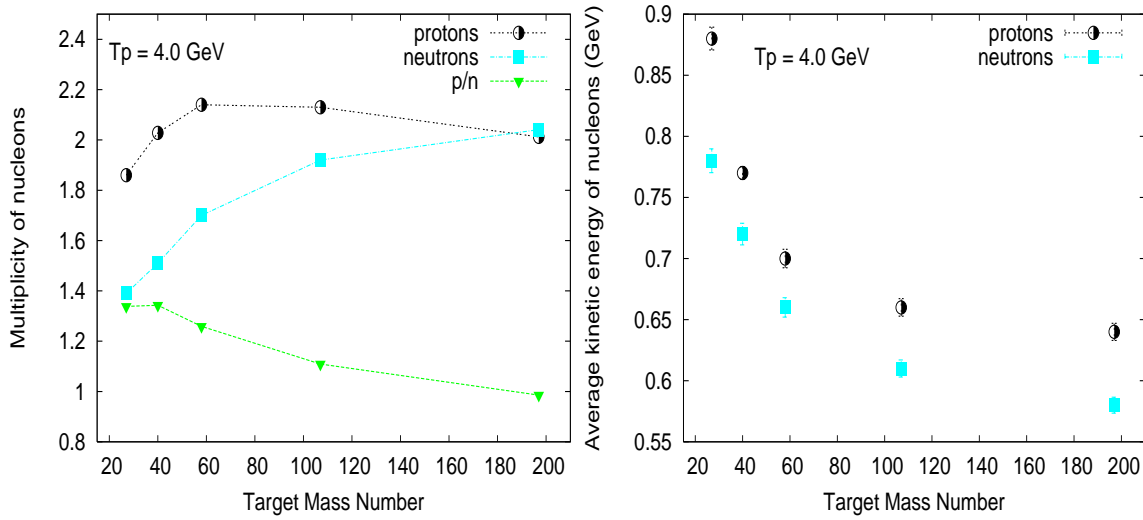
Figure 5.11: *Multiplicity (left) and average values of kinetic energy per individual nucleon (right) of nucleons emitted during first stage of 4.0 GeV proton induced reactions on a few targets, as function of target mass number; results of the HSD model calculations (error bars indicate values of standard deviation of the average values, divided by a square root of number of events)*
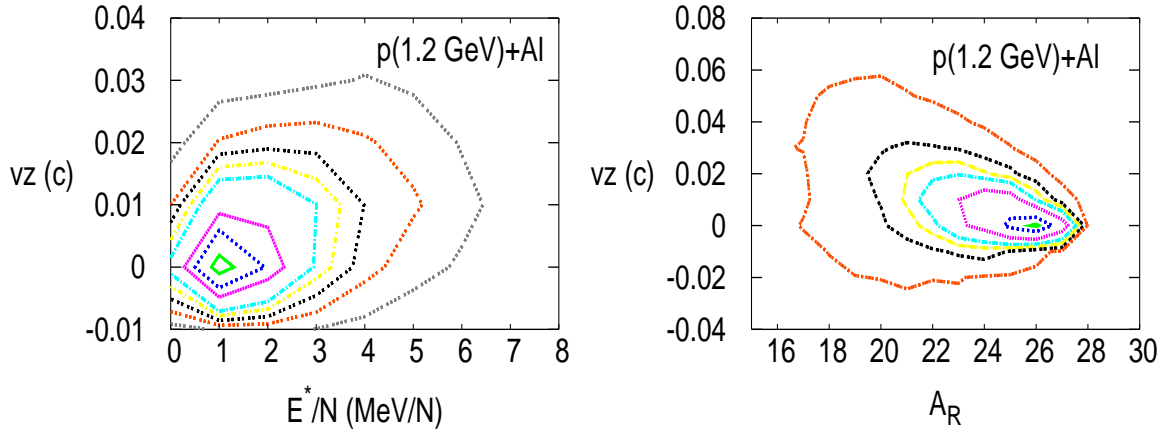
Figure 5.12: *Two - dimensional distributions of velocity in beam direction of residual nuclei and (a) excitation energy per nucleon of residual nucleus and (b) mass of residual nuclei, for exemplary reaction p+Al at 1.2 GeV of incident energy; results of the HSD model calculations (the most central contour line corresponds to a maximum of the distribution)*
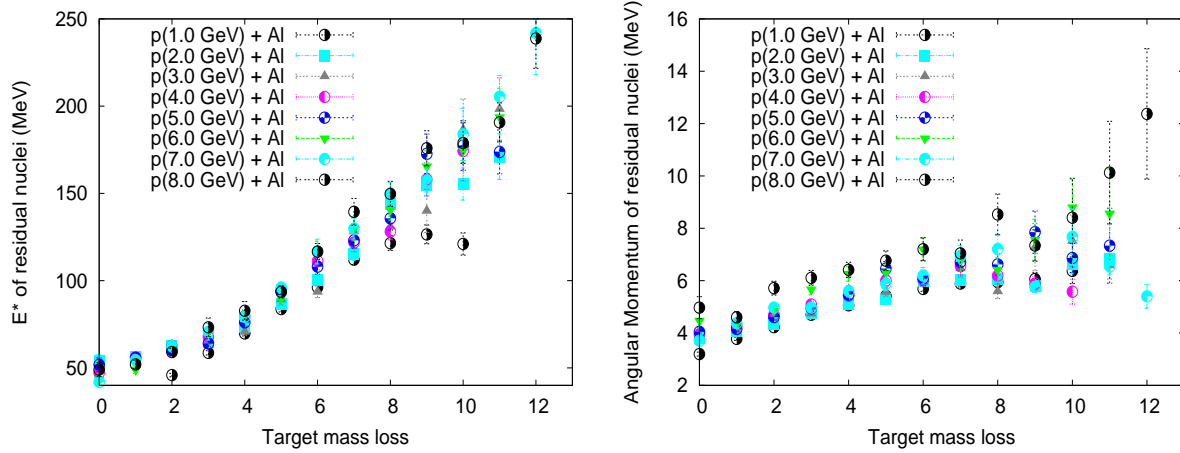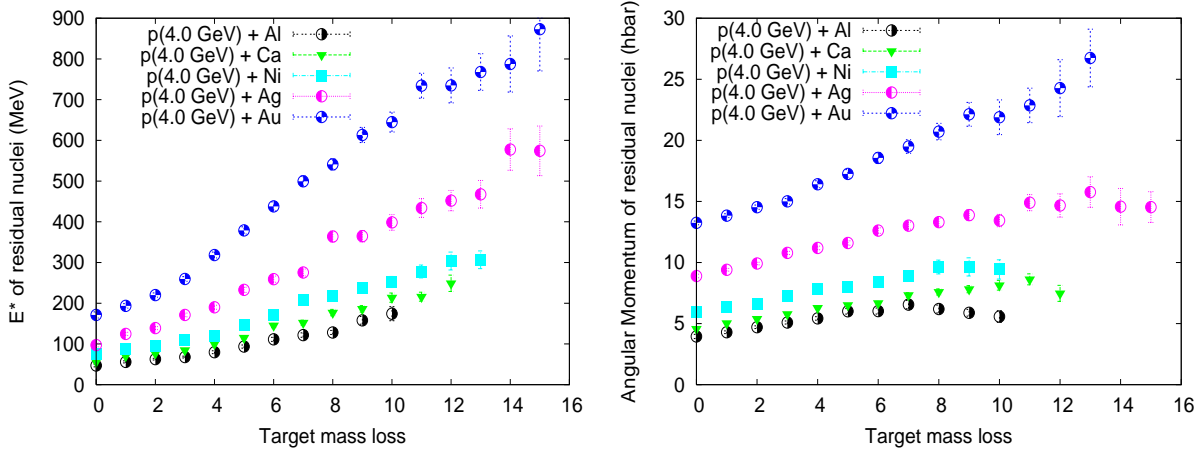

Figure 5.13: *Regression function of excitation energy (left) and angular momentum (right) of residual nuclei on target mass loss, for example p+Al reaction, at several values of incident energy; results of the HSD model calculations (error bars indicate values of standard deviation of average values of excitation energy and angular momentum, respectively, for adequate target mass loss, divided by a square root of number of events)*

Figure 5.14: *Regression function of excitation energy (left) and angular momentum (right) of residual nuclei on target mass loss, for proton induced reactions on Al, Ca, Ni, Ag and Au nuclei, at an example value 4.0 GeV of incident energy; results of the HSD model calculations (error bars indicate values of standard deviation of average values of excitation energy and angular momentum for adequate target mass loss, divided by a square root of number of events)*
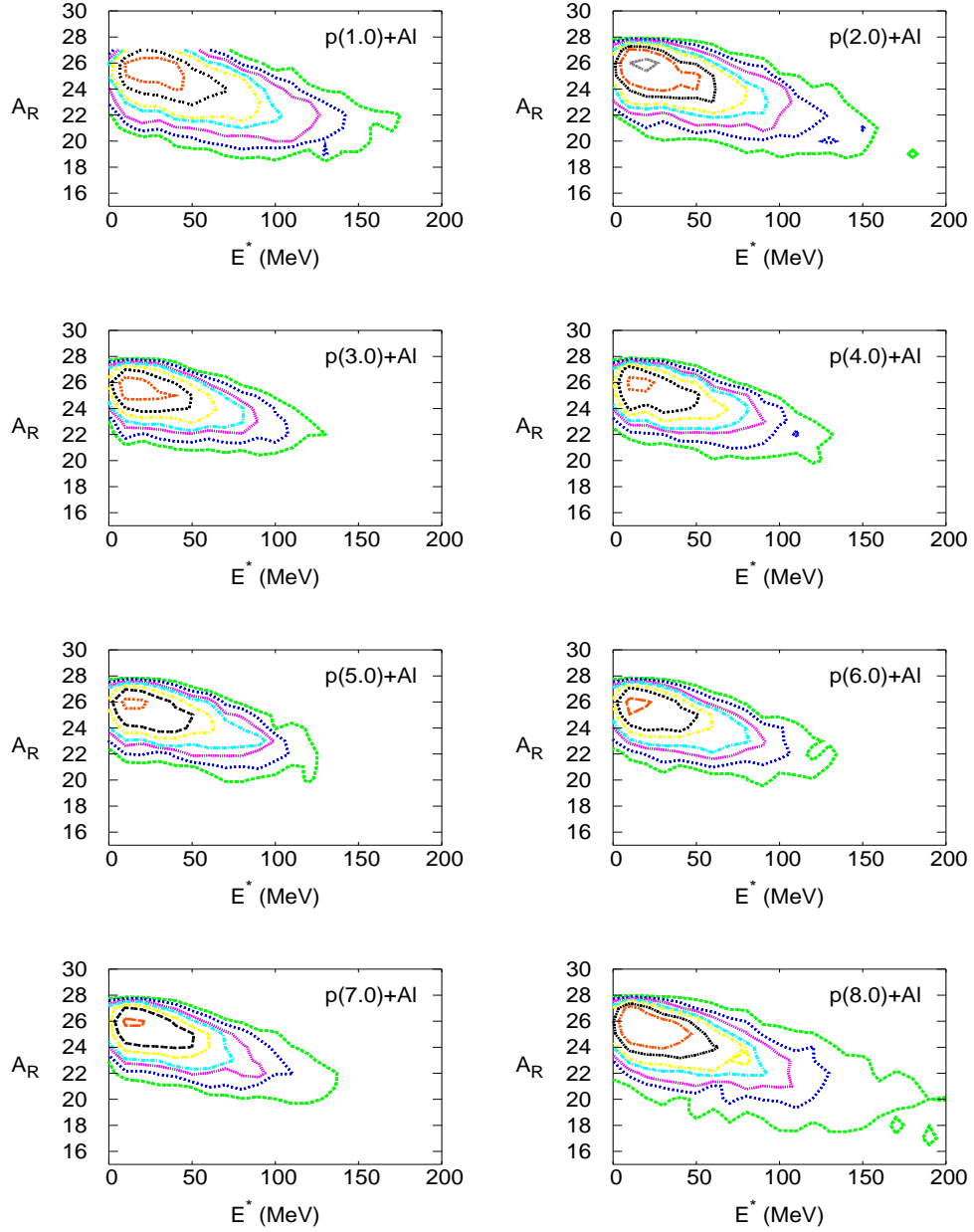
Figure 5.15: *Contour plots of the two-dimensional distributions of excitation energy and mass of residual nuclei at the end of first stage of proton induced reaction on Al target, at several values of incident energy; results of the HSD model calculations (the most central contour line corresponds to a maximum of the distribution, the more and more outer contours correspond to the decrease of a yield)*
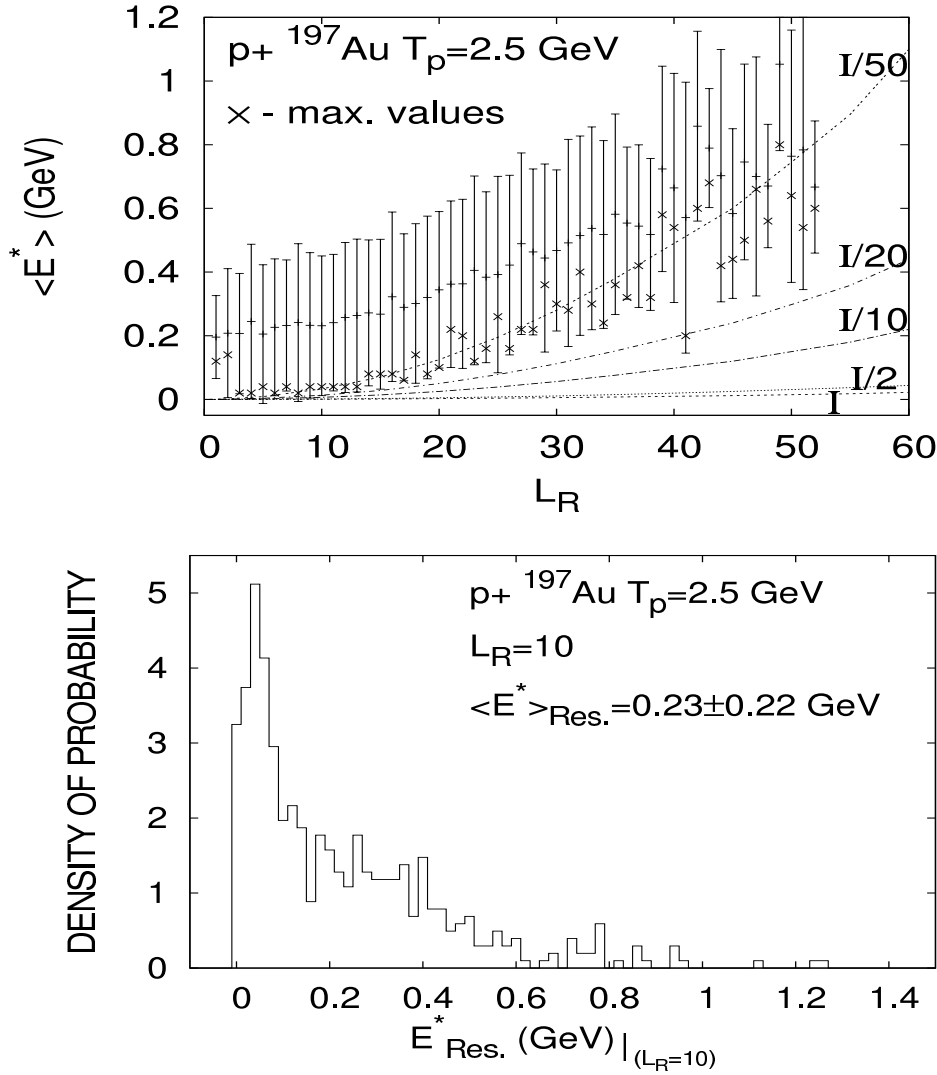
Figure 5.16: *Upper part: regression function of excitation energy on angular momentum of residual nuclei from an example proton induced reaction on Au target, at 2.5 GeV of incident energy; the five lines correspond to the Yrast lines calculated with different values of moment of inertia; lower part: distribution of the excitation energy for a chosen value (10 ℏ) of angular momentum; results of the HSD model calculations*
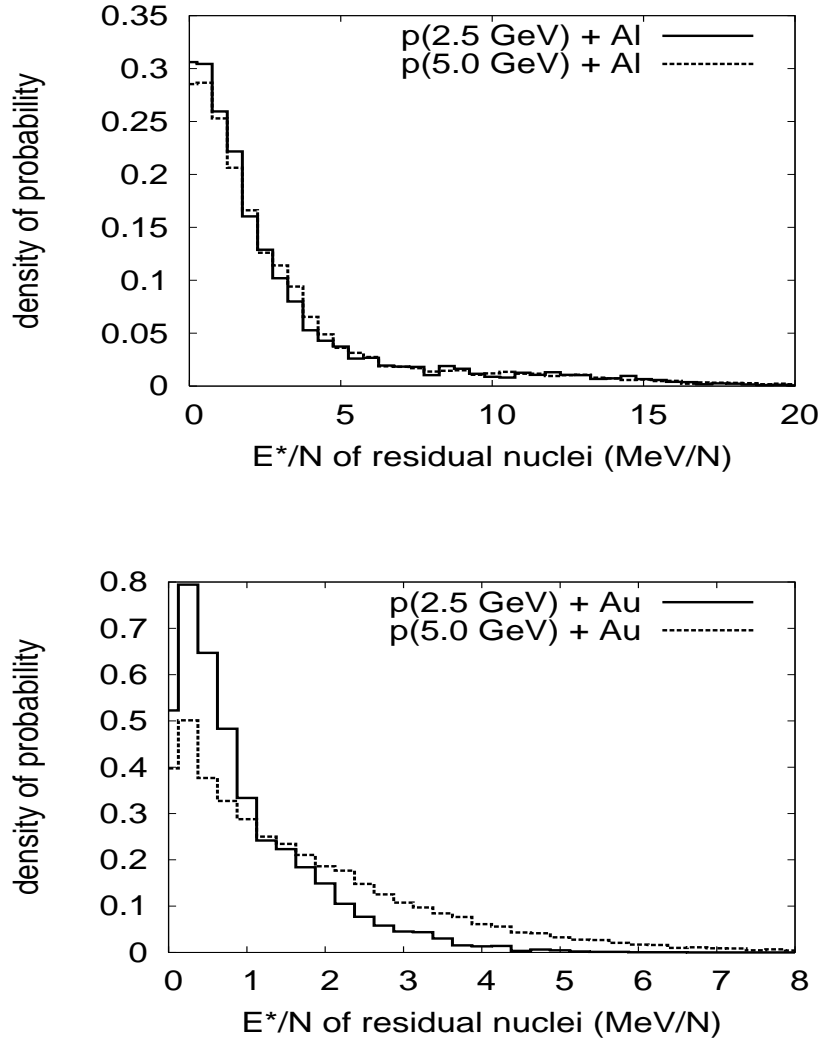
Figure 5.17: *Distributions of excitation energy per nucleon of residual nuclei from an example proton induced reaction on Al and Au target, at 2.5 GeV and 5.0 GeV of incident energy; results of the HSD model calculations*

5.1   Parametrization

It is impossible to measure or even to calculate the reaction of proton of all
energies on all target nuclei. One comes to idea to find a global parametriza-
tion for distributions of excitation energy versus mass of residual nuclei for
some chosen sample of targets and energies, involving finally dependency on
the target mass and projectile energy, in order to have the possibility to in-
terpolate for other energies and targets.
Two-dimensional distributions of excitation energy and mass of residual nu-
clei remaining after first stage of proton induced reaction, on a few targets,
at several projectile energies have been parametrized by a sum of at least
three two - dimensional Gaussians:

$$f(A_R, E^*) = \sum_{i=0,1,2} a_i \cdot exp(-b_i(A_R - A_{R0i})^2 - c_i(E^* - E_{0i}^*)^2) \qquad (5.1)$$

where: a_i stands for heights of the Gaussians, b_i and c_i - define widths in
A_R and E^* directions, likewise A_{R0i} and E_{0i}^* - the mean position of the
Gaussians in A_R and E^* directions, respectively. Example results of such
parametrization are presented in Figures 5.18 and 5.19. It is seen, that the
distributions, calculated with the HSD model, are very well described by a
sum of Gaussians (5.1).

Values of parameters of the Gaussians evolve rather smoothly with inci-
dent energy and mass of target nuclei. Example results of parametrization
of such dependences are presented in Figures 5.20 and 5.21.

Using the parametrizations, two-dimensional distributions of excitation
energy versus mass of residual nuclei could be obtained for any value of pro-
jectile energy and target nuclei from the chosen ranges, for the considered
cases. In order to verify the parametrization, interpolated distributions have
been compared to results of the HSD calculations. Comparisons of distri-
butions for example p+Al reaction at 2.5 GeV beam energy (interpolation
of parameters in function of projectile energy, see Fig. 5.20) and p+Zr re-
action at 2.0 GeV beam energy (interpolation of parameters in function of
mass of target nuclei, see Fig. 5.21) are presented in Fig. 5.22. Obtained
results are satisfactory. This indicates possibility of realization of such a
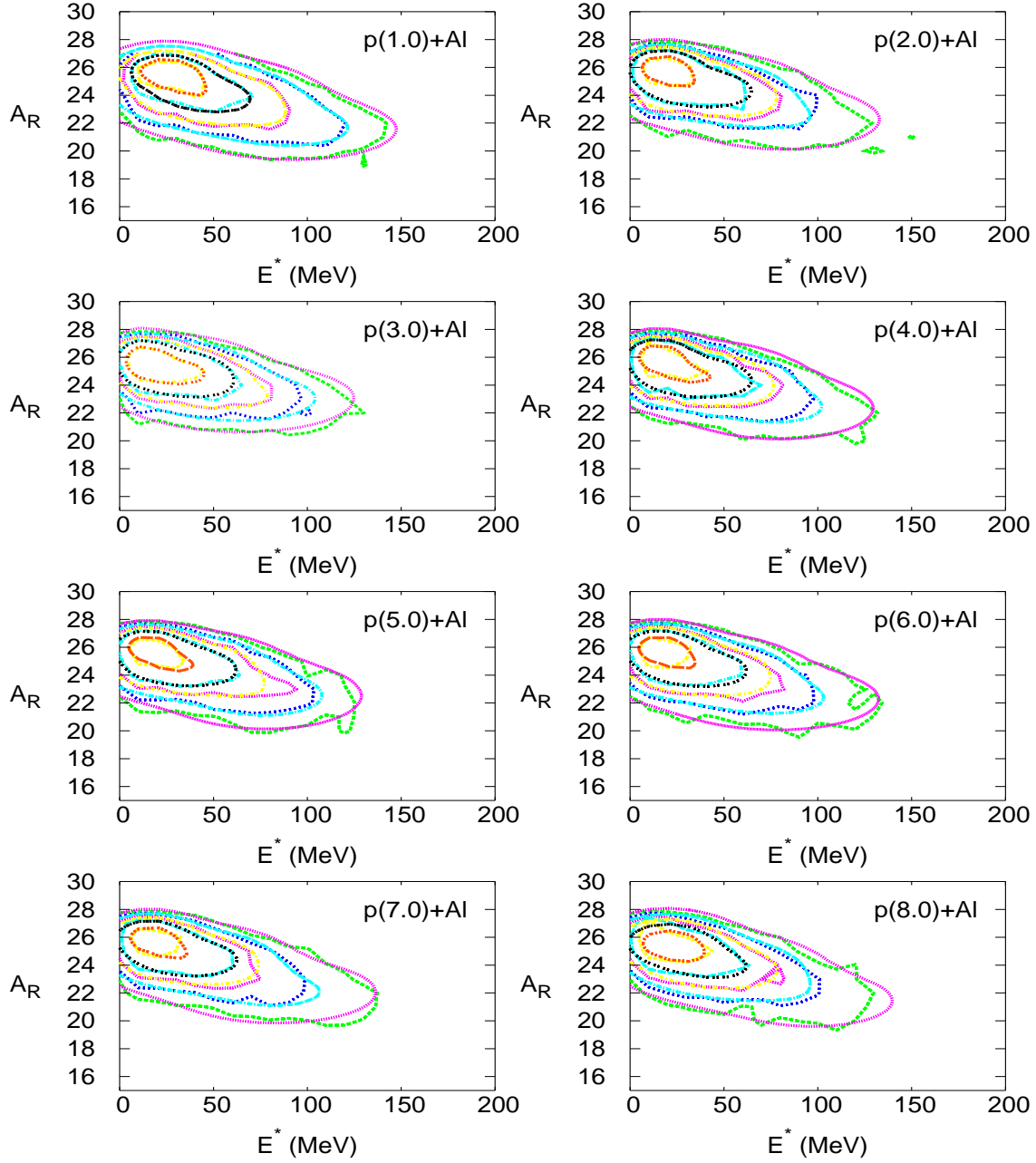parametrization for other target nuclei and other incident energies.

Figure 5.18: *Contour plots of the two-dimensional distributions of excitation energy and mass of residual nuclei in p+Al reactions, at several values of beam energy; jagged lines correspond to results of the HSD model calculations, smooth lines define parametrization (the most central contour line corresponds to a maximum of the distribution, the more and more outer contours correspond to the decrease of a yield)*
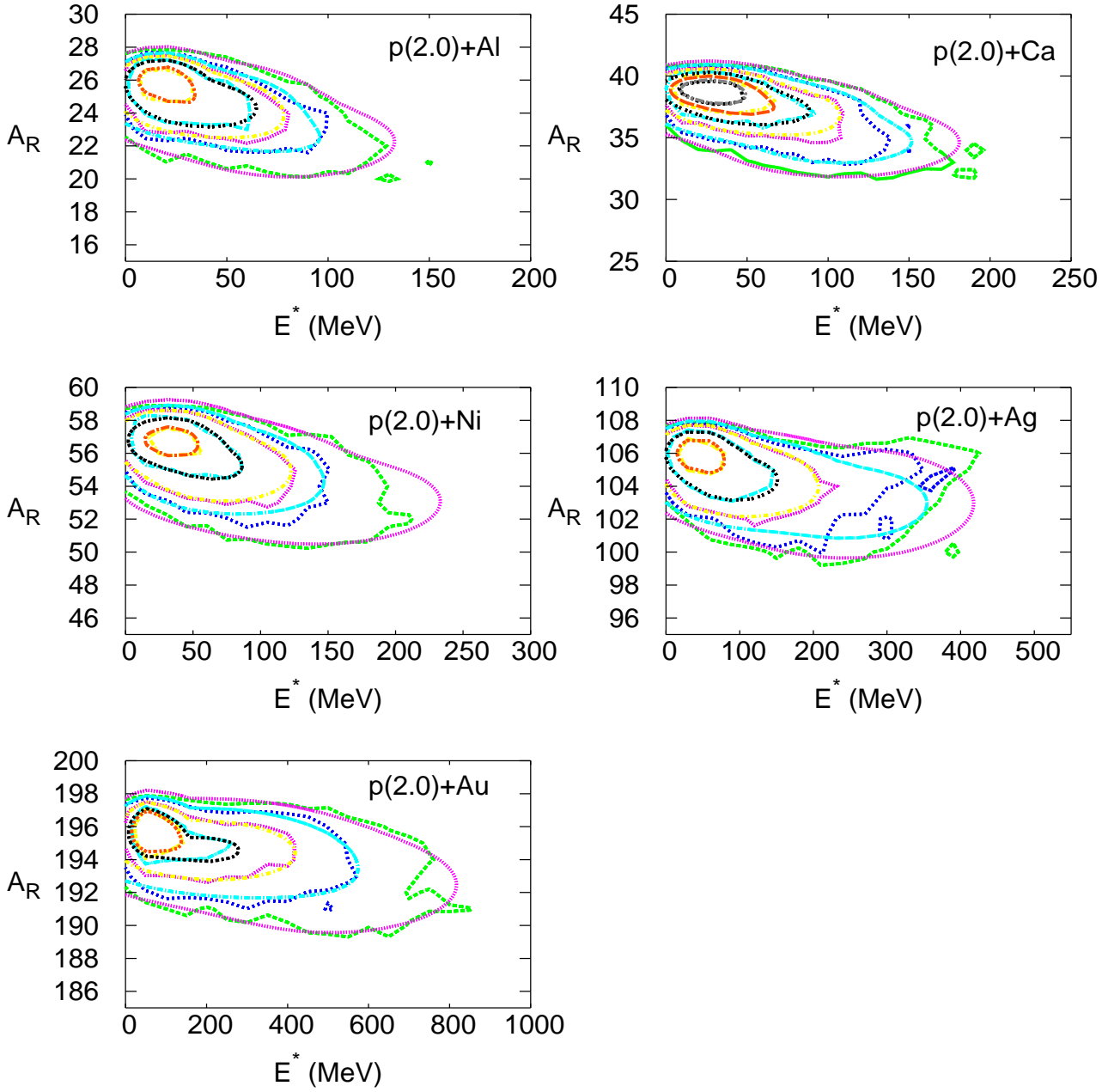
Figure 5.19: *Contour plots of the two-dimensional distributions of excitation energy and mass of residual nuclei in 2.0 GeV proton induced reaction on different targets; jagged lines correspond to results of the HSD model calculations, smooth lines define parametrization (the most central contour line corresponds to a maximum of the distribution, the more and more outer contours correspond to the decrease of a yield)*
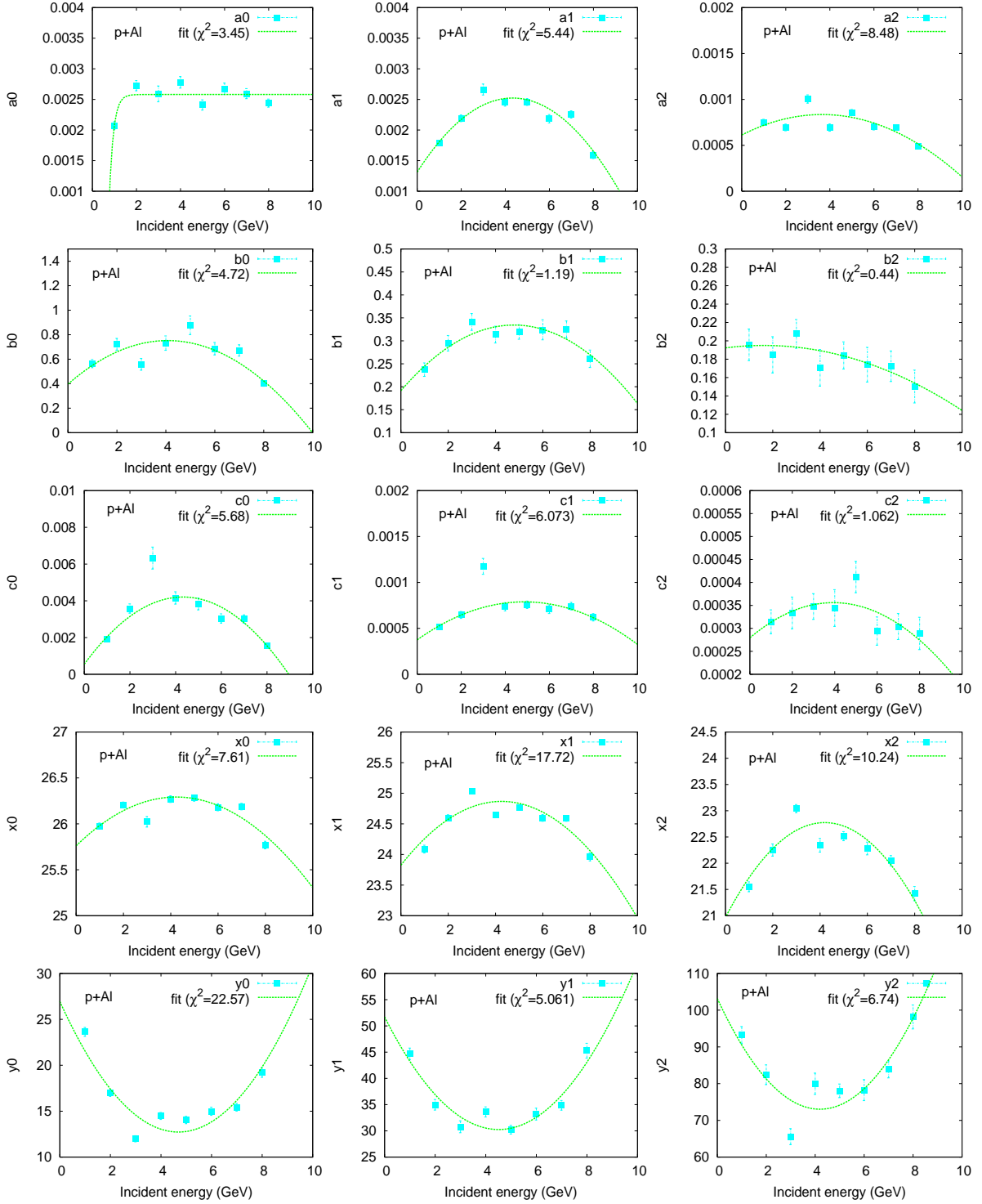
Figure 5.20: *Parametrization of values of the Gaussians parameters as function of incident energy for the p+Al reaction; e.g. $A_{R01} \equiv x1$, $E^*_{01} \equiv y1$, see formula 5.1 (χ^2 means chisquare per degree of freedom)*
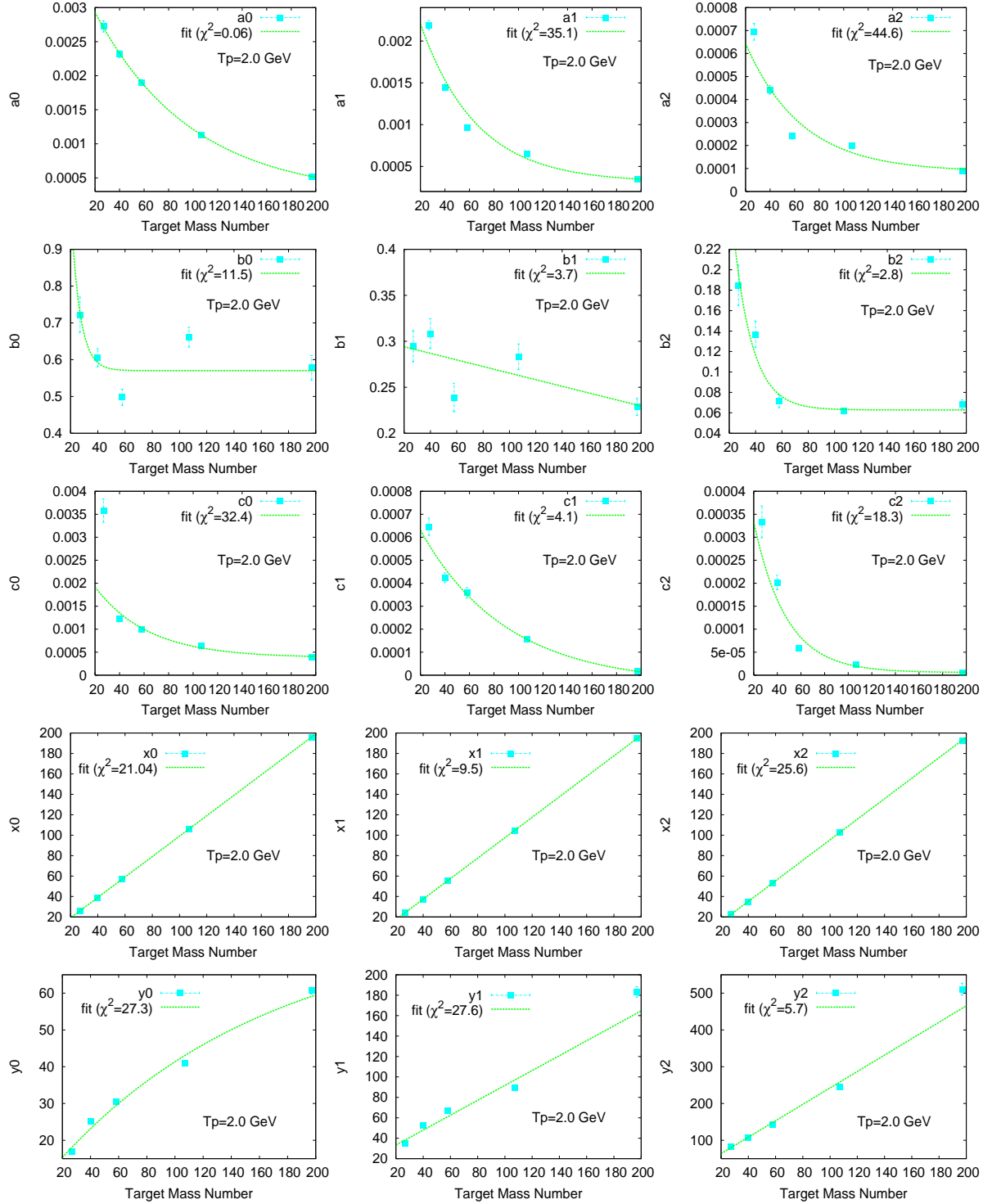
Figure 5.21: *Parametrization of values of the Gaussians parameters as function of target mass number for the 2.0 GeV proton induced reaction; e.g. $A_{R01} \equiv x1$, $E_{01}^* \equiv y1$, see formula 5.1 (χ^2 means chisquare per degree of freedom)*
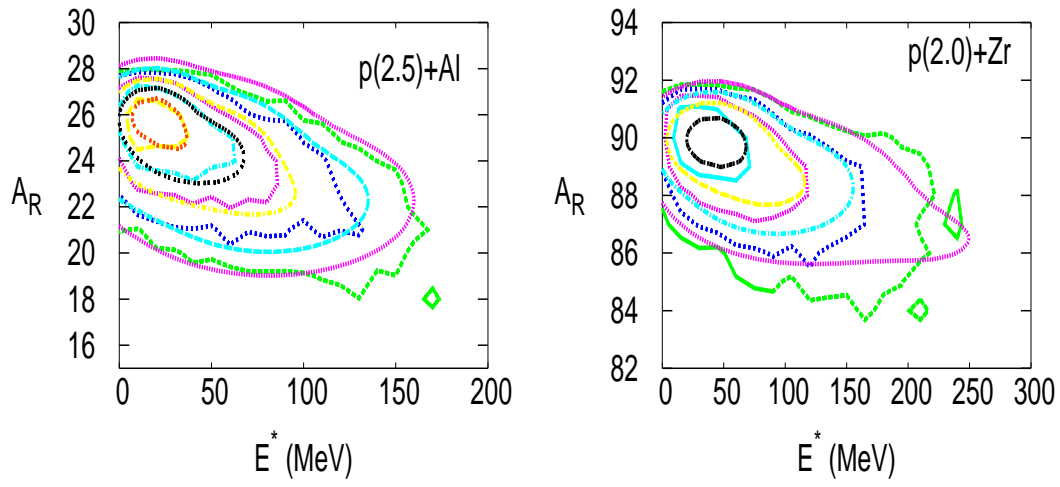
Figure 5.22: *Comparison of interpolated distributions and results of the HSD calculations (smooth and jagged lines) for example p+Al reaction at 2.5 GeV beam energy and p+Zr reaction at 2.0 GeV beam energy*

Chapter 6

Pion spectra

Pions are the most abundantly produced mesons during proton induced reactions on atomic nuclei. Creation of pions is very important process in the reactions due to the fact that they carry away significant part of four-momentum introduced by incoming particle during the first stage of the reaction. This is because pion mass (~ 140 MeV) is small enough to allow for copious production of pions in nucleon-nucleon collisions even at low beam energies, and large enough to contribute significantly to the energy and momentum transfer.

It should be emphasized that in spite of the fact that momentum carried away by pions is several times smaller than appropriate momentum of nucleons (see e.g. the energy balance presented in Sec. 8.1), the contribution of pions to the momentum and energy transfer may be comparable to that of nucleons. This is because pions, due to the low production threshold can be produced and reabsorbed several times during the reaction (threshold for charged pion production in free nucleon - nucleon collision is equal to about 289 MeV; inside nucleus, it can be decreased even up to about 141 MeV [56], due to the Fermi motion). Thus they influence the whole dynamical evolution of the reaction. Proper treatment of pion production and absorption may be crucial for realistic estimation of excitation energy and other properties of residual nuclei after the fast cascade of nucleon - nucleon collisions.

Calculations of the first stage of the reaction are sufficient in order to receive realistic pion spectra, since all pions are produced only in violent nucleon - nucleon collisions, where the locally available amount of four-momentum is large enough.

One can distinguish two components in pion angular and energy distributions: high energy anisotropic part, i.e. pions emitted dominantly in forward direction and isotropic part consisted of low energy thermal pions emitted in the whole angular range (0° - 180°).

Pions emitted from the first chance NN collisions have high energy, whereas those from secondary collisions are less energetic. Building up of pion spectra in time is presented in Figures 6.1 and 6.2. Typical momentum distributions of pions emitted from 1.0 GeV proton induced reaction on Al target are shown; P_Z corresponds to the momentum in beam direction. The time evolution of pion distributions is depicted more precisely in the Fig. 6.2, where double differential kinetic energy spectra of pions produced during the example reactions on light (Al) and heavy (Au) target, at low (1.0 GeV) and higher (2.5 GeV) projectile energy are displayed. It is seen, that in case of 1.0 GeV proton induced reactions, high energy anisotropic part of pion distribution is formed first. Then, the isotropic part is built up. Formation of the low energy part of pion spectra takes longer time, since it is result of several acts of absorption and emission of pions. In the Fig. 6.2, all produced pions at the chosen reaction time are plotted, at further time some of them can be absorbed or absorbed and re-emitted in other direction, so the number of presented pions can be lower than at ealier time. After 35 fm/c, all presented pions are emitted. The number of produced pions is higher in case of 2.5 GeV proton induced reactions. Pion distributions are evolving with reaction time only slightly. At fixed energy of incident protons, pions produced on heavy target are more abundant than those produced on light target and low energy pions are dominant. Pion on its way can be several times absorbed and emitted (its mean free path is equal to 1.0 - 1.5 fm), its initial direction could be changed and its energy is suppressed. So, it is much more difficult for pion to be emitted in forward direction in case of heavy target, where it has to pass a longer distance inside nuclear matter. Therefore, high energy pions emitted in forward direction dominate in case of light target. Quantitative comparison of yield of the produced pions is displayed in Table 6.1. It is noteworthy, that almost all of the pions have been produced due to Delta resonance decay; only a very few pions have been produced due to N(1440) decay.

Spectra of pions change significantly with projectile energy. It is seen in Fig. 6.3, where examplary distributions of transversal (P_T) versus longitudinal (P_Z) momentum of neutral pions emitted during proton induced reaction on Ni target are plotted for various incident energies. These are results of HSD model calculations, where P_Z corresponds to the pion momentum in beam direction and P_T is defined as $P_T = \sqrt{P_X^2 + P_Y^2}$.
It can be seen, how the evolution of pion spectra looks like with increase of incident energy. At low projectile energies pions have not enough energy to pass through a target nucleus, so they cannot be emitted in forward direction. In this case, only a small part of target is accessible for pions, the

Table 6.1: *Time evolution of multiplicity of pions from p+Al and p+Au reaction at 1.0 GeV and 2.5 GeV proton beam energy, results of the HSD model calculations*

	p(1.0 GeV)+Al			p(2.5 GeV)+Al		
	π^-	π^0	π^+	π^-	π^0	π^+
15 fm/c:	0.067	0.18	0.29	0.38	0.51	0.50
20 fm/c:	0.071	0.18	0.29	0.37	0.47	0.47
35 fm/c:	0.069	0.17	0.26	0.37	0.47	0.46
	p(1.0 GeV)+Au			p(2.5 GeV)+Au		
	π^-	π^0	π^+	π^-	π^0	π^+
15 fm/c:	0.010	0.045	0.060	0.35	0.46	0.41
20 fm/c:	0.085	0.19	0.26	0.53	0.60	0.52
35 fm/c:	0.11	0.17	0.23	0.49	0.53	0.46

rest of nucleus corresponds to the so-called *nuclear shadow*. Higher pion momenta are associated with increasing incident energy. With increase of the incident energy, the anisotropic part of distribution increases. It means, more and more pions have chance to be emitted in forward directions. The isotropic, low - momentum part of pion spectra at high projectile energy corresponds to thermal pions, which result from sequence of several absorptions and emissions. One should also notice that at high projectile energies (in the Fig. 6.3 - higher or equal to 2.0 GeV), the isotropic part of pion momentum spectra is symmetric around $P_Z = 0$. At low projectile energies (in the Fig. 6.3 - less than 2.0 GeV), the isotropic part of spectra, i.e. the most central contour line corresponding to a maximum of distribution is not symmetric around $P_Z = 0$, but shifted to negative values of P_Z; to large extent it is due to mentioned nuclear shadow. The isotropic part of pion spectra that consists of thermal pions has the Maxwell distribution. This is illustrated by Fig. 6.4, where the experimental distribution of negative pions, measured by Cochran et al. [57] at backward direction (150°), is presented. The following form of Maxwell function has been used for the parametrization:

$f(E_{\pi^-}) = A_0 \cdot ((E_{\pi^-} + m_{\pi^-})^2 - m_{\pi^-}^2) \cdot e^{-E_{\pi^-}/T_0}$

where: E_{π^-} and m_{π^-} are the kinetic energy of the pions and their mass, respectively. A_0 and T_0 are fitted parameters. The following values of the parameters are obtained: $A_0 = 11476.1 \pm 364.5$ [GeV^{-3}] and $T_0 = 0.024 \pm 0.00039$ [GeV].

It is interesting to see, how the average yield of pions produced in proton induced spallation reactions changes with projectile energy and mass of
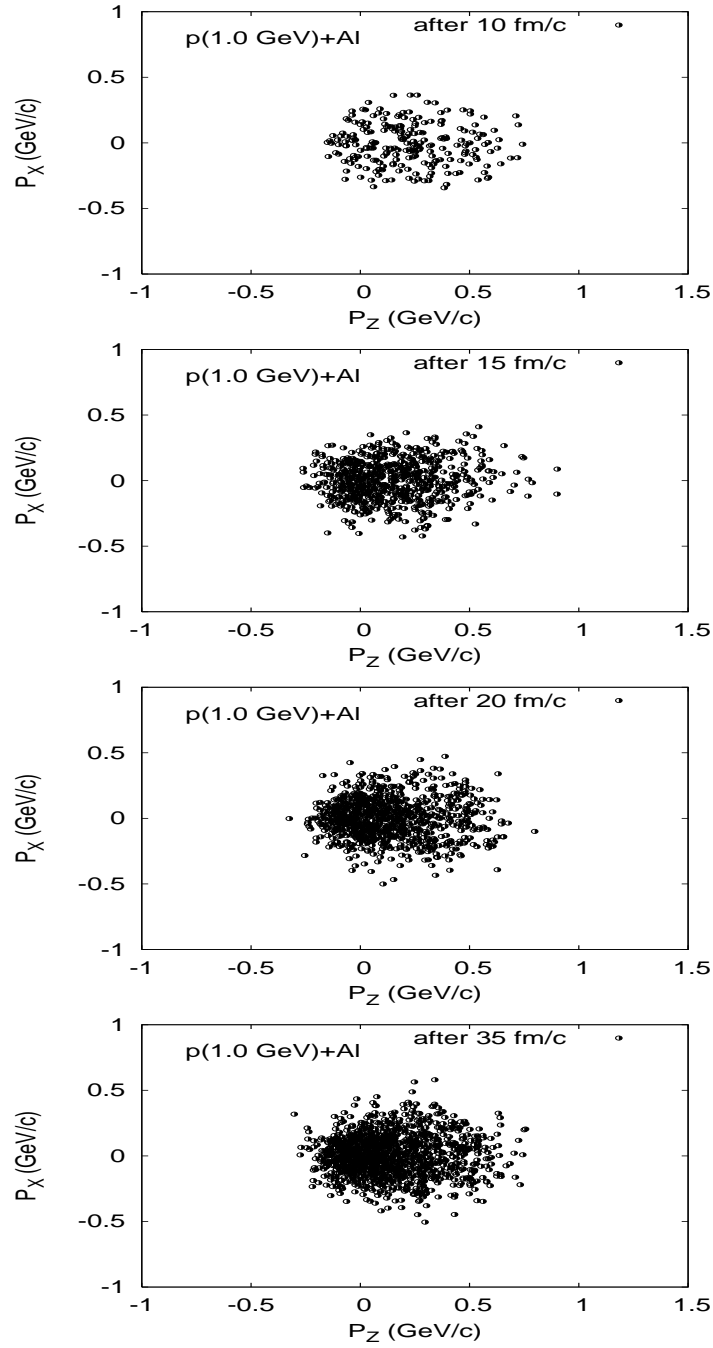
Figure 6.1: *Momentum distributions of pions emitted during p+Al reaction, at 1.0 GeV beam energy; P_Z corresponds to momentum in beam direction; results of the HSD model calculations (scatter plot)*
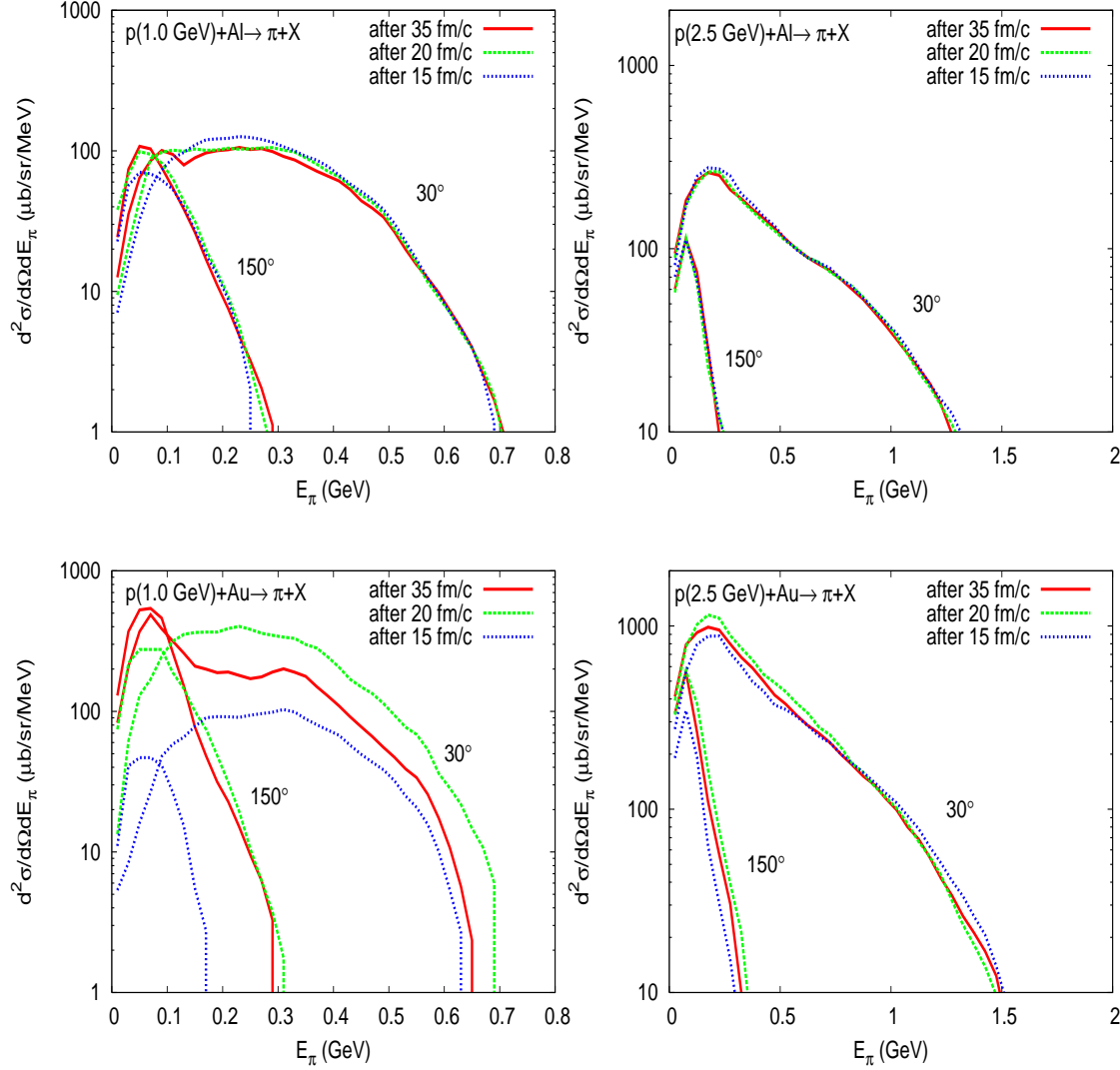
Figure 6.2: *Double differential kinetic energy spectra of all kind pions pro-
duced during p+Al and p+Au reactions, at 1.0 GeV and 2.5 GeV proton
beam energy; results of the HSD model calculations*

target. The HSD model calculations predict that multiplicity of pions, in
average, increases both with incident energy and mass of target. One can
expect that due to charge conservation, the relative yield of produced pions
should fulfill the relation: $\pi^+ > \pi^0 > \pi^-$. The incident energy dependence
(presented in Fig. 6.5) shows, that positive and neutral pion production is
favoured, as expected. For heavier targets, where there are more collisions,

multiplicity of positive pions decreases and for the heaviest target it is even lower than multiplicity of neutral and negative pions, as displayed in Fig. 6.6. The target mass dependence shows, that reabsorptions and secondary collisions play an important role, especially for heavy targets.

Looking at kinetic energy carried by individual emitted pions, it is seen (Fig. 6.5, right) that all kinds of pions produced in proton induced reactions on a chosen target carry, in average, the same amount of kinetic energy. The higher energy of the incident proton, the bigger amount of kinetic energy carried out by pions. In reactions on heavier targets (Fig. 6.6), emitted pions carry away, in average, less kinetic energy. In case of the heaviest targets, the negative pions take the least kinetic energy of all pions. The suppression of kinetic energy of emitted pions from heavier target is an expected result of numerous possible reabsorptions and emissions of pions, which become less and less energetic.

Inclusive differential kinetic energy spectra of pions emitted at different angles, calculated with the HSD model, have been confronted with available experimental data [57], as displayed in Fig. 6.7, for an example distributions of negative pions from p+Pb reaction, at 0.73 GeV of incident energy. One finds, that the calculations overestimate the experimental data. It is evident, that the pion dynamics in the HSD model needs to be improved, i.e. the number of produced pions should be reduced. Pions are created mainly due to decay of Delta(1232) resonances. It means, pions production and absorption proceeds mainly through the $NN \leftrightarrow N\Delta$ and $\Delta \leftrightarrow \pi N$ reactions (see description of the model in Chapter 3). Therefore, modifications of the cross section for the absorption of Delta resonance in reaction $N\Delta \rightarrow NN$ and the Delta lifetime should influence the amount of produced pions. In order to estimate the influence, the following corrections have been tested. First, the Delta resonance lifetime has been enlarged. Comparison of the pion spectra calculated with HSD model, with enlarged Delta resonance lifetime and the experimental data [57] is presented in Fig. 6.8 (the calculations are performed with 30 times longer lifetime of Delta resonance). It is seen, that this correction reduces number of pions emitted mainly in backward directions. This is due to the fact, that longer lifetime of Delta resonance implies smaller number of acts of absorption and emission of pions. If the cross section for the absorption of Delta resonance in reaction $N\Delta \rightarrow NN$ is enlarged (by factor 20), the number of pions emitted in forward directions is reduced, as it is shown in Fig. 6.9. Implementation of both of the corrections reduces the amount of produced pions both in forward and backward directions, as presented in the Fig. 6.10 (these are results of calculations performed with 30 times longer lifetime of Delta resonance and the cross section for its absorption enlarged by a factor 1.5). The improvement of agreement between

Table 6.2: *Multiplicity of pions from p+Au reaction at 0.73 GeV and 2.5 GeV proton beam energy, without any corrections and with enlarged cross section for the absorption of Delta resonance in reaction $N\Delta \rightarrow NN$ and enlarged Delta resonance lifetime*

	Tp = 0.73 GeV		Tp = 2.5GeV	
	without corrections	with corrections	without corrections	with corrections
π^+:	0.15	0.073	0.46	0.43
π^0:	0.11	0.053	0.54	0.48
π^-:	0.065	0.024	0.49	0.43

the data and model results is substantial, however, the introduced modifications are rather drastic. (Improvement of pion dynamics by modifications of Delta resonance lifetime and cross section for Delta absorption has been also performed in frame of the INCL model in [58], but obtained results also do not comply well with experimental data). Furthermore, it is tested, that the influence of the joined corrections on the pion spectra depends on the value of proton beam energy. The higher beam energy, the lower reduction of the pions yield by the corrections, as it is seen in Figs. 6.11 and 6.12, for spectra of pions produced in p+Au reaction, at low (0.73 GeV) and higher (2.5 GeV) beam energy, respectively. The quantitative distinction of the pions yield from the reactions at two different incident energies are collected in Table 6.2. It has been also verified that implemented corrections do not modify yield and shape of spectra of nucleons. Moreover, the corrections do not influence the properties of residual nuclei after the first stage of reaction. In particular, they do not change excitation energy of the remnants, because the average energy carried out by emitted pions with and without the corrections is the same; due to the corrections less pions are emitted, but they carried, in average, more kinetic energy.

The not very satisfactory agreement between calculations and experimental data is not too surprising, because pion production in proton - nucleus collisions is a complicated process. Although the elementary cross sections for pions production due to free nucleon - nucleon interactions are measured and very well known (see e.g. [59]), in-medium problem appears. In the HSD model, the in-medium effects are partly included through e.g. employment of the Pauli principle and cross section for Delta absorption. However, proper handling of modifications due to in-medium effects are hampered by a lack of experimental and theoretical knowledge.

Pion production mechanism is highly sensitive to pion and Δ - resonance dynamics. So, apart from tested above modifications of the Δ parameters, also introduction of density dependent width of Δ - resonance (increasing with density), introduction of pion potential, change of an angular distribution in order to describe possible anisotropic Δ decay into πN channel, etc. can influence the pions production. In fact, till now none of the trials have given satisfactory results, see [60, 61]. The propriety of description of pions dynamics and production due to proton - nucleus reaction could not be really verified, because experimental data are rather scarce, especially in projectile energy range of a few GeV order.

There exists also one more reason that influences the calculated pion spectra. In the HSD model, a target nucleus, i.e. the nuclear density distribution is constructed up to a constant limit $R + R_{CUT}$, where: $R = 1.12 \cdot A^{1/3}[fm]$ is a radius of nucleus, defined as a distance at which the value of nucleus density decreases to a half of the value of density in the center of nucleus; A is a mass number of the nucleus; $R_{CUT} = 1.5 fm$. This is due to difficulties with modelling of the infinite tail of nuclear density at nucleus surface, see [62]. Although the truncated part corresponds to only a small fraction of the whole nucleus density distribution, it can influence the pion spectra. This is because only pions produced close to the surface have a chance to be emitted, as the mean free path of pions is equal to about 1.0 - 1.5 fm, at standard density. The introduced cut off of nuclear surface neglects the possibility of further pion - nucleon interactions at surface, which are quite probable (since pion is a strongly interacting particle) and lead to spuriously higher multiplicity of emitted pions. The nucleus density cut off does not influence nucleons production, because most of nucleons are emitted closer to the center of nucleus, due to the fact that their mean free path is equal to about 3.0 fm. Therefore, the HSD model description of proton induced spallation reaction is not falsified by the used limited distribution of density of target nuclei, only outgoing pion distributions are to some extent misshapen.
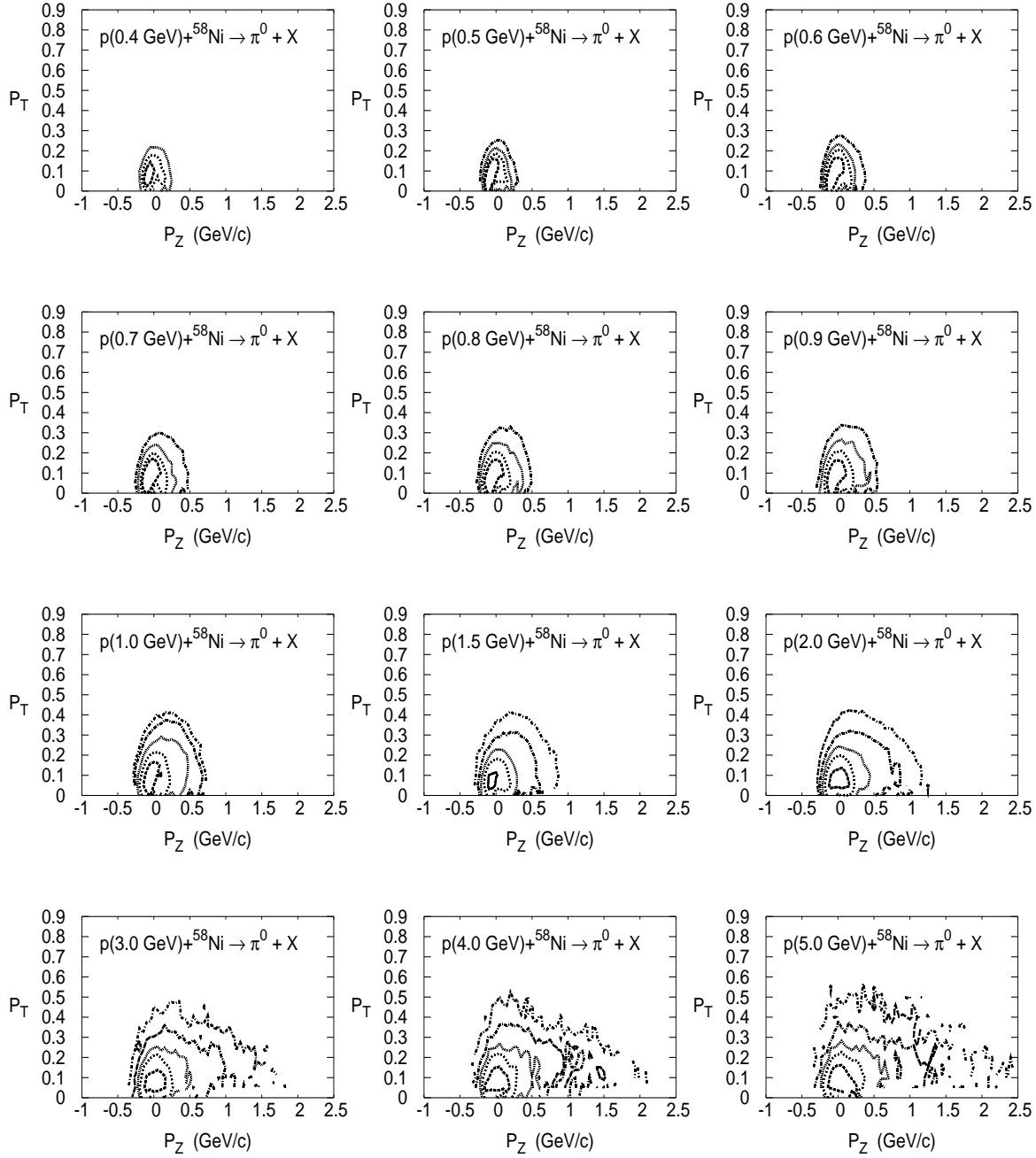
Figure 6.3: *Two-dimensional distributions of transversal versus longitudinal momentum of neutral pions emitted during proton induced reaction on Ni target, at various incident energies; results of the HSD model calculations (the most central contour line corresponds to a maximum of distribution)*
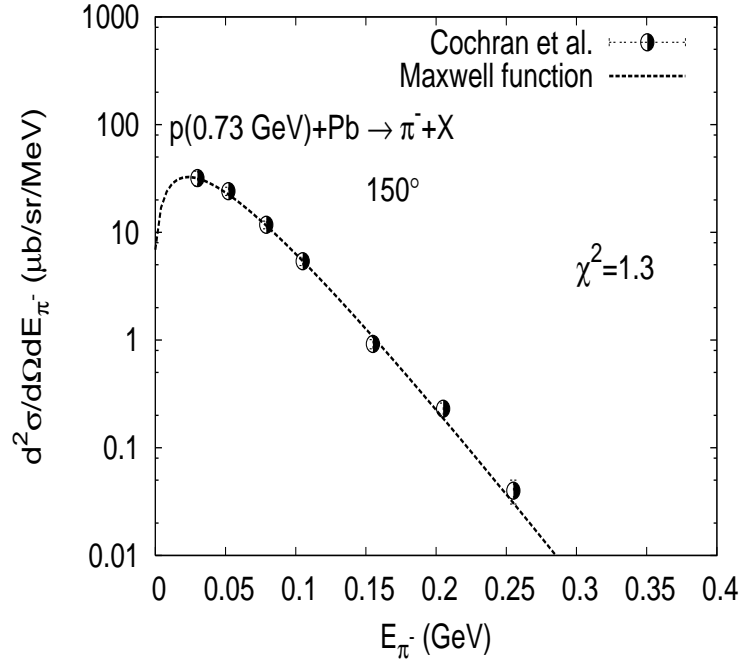
Figure 6.4: *Kinetic energy experimental spectrum of negative pions emitted in backward direction in p+Pb reaction, at 0.73 GeV proton energy, measured by Cochran et al. [57], parametrized by Maxwell function*
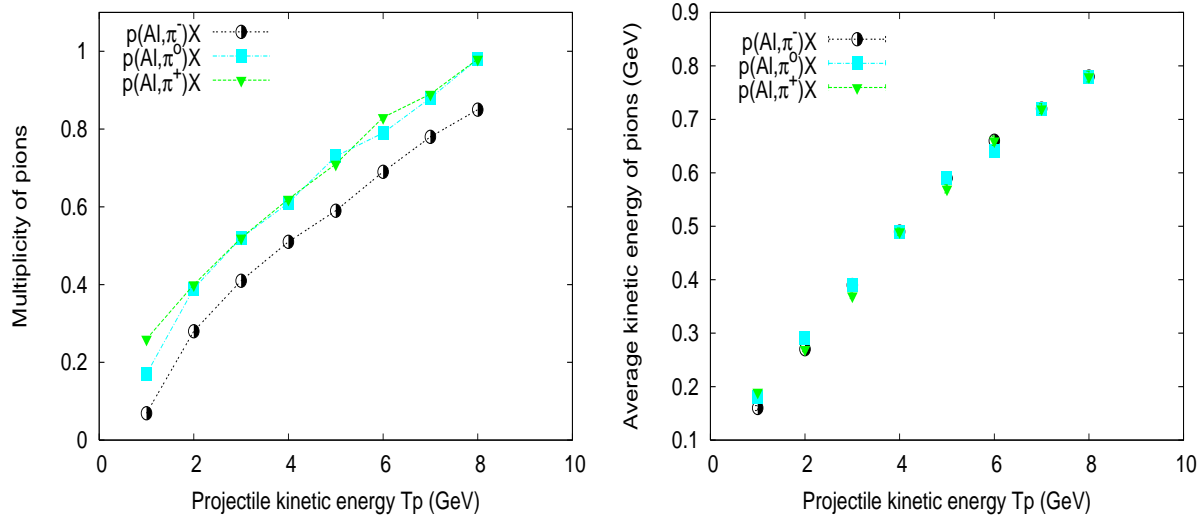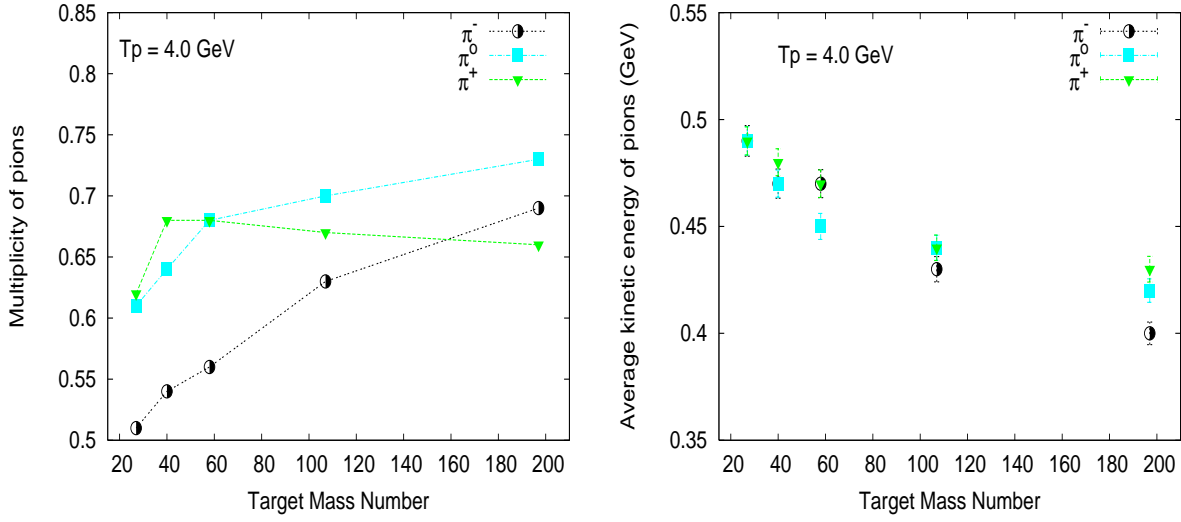

Figure 6.5: *Multiplicity (left) and average values of kinetic energy per individual pion (right) of pions emitted during proton induced reaction on Al target, in function of incident energy; results of the HSD model calculations (error bars indicate values of standard deviation of the average values, divided by a square root of number of events)*
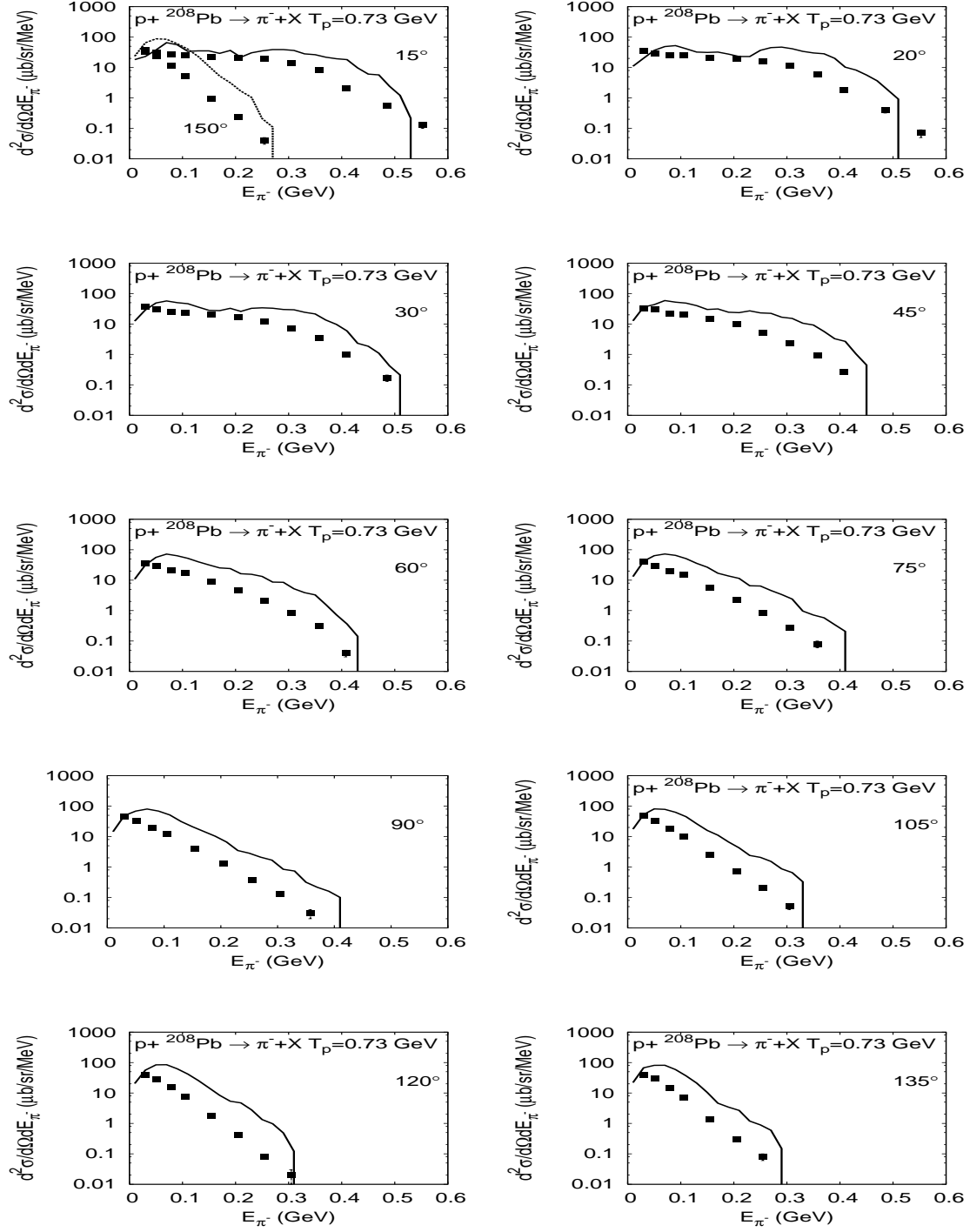
Figure 6.6: *Multiplicity (left) and average values of kinetic energy per individual pion (right) of pions emitted during 4.0 GeV proton induced reactions on a few targets, in function of target mass number; results of the HSD model calculations (error bars indicate values of standard deviation of the average values, divided by a square root of number of events)*

Figure 6.7: *Double differential negative pion spectra from p+Pb reaction at 0.73 GeV proton beam energy; lines show results calculated with HSD model, symbols indicate the experimental data [57]*
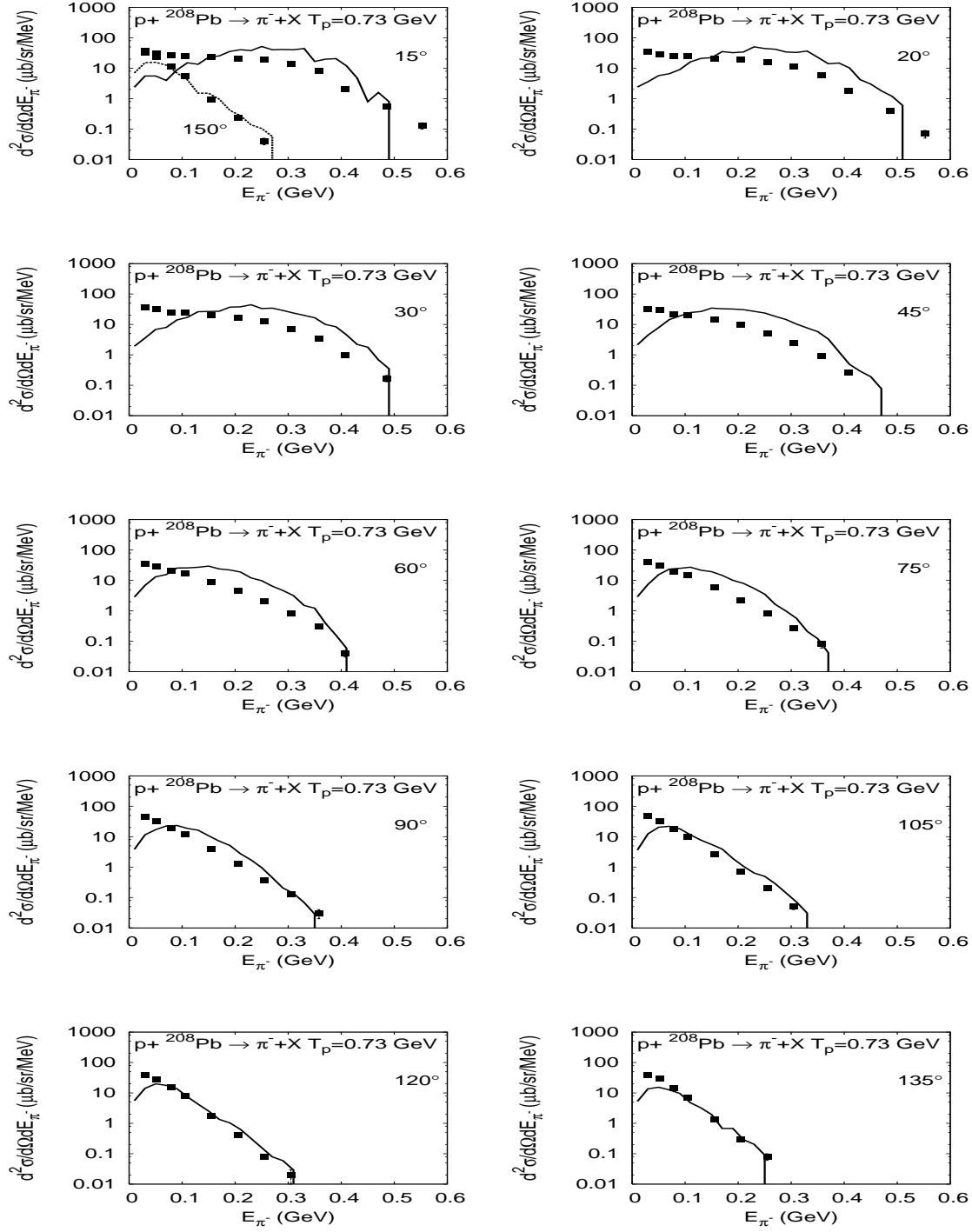
Figure 6.8: *Double differential negative pion spectra from p+Pb reaction at 0.73 GeV proton beam energy; lines show results calculated with HSD model, with enlarged Delta resonance lifetime, symbols indicate the experimental data [57]*
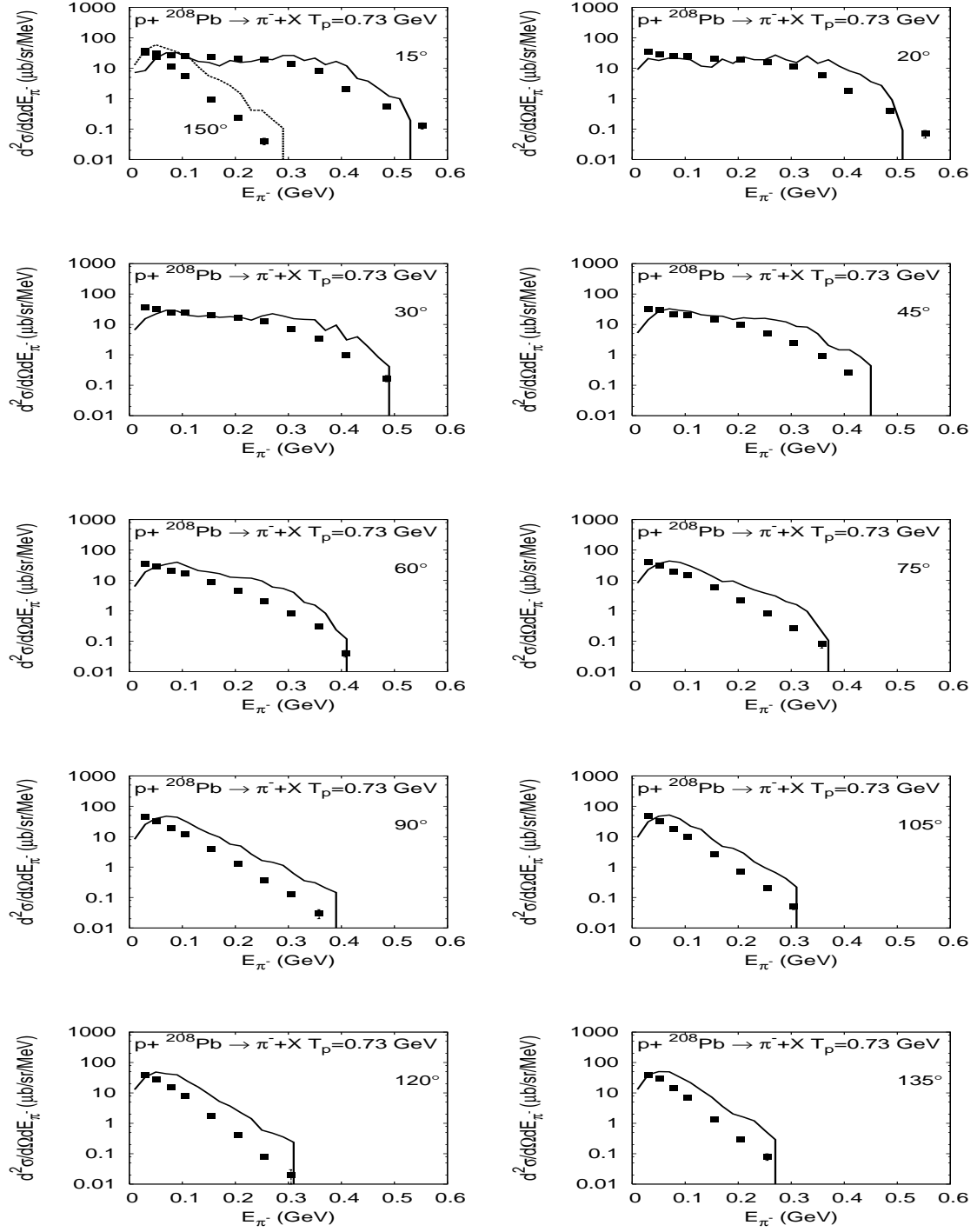
Figure 6.9: *Double differential negative pion spectra from p+Pb reaction at 0.73 GeV proton beam energy; lines show results calculated with HSD model, with enlarged cross section for the absorption of Delta resonance in reaction $N\Delta \to NN$, symbols indicate the experimental data [57]*
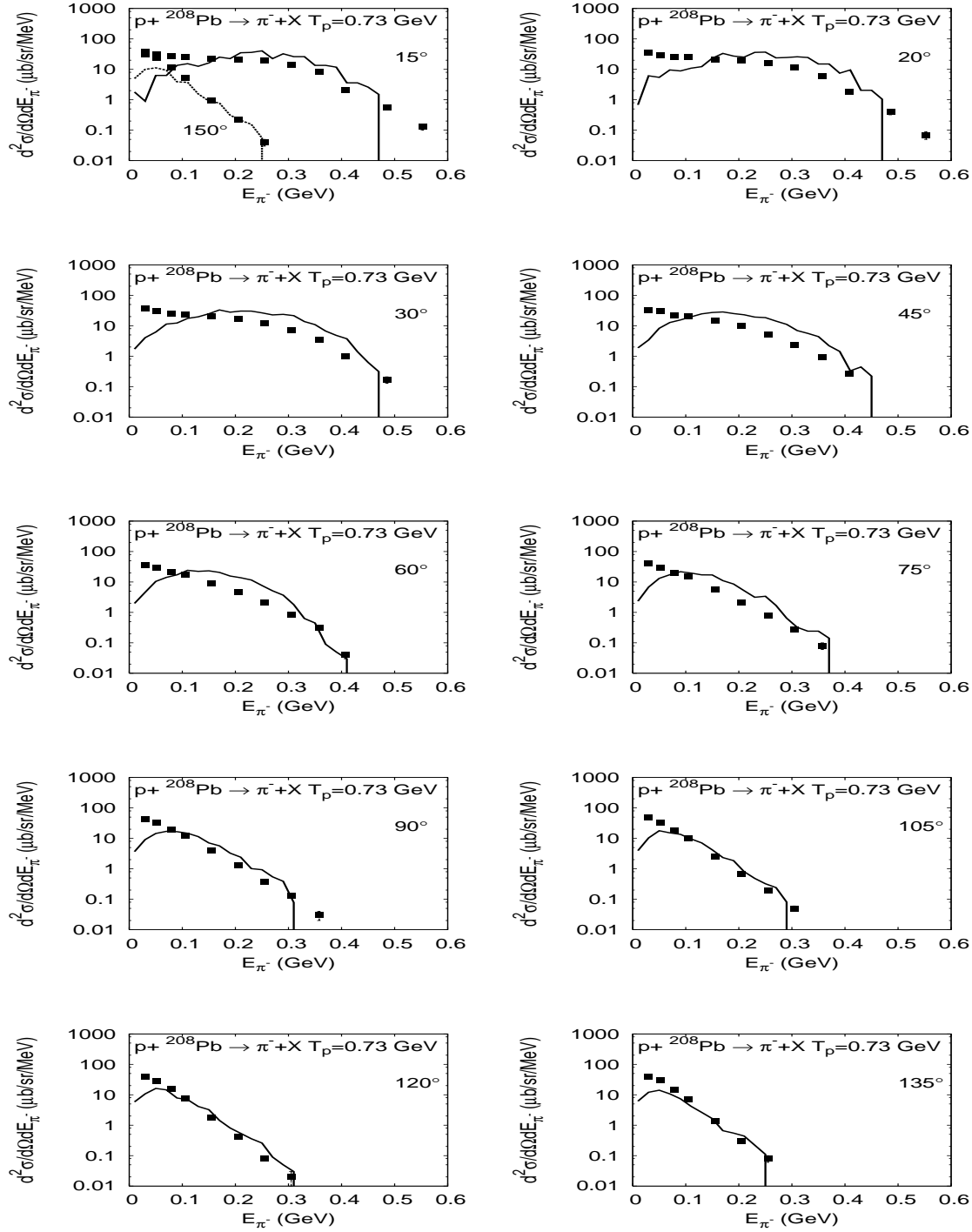
Figure 6.10: *Double differential negative pion spectra from p+Pb reaction at 0.73 GeV proton beam energy; lines show results calculated with HSD model, with enlarged both cross section for the absorption of Delta resonance in reaction $N\Delta \to NN$ and Delta resonance lifetime, symbols indicate the experimental data [57]*
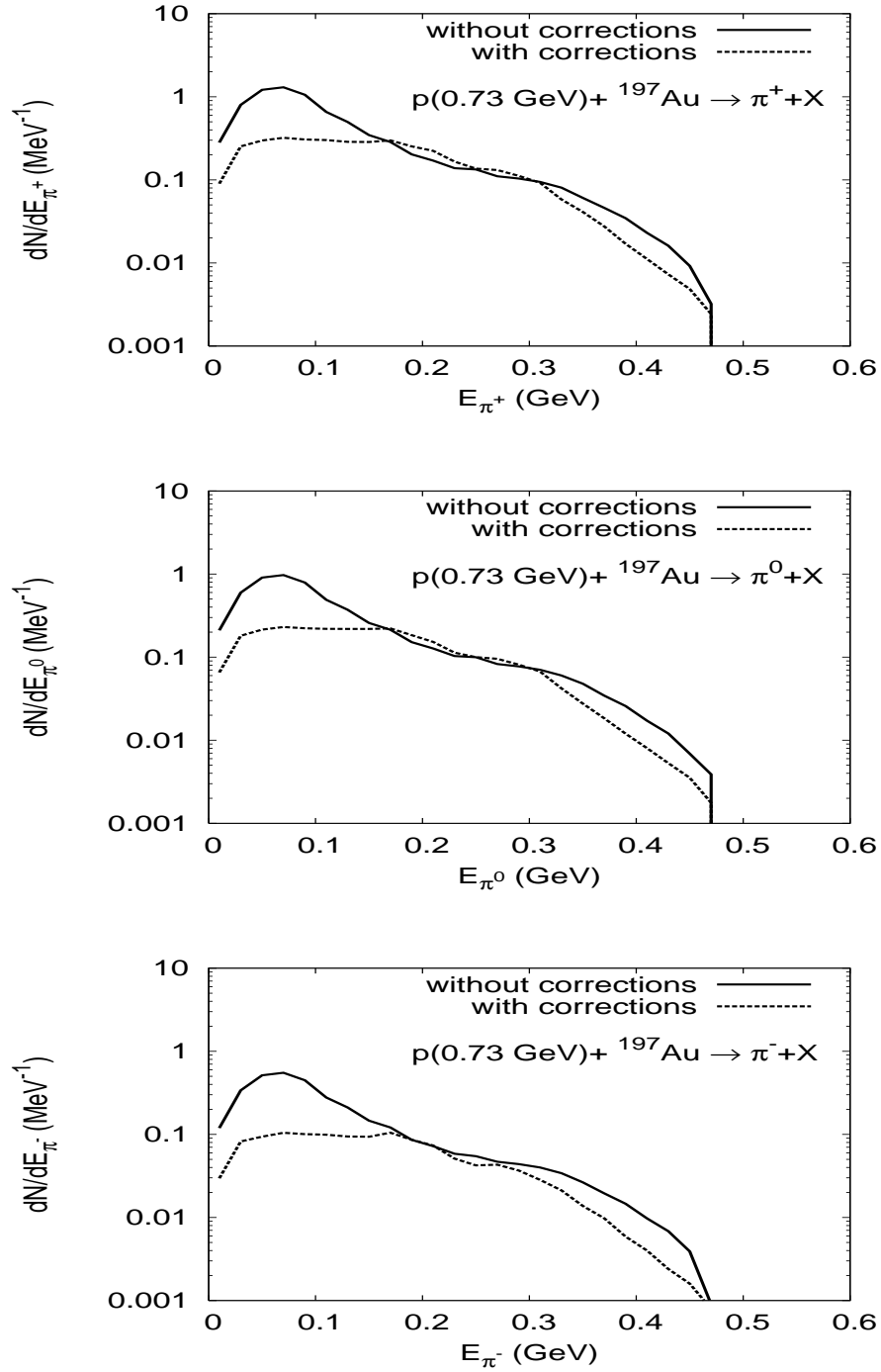
Figure 6.11: *Pions kinetic energy spectra from p+Au reaction at 0.73 GeV proton beam energy; solid lines show results calculated with HSD model, without any corrections, dashed lines show results calculated with enlarged cross section for the absorption of Delta resonance in reaction $N\Delta \rightarrow NN$ and enlarged Delta resonance lifetime*

Figure 6.12: *Pions kinetic energy spectra from p+Au reaction at 2.5 GeV proton beam energy; solid lines show results calculated with HSD model, without any corrections, dashed lines show results calculated with enlarged cross section for the absorption of Delta resonance in reaction $N\Delta \rightarrow NN$ and enlarged Delta resonance lifetime*
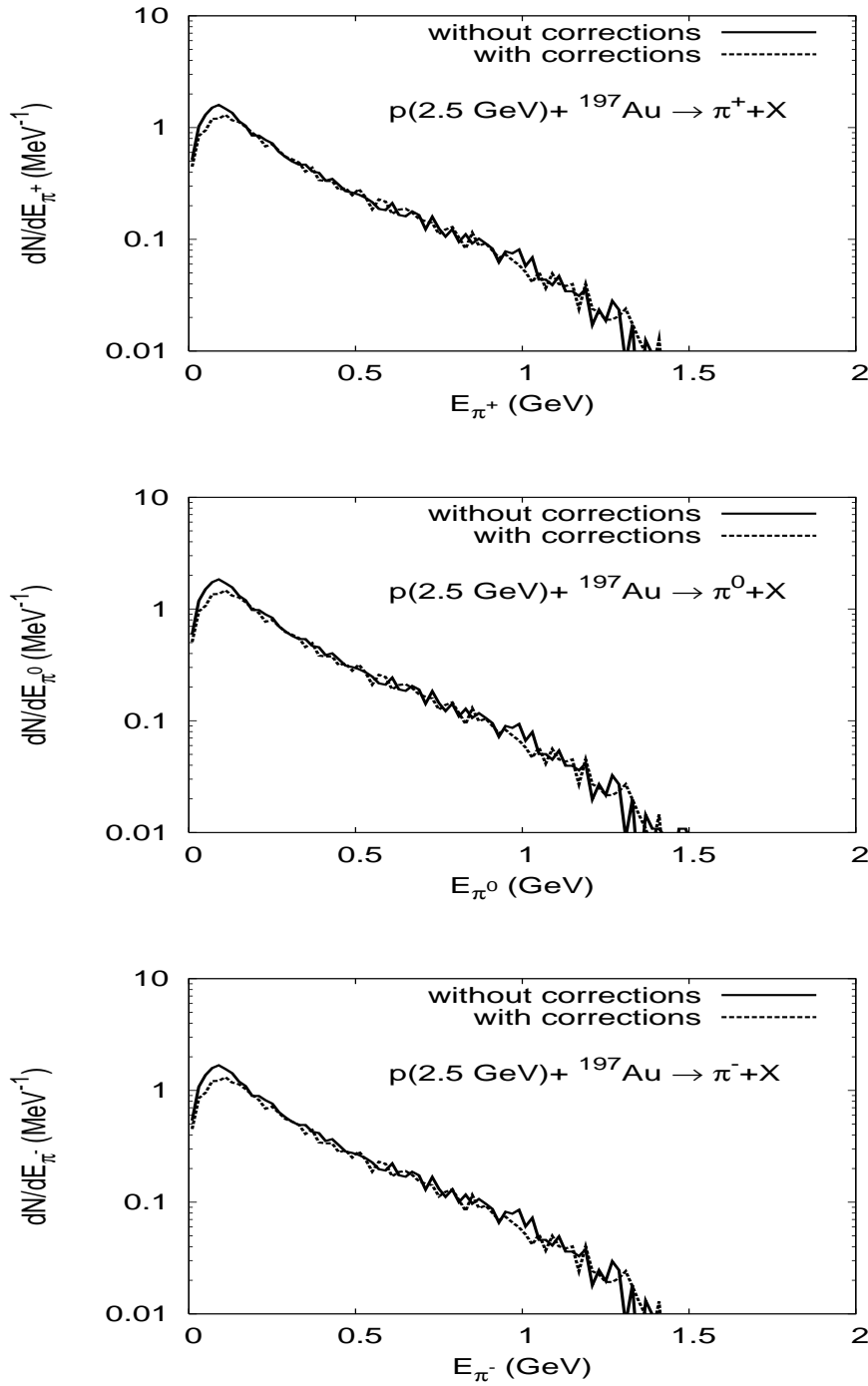
Chapter 7

Statistical emission of particles in the second stage of proton - nucleus collisions

The second stage of proton - nucleus reaction can be theoretically described with various statistical models. Historical origin of the models is related to Weisskopf's paper published in 1937 [4]. Weisskopf considers emission (evaporation) of a neutron with kinetic energy E_k from nucleus A, excited to energy E_A, transforming it to nucleus B, with excitation energy $E_B = E_A - B_n - E_k$. Probability of such emission is calculated using the principle of detailed balance. It can be determined if cross section for the inverse process $\sigma(E_A, E_k)$ is known (i.e. cross section for production of compound nucleus by collision of a neutron with nucleus B). The probability is expressed as:

$$W_n(E_k) = \sigma(E_A, E_k) g m E_k \omega_B(E_B) / \pi^2 \hbar^3 \omega_A(E_A) \qquad (7.1)$$

where: m stands for neutron mass, g is a spin degeneracy factor, ω_A and ω_B are the level densities of the initial and final nuclei, respectively.
In the Weisskopf expression, angular momentum effects are not taken into account. In order to consider the effects, one needs to use the Hauser-Feshbach formalism [63]. In this case, the decay probability is determined by level density $\rho(E_f, J_f)$ of the residual nucleus, depending both on its excitation energy E_f and angular momentum J_f, and transmission coefficient of emitted particle $T_l(E_k)$ (l is the orbital angular momentum removed by the particle, E_k is its kinetic energy).
Decay width Γ for state of energy E and angular momentum J into a specific

channel i is expressed as:

$$\Gamma_i(E, J) = D(E, J)/2\pi \sum_{I,l,J_f} \delta(I+l+J_f-J) \int_0^{E-BE_i} T_l(E_k)\rho_i(E-BE_i-E_k, J_f)dE_k$$

$$(7.2)$$

where: $D(E, J)$ is the level spacing (reciprocal of the level density) of the decaying nucleus, I stands for the particle spin. The following energy and angular momentum conservation constraints are employed:

$J = I + l + J_f$,

$E = E_f + E_k + BE_i$, where BE_i is the binding energy of the emitted particle in decay channel i.

The decay probability into channel i is evaluated as: Γ_i/Γ_{tot}, where: $\Gamma_{tot} = \sum_i \Gamma_i$, i runs over all open channels.
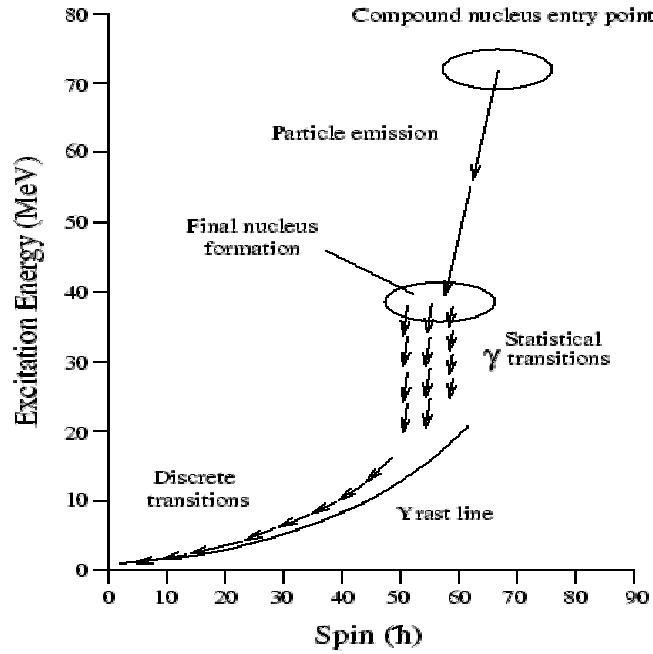

Figure 7.1: *The Statistical Evaporation Process*

Important step to comprehensive understanding of the dependence of the level density on angular momentum of compound nucleus was done by J. R. Grover [64]. He invented the "Yrast level" term to describe the lowest lying level at some given angular momentum. It means, that for any angular momentum J the nucleus has to have an excitation energy at least equals to the rotational energy $E_{rot}(J)$. Therefore, there cannot be any states with

excitation energy below $E_{rot}(J)$, i.e. below "Yrast level". Particle decay is inhibited close to the "Yrast line" (i.e. the level density is close to zero for the final states allowed by energy and angular momentum conservation). Deexcitation proceeds mainly by gamma emission along the "Yrast line", as illustrated in Fig. 7.1.

In the frame of this work, calculations of the second stage of proton - nucleus reactions have been done with use of PACE2 [20] and GEM [21] codes. Below, basic features and results of the models are presented.

7.1   Evaporation model - PACE 2

The statistical model code PACE2 (**P**rojection **A**ngular-Momentum **C**oupled **E**vaporation, version 2) [20] is based on the Hauser-Feshbach formalism. The decay sequence of an excited nucleus is calculated with use of a Monte Carlo procedure, which is followed until the nucleus reaches its ground state. At each stage of deexcitation, the decay probability is determined by calculating decay width for neutron, proton, alpha and gamma. Final states differ in excitation energy, angular momentum, nucleon number A and proton number Z.

The model contains several parameters, which has to be fixed. The main ingredients of the code are the level density and transmission coefficients. The level density $\rho(E, J)$, at a specific value J, is given by:

$$\rho(E, J) = (2J + 1)\omega(E - E_{rot}(J)) \tag{7.3}$$

where: $\omega(E)$ is the total level density at excitation energy E, evaluated according the following formula (given by Weisskopf for Fermi gas, see Ref. [4], [65]):

$$\omega(E) \approx exp[2(aE)^{1/2}] \tag{7.4}$$

with level density parameter $a = const$ (its dimension is MeV^{-1}).

For selecting the rotational energy contribution, $E_{rot}(J)$, model of A. J. Sierk [66] is used.

The transmission coefficients T_l are calculated with use of default potentials; for protons and neutrons taken from Perey and Perey [67], for alpha particles from Igo and Huizenga [68]. As the nucleus decays, it is assumed that transmission coefficients of charged particles are shifted in their kinetic energy dependence: $E_k - V_c(A, Z)$, where A and Z are the nucleon and proton numbers of the emitting nucleus, and V_c is the Coulomb barrier for the emitted particle.

Table 7.1: *Multiplicity of particles evaporated from excited Au nucleus, with excitation energy equal to 100 MeV and different values of angular momentum; results of the PACE2 model calculations*

	$0\ \hbar$	$10\ \hbar$	$20\ \hbar$
n:	7.80	7.80	7.70
p:	0.076	0.080	0.070
^{4}He:	0.031	0.031	0.031

Fission of the excited nuclei is also taken into account. The fission barrier of Sierk is used [66].

Gamma emission is considered statistically using $E1$, $E2$, $M1$ and $M2$ transition intensities.

7.2   Generalized Evaporation Model

Another model used for the Monte Carlo simulations of the second stage of the spallation reaction is the Generalized Evaporation Model (GEM), developed by S. Furihata [21], based on the Weisskopf-Ewing approach [4, 69]. In the GEM model, 66 nuclides up to Mg are included as ejectiles, not only the dominant particles emitted from an excited nucleus (i.e. nucleons and helium isotopes), as it is in the PACE2. The accurate level density function is used for deriving the decay width of particle emission, instead of an approximate form, as used in the PACE2 model (see the previous Section). Additionally, depending on the excitation energy and mass of the decaying nucleus, different parametrizations of the level density $\rho(E)$ are applied, see Ref. [21].
In the GEM model, contrary to the PACE2, the dependence of the level density on the angular momentum is neglected. Nevertheless, negligible difference between spectra of evaporated particles, calculated with the PACE2 model, with zero and non-zero values of angular momentum of emitting nuclei, has been noticed, as displayed in Fig. 7.2. Adequate multiplicities of evaporated particles, calculated with the PACE2 model, with different values of angular momentum of emitting nucleus are collected in Table 7.1.
Spectra of evaporated particles (nucleons and ^{4}He) calculated with the PACE2 and GEM models are in good agreement, as shown in Fig. 7.3 for an example Au nucleus, with the excitation energy set to 100 MeV and zero value of angular momentum. Adequate multiplicities of the emitted particles are collected in Table 7.2.

Table 7.2: *Multiplicity of particles evaporated from excited Au nucleus, with excitation energy equal to 100 MeV; results of the GEM and the PACE2 model calculations*

	GEM	PACE2
n:	8.86	7.80
p:	0.17	0.076
^{4}He:	0.029	0.031

Results of the GEM model calculations are very sensitive on the used level density parameter a [21]. There is a possibility to use a parameter equal to a quotient of mass of emitting nucleus and a constant number $a = A/const$ MeV^{-1} (see formula 7.4), where $const \approx 5 \div 20$ (see Ref.[6, 70]) or one can use the precise Gilbert - Cameron - Cook - Ignatyuk (GCCI) level density parametrization with the energy dependence taken into account, see Ref.[21, 71]. Dependence on the used method of level density parametrization is noticeable e.g. in multiplicities and spectra of evaporated particles. Comparison of spectra of various isotopes evaporated during the second stage of an example p+Au reaction, at 2.5 GeV beam energy, results of the GEM model calculations, with the different level density parameters are presented in Figures 7.4 and 7.5. It is seen from the Figures, that distributions of light particles (isotopes of hydrogen and helium) calculated with different level density parameters are very similar. Contrary, distributions of heavier isotopes (lithium, beryllium, etc.) differ significantly. Use of the GCCI level density parameter gives much higher abundance of the heavier isotopes, than use of the simple $a = A/8$ parameter. Moreover, calculations with the $a = A/20$ parameter result with even higher abundance than with the GCCI level density parameter. Adequate multiplicities of the evaporated particles are collected in Table 7.3. It is seen from the Figures, that choice of level density parameter affects not only heights of the spectra, but influences also their slopes. In the frame of the work, the GCCI level density parameter is used (confrontation with experimental data leads to conclusion, that use of the GCCI level density parameter gives the most reliable results).

Table 7.3: *Multiplicity of particles evaporated during p+Au reaction, at 2.5 GeV proton beam energy, calculated with the GCCI, a = A/8 and a = A/20 level density parameter*

|	GCCI	$a = A/8$	$a = A/20$
n:	14.78	14.90	9.016
p:	1.76	1.97	0.85
^{2}H:	1.11	1.11	1.17
^{3}H:	0.51	0.44	0.78
^{3}He:	0.063	0.062	0.12
^{4}He:	0.84	0.76	0.85
^{6}He:	0.012	0.0083	0.059
^{6}Li:	0.020	0.013	0.17
^{7}Li:	0.018	0.012	0.22
^{8}Li:	0.0055	0.0032	0.104
^{9}Li:	0.0011	0.00057	0.035
^{7}Be:	0.0021	0.0016	0.027
^{9}Be:	0.0039	0.0024	0.081
^{10}Be:	0.0045	0.0024	0.11
^{11}Be:	0.00041	0.00019	0.021
^{8}B:	0.00006	0.00004	0.0013
^{10}B:	0.0022	0.0013	0.060
^{11}B:	0.0018	0.00091	0.076
^{12}B:	0.0011	0.00053	0.039
^{13}B:	0.00013	0.00005	0.0049
C:	0.0027	0.0015	0.093
N:	0.0011	0.00055	0.071
O:	0.00041	0.00025	0.034
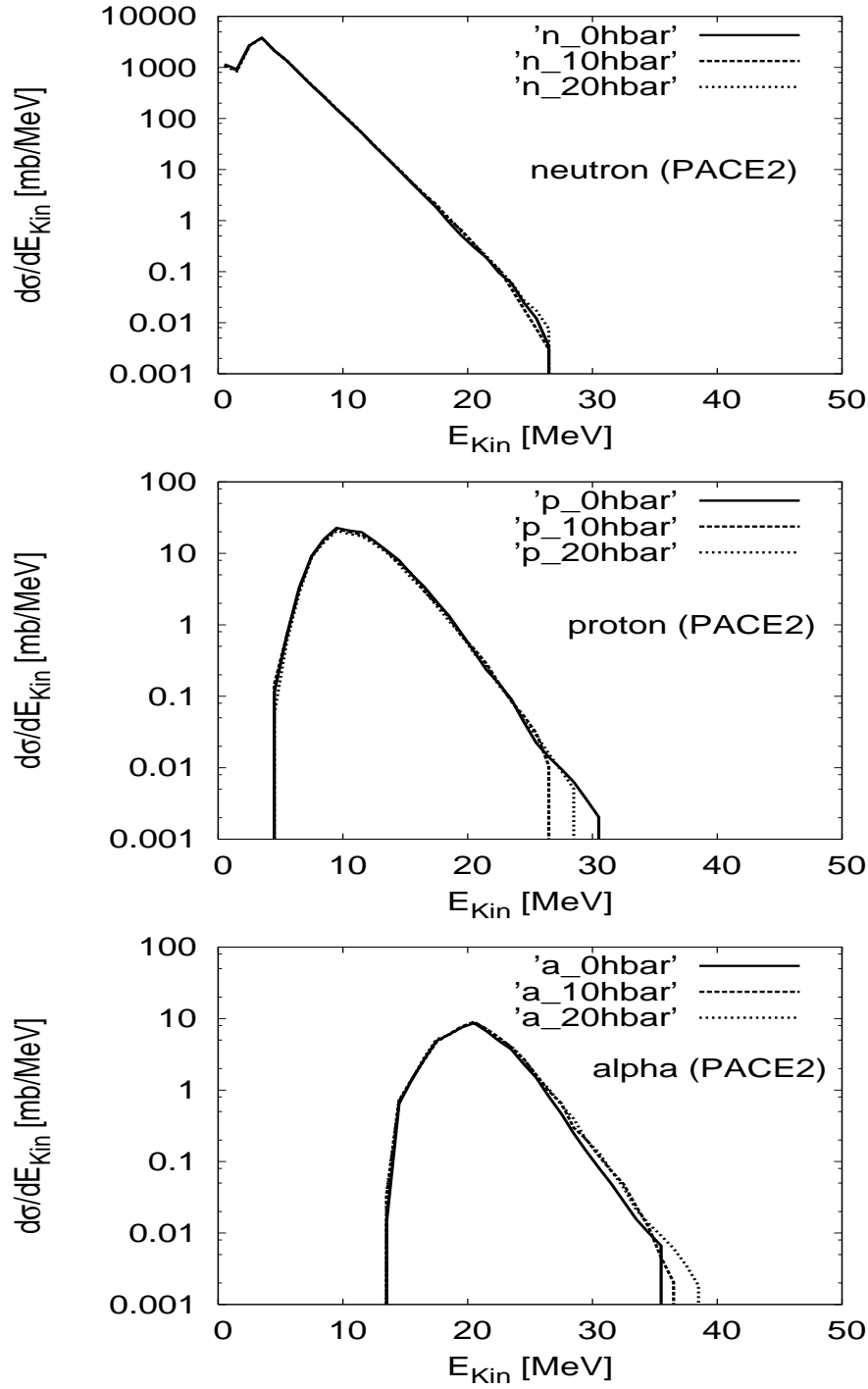
Figure 7.2: *Spectra of particles evaporated from excited Au nucleus, with the excitation energy equal to 100 MeV and different values of angular momentum; results of the PACE2 model (solid lines - zero value of angular momentum of the excited nucleus, dashed lines - angular momentum equal to 10 ℏ, dotted lines - 20 ℏ)*
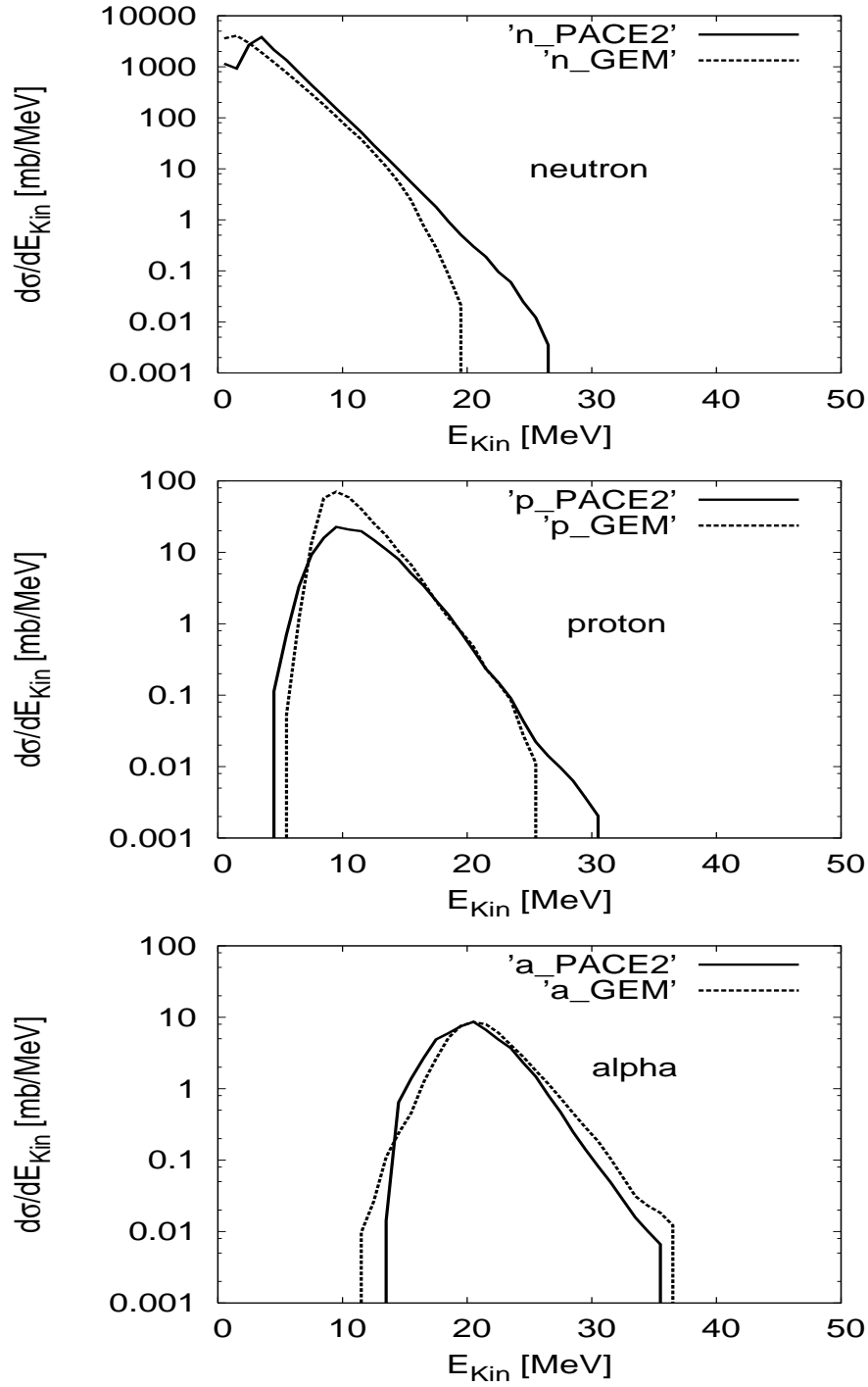
Figure 7.3: *Spectra of particles evaporated from excited Au nucleus, with the excitation energy equal to 100 MeV and zero value of angular momentum; solid lines - results of the PACE2 model, dashed lines - results of the GEM model*
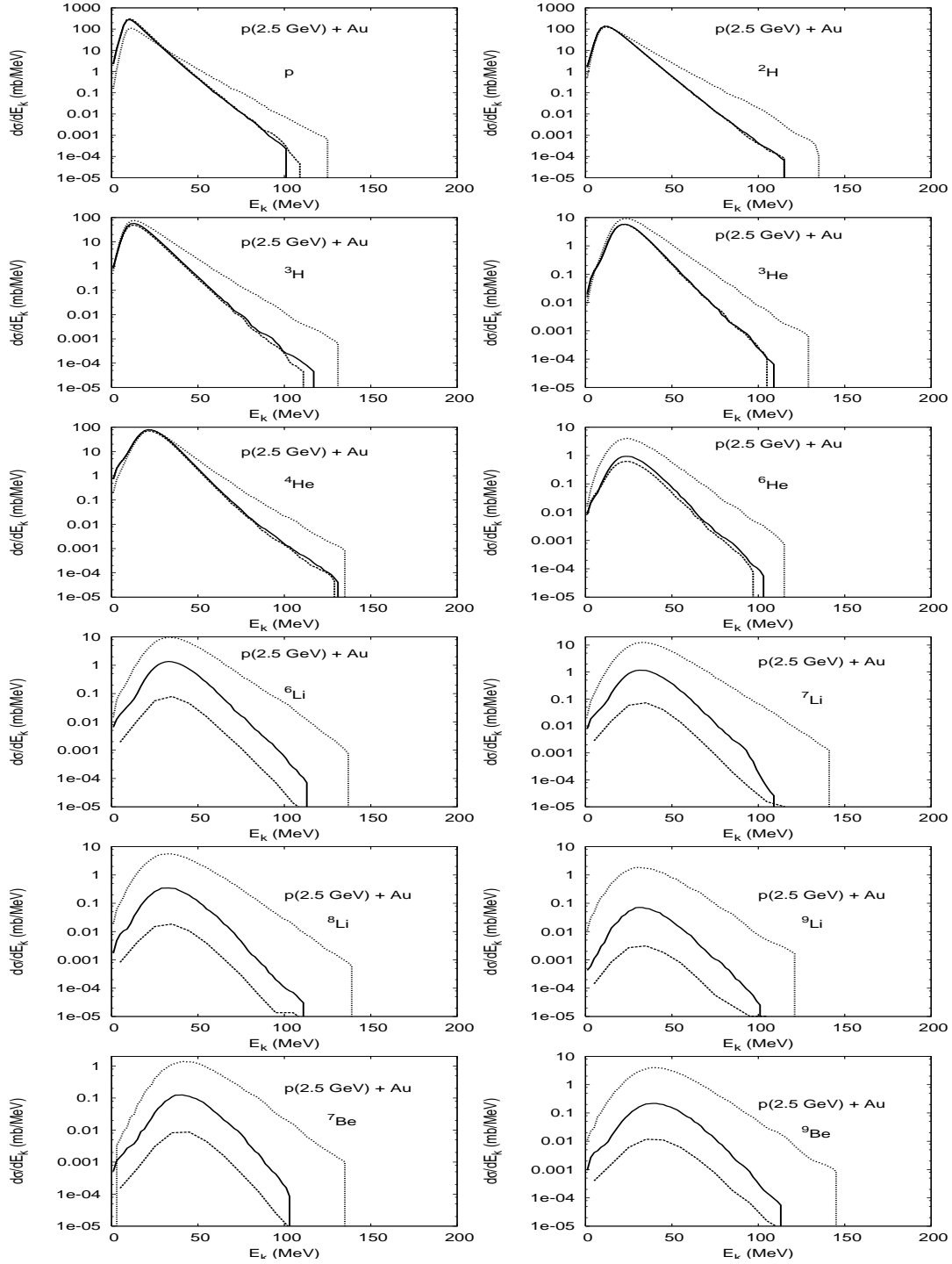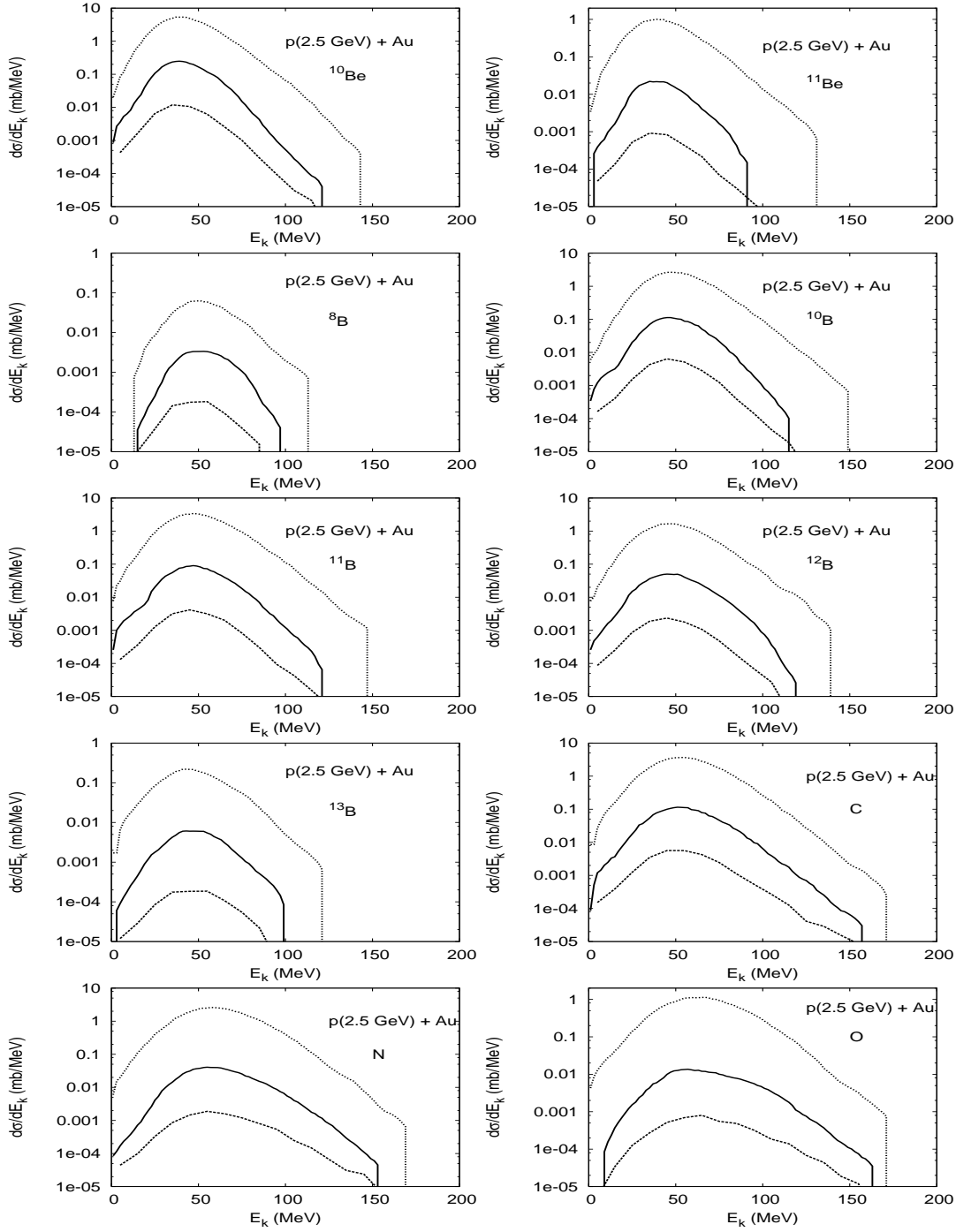
Figure 7.4: *Spectra of isotopes evaporated during p+Au reaction, at 2.5 GeV beam energy; results of the HSD+GEM model calculations (solid lines - calculations with the GCCI level density parameter, dashed lines - calculations with a = A/8, dotted lines - a = A/20)*

Figure 7.5: *Spectra of isotopes evaporated during p+Au reaction, at 2.5 GeV beam energy; results of the HSD+GEM model calculations (solid lines - calculations with the GCCI level density parameter, dashed lines - calculations with $a = A/8$, dotted lines - $a = A/20$)*

Chapter 8

Bulk models predictions for the proton induced nuclear reactions

8.1 Illustration of energy balance of the reaction

In order to show, how large fraction of energy is carried out during the first and the second stage of proton - nucleus reaction, respectively, a sample case of the HSD and statistical evaporation model calculations, for p + Au collision at 2.5 GeV proton beam energy is analysed in this Section.

The total initial kinetic energy introduced into nucleus by incoming proton is equal to 2.5 GeV. During the first stage of the reaction, about 1.7 GeV of the energy is carried away by nucleons and about 0.4 GeV - by pions. The multiplicity of nucleons is near 4.43, whereas the pion multiplicity, summed over all pion charges, is equal to 1.48. The average kinetic energy of one nucleon is about 0.4 GeV, whereas the average kinetic energy of one pion is equal to 0.29 GeV. Non-negligible amount of energy is taken away from the excitation energy and converted into rest masses of emitted pions, i.e. 0.2 GeV. Remaining energy of the excited nucleus after the first stage of the reaction, is equal to only about 200 MeV. This amount of energy is then evaporated in the second stage of the reaction by emission of mainly neutrons, protons, alphas and gammas. Emitted neutrons accumulate about 20 MeV of the energy, protons carried about 3 MeV, alphas - about 1 MeV, and gammas - about 6 MeV. The multiplicity of neutrons is equal to about 10 and the average kinetic energy of one neutron is equal to about 2 MeV, multiplicity of protons is equal to about 1 and the average kinetic energy of

one proton is equal to about 3 MeV. Multiplicity of alphas is equal to about 0.3 and the average kinetic energy of one alpha is equal to about 4 MeV and finally multiplicity of gammas is equal to about 6 and the average kinetic energy of one gamma is equal to 1 MeV. After taking into account the binding energy of nucleons inside nucleus, i.e. about 8 MeV per one nucleon, the whole amount of excitation energy of the residual nucleus (about 200 MeV) is carried out during the second stage of the reaction.

The presented balance shows, that the biggest amount of initial energy deposited in nucleus by incoming proton is carried out during the first stage of the reaction, i.e. about 85 %, and only about 15 % of the initial energy is carried away during the second stage of the reaction.

8.2   Participation of fission processes in spallation reaction

During the second stage of the proton - nucleus spallation reaction, deexcitation of the hot residual nucleus by evaporation of various isotopes takes place, as it is mentioned above in this work. However, there is a possibility, that during this process the evaporating nucleus undergoes fission. In such case, the particles emission is continued from the fission fragments. Probability of fission of particular nuclei depends on the ratio of Coulomb energy and surface energy of individual nucleus. The probability is strongly dependent on fissility parameter (f) defined as:

$$f = Z^2/A \tag{8.1}$$

where: Z is the charge of a nucleus and A is the mass number of a nucleus.

For example, the fissility parameter for Au nucleus, calculated according to the definition (8.1) is equal to 31.7. The experimental data collected in Ref. [72] indicate, that Au nucleus has rather low probability for fission, in comparison of Th and U nuclei. Distribution of the fissility parameter for residual nuclei emerged after the first stage of an example p+Au reaction, at 2.5 GeV beam energy (result of the HSD model calculations) is presented in Fig. 8.1. The average value of the fissility parameter distribution is equal to 31.40 ± 0.97.

On the base of a behavior of the fissility parameter in function of mass of residual nuclei, it can be tested if a ratio of charge and mass number is constant during the reaction and equal to the ratio of charge and mass number of the initial target nucleus. The fissility parameter in function of mass of residual nuclei for the example p+Au reaction, at 2.5 GeV proton beam
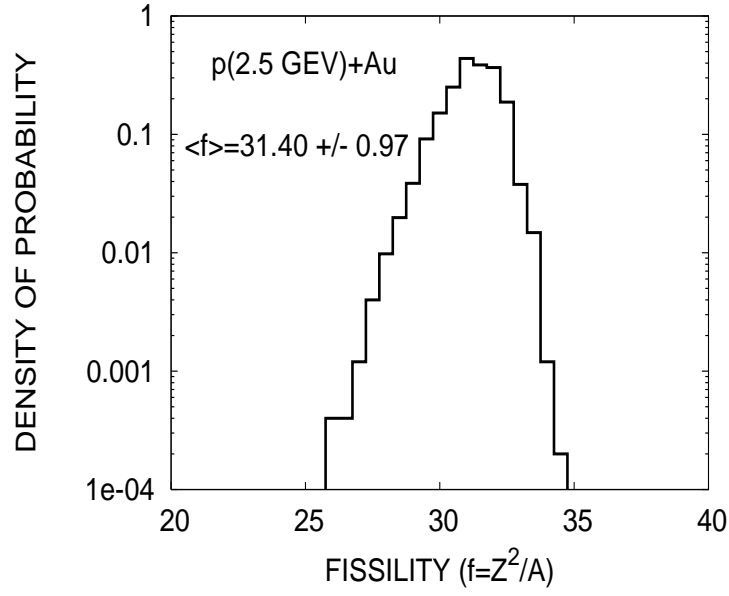
Figure 8.1: *Distribution of the fissility parameter for residual nuclei emerged after the first stage of p+Au reaction, at 2.5 GeV beam energy; results of the HSD model calculations*
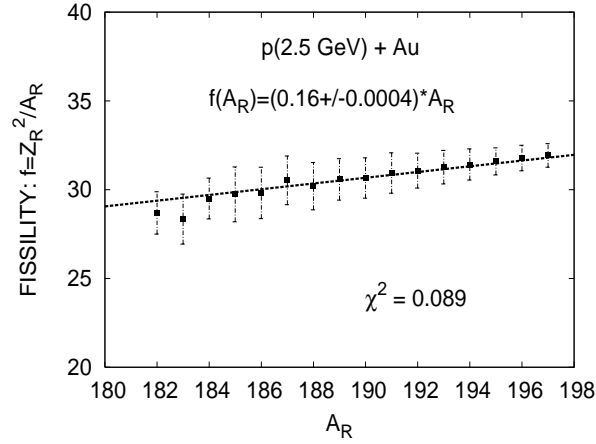

Figure 8.2: *The fissility parameter in function of mass of residual nuclei for the example p+Au reaction, at 2.5 GeV beam energy; results of the HSD model calculations (χ^2 means chisquare per degree of freedom)*

energy is presented in Fig. 8.2. The ratio of charge and mass number of the

Au initial target nucleus is equal to: Z(Au)/A(Au) = 79/197 = 0.40. Using the definition of the fissility parameter (8.1) and assuming that: Z=0.40·A, it is obtained that: f=0.16·A. Parametrization of the dependence presented in the Fig. 8.2, by a function proportional to the mass number give exactly the same result as received from the definition. This indicates, that in a first approximation, a ratio of charge and mass number is constant during the reaction and equal to the ratio of charge and mass number of the initial target nucleus. However, parametrization of the dependence by a function proportional to some power of the mass number (correcting a slope) gives a bit better accuracy, as presented in Fig. 8.3. It means, that the ratio of
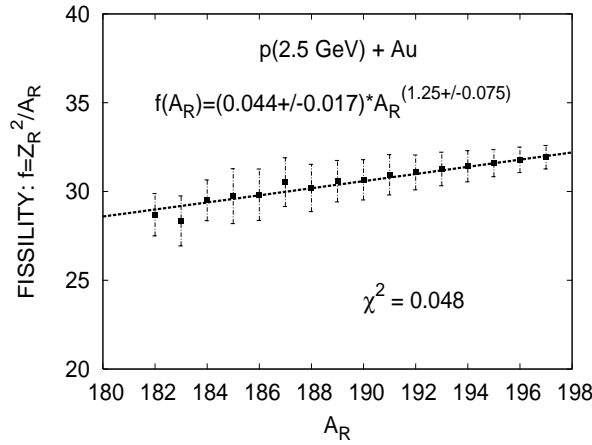

Figure 8.3: *The fissility parameter in function of mass of residual nuclei for the example p+Au reaction, at 2.5 GeV beam energy; results of the HSD model calculations (χ^2 means chisquare per degree of freedom)*

charge and mass number is not exactly equal to the ratio for the initial target nucleus. This is confirmed by multiplicities of protons and neutrons emitted during first stage of the p+Au reaction, at 2.5 GeV proton beam energy. Namely, due to interactions inside the target nucleus, multiplicity of emitted protons (equal to 1.66) is a bit higher than multiplicity of emitted neutrons (equal to 1.63). Contrary, in case of n+Au reaction, at 2.5 GeV neutron beam energy, multiplicity of emitted neutrons during the first stage of the reaction (equal to 1.89) is a bit higher than multiplicity of emitted protons (equal to 1.38). This indicates, that information about type of projectile is kept during the first stage of reaction.

If looking at the kinetic energy distributions of isotopes emitted during the second stage of p+Au reaction, calculated with blocked and allowed fission, differences are visible, because Au nucleus possesses non-zero, although

rather small fissility. The example spectra (result of the GEM model calculations) are presented in Fig. 8.4. It is clearly seen from the Figure, that
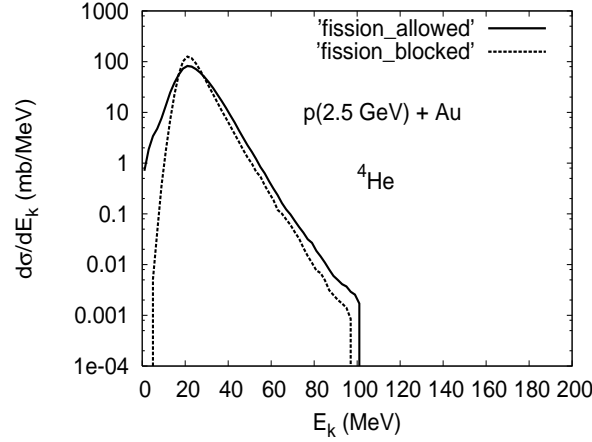

Figure 8.4: *The kinetic energy distributions of ^{4}He evaporated during the second stage of p+Au reaction, at 2.5 GeV beam energy; results of the HSD+GEM model calculations (solid line - fission allowed, dashed line - fission blocked)*

fission shifts spectra of emitted particles down in their maximum and causes them wider in energetical range, in direction of both lower and higher energies (in Fig. 8.4 the effect is shown for alpha particles). This is because of evaporation from fission fragments, which move in opposite directions. As a consequence there is a bit less particles with intermediate energies, emitted from the unfissioned residuum, but more particles with a bit lower and higher energies, emitted after fission, from excited fragments moving in backward and forward directions, respectively.

Cross section for the different fragments production in function of the fragments masses and charges (result of the HSD+GEM model calculations), for the example p+Au reaction, at 2.5 GeV proton beam energy, calculated with blocked and allowed fission, are presented in Fig. 8.5. Interesting result is obtained, when one subtracts the cross sections obtained with blocked and allowed fission. One can see in the Figures that fission diminishes amount of nuclei of masses close to 150 - 160 and increases amount of nuclei of masses in the range 60 - 100. One can conclude, that fission is much slower process than evaporation. First evaporation from a hot residual nucleus takes place. Due to evaporation both the mass and excitation energy of residuum decrease. Also the Coulomb energy and the surface energy of the nucleus is changing.

If the emission of particles is slow, a possibility of fission occurs. Fission is a collective slow process. This is confirmed by experimental data collected in Ref. [72], which show, that fission cross section decreases with increasing energy provided into nuclei. In case of very fast evaporation, fission has no possibility to occur. The second stage of spallation reaction is a competition between evaporation and fission.
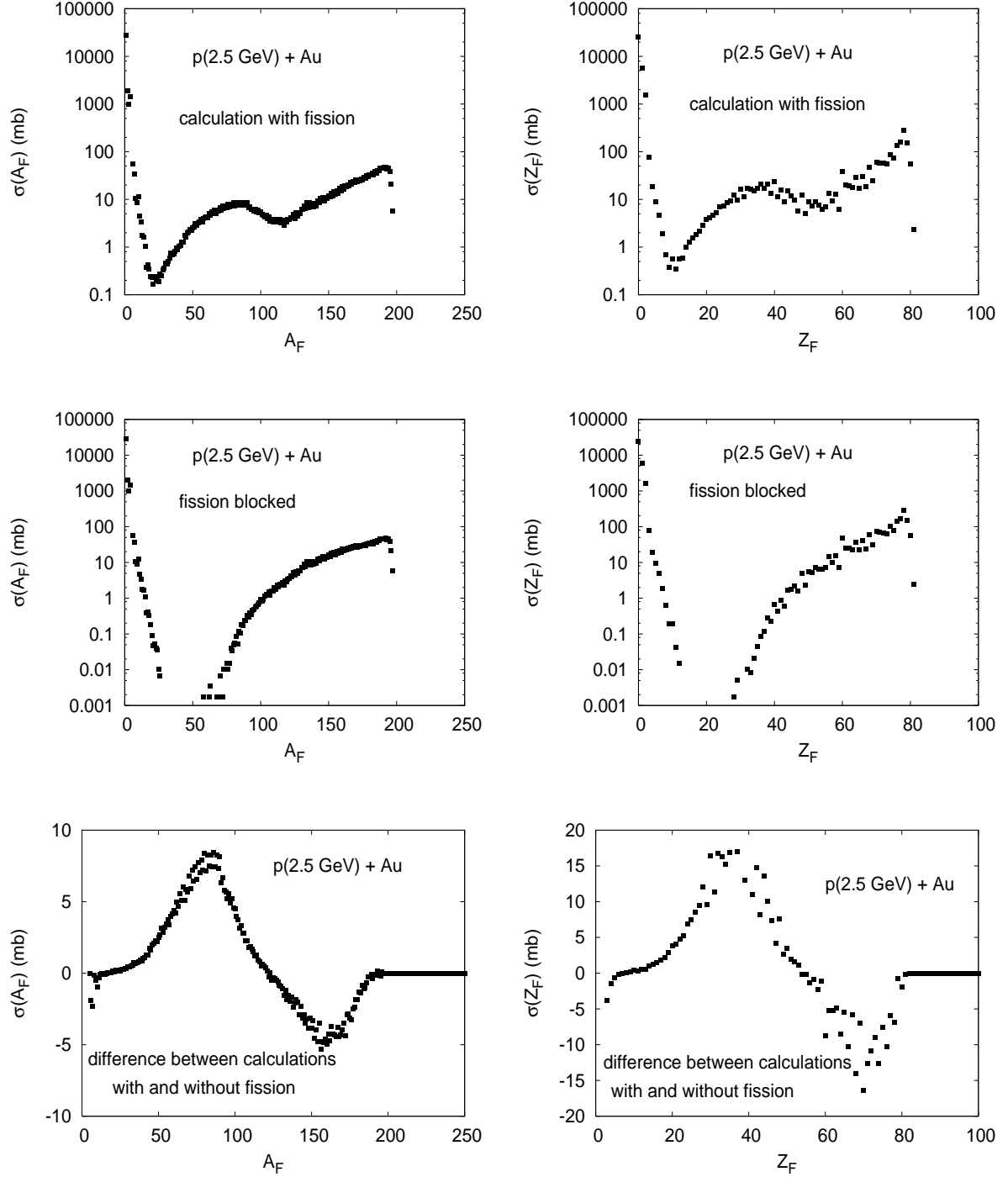
Figure 8.5: *Cross section for different fragments production in function of fragment mass and charge from p+Au reaction, at 2.5 GeV beam energy, with (a) allowed and (b) blocked fission; results of the HSD+GEM model calculations; (c) differences between calculations with and without fission*

Chapter 9

Comparison of results of the HSD plus evaporation model calculations with experimental data

Result of the HSD plus statistical evaporation model calculations have been examined by confrontation with existing experimental data. Effects are discussed in this Chapter.

9.1 Neutron spectra

Inclusive differential kinetic energy spectra of neutrons, emitted at different angles during proton - nucleus reactions on various target nuclei and at various impact energies, calculated with the HSD plus evaporation model and compared with available experimental data are analysed in this Section.

High energy part of neutron distribution, composed of so-called fast neutrons, produced during the first stage of the reaction is a result of the HSD model calculations. Such neutrons are emitted mainly in forward direction. Low energy part of neutron distribution, composed of slow neutrons produced during the second stage of the reaction is a result of evaporation model calculations. Such neutrons are emitted both in forward and backward directions. Neutron spectra obtained as a result of summing up these two parts are compared with the following experimental data. Distributions of spallation neutrons produced in proton induced reactions on Al, Fe, Zr, W, Pb and Th targets at 1.2 GeV beam energy and on Fe and Pb targets at 1.6 GeV proton beam energy, emitted at angles: 10°, 25°, 40°, 55°, 85°, 100°, 115°, 130°, 145°

and 160° are compared with data measured at the SATURNE accelerator in Saclay [73]. Similarly, calculated spectra of neutrons produced in proton induced reactions on Pb target at 0.8 and 1.5 GeV beam energies, emitted at angles: 15°, 30°, 60°, 90°, 120° and 150° are compared with experimental data measured by Ishibashi et al. [74]. The comparisons are presented in Figures: 9.1, 9.2, 9.3, 9.4, 9.5, 9.6, 9.7, 9.8, 9.9 and 9.10, respectively.

One can see, that independently on the value of projectile energy, the calculated neutron spectra produced in proton induced reactions on light targets (i.e. Al, Fe and Zr, presented in the Figures 9.1, 9.2, 9.3 and 9.7, respectively) are in perfect agreement with the adequate experimental data. Contrary, in case of spectra of neutrons produced in proton induced reactions on heavy targets (i.e. W, Pb and Th, presented in the Figures 9.4, 9.5, 9.6, 9.8, 9.9 and 9.10, respectively), the good agreement between calculations and proper experimental data is seen only in backward angles. In forward angles, calculations underestimate experimental data in the central parts of the distributions. Furthermore, based on the presented results of the several reactions, on the six target nuclei, the regular growth of the missing part of the calculated spectra is observed. The effect is continuous and increase monotonically with mass of target. The missing parts, in case of reactions on heavy targets indicate, that apart from the two stages of spallation reaction (fast and slow stage), there must be an additional intermediate stage, probably preequilibrium stage. It seems, that neutron production during this intermediate stage is dominant in case of reactions with heavy targets and negligible for reactions with light targets.

Multiplicities of neutrons emitted during first and second stage of the reactions are collected in Table 9.1. It is clearly seen, that neutrons are emitted mainly in the second stage of spallation reaction.

Table 9.1: *Multiplicities of neutrons emitted during fast and slow stage of reaction*

reaction	first stage	second stage
p(1.2 GeV)+Al	1.65	1.20
p(1.2 GeV)+Fe	2.16	2.84
p(1.6 GeV)+Fe	2.18	2.84
p(1.2 GeV)+Zr	2.24	6.15
p(1.2 GeV)+W	2.10	17.48
p(0.8 GeV)+Pb	1.31	21.02
p(1.2 GeV)+Pb	1.96	21.31
p(1.5 GeV)+Pb	2.19	20.57
p(1.6 GeV)+Pb	2.23	19.85
p(1.2 GeV)+Th	2.00	25.80
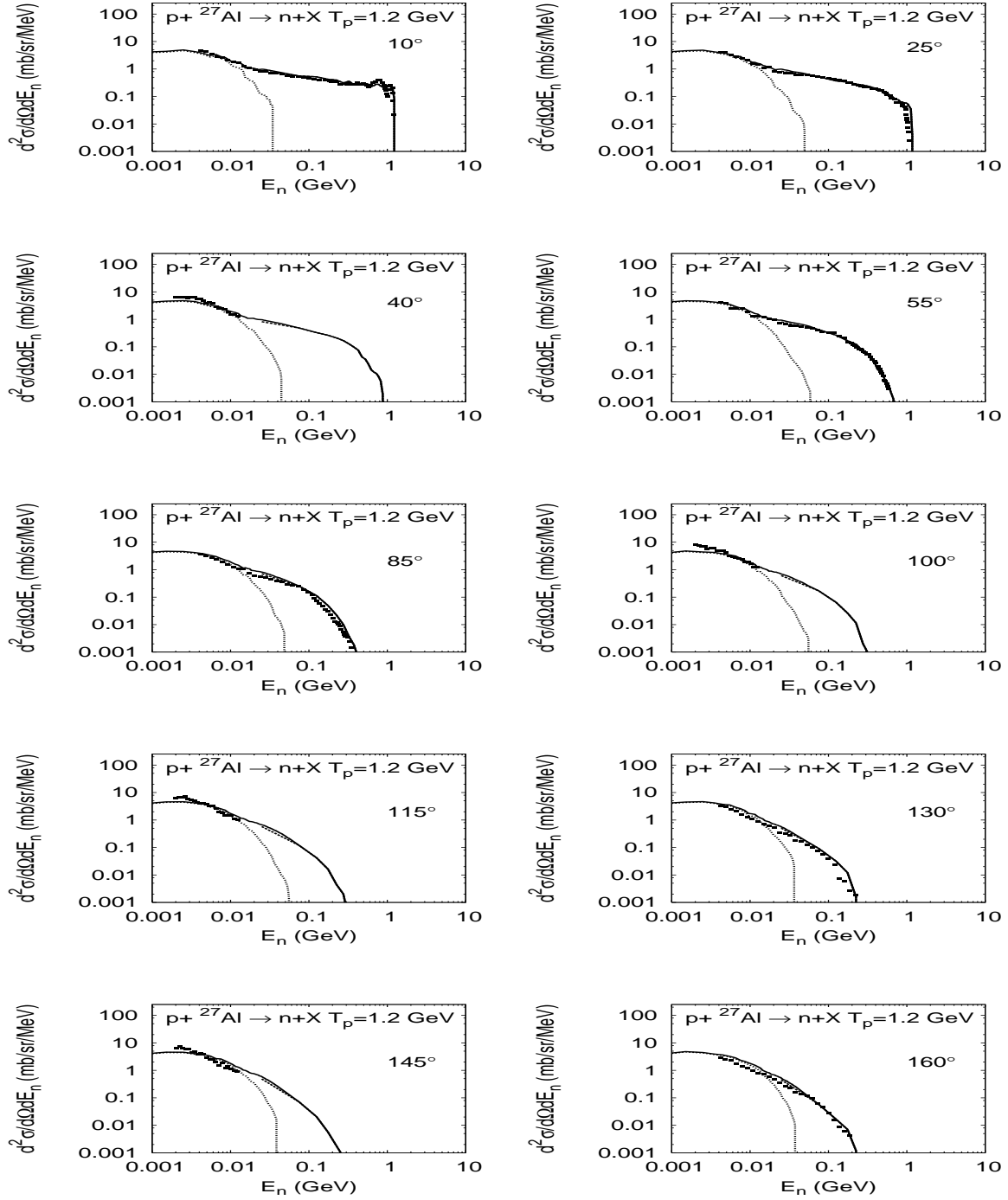
Figure 9.1: *Double differential neutron production cross section for p+Al reaction, at 1.2 GeV proton beam energy; lines show results of the HSD+GEM model calculations (dashed and dotted lines are contributions of first and second stage of reaction, solid line is their sum), symbols indicate the experimental data [73]*
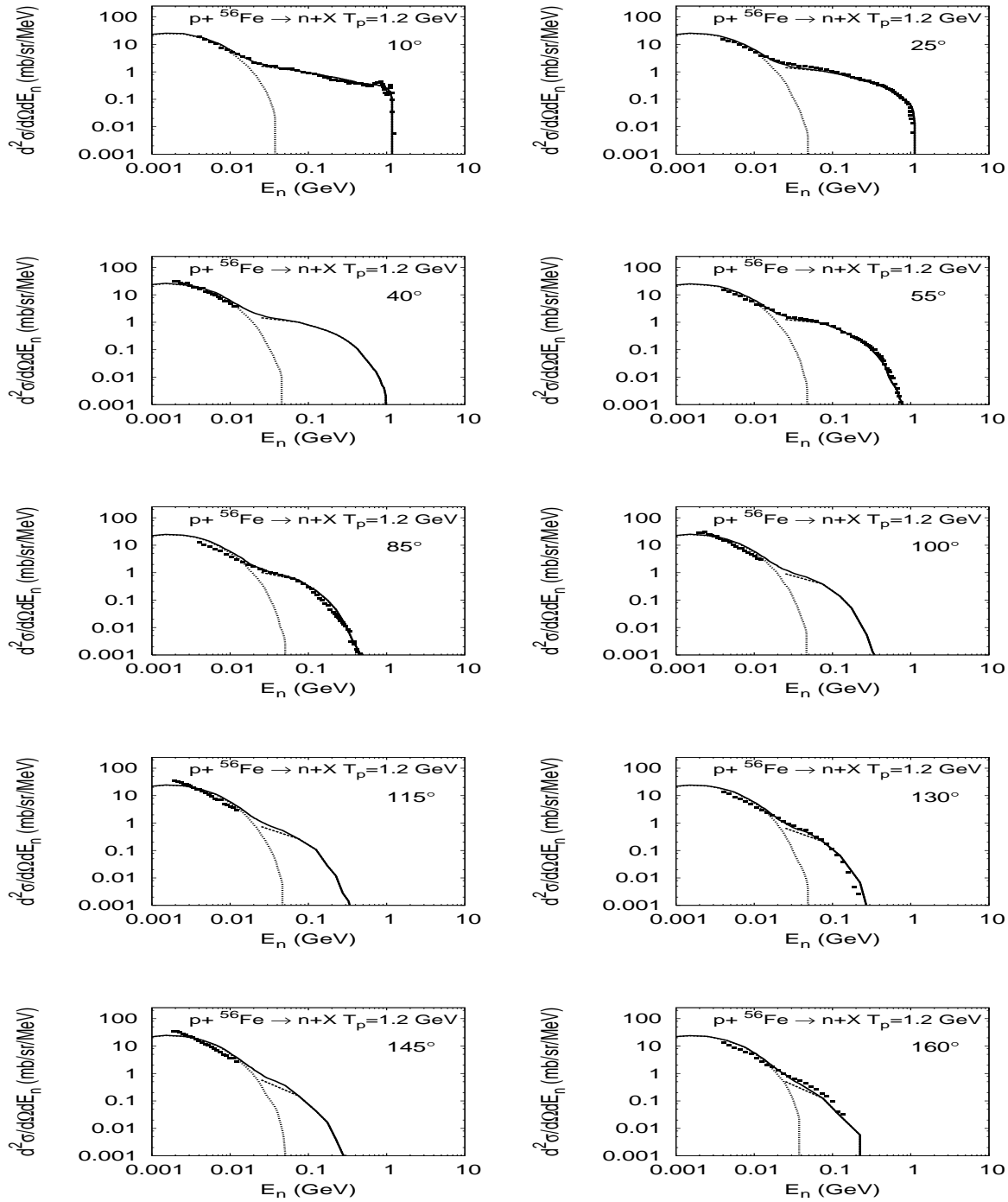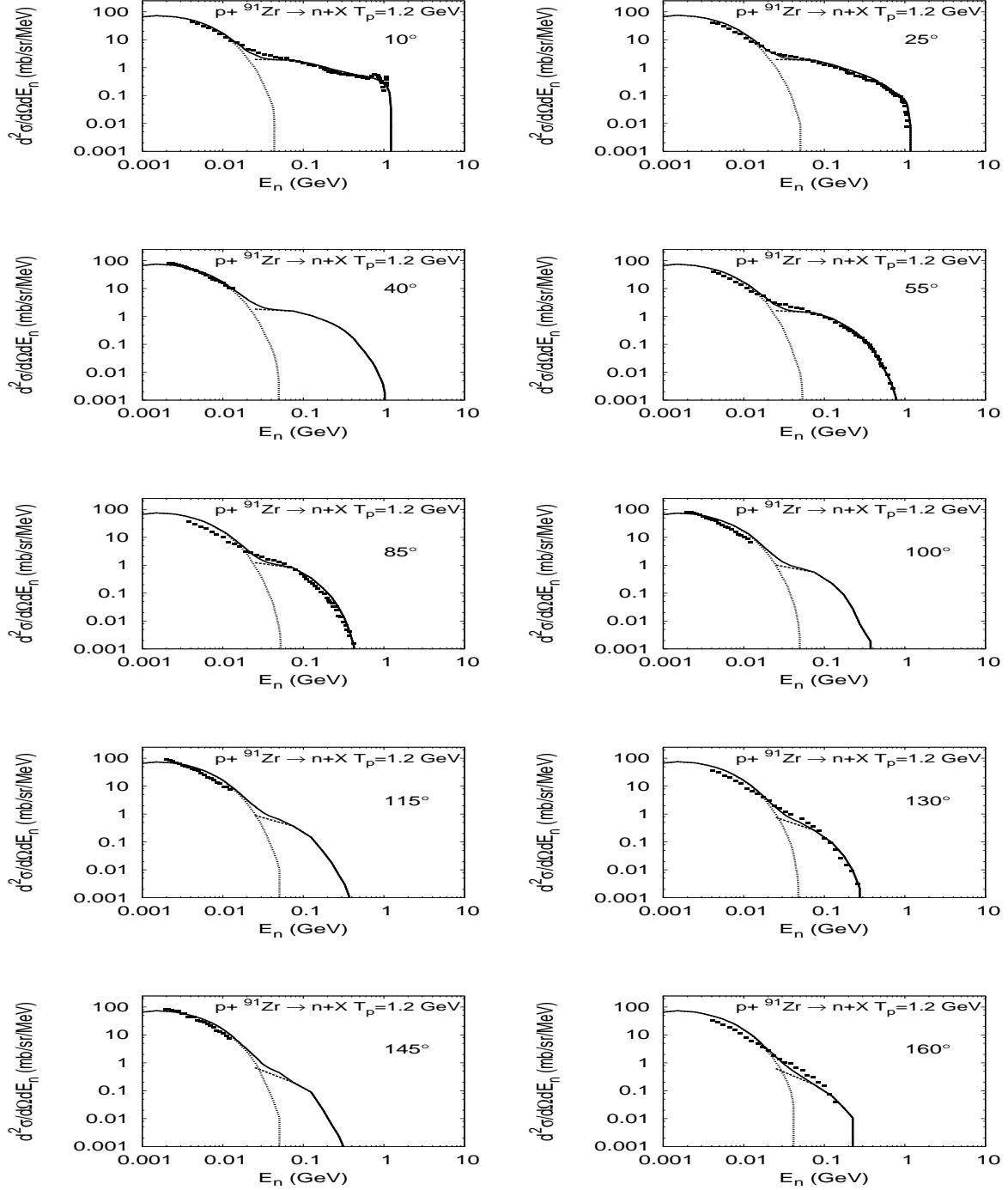
Figure 9.2: *Double differential neutron production cross section for p+Fe re-action, at 1.2 GeV proton beam energy; lines show results of the HSD+GEM model calculations (dashed and dotted lines are contributions of first and second stage of reaction, solid line is their sum), symbols indicate the exper-imental data [73]*

Figure 9.3: *Double differential neutron production cross section for p+Zr reaction, at 1.2 GeV proton beam energy; lines show results of the HSD+GEM model calculations (dashed and dotted lines are contributions of first and second stage of reaction, solid line is their sum), symbols indicate the experimental data [73]*
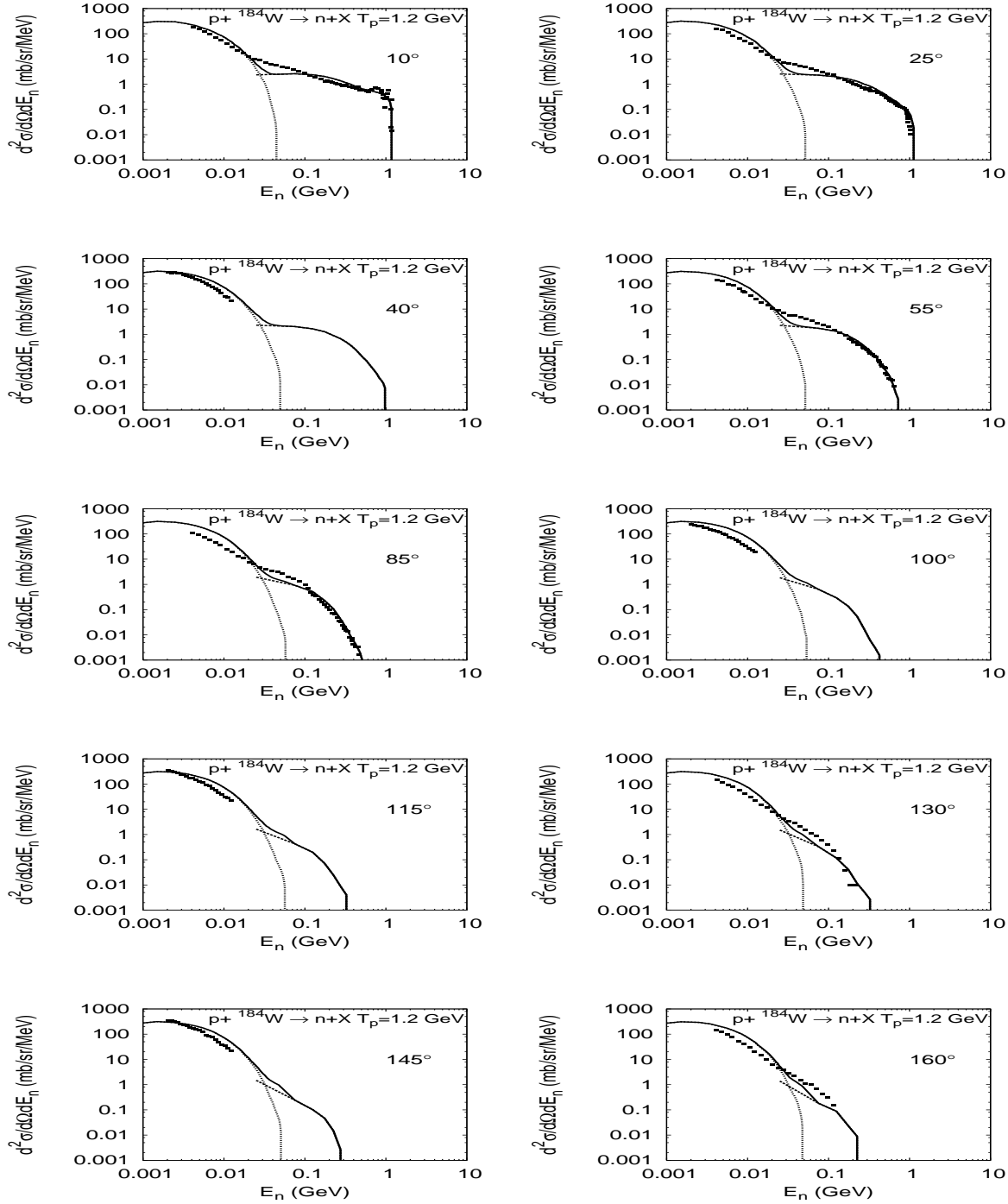
Figure 9.4: *Double differential neutron production cross section for p+W reaction, at 1.2 GeV proton beam energy; lines show results of the HSD+GEM model calculations (dashed and dotted lines are contributions of first and second stage of reaction, solid line is their sum), symbols indicate the experimental data [73]*
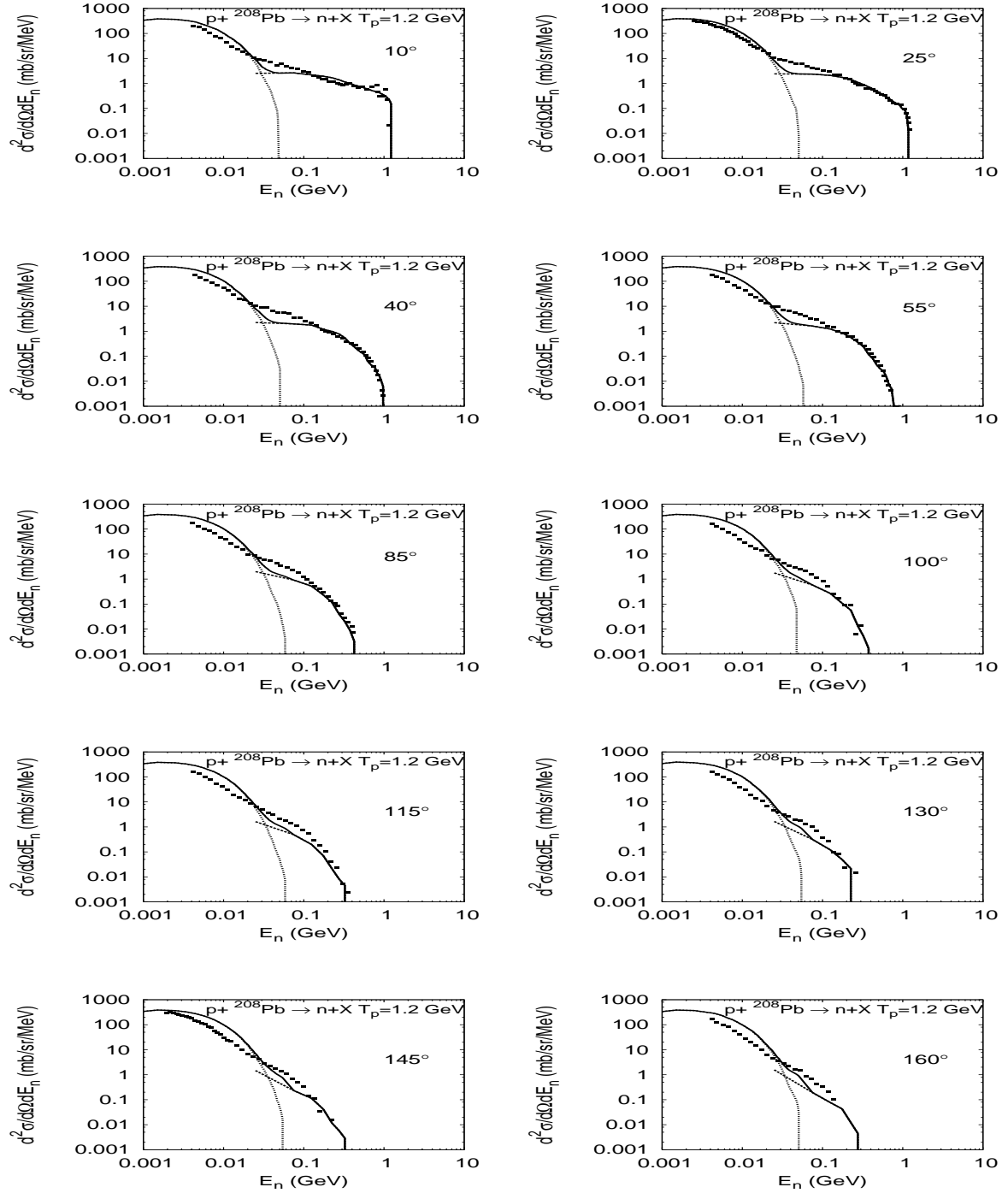
Figure 9.5: *Double differential neutron production cross section for p+Pb reaction, at 1.2 GeV proton beam energy; lines show results of the HSD+GEM model calculations (dashed and dotted lines are contributions of first and second stage of reaction, solid line is their sum), symbols indicate the experimental data [73]*

Figure 9.6: *Double differential neutron production cross section for p+Th reaction, at 1.2 GeV proton beam energy; lines show results of the HSD+GEM model calculations (dashed and dotted lines are contributions of first and second stage of reaction, solid line is their sum), symbols indicate the experimental data [73]*
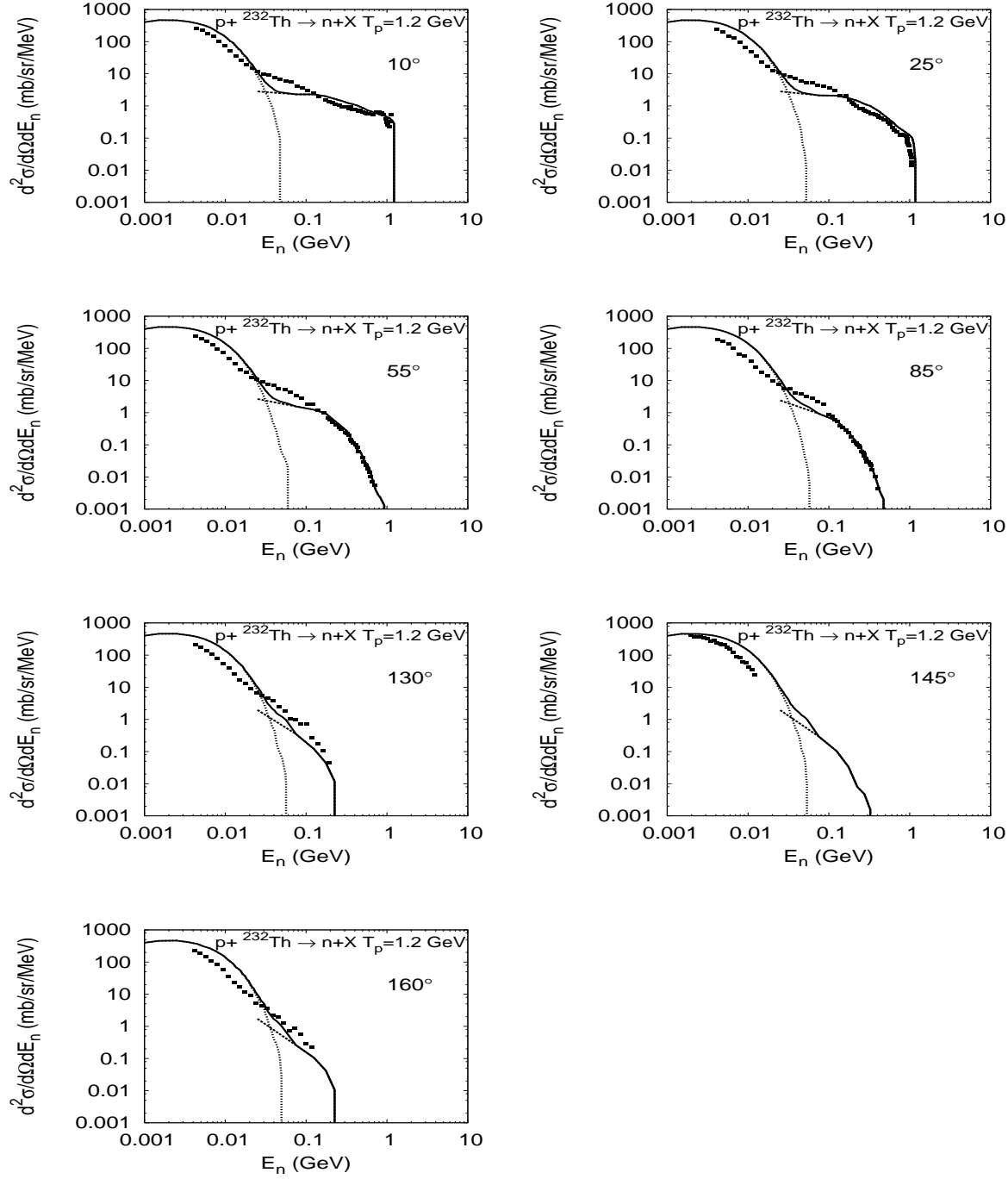
Figure 9.7: *Double differential neutron production cross section for p+Fe reaction, at 1.6 GeV proton beam energy; lines show results of the HSD+GEM model calculations (dashed and dotted lines are contributions of first and second stage of reaction, solid line is their sum), symbols indicate the experimental data [73]*
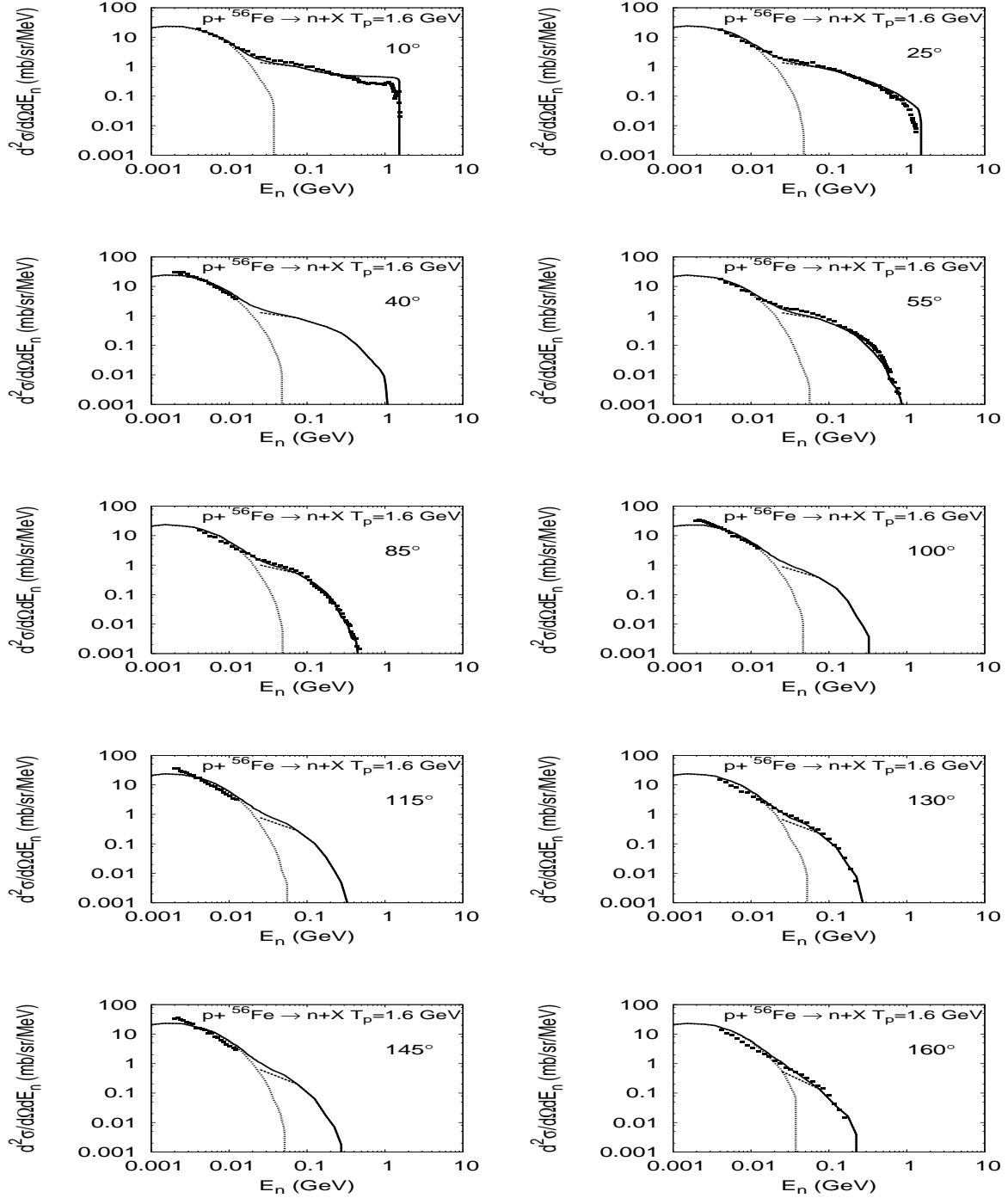
Figure 9.8: *Double differential neutron production cross section for p+Pb re-action, at 1.6 GeV proton beam energy; lines show results of the HSD+GEM model calculations (dashed and dotted lines are contributions of first and second stage of reaction, solid line is their sum), symbols indicate the experimental data [73]*
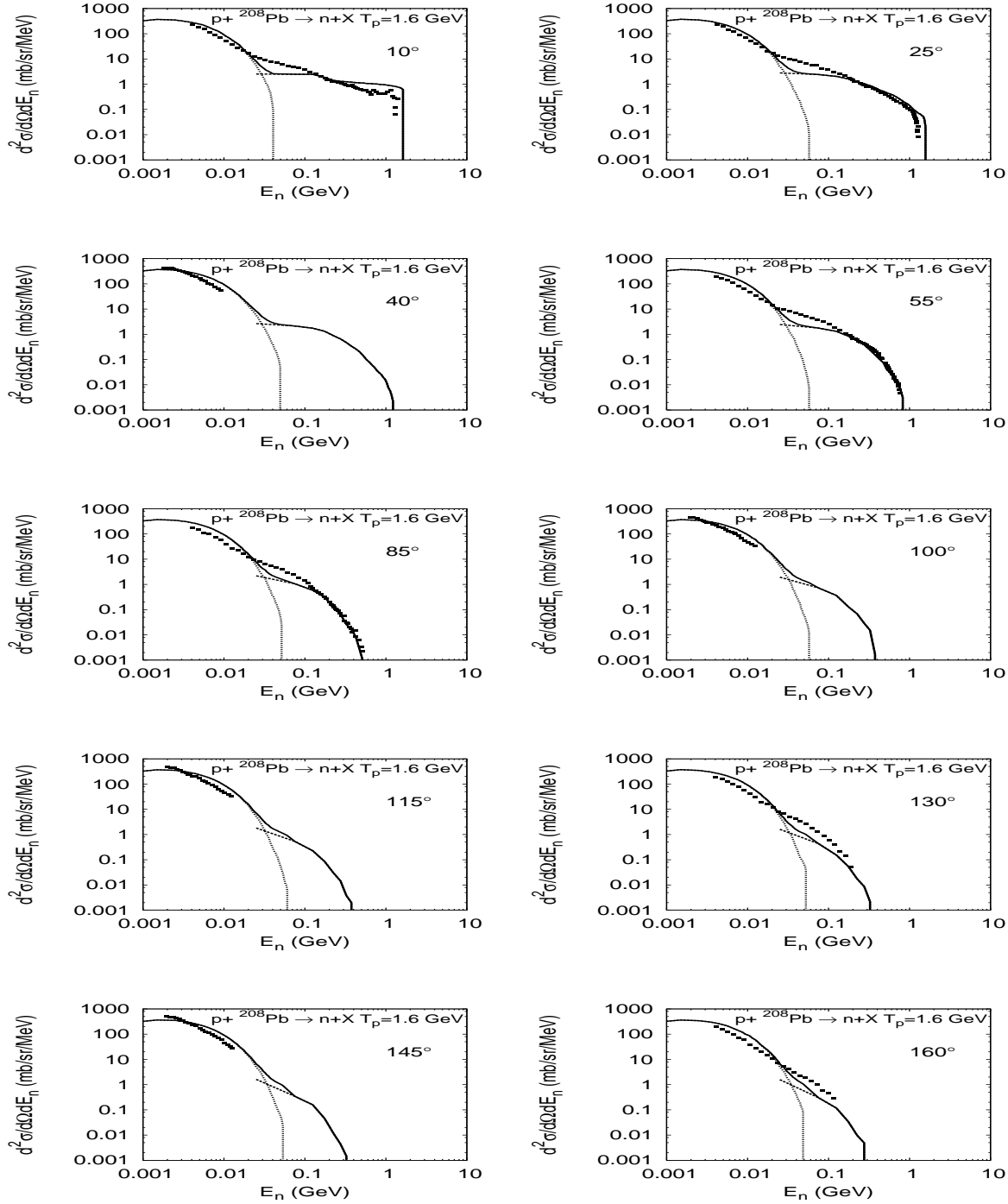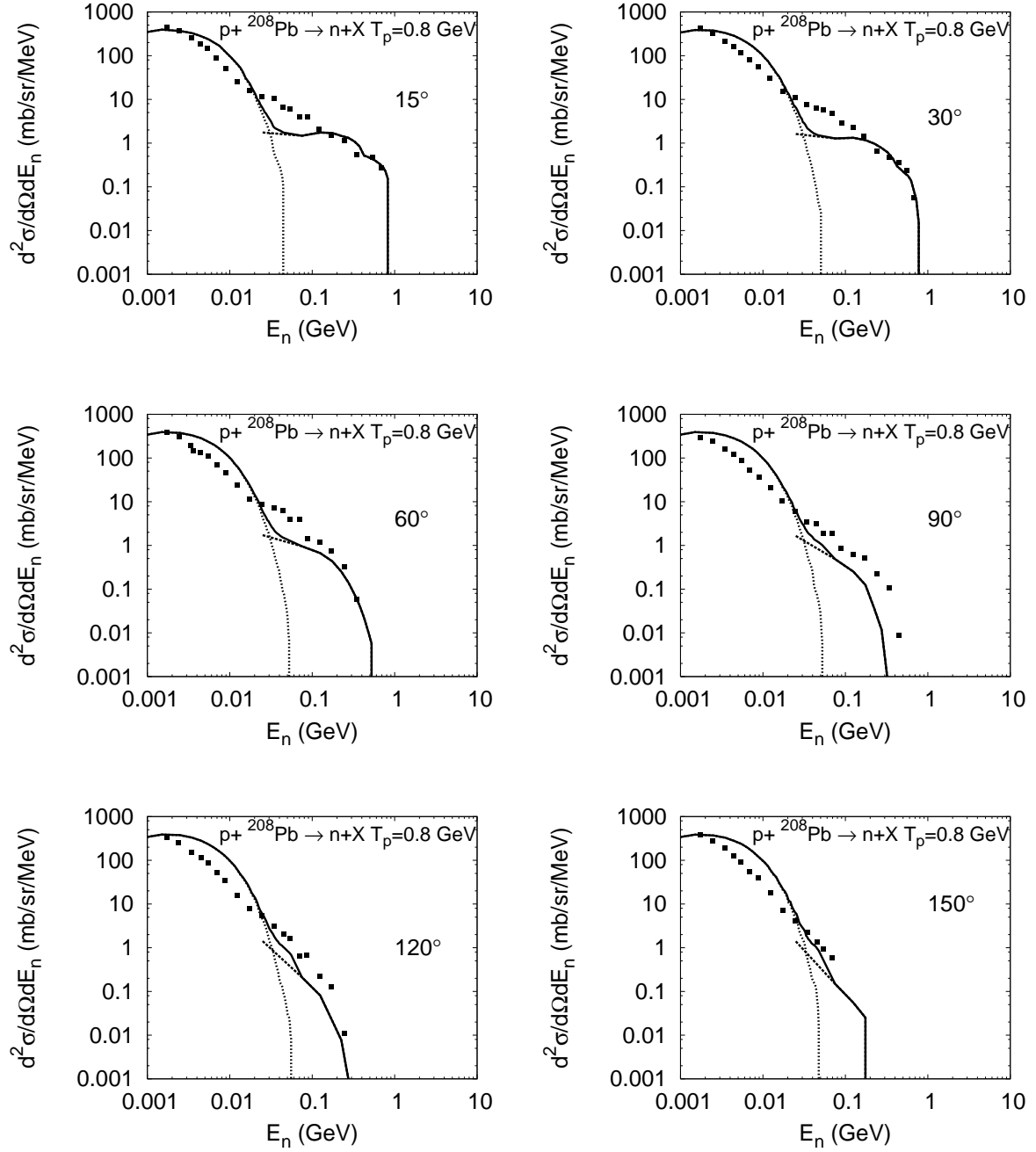
Figure 9.9: *Double differential neutron production cross section for p+Pb reaction, at 0.8 GeV proton beam energy; lines show results of the HSD+GEM model calculations (dashed and dotted lines are contributions of first and second stage of reaction, solid line is their sum), symbols indicate the experimental data* [74]

Figure 9.10: *Double differential neutron production cross section for p+Pb reaction, at 1.5 GeV proton beam energy; lines show results of the HSD+GEM model calculations (dashed and dotted lines are contributions of first and second stage of reaction, solid line is their sum), symbols indicate the experimental data [74]*
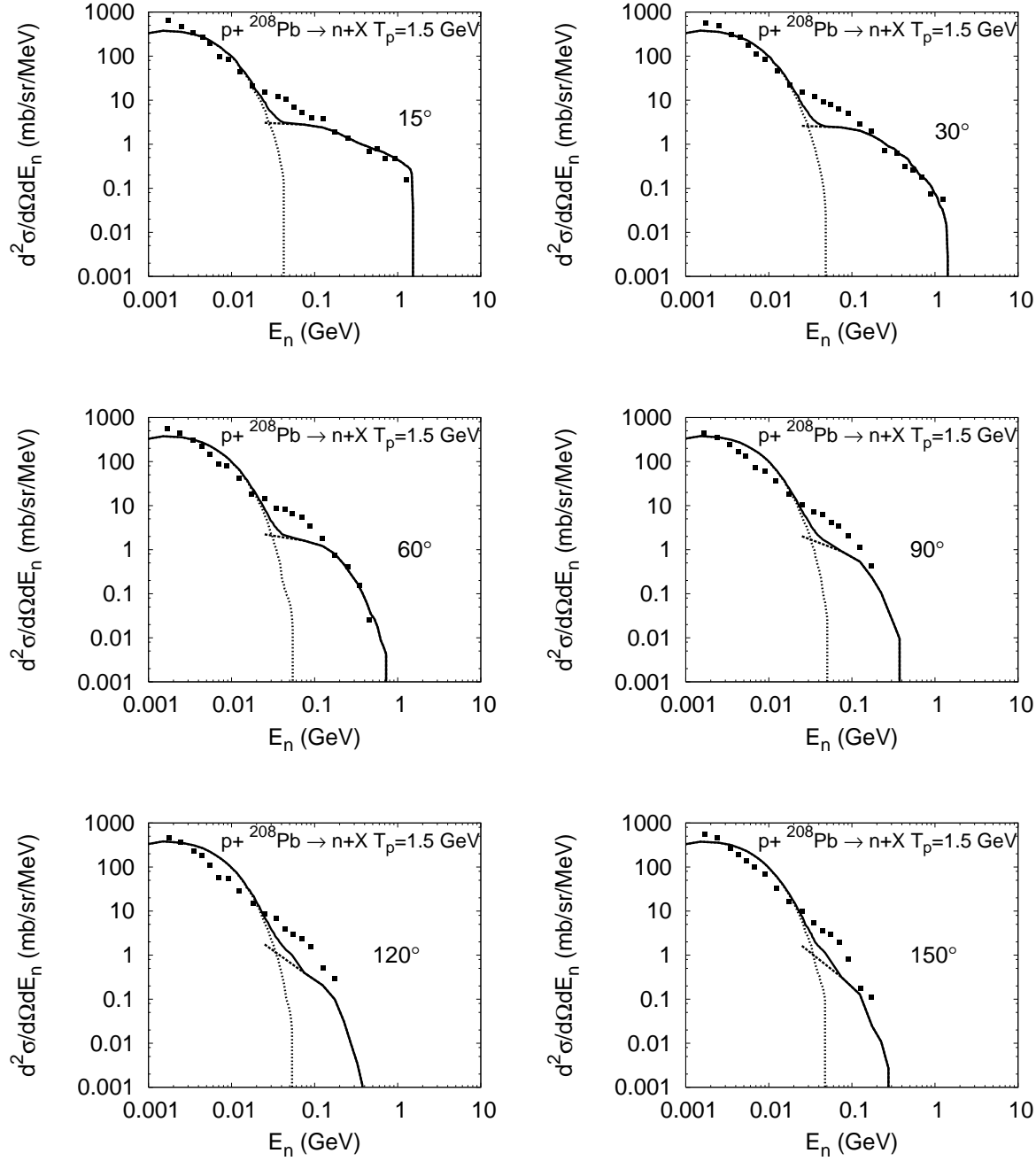
9.2 Proton spectra

Inclusive, double differential kinetic energy spectra of protons emitted at different angles in proton induced reactions on various targets, at broad range of incident energy, calculated with the HSD+GEM model, are compared with available experimental data. Model results of low energy reactions: p+Ni at 0.175 GeV beam energy (in this case, time of first stage calculations is equal to 55 fm/c), compared with experimental data measured by PISA collaboration [7] and p+Bi at 0.45 GeV beam energy (with time of first stage calculations equals to 65 fm/c), compared with data published in [75], are presented in Figures 9.11 and 9.12, respectively. Very good agreement between calculations and data is clearly seen.

Comparisons of calculated proton spectra produced in reactions induced by higher incident energies, e.g. p+Au at 1.2 GeV, 1.9 GeV and 2.5 GeV projectile energy (with time of first stage calculations equal to 45 fm/c), confronted with data measured by PISA collaboration [7], are shown in Figures 9.13, 9.14 and 9.15. In order to make the comparison easier, the high energy parts of the calculated distributions are plotted only up to 200 MeV of proton kinetic energy. It is seen, that in case of 1.2 GeV of incident energy (Fig. 9.13), the high energy parts of experimental distributions are described well, the low energy parts are slightly overestimated by calculations. In the case of 1.9 GeV beam energy (Fig. 9.14), the whole spectra, especially protons emitted in backward directions are described very well. Low energy part of experimental distributions of protons from reaction at 2.5 GeV (Fig. 9.15) are also very well described by calculations. The high energy parts are slightly underestimated. Nevertheless, the average agreement between the HSD+GEM model results concerning proton spectra and adequate experimental data is satisfactory.

In the presented Figures, contributions from intra-nuclear cascade (high energy part, result of the HSD model calculations) and evaporation (low energy part, result of the GEM model calculations) are visible. The cascade contribution evidently dominates. This indicates, that protons are emitted mainly in the first stage of spallation reaction. This is additionally confirmed by values of multiplicities of protons emitted during first and second stage of reaction, compared in Table 9.2 (quite contrary to the neutron case, consider Table 9.1).

Nucleon distributions depend strongly on projectile energy. The example two-dimensional distributions of transversal (P_T) versus longitudinal (P_Z) momentum of nucleons emitted during the first stage of proton induced reactions on Ni target, at various incident energies are presented in Fig. 9.16. These are results of HSD model calculations, where P_Z corresponds to the nu-

Table 9.2: *Multiplicities of protons emitted during first and second stage of reaction*

reaction	first stage	second stage
p(0.175 GeV)+Ni	1.61	0.91
p(0.45 GeV)+Bi	2.16	1.00
p(1.2 GeV)+Au	2.67	1.13
p(1.9 GeV)+Au	2.42	1.099
p(2.5 GeV)+Au	2.20	0.96

cleons momentum in beam direction and P_T is defined as $P_T = \sqrt{P_X^2 + P_Y^2}$. The two-dimensional distributions depict, how the nucleon spectra evolve with incident energy. In all the cases, low energy part is symmetric around zero value (it is not so in the case of pion production, see Fig. 6.3). With increase of projectile energy, the distribution is building up mainly in longitudinal (forward) direction. It spreads always up to a value corresponding to the value of beam momentum. That is because, it is possible that incoming proton will scatter only slightly on a surface of target nucleus and will appear in forward direction with almost unchanged momentum. In the Fig. 9.16, momentum spectra of all nucleons are presented, since distributions of protons and neutrons emitted during first stage of the reaction are very similar. The only exception concerns momentum corresponding to the beam momentum.

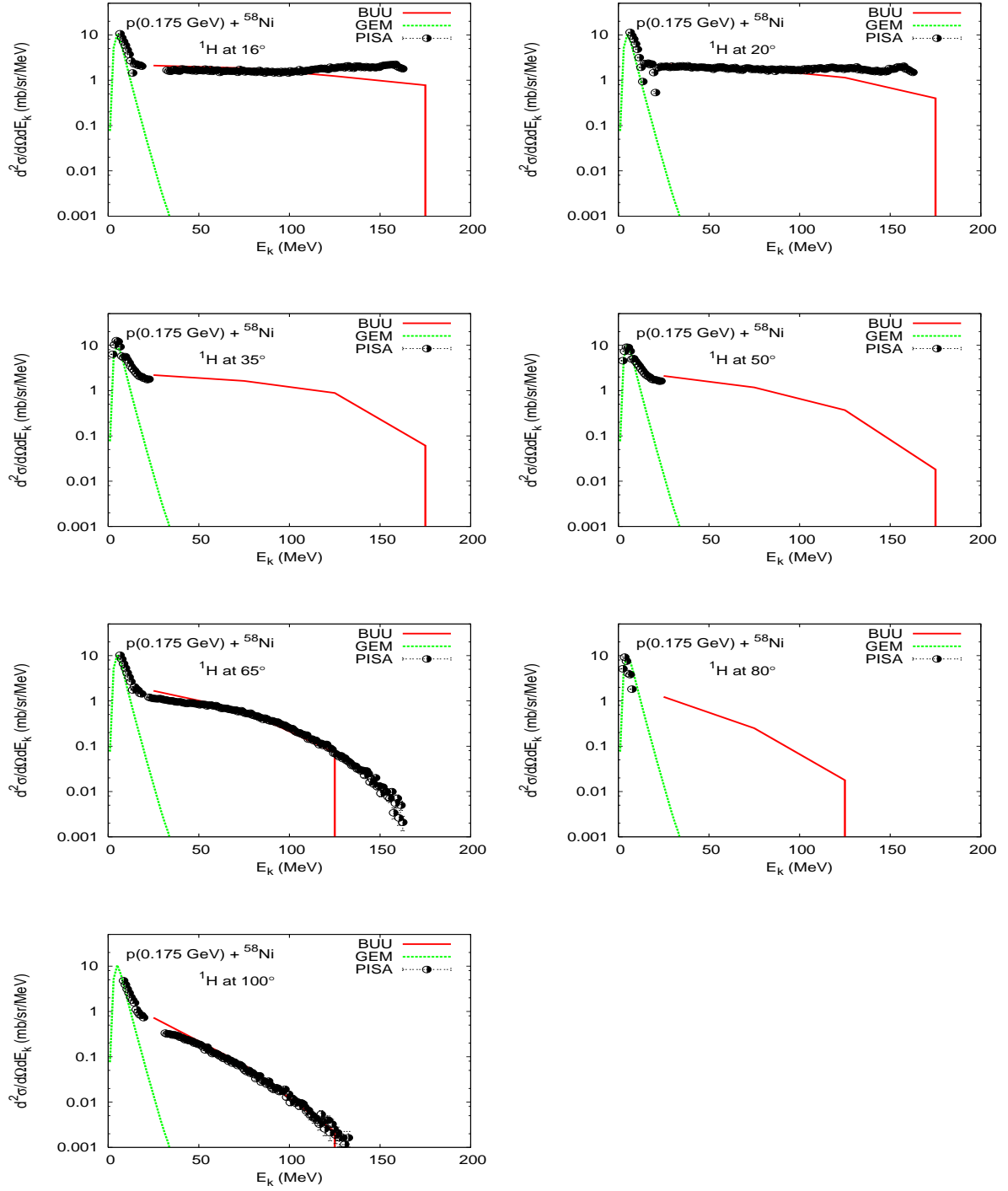Figure 9.11: *Double differential proton spectra from p+Ni reaction at 0.175 GeV incident energy; lines show results of HSD and GEM model calculations (solid line - first stage, dashed line - second stage), symbols indicate the experimental data measured by experiment PISA [7]*

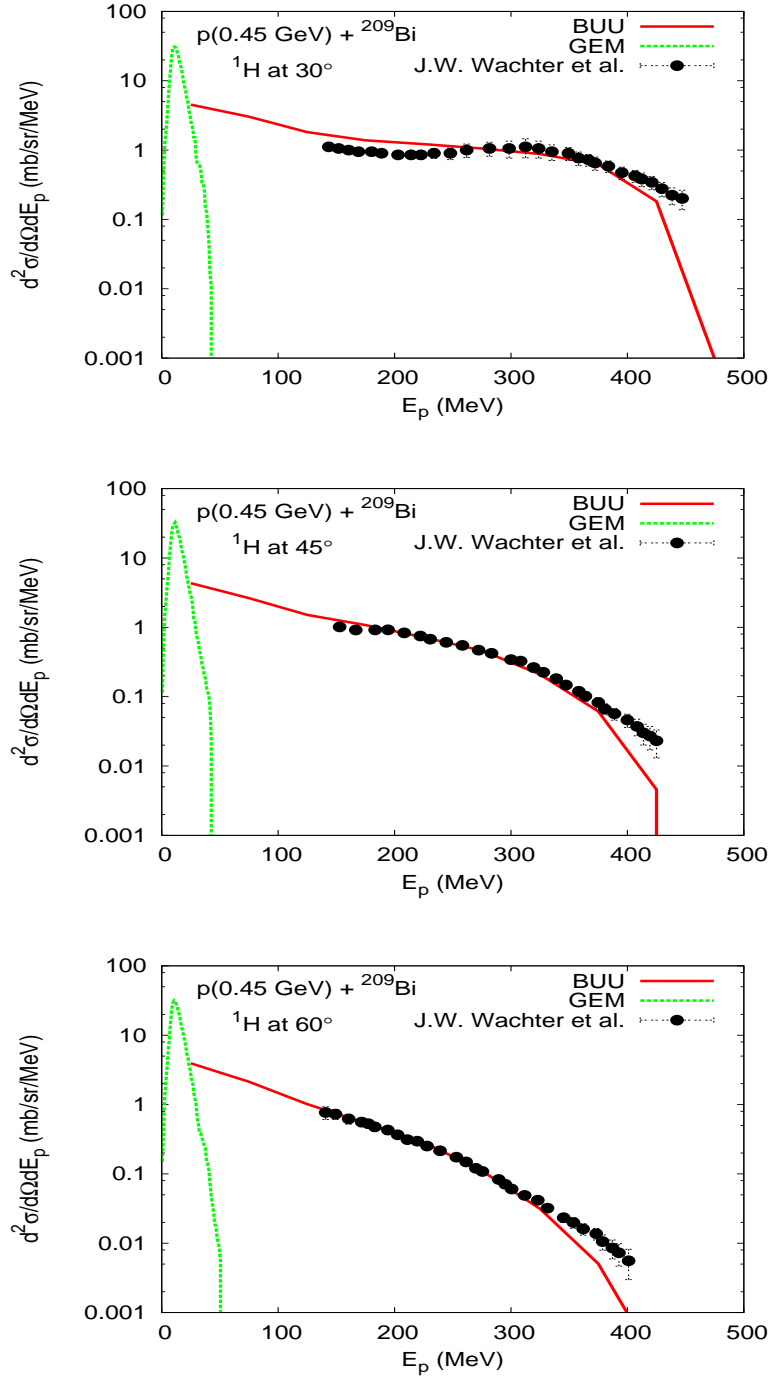Figure 9.12: *Double differential proton spectra from p+Bi reaction at 0.45 GeV proton beam energy; lines show results of HSD and GEM model calculations (solid line - first stage, dashed line - second stage), symbols indicate the experimental data [75]*

Figure 9.13: *Double differential proton spectra from p+Au reaction at 1.2 GeV proton beam energy; lines show results of HSD and GEM model calculations (solid line - first stage, dashed line - second stage), symbols indicate data measured by experiment PISA [7]*

Figure 9.14: *Double differential proton spectra from p+Au reaction at 1.9 GeV proton beam energy; lines show results of HSD and GEM model calculations (solid line - first stage, dashed line - second stage), symbols indicate data measured by experiment PISA [7]*
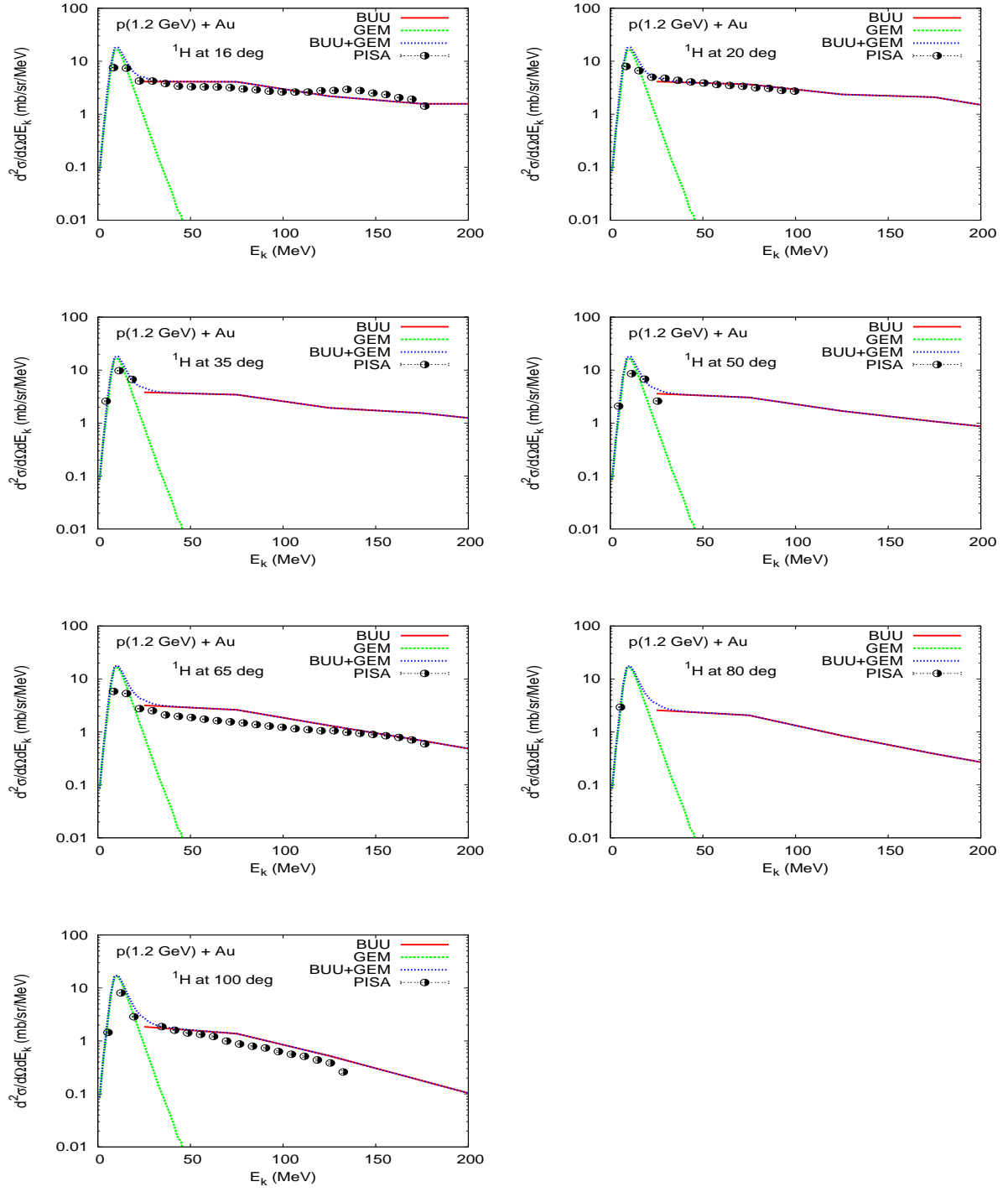
Figure 9.15: *Double differential proton spectra from p+Au reaction at 2.5 GeV proton beam energy; lines show results of HSD and GEM model calculations (solid line - first stage, dashed line - second stage), symbols indicate data measured by experiment PISA [7]*
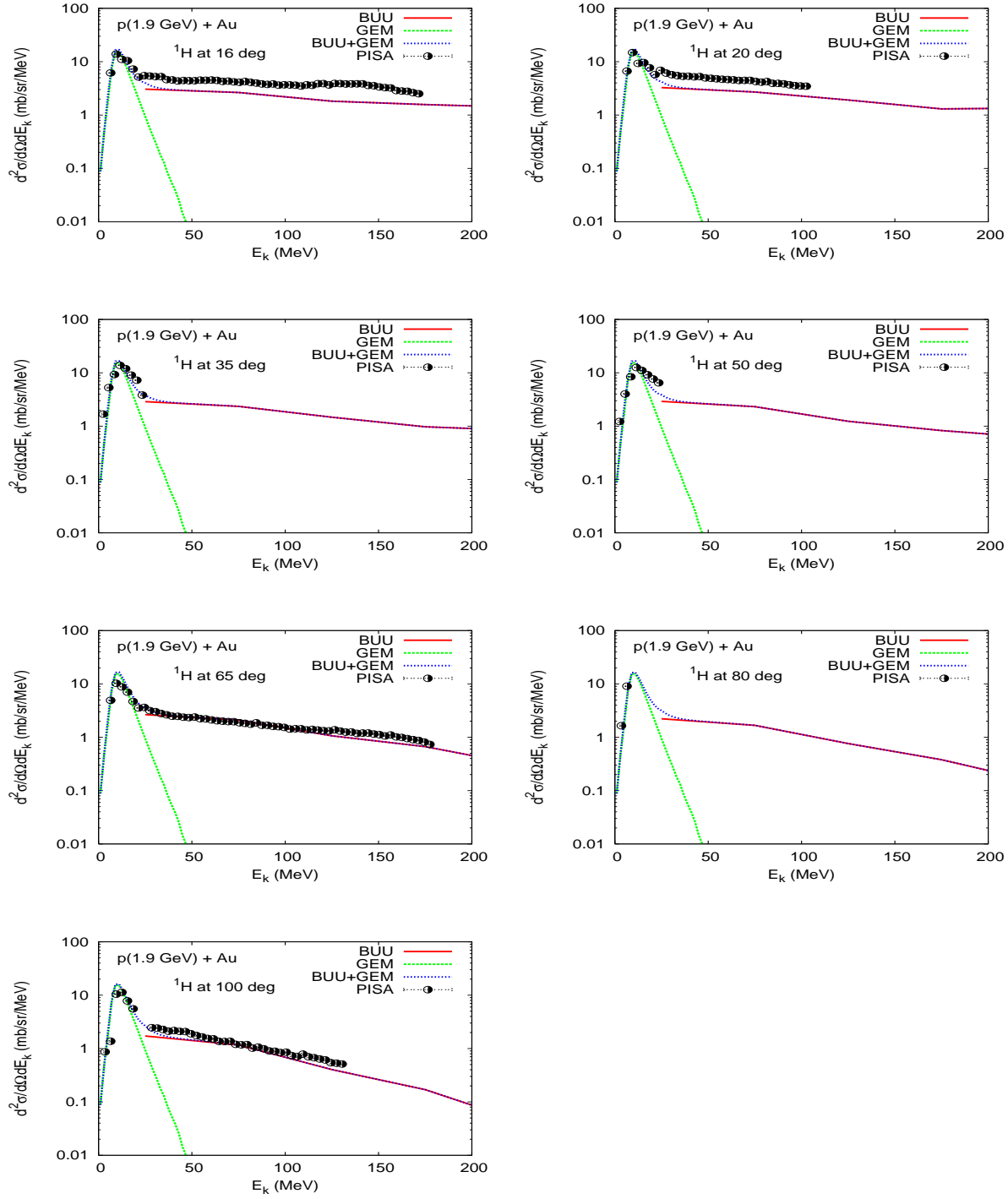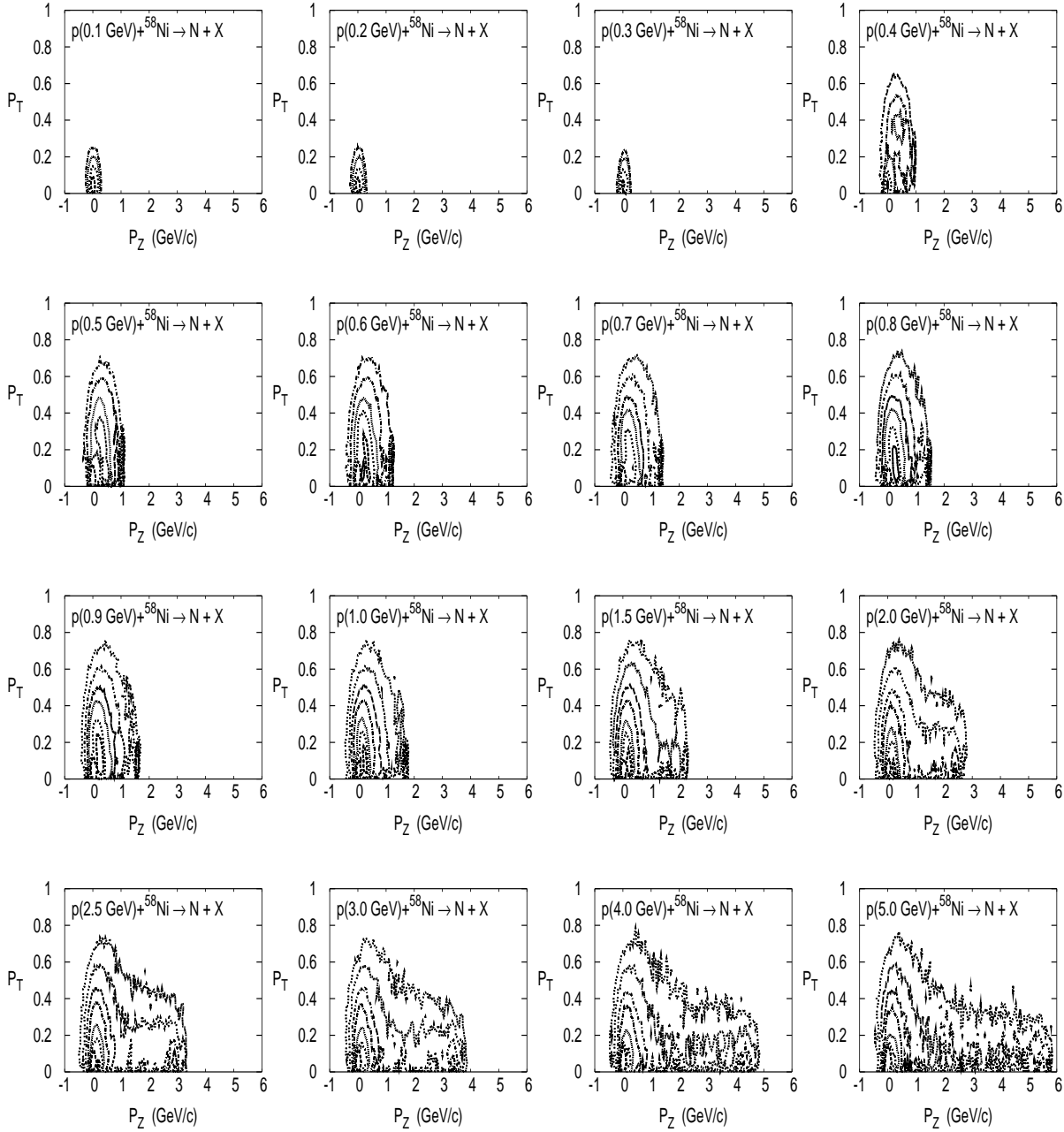
Figure 9.16: *Two-dimensional distributions of transversal versus longitudinal momentum of nucleons emitted during the first stage of proton induced reaction on Ni target, at various incident energies; results of the HSD model calculations (the most central contour line, symmetrical around zero value, corresponds to a maximum of distribution)*

9.3   Deuteron spectra

Comparison of inclusive differential energy spectra of deuterons calculated with the HSD+GEM model, with example experimental data is presented in Fig. 9.17.
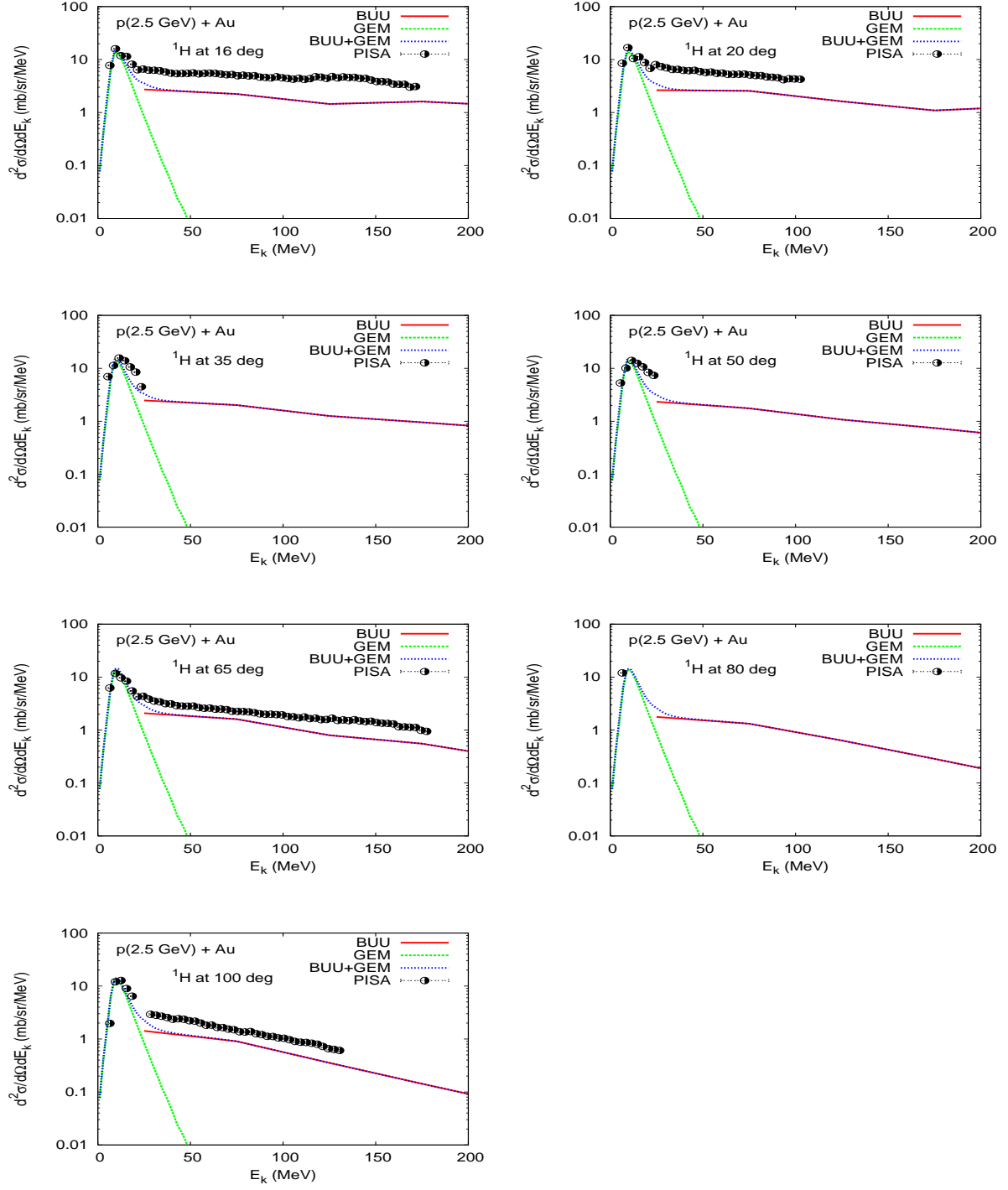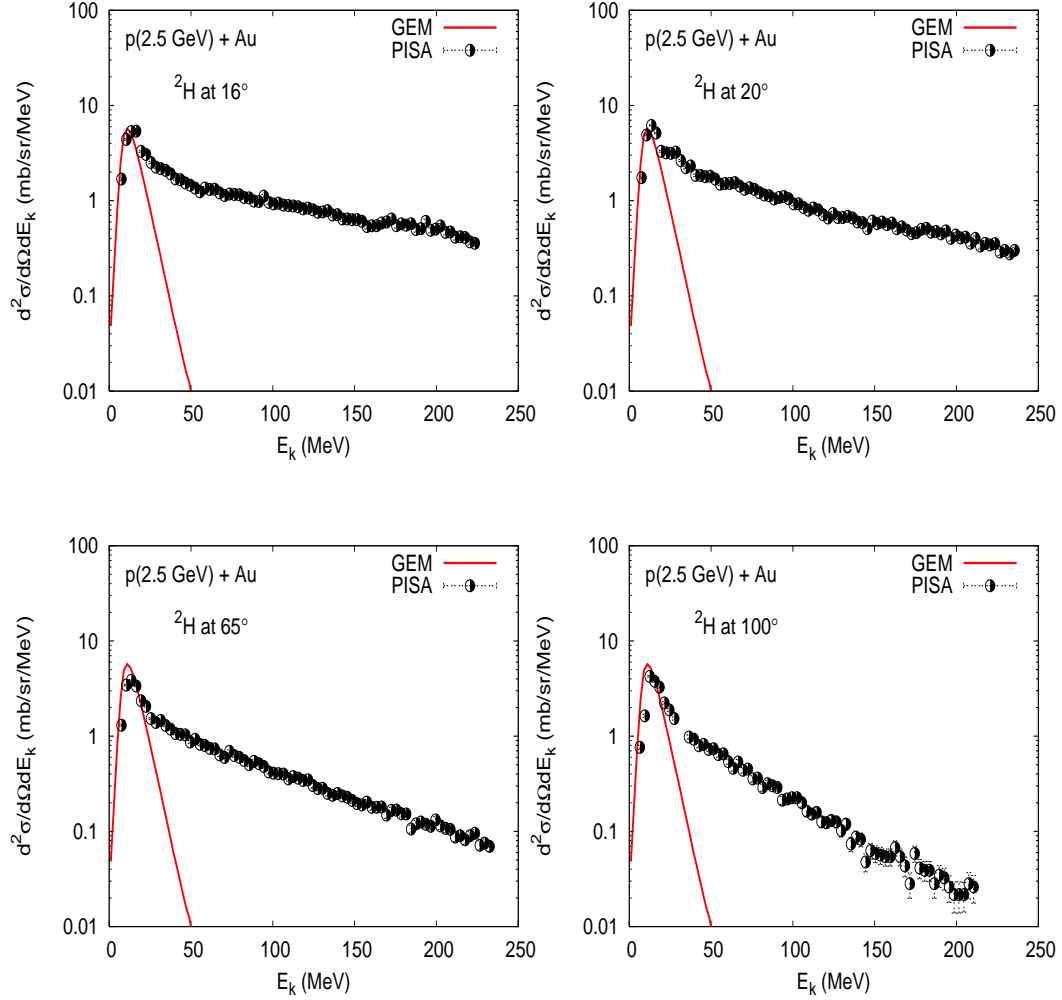

Figure 9.17: *Double differential deuteron spectra from p+Au reaction, at 2.5 GeV proton beam energy; lines show results of the HSD+GEM model calculations, symbols indicate data measured by PISA experiment [7]*

One can see, that only low energy part (i.e. deuterons evaporated from the residual nucleus during second stage of spallation reaction) is described by the model calculations. The absence of high energy part of modelled distributions indicates a lack of deuterons produced during first stage of the

reaction. Certainly, description of the whole distributions necessitates implementation of some additional mechanisms into the first stage model. Since deuteron spectra behave very similar as proton distributions (compare e.g. Figures 9.15 and 9.17), one can suppose that the high energy part of deuteron spectra are produced due to a coalescence of proton and neutron during first stage of reaction. Production of clusters (i.e. light ions) cannot be followed with the HSD approach, since it is a one body theory. Nevertheless, a trial of construction of deuterons from the fast stage of the spallation reaction, with use of informations provided by the HSD approach, have been undertaken in the frame of this work. The idea of generation of such deuterons, called here *deuterons of coalescence*, is based on the information of positions and momenta of nucleons belonging to the residual nucleus and nucleons being emitted during the first stage. The information is taken at a certain point of time, i.e. in the end of the first stage calculations. Deuterons can be built up in two manners: by fast proton and proper fast neutron, which are already emitted, or by fast proton emitted during fast stage of the reaction and proper neutron which belongs actually to the excited residual nucleus, but could have been glued with and taken away by the escaping proton during the first stage of reaction. In both cases, it is assumed that probability of creation a deuteron by defined above nucleon pair, depends on their relative momentum (Δp). It means, two nucleons are considering as a deuteron if their relative momentum fulfills assumed condition. The following conditions have been tested: each pair of neutron and proton can create a deuteron with the same probability (this gives the highest border of the absolute normalization), next, deuterons can be created by proton and neutron only if their relative momentum is lower than or equal to, respectively: $\Delta p \leq 0.45$ GeV/c, $\Delta p \leq 0.30$ GeV/c and $\Delta p \leq 0.15$ GeV/c.

All formed deuterons are additionally repulsed by Coulomb force. The Coulomb potential is approximated by potential of homogeneously charged sphere. This is because an incident proton does not cause any significant changes in the nucleon density distribution inside target nucleus, as shown in Chapter 4. Therefore, the kinetic energy of each deuteron is enlarged by value:

$$E_{Coul} = \frac{0.00144 * Z_T * Z_d}{R_T} \, [GeV] \qquad (9.1)$$

where: Z_T and Z_d are charges of target nucleus and deuteron, respectively, R_T is a radius of target.

Obtained differential energy spectra of deuterons produced in p+Au reaction at 2.5 GeV proton beam energy are presented in Figures 9.18 and 9.19. The calculated distributions are compared with experimental data measured by NESSI collaboration [76].

In more precise definition, deuteron is consider as a set of nucleons, which are sufficiently close to each other in phase space. Therefore, distributions of deuterons constructed of pairs of fast nucleons, with condition set not only on their relative momentum (Δp), but also their relative position (Δr) have been tested, too. The following unit volume of phase space have been selected: $\Delta p \Delta r \leq 0.387$ GeV·fm/c (= the Fermi momentum $\times$ 1.4 fm) [77]. The result underestimates experimental data, as shown in Fig. 9.18 and 9.19. That is because of lost of information about the time evolution of relative positions of the nucleons during the reaction. The condition of relative positions of nucleons, imposed on the situation at the end of first stage of reaction rejects nucleon pairs, that it has no record whether in some earlier period of time nucleons were close enough to create deuterons. Therefore, it determines, at most, the lowest border of coalescence effect.

There is also possible to define the probability (in fact the density of probability) of creation a deuteron by a pair of nucleons depending on their relative momentum, as equal to the modulus of the deuteron wave function squared: $|\psi_0(p)|^2 \cdot p^2$. The wave function can be parametrized itself as:

$$\psi_0(p) = \sum_i A_i exp(-\alpha_i p^2) \qquad (9.2)$$

Values of the coefficients A_i and α_i are taken from [78]. The used parametrization of the deuteron wave function is accurate within a few percent, up to momenta of 1 GeV/c, see Ref. [78].

Obtained in this way spectra of deuterons underestimate the experimental data, see Figures 9.18 and 9.19.

The calculated spectra of deuterons constructed by two fast nucleons (Fig. 9.18 and 9.20) are normalized absolutely. The spectra of deuterons constructed by fast protons and neutrons from the residual nucleus (Fig. 9.19) cannot be normalized absolutely. It is because the information, whether a fast proton before leaving target nucleus has been near a neutron long enough to create a deuteron is lost, what gives in this case evident overestimation of experimental data.

It is seen from the Fig. 9.20, that the high energy part of the experimental spectra are well described by deuterons of coalescence created by a pair of fast nucleons with relative momentum lower or equal to about 0.40 GeV/c. It is also seen that distributions of deuterons of coalescence are perfect continuation of the low energy part. As result, it gives full description of experimental data. However, taking into account shapes of the distributions from Fig. 9.19, one cannot reject possibility that some of the deuterons are produced as coalescence of e.g. fast proton and neutron from residual nucleus.
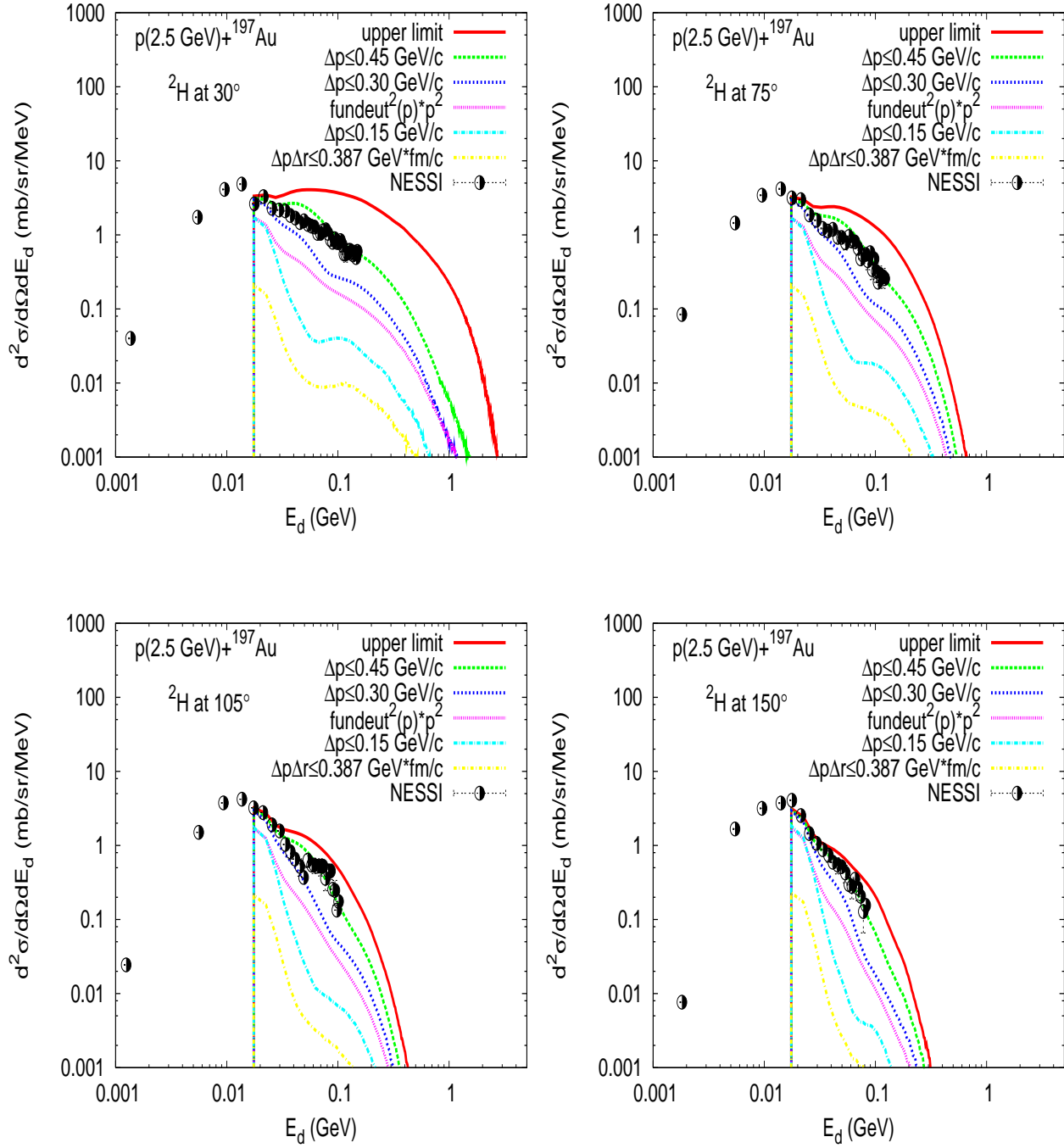
Figure 9.18: *Differential spectra of deuterons of coalescence of proton and neutron emitted during fast stage of p+Au reaction, at 2.5 GeV proton beam energy, compared with experimental data measured by NESSI [76] ("upper limit" means all proton - neutron pairs convert into deuterons)*
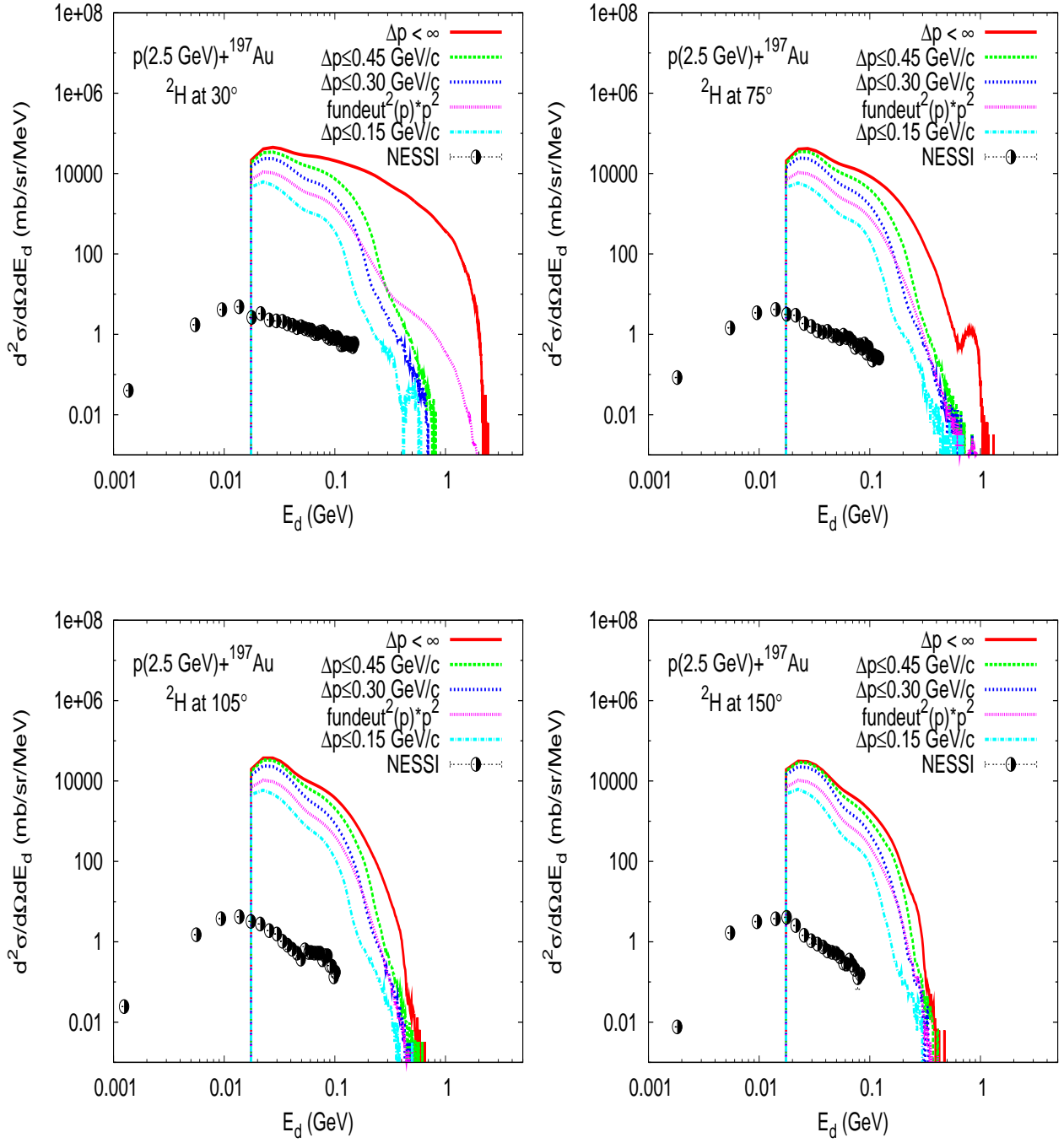
Figure 9.19: *Differential spectra of deuterons of coalescence of fast emitted proton and a neutron from residual nucleus remained after fast stage of p+Au reaction, at 2.5 GeV proton beam energy, compared to NESSI data [76]*
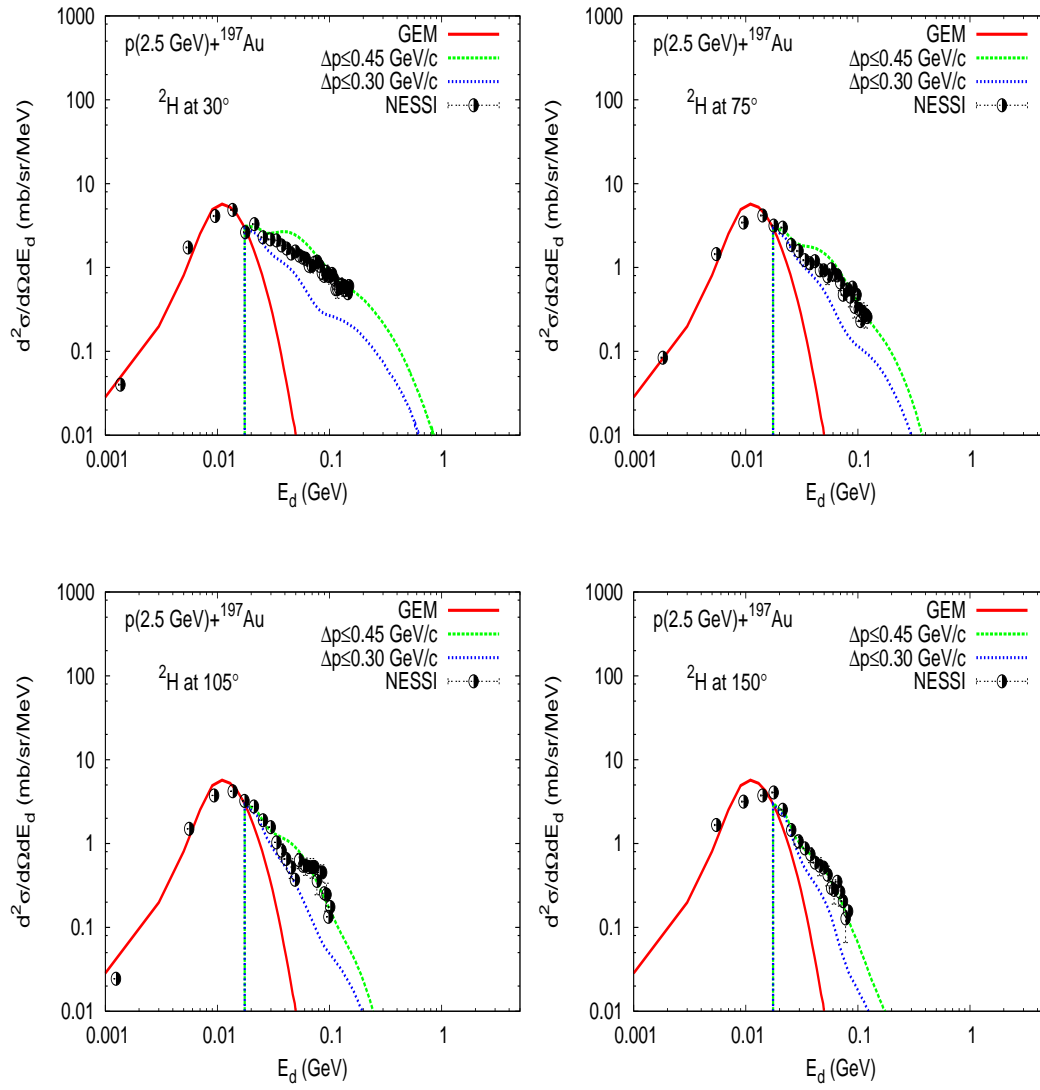
Figure 9.20: *Double differential deuteron spectra from p+Au reaction, at 2.5 GeV proton beam energy; lines show results of the HSD+GEM model calculations, symbols indicate the experimental data measured by NESSI [76] ("GEM" means "statistical evaporation only")*

9.4   Other Ejectiles

Looking at comparison of distributions of heavier particles emitted in proton - nucleus reaction, calculated with the HSD+GEM model with experimental data, displayed in Fig. 9.21, it is seen that only low energy part is described. That is because, in the frame of the model, the light composites are produced only in evaporation stage, as discussed in Sec. 9.3.

It is interesting to know, what is the predictive power of the model, how distributions of the evaporated composites vary with projectile energy and mass of target. Example energy spectra of different ejectiles (isotopes of H, He, Li, Be, B, ...) emitted in proton induced reaction on Au target, at a few chosen beam energies are presented in Figures 9.22, and 9.23. Spectra of particles ejected during 2.5 GeV proton induced reactions on few example targets are shown in Figures 9.24 and 9.25. Looking at the distributions of each ejectile, it is clearly seen, that shape of the particular distributions almost does not change with projectile energy, but strongly depends on used target. In all presented cases, the heavier target, the broader the distributions. Average kinetic energy of emitted particle increases with increase of mass of used target, but in this case neutrons are an exception. This indicates, that reason for such behavior is connected with charge of the particles, i.e. Coulomb repulsion force between the ejectiles and an emitting source. The higher charge of the emitting source, the higher average kinetic energy gained by charged ejectiles due to the Coulomb repulsion. Similarly, the particles yield almost does not change with incident energy, but varies significantly with mass of target. Multiplicities of the particles, produced due to discussed here reactions are compared in Tables 9.3 and 9.4. The yield of neutrons increases linearly with increase of the target mass. Multiplicity of each individual charged ejectile varies differently with the target mass. In some cases, it first decreases with the target mass number (for example presented in the Table 9.4, the minimal yield corresponds usually to Ni target) and then increases with further increase of mass of target (e.g. proton yield behaves in opposite way). In many cases, it is also observed roughly linear decrease of the multiplicity with increase of the target mass (as e.g. in case of ^6Li). The trends for the particles yield can be to some extent qualitatively understood, since it is known, that the particles emission is influenced by the Coulomb barrier, which is higher for heavier nuclei and by the binding energy, which in average first increases with mass number (A) of target (up to A equal to about 56) and then decreases with A. The relative yield of different ejectiles emitted in one chosen reaction (Tables 9.3 and 9.4) is also determined by separation energy of individual ejectile, which is not linear with the mass number of ejectile.
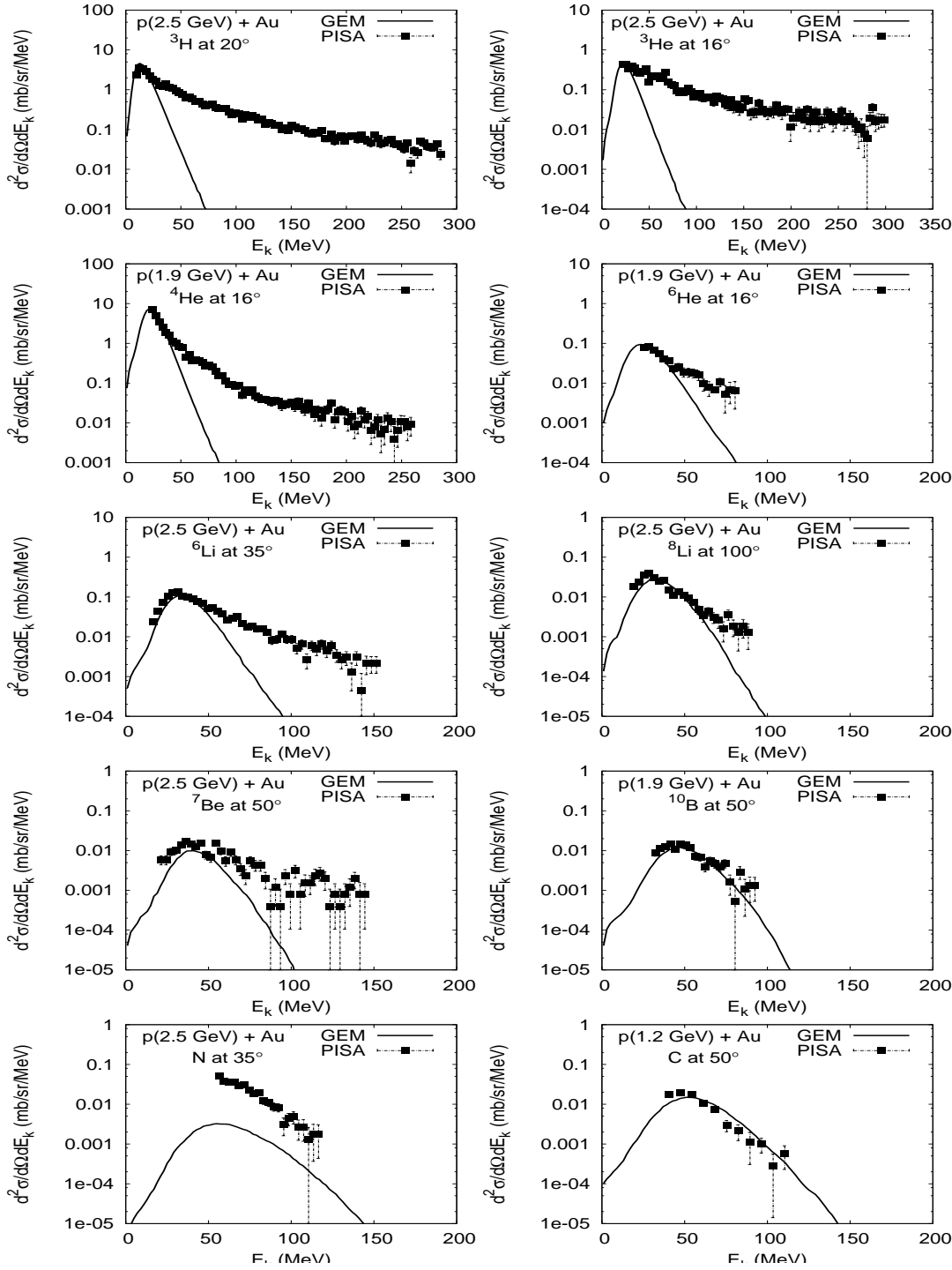
Figure 9.21: *Example double differential spectra of various ejectiles emit-ted during an example reaction p+Au, at few incident energies; results of the HSD+GEM model calculations (solid lines) compared with experimental data measured by PISA at COSY [7] (squares)*
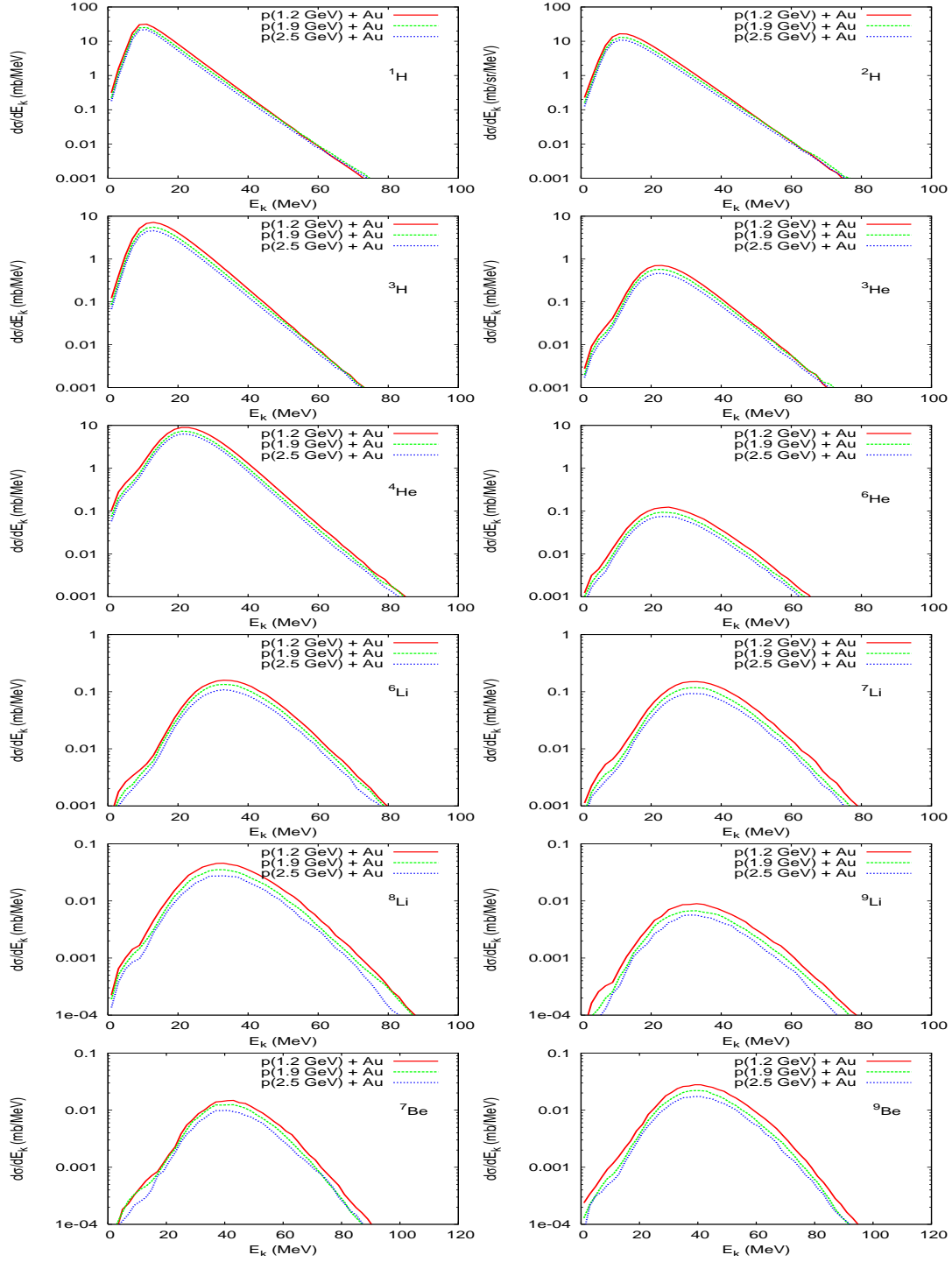
Figure 9.22: *Kinetic energy spectra of different ejectiles emitted in proton induced reaction on Au target, at several proton beam energies; results of the HSD+GEM model calculations*
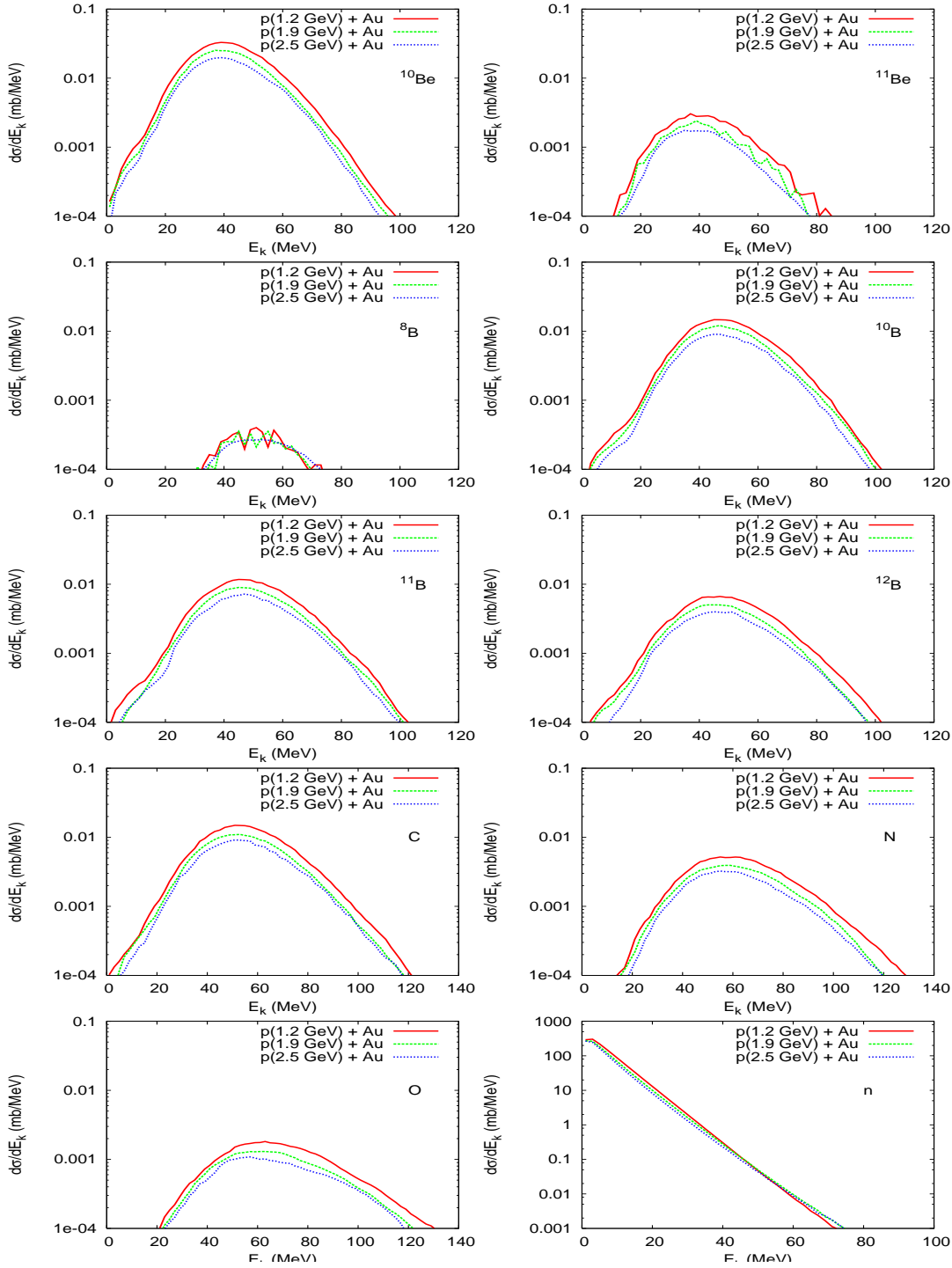
Figure 9.23: *Kinetic energy spectra of different ejectiles emitted in proton induced reaction on Au target, at several proton beam energies; results of the HSD+GEM model calculations*
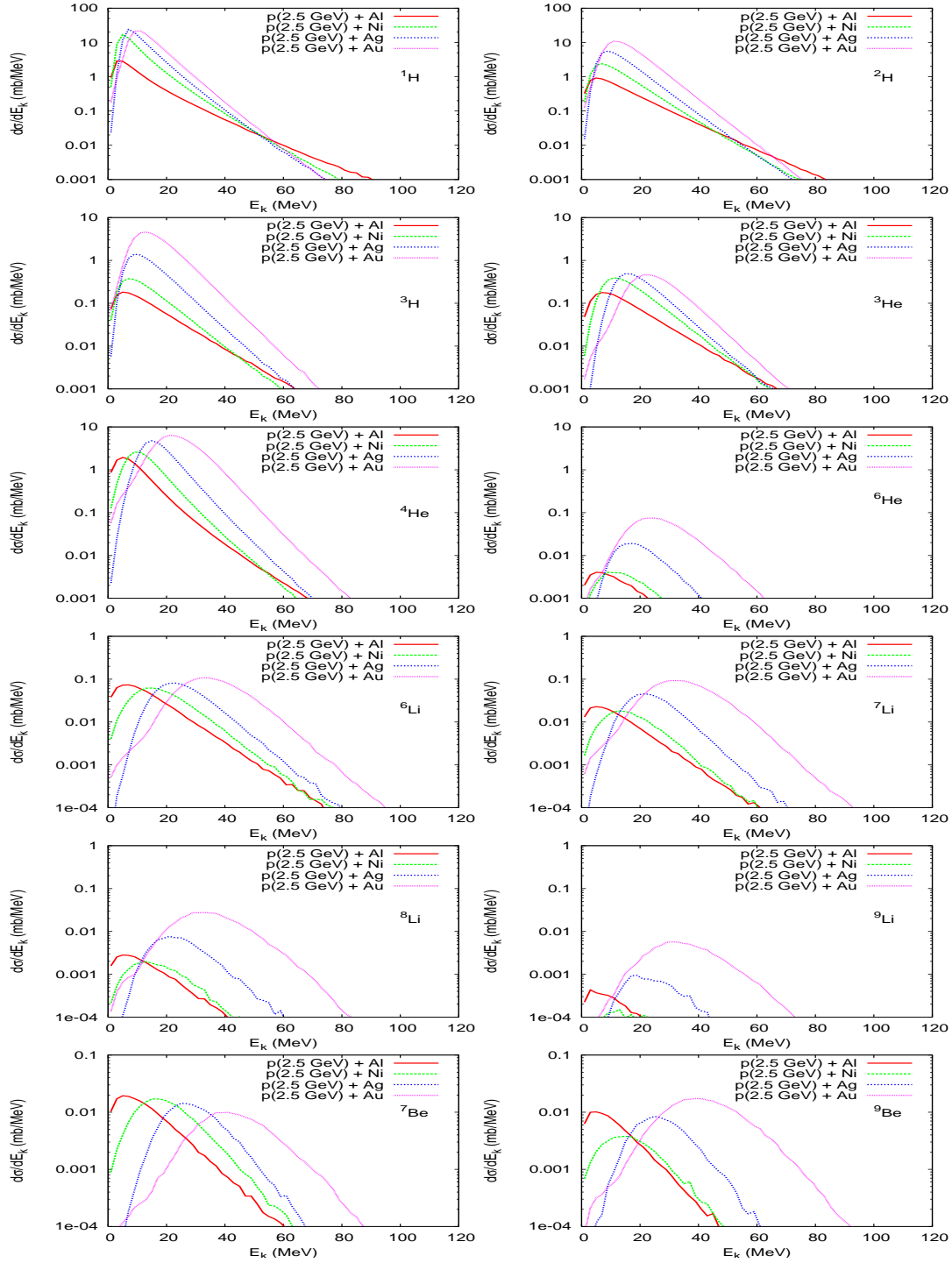
Figure 9.24: *Kinetic energy spectra of different ejectiles emitted in 2.5 GeV proton induced reaction on several targets; results of the HSD+GEM model calculations*
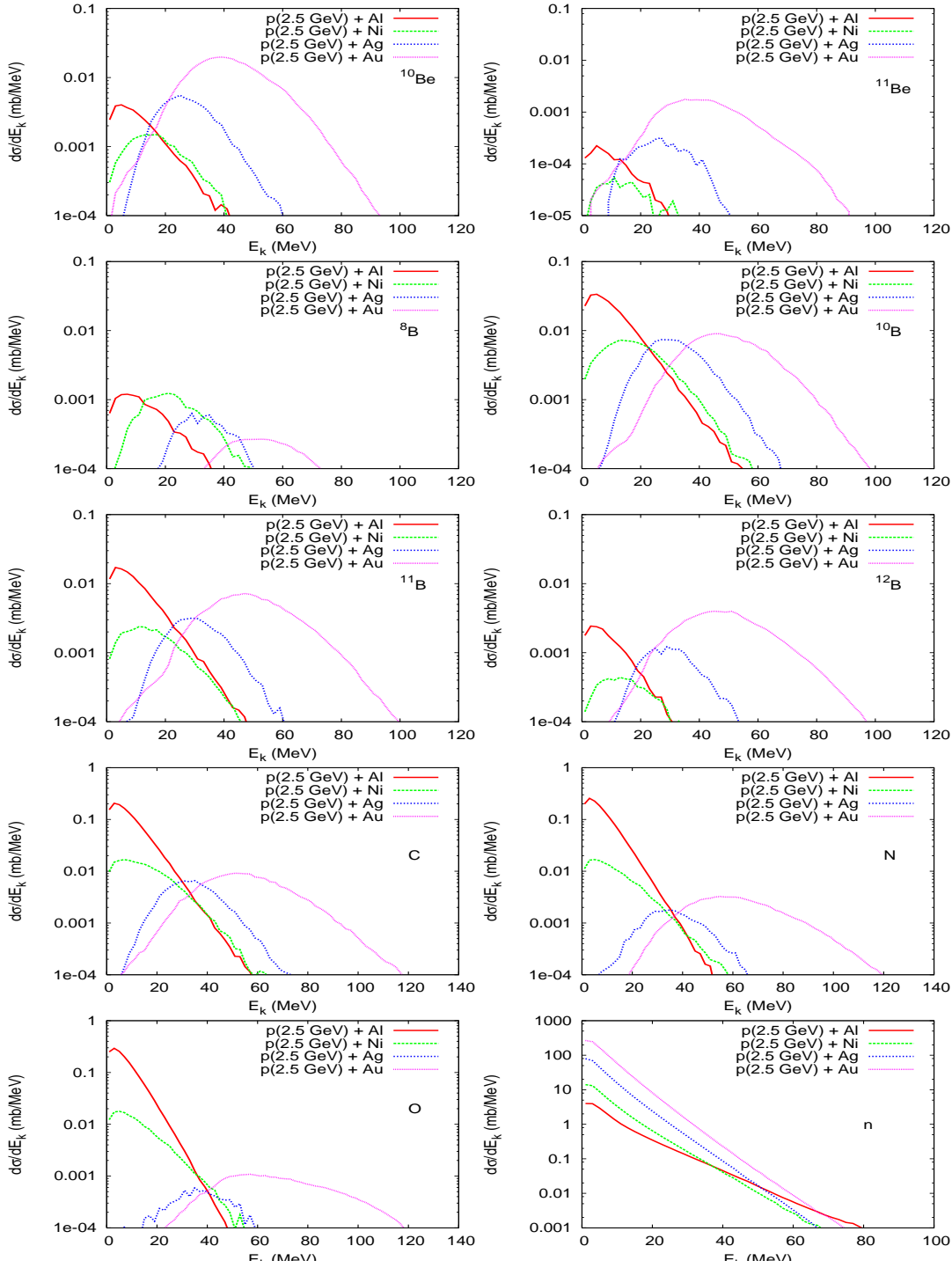
Figure 9.25: *Kinetic energy spectra of different ejectiles emitted in 2.5 GeV proton induced reaction on several targets; results of the HSD+GEM model calculations*

Table 9.3: *Multiplicities of various ejectiles emitted during second stage of proton induced reactions on Au target, at a few impact energies*

| impact energy	1.2 GeV	1.9 GeV	2.5 GeV
n:	14.17	12.79	11.88
^1H:	1.13	1.099	0.96
^2H:	0.59	0.59	0.51
^3H:	0.28	0.28	0.24
^3He:	0.020	0.023	0.021
^4He:	0.59	0.56	0.48
^6He:	0.0054	0.0058	0.0052
^6Li:	0.0045	0.0058	0.0056
^7Li:	0.0067	0.0076	0.0067
^8Li:	0.0018	0.0022	0.0019
^9Li:	0.00039	0.00045	0.00039
^7Be:	0.00045	0.00060	0.00055
^9Be:	0.0015	0.0017	0.0015
^{10}Be:	0.0018	0.0020	0.0017
^{11}Be:	0.00017	0.00017	0.00016
^8B:	0.000010	0.000018	0.000011
^{10}B:	0.00065	0.00081	0.00069
^{11}B:	0.00068	0.00078	0.00067
^{12}B:	0.00047	0.000497	0.00043
^{13}B:	0.000061	0.000051	0.000048
C:	0.0011	0.0012	0.0012
N:	0.00044	0.00045	0.00043
O:	0.0002	0.00021	0.00017

Table 9.4: *Multiplicities of various ejectiles emitted during second stage of 2.5 GeV proton induced reactions on several targets*

reaction	p+Al	p+Ni	p+Ag	p+Au
n:	0.97	1.76	6.11	11.88
^1H:	0.82	2.20	2.19	0.96
^2H:	0.36	0.51	0.75	0.51
^3H:	0.076	0.089	0.20	0.24
^3He:	0.082	0.10	0.082	0.021
^4He:	0.58	0.53	0.64	0.48
^6He:	0.0017	0.0012	0.0036	0.0052
^6Li:	0.033	0.021	0.017	0.0056
^7Li:	0.0097	0.0057	0.0092	0.0067
^8Li:	0.0012	0.00065	0.0016	0.0019
^9Li:	0.00016	0.000046	0.00020	0.00039
^7Be:	0.0087	0.0059	0.0032	0.00055
^9Be:	0.0040	0.0013	0.0019	0.0015
^{10}Be:	0.0016	0.00055	0.0013	0.0017
^{11}Be:	0.000075	0.000015	0.000068	0.00016
^8B:	0.00059	0.00046	0.00015	0.000011
^{10}B:	0.013	0.0029	0.0019	0.00069
^{11}B:	0.0061	0.00088	0.00079	0.00067
^{12}B:	0.00087	0.00016	0.00030	0.00043
^{13}B:	0.000092	0.0000069	0.000018	0.000048
C:	0.064	0.0062	0.0018	0.0012
N:	0.070	0.0049	0.00053	0.00043
O:	0.077	0.0048	0.00018	0.00017

9.5   Massive Fragments

As it is mentioned above, spallation is characterized by observations of one heavy (in respect to the mass of initial target) nucleus, a small number of light fragments and several individual nucleons. Mass distributions of the heavy fragments, produced as result of proton induced spallation reaction on a chosen target vary with incident energy. In Figure 9.26, mass distributions

Table 9.5: *Average values and corresponding standard deviations of mass of heavy nuclei remained after first and second stage of p+Pb reaction, at different incident energies (Tp)*

incident energy	after first stage	after second stage
Tp = 0.5 GeV	208.36±1.14	188.21±7.17
Tp = 1.0 GeV	206.73±1.48	186.65±7.31
Tp = 2.0 GeV	205.79±2.24	188.33±9.70
Tp = 3.0 GeV	205.70±2.39	189.53±9.98
Tp = 4.0 GeV	205.26±2.82	188.68±10.24
Tp = 5.0 GeV	204.57±3.25	187.70±10.58
Tp = 7.0 GeV	203.86±3.92	186.89±11.28
Tp = 9.0 GeV	202.78±4.73	185.04±11.83

of heavy fragments formed in example p+Pb reactions, at several incident energies (calculated with the HSD + statistical evaporation model), set together with mass distributions of corresponding residual nuclei remaining after first stage of the reactions (results of the HSD model only), are shown. It is seen, that both of the distributions (after first stage and after whole reaction) broaden with increase of incident energy. Additionally, the higher projectile energy, the lower average mass of nuclei after the first stage of the reaction. Distribution of mass of nuclei produced after the second stage of the reaction is much broader than mass distribution of the remnants of the first stage. The following changes of the distribution of mass of nuclei produced after the second stage, as function of projectile energy are observed. At the lowest presented projectile energy, a maximum at low masses is seen and very small amount of nuclei with masses close to masses of nuclei after first stage of reaction (which are close to mass of the initial target). With increase of incident energy, the distribution broadens. The higher the incident energy, the smaller is the maximum at lower masses. The lighter and lighter nuclei appears. Also more nuclei with masses close to mass of the initial nucleus are produced. Quantitative differences are presented in Table 9.5.

In Figure 9.27, comparison of calculated mass and charge distributions of products of the proton induced reaction on Au target, at a few incident energies, with experimental data [79] and [80], is presented. Agreement between the calculations and measurements is quite good.

If one compares mass and charge distributions of products of proton induced reactions on a chosen target, at different projectile energies, significant dif-

ference is seen in mass range $A > 25$ and charge range $Z > 10$, as shown in Fig. 9.28. At the lower projectile energy, two almost separate distributions are visible: one ($25 < A < 130$, $10 < Z < 60$, lower yield) corresponds to fission products, the second ($130 < A < 200$, $60 < Z < 80$, higher yield) indicates spallation products (fission process is discussed in Sec. 8.2). At higher incident energy, the split of the distributions vanishes.
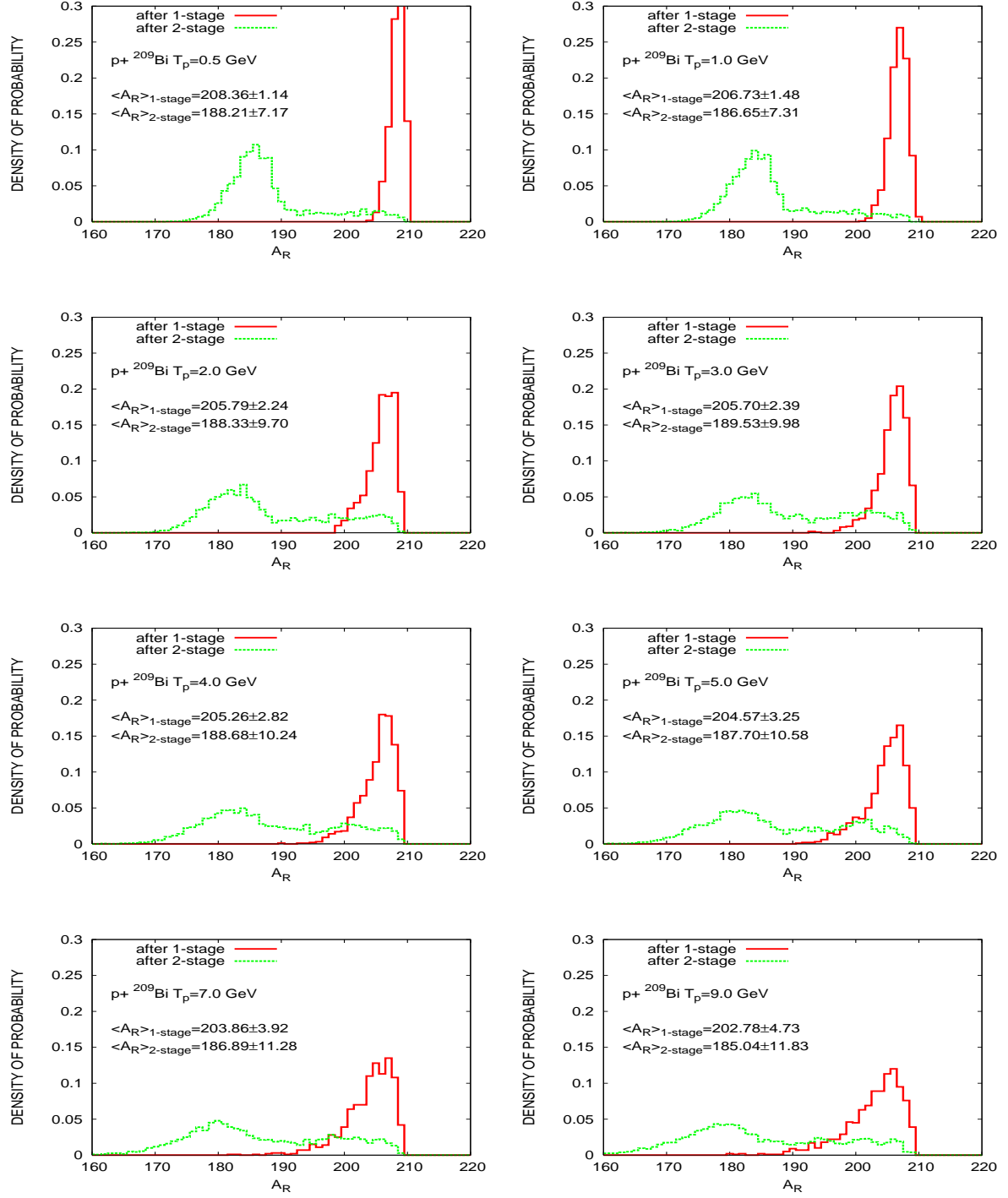
Figure 9.26: *Mass distributions of heavy fragments remained after first and second stage of p+Pb reaction at few proton beam energies; results of the HSD (first stage) and PACE2 (second stage) model calculations (see also Table 9.5)*
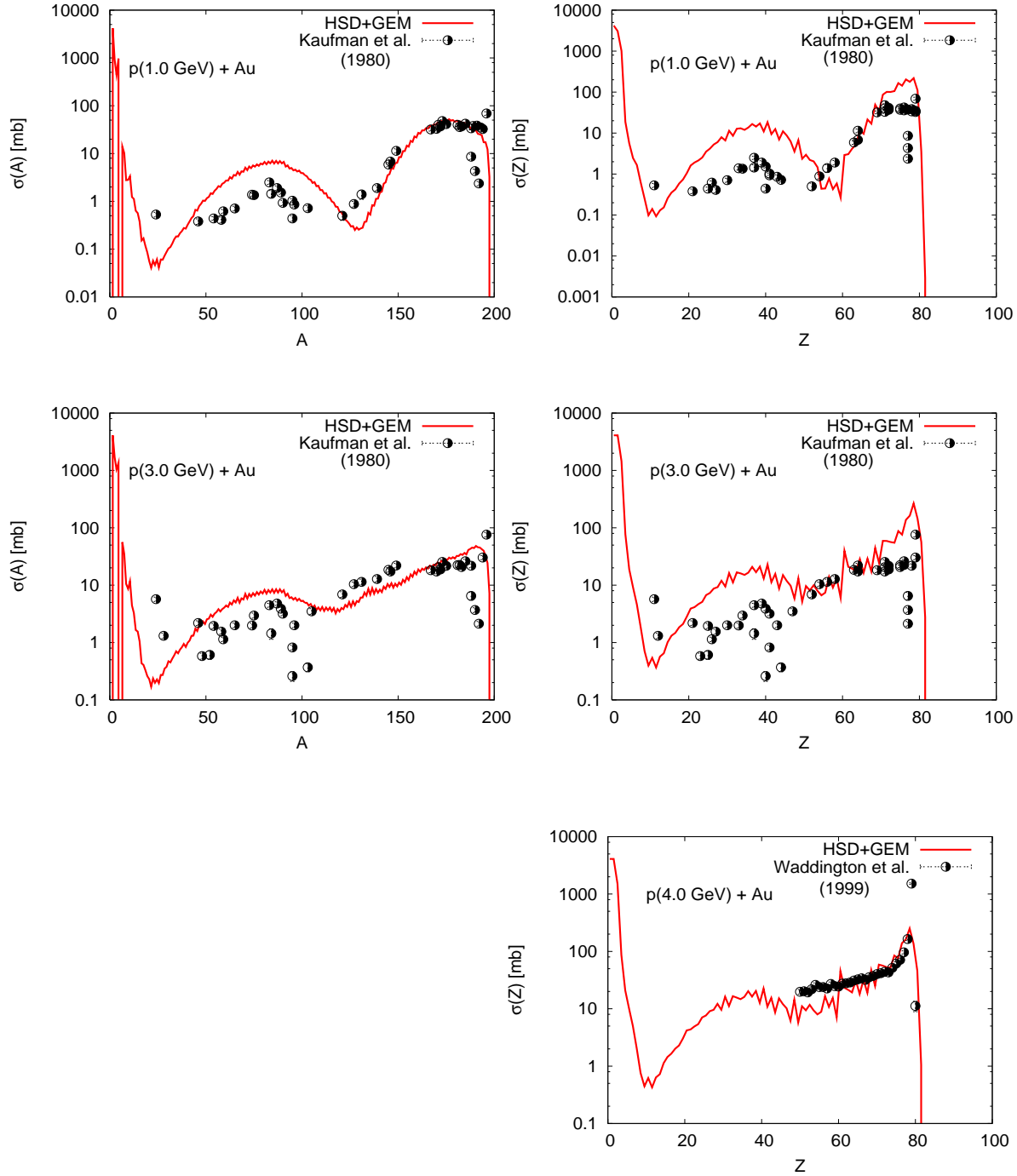
Figure 9.27: *Mass (left) and charge (right) distributions of products of the second stage of p+Au reaction, at a few proton beam energies; results of the HSD+GEM model calculations (solid lines), compared to experimental data [79] and [80]*

Figure 9.28: *Comparison of mass and charge distributions of products of the second stage of p+Au reaction emitted at different proton beam energies; results of the HSD+GEM model calculations (one observes that for higher incident energies of proton, the dips in the distributions become shallower)*

Chapter 10

Comparison of different models predictions on the first stage of proton induced reactions

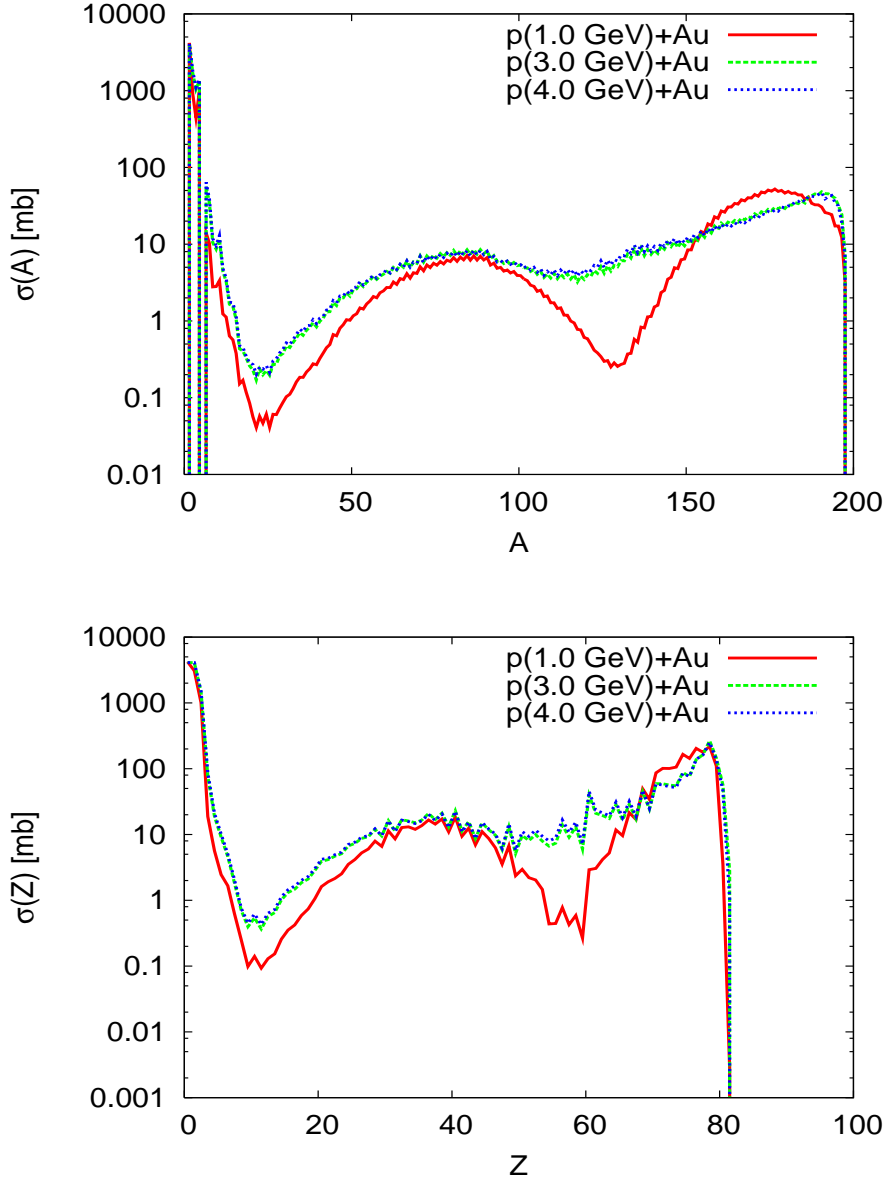Apart from the HSD model, a few other microscopic models have been developed in order to describe the fast stage of proton - nucleus reaction. All the models are based on different assumptions or simplifications (as described in Chapters 2 and 3). It is interesting to compare their predictions. In this chapter, results of the HSD, INCL4 ([17]) and QMD ([19]) models are examined.

The most important issue for comparison of results of various models of the first stage of proton - nucleus reaction are: particles production during the first stage of the reaction and properties of residual nuclei remaining after the stage. Predictions on pion production are particularly interesting for comparison. This is due to the fact, that calculations of the first stage of reaction are sufficient in order to receive realistic pion spectra, as all pions are produced only in the fast cascade of nucleon - nucleon collisions, where the available amount of four-momentum is large enough. One of the important features which can influence the magnitude of pion production and absorption is treatment of the nucleon-nucleus mean field (that corresponds to the main difference between the models). To check whether assumptions concerning the mean field in the model calculations affect significantly multiplicity of produced pions, results of the HSD model are compared with the INCL4 and QMD models calculations and presented in Tables 10.1 and 10.2, for 2.5 GeV proton induced reactions on Ni and Au target, respectively.

It is seen that the relative behavior of the pion multiplicities obtained from the different models is similar: for lighter target (Ni) the $\pi(+) : \pi(0) : \pi(-)$ ratio is equal to 1 : 0.86 : 0.67 for QMD [82], 1 : 0.97 : 0.51 for INCL4

Table 10.1: *Multiplicity of pions produced during p+^{58}Ni reaction at 2.5 GeV proton beam energy; results of the HSD, INCL4 [81] and QMD [82] model calculations*

	HSD	INCL4	QMD
π^+	0.51	0.35	0.42
π^0	0.46	0.34	0.36
π^-	0.38	0.18	0.28

Table 10.2: *Multiplicity of pions produced during p+^{197}Au reaction at 2.5 GeV proton beam energy; results of the HSD, INCL4 [81] and QMD [82] model calculations*

	HSD	INCL4	QMD
π^+	0.49	0.29	0.34
π^0	0.53	0.35	0.34
π^-	0.46	0.25	0.32

[81] and 1 : 0.90 : 0.75 for the HSD, while for the heavy target (Au) 1 : 1 : 0.94 (QMD [82]), 1 : 1.21 : 0.86 (INCL4 [81]) and 1 : 1.08 : 0.94 (HSD). However, absolute values of pion multiplicities obtained from the HSD model are always higher by factor ∼1.5 than the values received from the INCL4 and the QMD models, although results of the HSD model are closer to that of the QMD model.

Let's compare now also an amount of kinetic energy carried out by the most abundantly produced particles during the first stage of the reaction, i.e. nucleons and pions. The average multiplicity and average kinetic energy of nucleons and pions emitted during the first stage of example 2.5 GeV proton induced reaction on Au target are displayed in Table 10.3. The values collected in Table 10.3 indicate, that although the average multiplicity of emitted particles provided by the models are slightly different, the average amount of kinetic energy carried out by the particles is almost identical in all of the models. Consequently, properties of residual nuclei evaluated by the different models should be similar. In Figure 10.1, comparison of the properties of residual nuclei, i.e. distributions of mass, charge, excitation energy and momentum in beam direction of the residual nucleus created in example p+Au reaction, at 2.5 GeV beam energy, are shown. The adequate average values are listed in Table 10.4. One observes that the HSD and

Table 10.3: *Multiplicity, average values and standard deviations of total kinetic energy of nucleons and pions emitted during first stage of p+Au reaction, at 2.5 GeV proton beam energy; comparison of results of the HSD, INCL4 [81] and QMD [82] model calculations*

	HSD		INCL4		QMD	
	M	$<E_k>[GeV]$	M	$<E_k>[GeV]$	M	$<E_k>[GeV]$
n	2.23	0.78±1.27	3.48	0.80±1.46	7.63	0.76±1.83
p	2.20	0.90±1.36	2.68	0.96±1.58	5.63	0.96±2.31
π^-	0.49	0.14±0.13	0.25	0.07±0.08	0.32	0.09±0.11
π^0	0.53	0.15±0.15	0.35	0.13±0.13	0.34	0.10±0.12
π^+	0.46	0.13±0.13	0.29	0.11±0.11	0.34	0.11±0.12

Table 10.4: *Average values and standard deviations of properties of residual nuclei after first stage of p+Au reaction, at 2.5 GeV proton beam energy; comparison of results of the HSD, INCL4 [81] and QMD [82] model calculations*

	HSD	INCL4	QMD
$<A_R>$	193.0±3.3	191.8±4.03	183.5±10.1
$<Z_R>$	77.6±1.8	77.3±1.9	73.8±4.3
$<E^*>[MeV]$	201.7±171.3	253.6±226.3	195.5±165.8
$<(p_z)_R>[GeV/c]$	0.28±0.35	0.44±0.51	0.58±0.62

INCL4 predictions are quite similar.

Results of the models are sensitive to used parameters (in particular time duration of the first stage calculations, which is determined for each model individually, see [17, 19]). Therefore it is worthy to compare results obtained from each of the model and estimate their predictive power by confrontation with experimental data. In order to describe the nuclear reaction in unified way to verify predictions of the different models with experimental observations, the first stage models have been incorporated with one chosen statistical evaporation model applied for the second stage of reaction, i.e. GEM [21]. Output of the HSD, INCL4 and QMD model, respectively (i.e. mass, charge, momentum and excitation energy of the residual nuclei) defines input for the GEM model.
In order to verify which of the distributions of the properties displayed in the
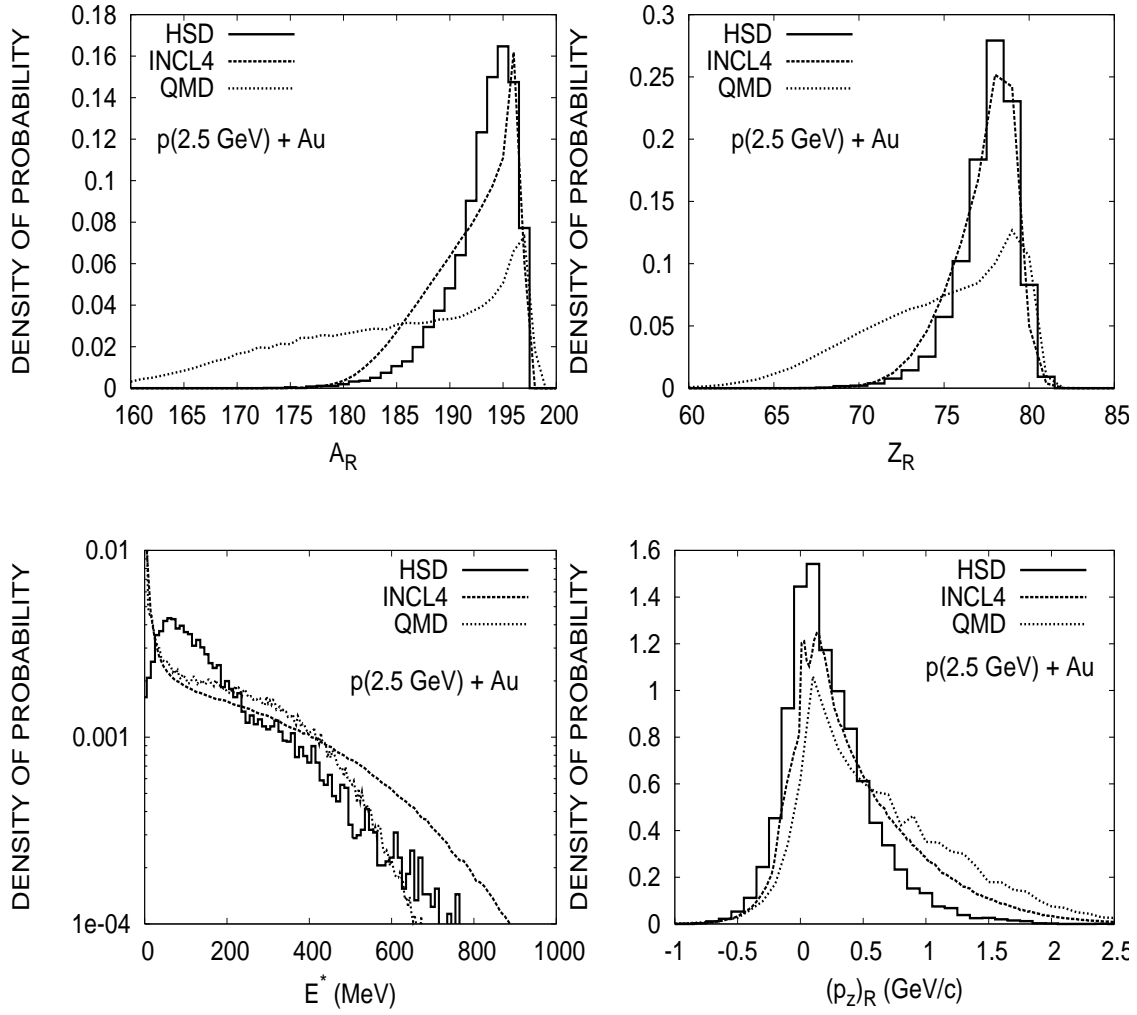
Figure 10.1: *Distributions of properties of the residual nuclei after first stage of p + Au reaction, at 2.5 GeV proton beam energy; comparison of results of the HSD (solid lines), INCL4 [81] and QMD [82] (scatter lines) model calculations*

Fig. 10.1 is the most reliable, calculated double differential kinetic energy spectra of ^{4}He emitted at two different angles during p+Au reaction at 2.5 GeV incident energy are compared with experimental data [7], and shown in Fig. 10.2. Distributions of ^{4}He are the best choice for such a comparison due to the fact, that in the ^{4}He channel evaporation is dominant. As it is shown in Ref.[7], about 90% of the ^{4}He spectrum consists of the particles produced during the evaporation stage. One can see, that the models give similar results, although the HSD and the QMD model results are somehow closer to experimental data.

In Figure 10.3, comparison of calculated example fragment mass and charge distributions compared with experimental data [79] and [80] are displayed. It is seen, that also in this case the models give similar results. In particular, results of the HSD and the INCL4 models are almost identical. If looking at the QMD model calculations, plotted for reaction p+Au at 1.0 GeV beam energy, in the emitted fragment mass number and charge range corresponding to the fission peak (i.e. $50 < A < 100$ and $20 < Z < 50$), they are lower than calculations of the other models, but closest to the experimental data. However, outside the range (i.e. $A < 50$, $A > 100$ and $Z < 20$, $Z > 50$) results of all considered here models are very similar.
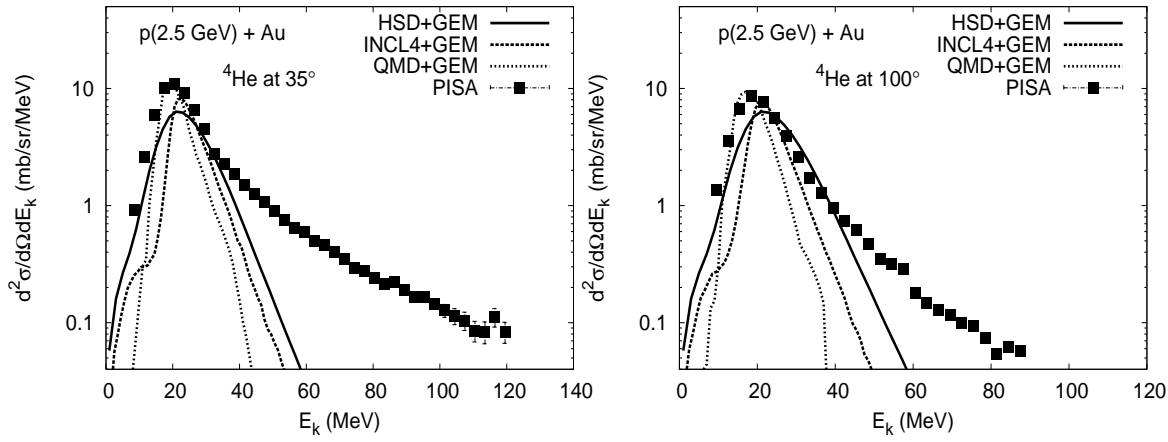

Figure 10.2: *Double differential distributions of ^4He emitted during p+Au reaction, at 2.5 GeV incident energy; results of the HSD+GEM, INCL4+GEM ([81]) and QMD+GEM ([82]) model calculations compared to experimental data measured by PISA collaboration [7]*

Based on the comparisons, one can conclude that results of the HSD model do not differ significantly from results of the other models. The additional verification by confrontation of the calculations with experimental data indicates, that results of the HSD and the QMD model are particularly close to the experimental data. As results of the HSD model are not distinctly different from that of the QMD model (which is actually the most advanced one), a big advantage of the HSD model, connected with respectively short time of calculations should be mentioned. The average time needed to calculate a reaction with the QMD model is of the order of a few days, while time needed to calculate the adequate reaction with the HSD model - only few hours.
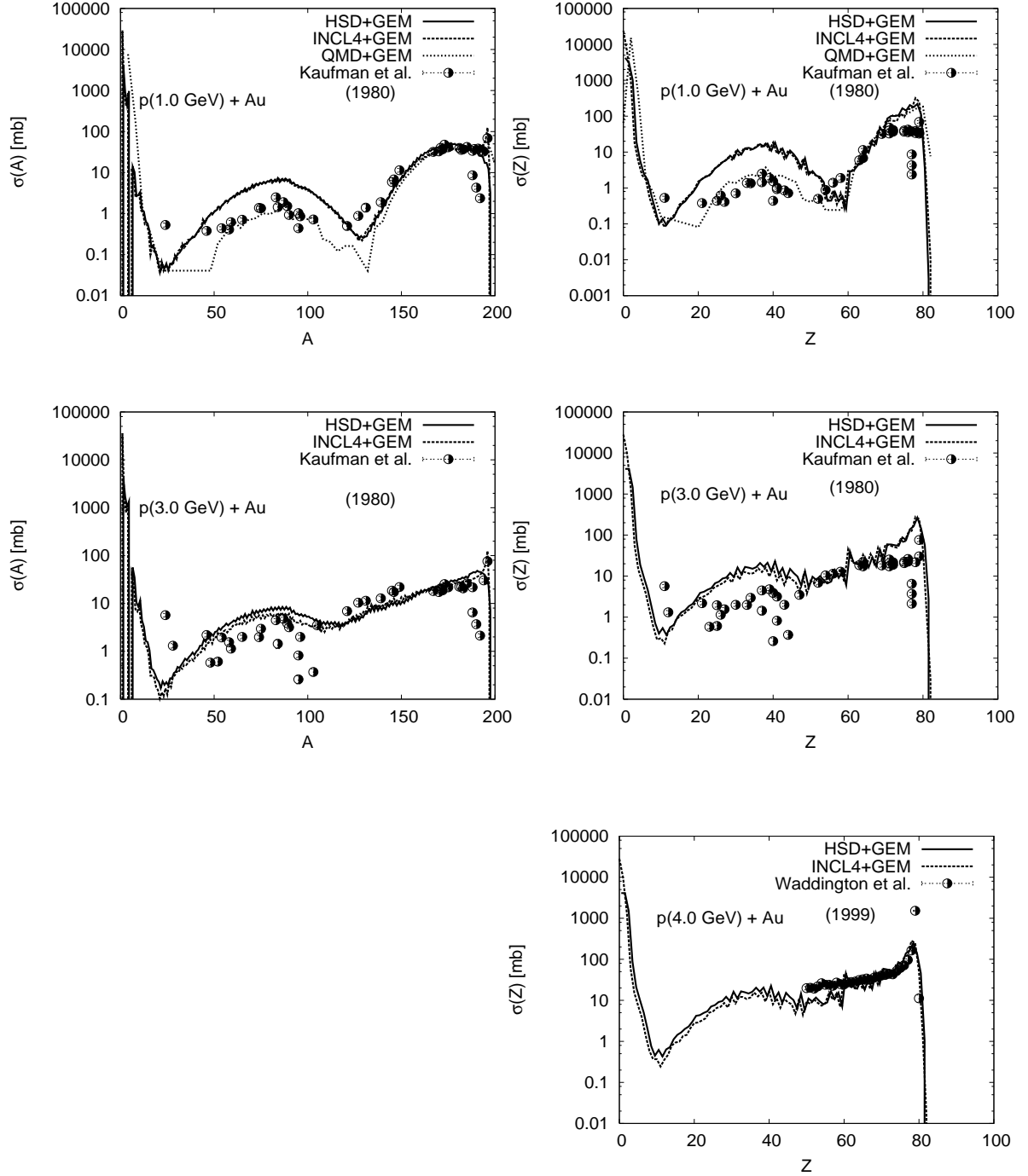
Figure 10.3: *Comparison of mass (left) and charge (right) distributions of products of the second stage of p+Au reaction emitted at different proton beam energies; results of the HSD+GEM, INCL4+GEM ([81]) and QMD+GEM (for T_p = 1.0 GeV only, [82]) model calculations compared to experimental data [79] and [80]*

Chapter 11

Summary and Conclusions

Global information of properties of proton - nucleus reactions (i.e. particles production, properties of residual nuclei after first stage of the reactions) has been presented in wide range of projectile energy and mass of target nuclei, with the Hadron String Dynamics (HSD) [38, 39] model for the first stage of the reaction, incorporated with statistical evaporation model (GEM [21] and PACE2 [20]) for the second stage. It has been confronted with experimental data and results of other models.

The version of the HSD code [38] has been developed in order to describe proton induced spallation reactions in wide energy range in the following aspects. First of all, to calculate properties of residual nuclei after first stage of the reaction, defining an input for models of the second stage calculations. The code has been developed for description of pion production in proton - nucleus reactions. Additionally, a version of HSD code that allows for calculations of pion induced reactions has been prepared.

Stopping time for the first stage model calculations has been established based on behaviors of excitation energy, longitudinal momentum and angular momentum as a function of time. These are decisive for determination of the duration time of the first stage of proton - nucleus collisions, due to the fact that in the dependences two phases can be distinguished: a phase of rapid variations, followed by a phase of much slower variations, indicating thermodynamical equilibrium of the nucleus. Properties of residual nuclei are evaluated by exploring conservation of energy, mass, charge, momentum and angular momentum.

It has been shown, that distributions of properties of residual nuclei (i.e. mass, charge, excitation energy, momentum, angular momentum) differ significantly with mass of target, but behave similarly for varied projectile energies. Multiplicity of emitted pions increases with incident energy and with target mass number. Contrary, e.g. average kinetic energy of other individ-

ual emitted particles (i.e. nucleons, pions) increases with kinetic energy of incoming proton, but decreases with target mass number. Higher nucleon and pion momenta and their increasingly forward peaked distributions are associated with increasing incident energy. That is connected with increasingly forward focused nature of nucleon - nucleon collisions with increase of incident energy; the total nucleon - nucleon scattering cross section remains approximately constant, but ratio of inelastic to elastic collisions increases rapidly with impact energy [45].

It has been shown, that the biggest amount of initial energy deposited in nucleus by incoming proton is carried out during the first stage of the reaction, i.e. about 85 %, and only about 15 % of the initial energy is carried away during the second stage of the reaction. Most of the initial energy is carried out by nucleons and pions. Neutrons are emitted mainly in the second stage of reaction, whereas protons - mainly during the fast cascade stage. Pions are emitted only in the first stage of reaction, where the locally available amount of four-momentum is large enough. In case of light composites, only low energy part of distribution, corresponding to a result of evaporation stage, is described by the HSD plus evaporation model. E.g. for deuterons, the absence of high energy part of modelled distributions indicates a lack of deuterons produced during first stage of the reaction. Description of the whole distributions necessitates future implementation of some additional mechanisms into the first stage model, e.g. coalescence processes. It is observed already in neutron spectra that these additional mechanisms have to depend strongly on size of the system: for heavier targets the neutron spectra in some region are visibly underestimated by model calculations, see Fig. 9.10.

Very interesting conclusion of the work is a prevision for a negligible probability for fragmentation in proton induced reactions, at considered here range of incident energy. This statement is based on results of the HSD model calculations of excitation energy per nucleon of residual nuclei and time evolution of nucleon density. Results of the HSD model show, that a value of excitation energy greater than 5 MeV/N occurs very rarely, in only few percent of cases (studies of fragmentation have found that it occurs at a value of excitation energy per nucleon of a residual nuclei at least equal to about 5 MeV/N [54, 55]). Fragmentation could be more probable if a part of nuclei takes part in excitation, i.e. the excitation energy should be calculated only per some amount of the *active* nucleons; only this part of nucleus would undergo fragmentation. However modelling of nucleon density evolution with the reaction time shows, that proton induced reactions are very low - invasive processes. Incoming proton causes insignificant modifications of the nuclear density. Energy is rather uniformly distributed among the nucleons of resid-

ual nuclei. A situation, when two differently excited parts of nucleus appear, occurs only in about 1% of proton - nucleus reaction cases and rather in peripheral collisions, whereas experimentalists associate fragmentation with central collisions.

It has been shown that in proton induced reaction, in the considered here incident energy range, spallation is evidently dominant process. Moreover, the second stage of spallation reaction is a competition between evaporation and fission.

Results of the HSD model calculations have been compared with available experimental data and with adequate results of other microscopic models (i.e. INCL4 [17] and QMD [19]). The comparisons model - model show that results of the HSD model do not differ significantly from results of the other models calculations. Results of the HSD model are also consistent with various experimental data. Qualitatively, the data are well described by the calculations. Quantitatively, the maximal noticed discrepancy is of factor 2. It concerns pion spectra, which are the worst described cases, i.e. overestimated by a factor of 2. That is because, despite description of NN interactions is well established, details of pions propagation in nuclear matter are very delicate. Legth of free path for pions in nuclear matter of standard density is 1 - 1.5 fm. It means, pions that arrive to detectors stem from surface of nucleus. In models like HSD it is just the surface that is described only approximately. Pions production due to proton - nucleus collisions is a complicated process, since they are not emitted directly, but result from a succession of productions and absorptions inside a nucleus, mediated by Delta resonance.

The comparisons indicates that assumptions and simplifications employed in the HSD model are correct.

In order to obtain the possible best description of proton induced reactions, trials of various feasible modifications of the HSD model parameters has been investigated. However, the possible modifications, as in case of each of semi-classical models are limited. A necessity of the exact fully quantum model appears. Unfortunately, construction of such model of many body strongly interacting system is at present practically impossible.

Summarizing, the global properties of proton induced reactions have been presented in wide range of mass of target and incident energy. It has been shown, that these are quite non-invasive reactions, where spallation is the dominant process. Properties of residual nuclei after the first stage of the reaction are weakly dependent on incident energy, but strongly dependent on mass of target. High momenta of emitted particles are associated with high incident energies. The second stage of the reaction is a competition of evaporation and fission. The agreement of results of the HSD calculations

with experimental data and with results of the other microscopic models calculations indicates that proper assumptions have been employed in the HSD model. As discussed in Sec. 5.1, results obtained from the HSD model vary smoothly as function of proton incident energy and mass of target, so interpolation of results is quite feasible.

Acknowledgments

I would like to thank all the people who helped me during the years of Ph. D. studies.

First of all I would like to express my enormous gratitude to Dr hab. Zbigniew Rudy, for devoting his time, many ideas that helped to bring this dissertation into existence, for his guidance, patience, support, encouragement and help whenever I need it.

I am grateful to Prof. Bogusław Kamys for allowing me to prepare this dissertation in the Faculty of Physics, Astronomy and Applied Computer Science of the Jagiellonian University.

I am extremely grateful to Prof. Bogusław Kamys and Prof. Lucjan Jarczyk for giving me an opportunity to work in PISA collaboration. I am indebted to them for their helpful ideas, suggestions, their kindness, support and encouragement during all the years of my studies.

A big "thank you" to all colleagues from the PISA collaboration, especially to: Prof. D.Filges, Dr F.Goldenbaum, Prof. L.Jarczyk, Prof. B.Kamys, Dr M.Kistryn, Dr hab. St.Kistryn, Dr E.Kozik, Prof. A.Magiera, B.Piskor-Ignatowicz, M.Puchała, Dr K.Pysz, Dr hab. Z.Rudy and M.Wojciechowski.

I'd like to express my gratitude to Dr Małgorzata Kistryn and Małgorzata Puchała for communication concerning results of INCL and QMD model calculations.

I would like to acknowledge Prof. Ulrich Mosel for allowing me to work in his group, at the Institut of Theoretical Physics of Justus-Liebig University in Giessen.

I am extremely grateful to Prof. Wolfgang Cassing for giving me an opportunity to work under his guidance at the Institut of Theoretical Physics in Giessen and ability to use his HSD code. I am indebted to him for help in developing of the code, for sharing his experience, devoting his time and for his patience.

I would like to acknowledge Prof. Jim Ritman for allowing me to work in Research Center Juelich.

I am grateful to Dr Frank Goldenbaum, for the invitation to the Research Center Juelich, for his kindness and help.

I am very grateful to Dr hab. Zbigniew Rudy for careful reading and correcting this dissertation. I am also very grateful to Prof. Bogusław Kamys, Prof. Lucjan Jarczyk and Dr Frank Goldenbaum for correcting some parts of this thesis.

Thanks to all my colleagues from "the room 03A", from Giessen and from IKP for the pleasant atmosphere of the daily work.

Bibliography

[1] N. Bohr, Nature 137(1936)344

[2] B. B. Cunningham et al., Phys. Rev. 72(1947)739

[3] R. Serber, Phys. Rev. 72(1947)1114

[4] V. Weisskopf, Phys. Rev. 52(1937)295

[5] N. Metropolis et al., Phys. Rev. 110(1958)185

[6] I. Dostrovsky et al., Phys. Rev. 111(1958)1658

[7] A. Bubak et al., *Non-equilibrium emission of complex fragments from p+Au collisions at 2.5 GeV proton beam energy*, accepted for publication in Phys. Rev. C, 2007.

[8] F. Goldenbaum et al., Phys. Rev. Lett. 77(1996)1230

[9] W. Przygoda et al., Nucl. Phys. A 783(2007)583

[10] S. Aiello et al., Nucl. Phys. A 583(1995)461

[11] B. S. Brown, A. D. Taylor, ICANS XIII, *13th Meeting of the International Collaboration on Advanced Neutron Sources*, Report PSI-Proc. 95-02, November 1995, ISSN 1019-6447

[12] R. Pynn, ICANS XI, *11th Meeting of the International Collaboration on Advanced Neutron Sources*, Report KEK 90-25

[13] G. S. Bauer, ICANS XIV, *14th Meeting of the International Collaboration on Advanced Neutron Sources*, Report ANL-98/33, ISSN 1560-859X

[14] C. D. Bowman et al., Nucl. Inst. Meth. in Phys. Res. A 320(1992)336

[15] R. Silberberg, C. H. Tsao, Phys. Rep. 191(1990)351

[16] S. G. Mashnik, *On Solar System and Cosmic Rays Nucleosynthesis and Spallation Processes*, LANL, Report LA-UR-00-3658, (2000)

[17] J. Cugnon et al., Nucl. Phys. A, 620(1997)475

[18] K. Niita, W. Cassing and U. Mosel, Nucl. Phys. A, 504(1989)391

[19] J. Aichelin, Phys. Rep. 202(1991)233

[20] A. Gavron in *Computational Nuclear Physics 2, Nuclear Reactions*, edited by K. Langanke et al., Springer-Verlag 1993, p. 108

[21] S. Furihata, Nucl. Inst. Meth. in Phys. Res. B 171(2000)251

[22] H. W. Bertini, Phys. Rev. 131(1963)1801

[23] Y. Yariv and Z. Fraenkel, Phys. Rev. C, 20(1979)2227

[24] K. Niita et al., Phys. Rev. C 52(1995)2620

[25] E. Wigner, Phys. Rev. 40(1932)749

[26] J. Cugnon et al., Nucl. Phys. A 352(1981)505

[27] J. Richert, P. Wagner, Phys. Rep. 350(2001)1-92

[28] W. Bauer, D. R. Dean, U. Mosel, U. Post, Phys. Lett. B, 150(1985)53

[29] W. Bauer, U. Post, D. R. Dean, U. Mosel, Nucl. Phys. A, 452(1986)699

[30] X. Campi and J. Desbois, in *Proceedings of the 23rd Bormio Conference* (Ricerca Scientifica ed Educatione Permanente, Milano, 1985), p. 497

[31] W. Bauer, Phys. Rev. C, 38(1988)1297

[32] A. S. Hirsch et al., Phys. Rev. C, 29(1984)508

[33] T. Murakami et al. (MULTI collab.), *Proc. of the Int. Symp. on Clustering Aspects of Quantum Many-body Systems* (World Scientific, 2002), p.177

[34] D. R. Fortney et al., Phys. Rev. C, 21(1980)2511

[35] Y. Hirata et al., nucl-th/0111019

[36] S. Yamaguchi and A. Ohnishi, Prog. Theor. Phys. 156(2004)150

[37] G. F. Bertsch and S. Das Gupta, Phys. Rep. 160(1988)189

[38] W. Cassing, private communication

[39] J. Geiss, W. Cassing, C. Greiner, Nucl. Phys. A, 644(1998)107

[40] B. Anderson, G. Gustafson, Hong Pi, Z. Phys. C, 57(1993)485

[41] Donald H. Perkins, Introduction to High Energy Physics, (University Press, Cambridge, 2000)

[42] B. Anderson, G. Gustafson, G. Ingelman, T. Sjoestrand, Phys. Rep. 97(1983)31

[43] A. E. Uehling and G. E. Uhlenbeck, Phys. Rev. 43(1933)552

[44] G. F. Bertsch, H. Kruse and S. Das Gupta, Phys. Rev. C, 29(1984)673

[45] Particle Data Group, Phys. Rev. D, 50(1994)1173

[46] J.H. Koch et al., Ann. Phys. 154(1984)99

[47] S. Teis et al., Z. Phys. A 356(1997)421

[48] J. Geiss, PhD thesis, 1998, not published

[49] W. Cassing, E.L. Bratkovskaya, U. Mosel, S. Teis and A. Sibirtsev, Nucl. Phys. A, 614(1997)415

[50] W. Ehehalt and W. Cassing, Nucl. Phys. A, 602(1996)449

[51] J. Geiss, C. Greiner, E. L. Bratkovskaya, W. Cassing, U. Mosel, nucl-th/9803008

[52] A. Strzałkowski, Wstęp do fizyki jądra atomowego, W-wa 1979, PWN

[53] A. Bubak, B. Kamys, M. Kistryn, B. Piskor-Ignatowicz, Nucl. Instr. Meth. B 226(2004)507

[54] L. Beaulieu et al., Phys. Rev. Lett. 84(2000)5971

[55] V. E. Viola et al., Phys. Rep. 434(2006)1

[56] J.Martensson et al., Phys. Rev. C 62(2000)014610

[57] D. R. F. Cochran et al., Phys. Rev. D 6(1972)3085

[58] A. Boudard et al., Phys. Rev. C 66(2002)044615

[59] Baldini et al.: Landolt-Boernstein vol. 12, Springer, Berlin (1987)

160

[60] Th. Aoust and J. Cugnon, Phys. Rev. C 74(2006)064607

[61] A. Engel et al., Nucl. Phys. A 572(1994)657

[62] A. Kowalczyk, Diploma Thesis, Jagiellonian University 2002, not published

[63] W. Hauser and H. Feshbach, Phys. Rev. 87(1952)366

[64] J. R. Grover, Phys. Rev. 127(1962)2142

[65] A. Bohr and B. R. Mottelson, Struktura Jądra Atomowego, W-wa 1957, PWN

[66] A. J. Sierk, Phys. Rev. C, 33(1986)2039

[67] C. M. Perey and F. G. Perey, At. Nucl. Data Tables 17(1976)1

[68] J. R. Huizenga and G. Igo, Nucl. Phys. 29(1962)462

[69] V. Weisskopf and P. Ewing, Phys. Rev. 57(1940)472

[70] I. Dostrovsky et al., Phys. Rev. 116(1959)683

[71] A. Gilbert and A.G.W. Cameron, Can. J. Phys. 43(1965)1446

[72] H. G. de Carvalho et al., Nucl. Phys. 53(1964)345

[73] S. Leray et al., Phys. Rev. C, 65(2002)044621

[74] S. Meigo et al., Nucl. Instr. Meth. A 431(1999)521
K. Ishibashi et al., J. Nucl. Sci. Technol. 34(1997)529

[75] J. W. Wachter et al., Phys. Rev. C 6(1972)1496

[76] A. Letourneau et al., Nucl. Phys. A, 712(2002)133

[77] A. Boudard et al., Nucl. Phys. A, 740(2004)195

[78] G. Alberi, L. P. Rosa, Z. D. Thome, Phys. Rev. Lett., 34(1975)503

[79] S. B. Kaufman and E. P. Steinberg, Phys. Rev. C 22(1980)167

[80] C. J. Waddington et al., The Astrophysical Journal, 519(1999)214

[81] M. Kistryn, private communication (2007)

[82] M. Puchała, private communication (2007)